UNIVERSITY OF OKLAHOMA

GRADUATE COLLEGE

EXPERIMENTAL INVESTIGATION, CORRELATION, AND DIMENSIONAL ANALYSIS OF NEAR-WELLBORE FORMATION TREATMENT BY GEL PARTICLES AND PARTICLE-GEL SYSTEM

A DISSERTATION

SUBMITTED TO THE GRADUATE FACULTY

in partial fulfillment of the requirements for the

Degree of

DOCTOR OF PHILOSOPHY

By

ADNAN L. MUHSIN AL-IBADI
Norman, Oklahoma
2014

EXPERIMENTAL INVESTIGATION, CORRELATION, AND DIMENSIONAL ANALYSIS OF NEAR-WELLBORE FORMATION TREATMENT BY GEL PARTICLES AND PARTICLE-GEL SYSTEM

A DISSERTATION APPROVED FOR THE
MEWBOURNE SCHOOL OF PETROLEUM AND GEOLOGICAL ENGINEERING

BY

_____
Dr. Faruk Civan, Chair

_____
Dr. Deepak Devegowda

_____
Dr. Ramadan Ahmed

_____
Dr. Maysam Pournik

_____
Dr. Jeffrey Harwell

Acknowledgements

I would like to express sincere gratitude to Dr. Faruk Civan, chairman of my committee and advisor of this dissertation work, for providing the best graduate school experience that I could have hoped for. I am deeply indebted for his ultimate support, guidance, patience, and generosity throughout this dissertation work.

I would like to thank Dr. Deepak Devegowada, Dr. Ramadan Ahmed, Dr. Maysam Pournik, and Dr. Jeffrey Harwell for serving in my dissertation committee and their helpful comments, and suggestions.

I would like to thank Dr. Ian Robb of Halliburton Energy Services, who past away, of his valuable discussions and support during the initiation of our experimental studies related to the near-wellbore formation treatment by gel particles suspension. I would also like to thank Dr. Larry Eoff with Halliburton for his support on the work related to the near-wellbore water shutoff treatment studies, both supplying equipment and chemicals for lab testing and discussion of lab results. I would also like to thank Dr. Cengiz Altan and Dr. Levent Aktas of the University of Oklahoma for use their microscope to obtain the photomicrographs included in this work.

Finally, I would like to thank my wife, my two sons, and my sweet daughter for their understanding, support, and encouragement. This work is dedicated to the memory of my parents.

Table of Contents

List of Tables

List of Figures

Abstract

Reservoir permeability heterogeneity with high permeability zones can create many problems in petroleum reservoirs such as lost circulation of drilling fluids and high water production in hydrocarbon producing wells. These problems cause high cost to the oil and gas industry. Thus, the conditions leading to plugging of the high permeability zones during the treatment and conditioning of high permeability porous formations by suspended gel particles and silica flour particle-gel systems were studied and useful empirical correlations, dimensionless correlations, and charts were developed which can be used for effective and successful design of formation-plugging treatment.

First, conditioning and plugging of high permeability formations and the resulting permeability impairment occurring during injection of suspensions of deformable gel particles are investigated experimentally to treat reservoir permeability heterogeneity which can prevent lost circulation of drilling fluids. Appropriate dimensionless groups are used to develop several empirical correlations of the experimental data, which can assist in choosing suitable gel-particle suspensions and proper conditions required for effective near-wellbore-formation treatment.

Second, the plugging and permeability impairment processes involved in the treatment and conditioning of high permeability porous formations is investigated at various temperatures by flowing a suspension of gel particles through unconsolidated proppant packs. The effective mechanisms of the consecutive plugging and unplugging processes occurring during the flow of gel particles suspension through the proppant pack are identified and the best-estimate values of their rate coefficients are determined.

Various empirical correlations of practical importance developed in this work can be used for effective design of the suspended gel particles treatment in highly permeable near-wellbore formations. These correlations can predict the effect of temperature on conditioning of the high permeability formations by injection of suspensions of gel particles.

Third, analysis and interpretation of experimental data of laboratory tests of porous formation treatment by gel particles conducted at different gel particles suspension and application conditions are presented based on the dimensional analysis method. The measured permeability reduction caused by gel particles suspension injection into sand packs is correlated successfully by using the dimensionless groups developed from the relevant variables of sand packs, gel particles suspensions, and application operation conditions. Dimensionless correlations are developed from the dimensionless groups which can assist in evaluating the treatment of highly permeable near-wellbore formations by suspension of gel particles under varying application conditions.

Fourth, the performance of several particle-gel systems is investigated for near-wellbore formation treatment to prevent or control water production in waterflooded mature oil fields. Effects of particulate concentration, leak-off, and threshold-pressure are investigated by the laboratory fluid loss tests conducted at constant pressure. Useful empirical correlations and charts for the fluid loss, pressure initiation for flow, and critical silica flour concentration are developed for practical applications which can assist in choosing suitable particle-gel systems for effective near-wellbore-formation treatment. A methodology using these correlations and charts

is presented for design of optimal conformance control treatments for effective mitigation of water production in waterflooded mature oil fields.

Fifth, analysis and interpretation of experimental data of laboratory tests of several particle- gel systems and different application conditions are presented based on empirical correlations. The rate constant of filtrate and spurt loss volume are determined and correlated at different silica flour concentrations, sand sizes, and pore diameters of filter discs. Exponential relationship is used to correlate the experimental filtrate volume during the leak off tests at different sand sizes, pore diameters of filter discs, and silica flour concentrations. The present empirical correlations can predict the evolving filtrate volume of particle-gel system under varying conditions. The proposed empirical correlations can assist in effective design of particle-gel systems used for treatment of high-permeability near-wellbore formations for avoiding and mitigation of water production in waterflooded mature oil fields.

Sixth, treatment design for near-wellbore field application is demonstrated using the empirical correlations that developed by this study. Two synthetic field cases, involving the drilling of an oil well and producing from an oil well, are studied for treatment design. The treatment fluid properties and the conditioning and treatment of high permeability near-wellbore formation are determined.

Chapter 1: Introduction

The high permeability zones of the heterogeneous petroleum reservoirs can cause many problems to the oil and gas industry such as lost circulation of drilling fluids and high water production in hydrocarbon producing wells. Injection of suspension of deformable gel particles and silica flour particle-gel systems as methods of near-wellbore formation treatment is considered in the present study. The goal of the present study is to determine the effects of various factors that participate in plugging of high permeability zones during the treatment and conditioning of high permeability porous formations by suspended gel particles and silica flour particle-gel systems and to develop empirical correlations, dimensionless correlations, and charts which can assist in choosing suitable conditions for effective near-wellbore formation treatment.

1.1 Near-Wellbore Formation Treatment

The lost circulation of drilling fluids during drilling operations and excessive water production in oil producing fields are undesirable problems because of high cost to the oil industry. These problems are caused by reservoir heterogeneity in high permeability zones with large and highly connective pores, open fractures, and worm holes. Therefore, near-wellbore formation treatment by injection of suspensions of deformable gel particles and silica flour particle-gel system is explored as a method of preferentially plugging the large pores, thus reducing the undesirable high formation permeability and handling of reservoir permeability heterogeneity to prevent lost circulation of drilling fluids and control water production in mature waterflooded oil

fields containing highly permeable zones. The gel particles suspension and silica flour particle-gel system are insensitive to lithology. Thus, these can be applied in sandstone, carbonate, and shale formations needing a near well-bore treatment.

Fig. 1.1 shows a schematic of the various zones and the gel particles suspension and silica flour particle-gel system applications in the near- wellbore formation. Study of the performance of gel particles during the injection into the porous media and the factors affecting the gel particles plugging mechanisms are important issues to consider for successful applications for this technology.

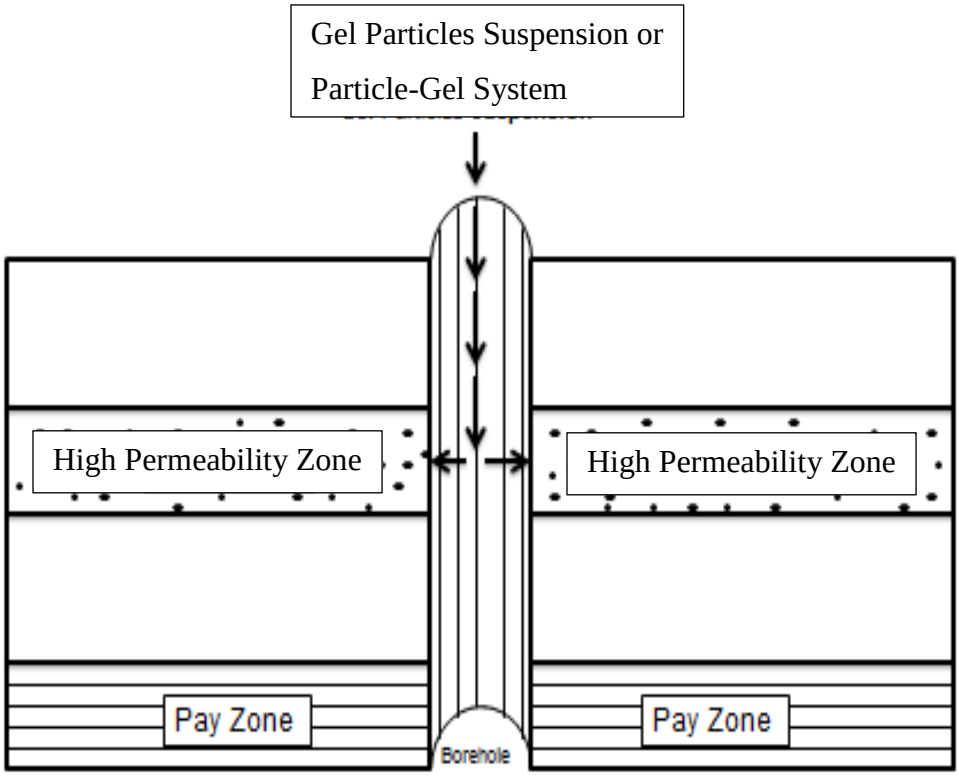

Fig. 1.1: Schematic of various zones and the gel particles suspension and silica flour particle-gel system applications in the near- wellbore formation

1.2 Objectives of the Study

The primary objectives of this study are several fold described as follows.

1.2.1 Experimental approaches

- Investigate the conditions leading to plugging of highly permeable formations by studying the permeability impairment of porous media during flow of a suspension of deformable gel particles and by studying the pressure required to initiate flow after the silica flour particle-gel process.
- Describe the relevant processes and mechanisms of pore plugging by gel particle suspensions and silica flour particle-gel system at different operation conditions.
- Describe the effect of the variation in gel particle and silica flour concentrations, flow rates, gel particle diameter, ratio of gel particle sizes-to-pore-throat diameter, pore space of the permeable filter disc, and sand sizes on the plugging conditions of the high-permeability formations.
- Determine the thermal effect on treatment of high permeability formations and the relevant processes and mechanisms of pore plugging by a suspension of deformable gel particles and silica flour particle-gel system.
- Evaluate the near well-bore treatment of high permeability formations by gel particles suspension using dimensional analysis.

1.2.2 Data analysis approaches

- Determine and describe the relevant dimensionless groups of gel particles application processes at different operation conditions and develop dimensionless correlations from these dimensionless groups for the

- permeability reduction by gel particles injection and investigate the functional trends of these correlations to assist in scaling from laboratory to field conditions.
- Develop empirical correlations and charts from the experimental data of the gel particles process and silica flour particle-gel system for the suspended gel particle size distributions before and after flow, differential pressure build-up across porous media, permeability reduction of porous media, resistance factor against suspended flow, fluid loss, pressure required to initiate flow, and critical silica flour concentration.
- Investigate the permeability-impairment trapping mechanisms of gel particles by means of the diagnostic equations of Wojtanowicz et al. (1987).
- Apply a Vogel-Tammann-Fulcher (VTF) - type equation to develop empirical correlations for the viscosity, differential pressure build-up across porous media, permeability reduction of porous media, resistance factor against the suspended gel particles flow, fluid loss and pressure required to initiate flow of the silica flour particle-gel system from the experimental data involving the temperature effects.
- Correlate the thermal effects on the sequential plugging and unplugging events during the injection of gel particles suspension into porous media.

1.3 Description of Various Chapters

Chapter 2 presents a literature review of the experimental studies of the

operation conditions involving the particulate processes which lead to plugging in the pores of porous media. A literature review of the mathematical and numerical models of the particulate processes of porous formations is also presented.

Chapter 3 describes the factors affecting the near-wellbore formation treatment by gel particles such as gel particle deformation and break-up, gel particle coagulation and detachment**,** carrier fluid properties, suspension viscosity, gel particle diameter, suspension concentration, porous media, and operation conditions which can affect the plugging of pores and thus the conditioning of the high permeability formations.

Chapter 4 presents the experimental studies undertaken to investigate the conditions favorable for plugging in highly permeable formations by gel particle suspensions and silica flour particle-gel systems. The experimental flow apparatus used at isothermal and thermal conditions, the experimental testing procedures, gel particle suspension preparation, silica flour particle-gel system preparation, and the measurements of viscosity, pore throat size, and particle gel size are described in this chapter.

Chapter 5 presents the conditioning and plugging of high permeability formations by suspension of deformable gel particles. The Effect of concentration, flow rate, gel-particle sizes of suspensions, and particle diameter to pore-throat size on the prevailing pore- plugging processes is inferred by flow tests conducted with 3800-md 16- to 20-mesh sandpacks. Prevailing particle-entrapment and –permeability impairment mechanisms are identified under various conditions by means of specially formulated diagnostic equations and the results of data analysis for pore plugging are described. This reveals valuable insights and information about the functional trends of

sandpack plugging by gel-particle suspensions, which can help in successful design and mitigation of formation-plugging treatment in the field. Empirical correlations of the experimental data are developed which can assist in choosing suitable operation conditions for successful near-wellbore formation treatment.

Chapter 6 studied the thermal effects on near-wellbore formation treatment by suspension of gel particles. Gel particles treatment applications in reservoirs are subject to high temperature conditions significantly different than the above-mentioned laboratory test conditions and hence the characteristics of the in situ gel particles plugging mechanisms are affected by the prevailing temperature conditions, as demonstrated in the present studies. Consequently, an experimental study was undertaken to gain an understanding of the effect of temperature on the transient behavior of gel particles plugging in high permeability porous media for purposes of treating the reservoir heterogeneity to prevent the loss circulation and control water production.

The permeability reduction and resistance factor are inferred by measurements of the pressure differentials with time across the proppant pack. Temperature effect is observed to be an important factor in suspended gel treatment of high permeability near-wellbore zones because temperature affects the gel properties and placement rate processes significantly. The effect of temperature on viscosity, differential pressure, permeability reduction, and resistance factor are investigated and useful correlations are developed from the experimental data by using the Vogel-Tammann-Fulcher (VTF)-type equations. Mechanisms of plugging and unplugging phenomena are investigated during the near-wellbore formation treatment by gel particles. The rate constants of

plugging and unplugging processes are determined at various temperatures and correlated by using the Vogel-Tammann-Fulcher (VTF)-type equations.

Chapter 7 presents the dimensionless analysis for interpretation of near-wellbore formation treatment by gel particles at different application conditions. Several dimensionless groups are developed from the relevant variables of sand packs, gel particles suspensions, and operation conditions. The dimensionless correlations are shown to assist in quantifying the effect of the particle-diameter to pore-throat size ratio on permeability reduction, evaluating the treatment of highly permeable and weak near well-bore formations by gel particles, and extrapolating from laboratory to field conditions. The present dimensionless correlations can predict the evolving permeability reduction under the varying conditions of gel particles suspension injection processes. The proposed dimensionless correlations can assist in effective design and mitigation of treatment of high-permeability near-wellbore formations by gel particles for avoiding drilling-fluids lost circulation.

Chapter 8 studied the performance of silica flour particle-gel system for near-wellbore formation treatment. Effects of particle concentration, leak off, and threshold pressure gradient on controlling water production in waterflooded mature oil fields are investigated. The filtrate volume is measured to determine the leak off under different treatment and formation conditions. Effects of particle concentration, pore space of the permeable filter disk, sand sizes and temperature on the leak off and the pressure required to initiate flow are measured by adding different amounts of silica flour to the gel systems and using permeable filter disks with different size pore spaces and sand of different sizes at different temperatures. The sand represents a gravel pack and the filter

disc represents the formation. The threshold pressure gradients which must be overcome to initiate water flow after the fluid loss tests were determined in each case. The experimental results show that the filtrate loss decreases with increasing silica flour concentration and increases with increases in the pore size of the permeable filter disk, the sand mesh size, and temperature. The threshold pressure gradient increases with increase in the silica flour concentration and decreases with increase in the sand mesh size, with increase in the pore size of the permeable filter disk, and with increase in temperature. Correlations and charts for the fluid loss, the pressure required to initiate flow, and the critical silica flour concentration are developed for practical applications.

Chapter 9 presents filtration analysis of the leak off tests of the silica flour particle-gel system. Exponential relationship is used to correlate the filtrate time with the filtrate volume of the silica flour particle-gel system. Empirical correlations of the filtrate volume were developed at different sand sizes, pore diameters of filter discs, and silica flour concentrations. The empirical correlations can assist in successful design of silica flour particle-gel system used for near-wellbore formation treatment for mitigation of water production in waterflooded muture oil fields.

The filtrate volumes of the silica flour particle-gel system during the fluid loss tests are modeled and represented as straight line plots at different silica flour concentrations, pore diameters filter discs, and sand sizes. The rate constants of filtrate and the spurt loss volumes are determined from the straight line plots of relevant equations and correlated by using the exponential relationship at different sand sizes and pore diameters filter discs. The empirical correlations of the rate constant of filtrate and spurt loss volume can be used to predict the filtrate volume at any conditions.

Chapter 10 demonstrated the importance of the empirical correlations, which developed in this study, in the treatment design of the near-wellbore formation. Synthetic oil well under drilling operations, which have fluid loss problem, is studied. Gel-particles suspension is used to treat the near-wellbore formation and the developed empirical correlations are used to determine the gel-particle properties and the modification of the near-wellbore formation. Synthetic oil producing well is studied for high water cut problem. Silica flour particle-gel system is used to plug the perforation zone that produce high water. The components of the silica flour particle-gel system and the treatment design for the near-wellbore formation are presented using the developed empirical correlations.

Chapter 11 summarizes the accomplishments and conclusions of the present study.

Chapter 2: Literature Review

This chapter is a review of the relevant literature on the experimental and theoretical studies which may be applicable for the present gel-particles treatment.

2.1 Review of Experimental Studies

Lost circulation of drilling fluids is an undesirable problem because it can increase the wellbore non-productive time (NPT) in drilling operations, especially in highly permeable formations. The flow paths causing a fluid leak-off may be of the natural and induced types (Wang et al. 2008). Natural lost circulation occurs when drilling operations penetrate formations of large and highly connective pores, classified as highly permeable and high-coordination-number (high degree of pore connectivity) porous formations. Taking proper measures for drilling of wells of various types in such formations without losing a substantial amount of drilling fluid is of great concern. Injection of gel- particle suspensions into these formations can help avoid the lost circulation during a drilling operation by plugging large pores, thus reducing the undesirable high formation permeability.

Gruesbeck and Collins (1982), Civan and Nguyen (2005), and Civan and Rasmussen (2005) have shown that the pathways in porous media can be classified into two groups as being the plugging and nonplugging pathways, relative to the particle size. Hence, particle retention in plugging pathways can occur by bridging across porethroats, and particle retention in nonplugging pathways can occur by deposition over the pore surface. The first mechanism leads to a severe permeability

reduction, and the latter usually causes a negligible permeability reduction. Therefore, particles with sizes comparable to pore-throat sizes can accomplish effective permeability impairment in high-permeability formations, as demonstrated by Civan (2000, 2007, 2010), Iscan and Civan (2006), and Iscan et al. (2009).

In many cases, lost circulation problems can be circumvented conveniently by using suitable lost circulation materials (LCM) as additives in drilling fluids, including certain types of granular and fibrous materials, calcined petroleum coke, calcium carbonate, and gelling polymers (Messenger 1981). Several researchers (Bai et al. 2007; Chaveteau et al. 2000, 2001, 2003; Coste et al. 2000; Feng et al. 2003) investigated the use of gel particles for plugging of pores for circumventing the problems associated with the high permeability of "thief zones" by conditioning and preparing such unfavorable formations for drilling operations.

Polymer-crosslinker mixtures, frequently referred to as gelants, are commonly applied in high-permeability reservoirs for controlling of the fluid-loss during drilling operations, improving the conformance, and reducing the water or gas channeling. Injection of gels into formations containing fractures or channels (high permeability) has been studied extensively (Fielding et al. 1994; Lane and Seright 2000; Sydansk and Southwell 2000; Wang et al. 2001). Mostly the preformed gels instead of in-situ formed gels are preferred to avoid the difficulties associated with controlling of the gelation time and gel compositions during gel placement in porous media. Seright (1997, 2000) studied the performance of gel behavior and placement in fractured formations and determined that preformed gel can penetrate deeper into a fracture than in-situ formed gel and causes much less gel damage in oil-bearing formations or matrix. Chaveteau et

al. (2000, 2001, and 2003) investigated the performance of preformed soft and size-controlled microgel particles which can crosslink by the shear effect which are insensitive to the physico-chemical conditions of reservoir formations. Preformed microgels were found to achieve an in-depth permeability treatment by adsorbing over the pore surface.

Coste et al. (2000) examined the effectiveness of the preformed gel particles (PPG) prepared by using 15wt% acrylamide monomer in a 400 mg/L crosslinker. They crushed and then sieved dry gels to obtain powdered gel particles which can swell several folds to their original size in water to form a suspension. Preformed gel particles effectively resist the high salinity and high temperature reservoir conditions. They conducted glass micro-models and core experiments using the PPG suspensions and observed the three distinct processes, namely deformation, shrinking, and breaking, which occur during a big PG particle passing through a pore throat. They demonstrated that weaker-strength gels penetrate deeper into porous media.

Bai et al. (2007) investigated the movement of the preformed particle gel (PPG) through porous media by visual micro-model experiments. They observed that the transport of PPG through porous media can occur in six different ways: direct pass and adsorption (for particle sizes smaller than the pore-throat size), deform and pass, snap-off and pass, shrink and pass, and entrap (for particle sizes greater than the pore-throat size). Three ways of the PPG motion through porous media were determined from the macroscopic scale (coreflooding) experiments: pass, break-into-pieces and pass, and plugging or jamming. The occurrence of these gel transport patterns depends on the pressure change over time, injected to produced suspension particle size ratio,

and residual resistance factor of porous formation. PG particle can move through porous media only when the driving pressure gradient exceeds the threshold pressure gradient (Prada et al. 2000) which in turn depends on the particle-to-pore throat size ratio (Civan 2000, Iscan and Civan 2006) and the particle strength.

Zhang and Bai (2010) studied the factors affecting PPG injectivity and plugging efficiency during transport of PPG through open fractures. They observed that the PPG injection pressure increases with injection flow rates and decreases with the fracture width and the resistance factor decreases when the flow rate increases. They correlated the injection pressure and resistance factor vs. flow rate by use of empirical power-law equations.

Zheng et al. (2012) developed a fuzzy ball working fluid with pocket air inside for plugging of fluid-losing channels in depleted reservoirs. The fuzzy ball working fluids of density 0.80, 0.85, 0.90, and 0.95 g/cm³ were prepared by mixing 100 mL of water with a predetermined weight of sodium carbonates, caustic soda, nucleating agent, film-forming agent, layering agent, and spotting agent. The rheological properties of the fuzzy ball working fluid at the room temperature and at HPHT were measured by using an adequate rheometer. The observed relationship between the shear-rate and shear-stress indicate a Bingham fluid. It is a plastic fluid having high yield points and plastic viscosity ratios. They determined that the fuzzy ball working fluid can be used for cuttings removal in the oil and gas wells as normal working fluid. They studied the microstructure of the fuzzy ball working fluid by using a microscope by enlarging 1000-2000 times which show a size of 15-150 μm and thickness of 3-10 μm. The density of the fuzzy ball working fluid decreases by

temperature and increases by pressure at constant temperature because the fuzzy ball contains air. Their plugging tests using static sand filling, static core, and dynamic core proved that the fuzzy ball working fluid can plug effectively the losing channels in the lost circulation formations.

Wang et al. (2012) examined pre-gelled particle (PPG) flow through single and double sand packs to determine the flow behavior in porous media, analyze the mechanism of profile control, and investigate the effect of the surface and plugging depositions on permeability reduction. Sand pack of 30 cm long and 2.5 cm diameter was filled with 20-mesh unconsolidated sand and the porosity and permeability were estimated at 0.32 and 6.53 μm^2, respectively. During the injection process, the pressure of the sand pack is recorded by a data acquisition system at four pressure taps located at the inlet, the outlet, and the two locations in between them. The effluent sample is collected at a cylinder and tested by Malvern Mastersize 2000 to obtain the particle size distribution. The particle shape is approximately sphere and the particle expanded in volume because of the water swelling. PPG suspension of 20,000 parts per million (ppm) concentration is injected at 5 mL/min flow rate into the sand pack and the pressure at the four equally-spaced different points is recorded. They proved that there is a critical pressure below which the particles will deposit at the pore-throat and above which the particles can pass through the pore-throat without plugging. Double parallel sand packs with a permeability ratio 4:1 were used to study the fractional flow. They show that for the low permeability sand pack, the particles will accumulate at the inlet side of the pore throats and form new pores causing a small decrease in the permeability. For the high permeability sand pack, the PPG suspension initially flows

into the high permeability sand pack leading to a pressure increase because the occurring deposition causes deformation and pushing of the particle to move ahead and decreases the permeability and therefore the fractional flow. For the surface deposition experiments, they used particles of diameters smaller than the pore-throat size and show that for low injection concentration, the bridging pore-blocking did not occur and only the pore surface deposition happened. For the higher injection velocity, the amount of particle deposition at the surface decreased and particles concentration at the outlet increased, because the drag force causes mobilization of particles at the high injection velocity (Pu 2008; Zamani and Maini 2009). For the plugging deposition experiments, they used particles of diameter greater than the pore-throat size to cause particle deposition or plugging at the throat. They showed that the permeability variation happened by retention of the PPG because the deposition of particles on the surface causes a porosity decrease and hence permeability decrease, and the plugging deposition causes a decrease in the quantity of filtering channels which lead to permeability reduction.

Tran et al. (2010a) studied the formation damage caused by the suspended particles of the drilling fluid by using the Nuclear Magnetic Resonance (NMR) and X-ray (CT) methods. Water-based drilling fluid of suspended barite particles with different diameters and concentrations injected into Berea core samples saturated with 3% KCl brine and the permeability reduction was measured. The pore size distribution and the porosity of the core samples were measured before and after porous media damage by using the NMR technique and showed that the porosity reduced due to particle capturing and blocking in the pores. By the injection process, the small pores were

blocked and the large interconnected pores provided the flowing path. Thus, when the capture probability decreased, then the porosity reduction decreased. The particle size distribution of the original and effluent fluids was measured by using the laser diffraction particle size distribution analysis (LDPSDA) technique and showed that the large particles were captured inside the pores while the small particles were remained in the flowing fluid. The X- ray computed tomography (CT) method was used to estimate the porosity of the core samples. Tran et al. proved that the particle capture probability and permeability reduction increase by increase in the particle size and concentration. They developed a model of fines migration and deposition in porous media from the empirical parameters determined from the injection processes.

Tran et al. (2010b) studied the conditions leading to plugging of natural fractures and slotted liners by suspended particles of different diameters and concentrations. The carrier fluid consisted from water and Diutan with concentration of 1.86% and viscosity of 65 cp to avoid particle settling. The suspended particles in the carrier fluid are the glass beads of 2.54 g/cm^3 density and the ceramic proppant of 2.72 g/cm^3 density. To study the plugging conditions, the Diutan particles suspension was injected into different slot geometries and the weight of the effluent during the injection process was measured. The experimental data were correlated by using the slot width-to-particle size ratio and the particle volume fraction Reynold number dimensionless groups. They developed exponential curve from the empirical dimensionless groups and the region below the curve is shown to represent the plugging conditions. They showed that the plugging conditions were affected essentially by the width and length of the fracture opening, and the particle size and concentration. They studied also the time

required for plugging of fractures and slots at different particle concentrations and different shape factors, and developed empirical correlations of dimensionless plugging time versus particle volume fraction.

Feng et al. (2013) studied experimentally the gel particles migration and deposition in porous media after polymer flooding. The shear breaking, synergy with remaining polymer, deformation migration, and swelling of gel particles were examined after polymer flooding. For swelling process of gel particles in water, the particle diameter was measured at different times by laser particle size analyzers which indicated that the aging time of gel particle swelling is very short. For synergy with remaining polymer, they demonstrated that the gel particle diameter increases by the polymer concentration because the gel particles adsorbed the remaining polymer in porous media. They proved that because of the shearing breaking of the gel particles when migration through porous media, the diameters of gel particles decrease quickly to ultimate value. To demonstrate the deformation and migration of gel particles in porous media, they studied the injection pressure during the gel particles injection process in cores. They showed that oscillation phenomenon happened because of the deformation during the migration of the gel particles.

Muhammed et al. (2014) evaluated experimentally the strength of gel particles by using a simple apparatus which consists of a hand pump and a specially designed piston accumulator with screen plate having multiple holes. The threshold pressure gradient was determined during the experiments as the minimum pressure gradient required for the gel particles to pass through the screen holes. The same apparatus was also used to measure the apparent viscosity. They showed that there is a

significant effect of the hole size and hole density per screen on the threshold pressure gradient but they do not effect the apparent viscosity. They observed that the threshold pressure gradient increased when the brine salinity increased. The gel particles elastic modulus was measured using a rheometer and correlated with the threshold pressure gradient. Two models were developed based on the experimental data. First model represents the correlation of the threshold pressure gradient with the gel strength and the other represents the correlation of the apparent viscosity with the shear rate.

Almohsin et al. (2014) studied the effects of the nanogel particle concentration, flow rate, particle deformability, and rock permeability on the resistance factor and the particle propagation. Sandstone cores of permeabilities 42 to 1038 mD were used in the core flooding tests of deformable nanoparticles of diameters 100 to 285 nm. The experimental results show that the resistance factor increased when the nanogel particles concentration increased and the resistance factor decreased when the rock permeability and flow velocity increased. For the same dry nanoparticles size, the resistance factor decreased when the swollen particles size increased because the larger particle is weaker than the smaller particle. They showed that the nanogel adsorption layer thickness increased when the nanoparticle concentration and decreased with the shear rate.

A summary of the findings by the above review and evaluation of the previous experimental studies is presented in **Table 2-1**.

TABLE 2-1: SUMMARY OF THE EXPERIMENTAL STUDIES				
Investigators	Operation Conditions	Porous Media	Results and Analysis	Comments
Zhang and Bai (2010)	- PPG concentration: 0.903, 1.597, 2.731, and 2.961 %. -Flow rates: 5,10, 15, 25 , and 30 mL/min. -Brine concentration: 0.05, 0.25, 1, and 10%.	- Fracture length: 55 cm. - Fracture height: 10 cm. – Fracture width: 0.55, 1.0, and 1.5 cm.	- The Injection pressure increased by the flow rate and the brine concentration and decreased by the fracture width. - The resistance factor increased by the fracture width and the brine concentration and decreased by the flow rate. -The PPG injectivity increased by the flow rate and the fracture width and decreased by the brine concentration.	- The resistance factor is the ratio of the gel particle injection pressure drop to the particle-free water injection pressure drop. - The PPG injectivity is the ratio of the flow rate to the pressure difference.
Zheng et al. (2012)	- Density of the fuzzy ball working fluid: 0.80, 0.85, 0.90, and 0.95 g/cm³. - Size of the fuzzy ball is 15-150 µm and thickness is 3-10 µm. - PH of the fuzzy ball working fluid is 9. - Maximum injection pressure of the sand packs and the cores are 6 and 20 µPa, respectively.	- Permeability of the sand packs are 15-20, 40-60, and 140-300 µm² for 80-100, 40-60, and 20-40 mesh, respectively. - Range of permeabelities of the cores are 2.36-244.2*10^{-3} µm².	- The fuzzy ball working fluid can be used for cuttings removal in the oil and gas wells and can plug effectively the losing channels in the lost circulation formations.	-The fuzzy ball working fluid composite from water, sodium carbonates, caustic soda, nucleating agent, film-forming agent, layering agent, and spotting agent and the fuzzy ball contains air.

Investigators	Operation Conditions	Porous Media	Results and Analysis	Comments
Tran et al. (2010a)	- The core samples are saturated with 3% KCl. - Barite particles of diameter range 0.5-15 µm are added to water-based drilling muds. - The flow rate for permeability impairment experiments is 90 cm^3/hr and for porosity variation experiments is 36 cm^3/hr.	- Berea core samples of 6 in long and 1 in diameter are used. - The permeabilities of the core samples are 1240 and 265 mD, the porosities are 0.206 and 0.175, and the mean pore diameters are 26.1 and 15.7 µm.	– The porosities of the core samples reduced from 0.209 to 0.176 and from 0.175 to 0.169 after 5 hrs flooding. - For 5.4 µm mean diameter of particles injected, the large particles are captured inside the pores while the smaller are flushed out.	- External filter cake observed because of the pore-throat bridging mechanism. - The pore deposition and pore filling are the dominant mechanisms.
Tran et al. (2010b)	- Geovis XT fluid of 1.86 % Diutan concentration and 65 cp apparent viscosity at ambient temperature 75 °F is used. - The suspended particles are glass beads of 2.54 g/cm^3 density and 0.10, 0.12, 0.15, 0.20, and 0.25 cm diameters and ceramic proppants of 2.72 g/cm^3 density and 20/40, 30/50, and 30/70 mesh.	- Transparent-plastic testing cell of 2 ft long and 1.5 in ID. - For glass beads suspended, slots of 0.32 cm width and different lengths of 0.64, 1.28, and 2.56 are used. - For ceramic proppant suspended, slots of 0.16 cm width and different lengths of 0.64, 1.28, and 2.58 cm are used.	– No plug is observed for $\beta' > 2$ and the plug happened for $0.795 < \beta' < 2$. - No plug is observed up to concentration of 0.25 by volume fraction and the plug happened at 0.30 concentration.	- β' is a modified slot size-to-particle size ratio.

Investigators	Operation Conditions	Porous Media	Results and Analysis	Comments
Feng et al. (2013)	- Bicarbonate-sodium type water of salinity 2841.2 mg/L is used. - Polymer of 16-19 million molecular weight, 20% hydrolyzing degree, and 1000 mg/L concentration is used. - Cationic gel particles with 2000 mg/L concenitration are used. - The median gel particle diameter is 160 µm. - The temperature is 45 °C. - The injection pressure is 2-10 µM.	- Artificial quartz sandstone cores of porosities 0.20, 0.21, and 0.24, and permeabilities 1.037, 3.674, and 4.409 µm² are used. –The threshold pressure gradient is 16.7 µPa/m.	- The agin time of gel particle swelling is about 4 hr. - The gel particle diameter increases by the polymer concentration. - Because of the shearing braking, the gel particle diameter decreases by about 27.3%.	- The oscillation phenomenon of the pressure is happened because of the deformation migration of the gel particles.
Muhammed et al. (2014)	– Medium size of the dry PPGs is 0.92 mm. - Brine (NaCl) concentration are (0.05, 0.1, 0.25, 0.5, 1.0, and 5.0 wt%) - Flow rates are 0.1,0.2, 0.5, 0.75, 1.0, 1.5, 2.5, 3, 5.0, 7.5, and 10 ml/min.	- Screen plates were used as porous media of 40 holes/plate and and 122 holes/plate. – The screen plates have hole sizes (0.5, 1, 1.5, and 5.0 mm).	- The threshold pressure were 84.1 Kpa of 122 holes/plate and 372.3 kPa of 40 holes/plate for PPGs swollen in water. – The stabilized pressure was 300 kPa for 0.5 mm hole and PPGs swollen in 5 wt% and decreased for 1.5 mm hole size. - Threshold pressure increased by salinity.	- Threshold pressure is the minimum pressure required of the gel particle to pass through hole.

Investigators	Operation Conditions	Porous Media	Results and Analysis	Comments
Coste et al. (2000)	– PPG consists from 15% acrylamide monomer and 400 mg/L crosslinker. - Concentration of the sus-Pension was 1000 mg/L. - Flow rate was 2 ml/min.	- Glass plates with pore network saturated with water were used. - Sand-packed columns at residual oil saturation with 30 cm long and 2.2 cm diameter filled with sand of 40 to 120 mesh were used.	– Three mechanisms of particles passing were investigated: deformation, shrinking, and breaking – Weaker-strength gels penetrate deeper into porous media.	- The PPG particles can be used for water control applications.
Bai et al. (2007)	- PPG is a kind of xerogel that can swell by water. - For sand-packed experim-ents, 1000 mg/L particle su-spension was injected at 1 cm^3/hr flow rate and 3 MPa pressure. - 5 cm^3 of PPG suspension with a concentration of 0.1% was injected into the micromodels. - Average particle diameter is 150 µm. - Pore-throat diameters varies from 90 µm to 250 µm.	- Two etached glass micromodels were used: irregular and regular pore models. - sand- packed core model of 30 cm long and 2.2 diameter was used. - The sandpacked filled with quartz sands of 20 to 100 meshes size.	- PPG transport ways through micromodels are: direct pass, adsorption, deform and pass, snap-off and pass, shrink and pass, and entrap. - PPG motion through sand packed are: pass, break and pass, and plugging.	– PPG particle moves when the driving pressure gradient is greater than the thre-shold pressure gradient.

Investigators	Operation Conditions	Porous Media	Results and Analysis	Comments
Wang et al. (2012)	– Concentration of PPG suspension is 20,000 ppm. - Injection flow rate is 5 ml /min. - Stable injection pressure is 0.24 MPa.	- Sand pack of 30 cm long and 2.5 cm diameter filled with 20 mesh sand was used with 0.32 porosity and 6.53 µm² permeability. - Double parallel sand packs with permeability ratio 4:1 were used to study the fractional flow	– There is a critical pressure below which the particles deposit at the pore-throat and above which the particles pass through the pore-through. - At high injection velocity, the particle deposition decreases.	- For high velocity, the drag force causes mobilization of the deposited particles.
Almohsin et al. (2014)	– The nanogel was an acrylamide-based crosslinked polymer. - 1 wt% of potassium chloride (KCl) was used to prepare the nanoparticle solutions. - Average particle diameter was 158 µm. - Injection flow rate is 0.25 to 5 ml/min. - The injection pressure is 2379.21 psi at 1.75 ml/min flow rate.	- Berea sandstone cores of 41.2 to 555.4 mD permeability and Missouri sandstone cores of 1038 mD were used - The cores of 6.95 to 7.1 cm length and 2.5 to 2.53 diameter.	– The resistance factor increased by the particles concentration. - The resistance factor decreased by the rock permeability and the flow velocity. – The resistance factor decreased with the swollen particle size increased.	- The nanoparticles adsorption layer thickness decreased by the shear rate.

2.2 Review of Theoretical Studies

Zeinijahromi et al. (2012) derived the basic equations required for detachment and mobilization of fine particles by the drag and lifting forces applied on the particles during flow through porous media, and the size exclusion of the pores which causes formation permeability decrease and hence the well productivity decrease. They developed analytical models for steady-state well production, velocity, and particles suspension concentration near the wellbore. The reservoir fine particles production and accumulation cause a skin factor growth by time. The productivity index and the skin factor versus time are studied by the analytical model showing that the skin factor growth coefficient increases by the filtration coefficient. The analytical model assumes small retention concentration. Therefore, the model can be applied to predict the well behavior only at the early stage of the well clogging process and cannot be applied at the late stages of well clogging. The analytical modeling results show good agreement of matching with the field producing data.

Goldszten (2005) developed a mathematical model to predict the volume of suspension flowing through a small orifice until clogging occurs. The mathematical model describes the clogging and choking of a single pore throat present in a container as a circular hole on its wall and filled with a suspension of incompressible liquid and spherical particles. The mathematical model assumed that the liquid is incompressible, the particle velocity is same as the liquid velocity, uniform flow, and the particle is randomly placed in the container before opening the hole to allow flow. The mathematical model provides an understanding of pore throat clogging in porous media and efficient numerical algorithm for upper and lower bounds of the effluent volume.

Civan (2010) developed a practical phenomenological mathematical model which considered temperature variation and particle transport by dispersion and advection. The particle deposition and migration and the permeability impairment resulting from particle deposition and migration are investigated by this model. Effects of temperature and particle deposition on the permeability impairment of porous media are described by dimensionless numbers and special correlations of the relevant variables. The permeability impairment is affected strongly by temperature variation because the filter coefficient, pore-throat constriction, and porous matrix thermal deformation depends on temperature. The numerical simulation results obtained with and without considering the dispersion and temperature effects are compared to show the effect of temperature and dispersion on the fines deposition and migration, and the resulting permeability impairment. This improved model can assist in scientifically guided experimentation, analysis, and design of fines particles transport process through porous media.

Sato et al. (2013) numerically studied the effect of the trapping fines particles on formation permeability by using a three-dimensional (3D) Lattice Boltzmann method (LBM). They showed that the absolute permeability of porous media is reduced by 60-90% due to fine particles trapping for the volume fraction of the fine particles to the pore volume of 0.15-0.29. However, the permeability reduction is not only due to fine particle saturation but also the fine particle size distribution. The geometrical properties of sand grains are digitally described by series expansion of spherical harmonics using computed tomography (CT) scans of real sand grains. The migrating fine particles are assumed spherical and the volume distributions are log-normal. The permeability

alteration is modeled theoretically using volume saturations and specific surface areas of the fine particles and the frame sands.

Tran et al. (2009) analyzed their experimental data and developed empirical correlations for perforation and pore plugging conditions and plugging time by suspended particles which can be help in avoiding the perforation/pore plugging in the field by migrating particles. The pore throat-to-particle size ratio was correlated satisfactorily against the particle volume fraction Reynolds number depending on the experimental data and using an exponential-law model. They showed that the exponential-law model worked well for the suspension of nylon particles of diameters range of 0.16-0.48 cm and of different particles size distributions and for the Carbo proppant suspension particles in Geovis XT fluid. They developed exponential curves, below which indicates the conditions leading to plugging and above which shows the conditions leading to non-plugging. Therefore, to avoid the plugging of the pores or the perforations, the value of perforation diameter to particle diameter ratio versus particle volume fraction Reynolds number should be located above the correlated curves. They correlated also the time for perforation and pore throat plugging by using exponential model of the particle volume fraction and demonstrated that higher the volume fraction of particles in the suspension, shorter the plugging time. They studied the effect of the particle size distribution on the plugging time and showed that the fines particles did not affect the plugging time but after plugging the fine particles deposited at the pore throats to form a bridge and worked as a membrane.

Feng et al. (2013) developed a numerical model to interpret their experimental data which demonstrates the gel particles transportation after polymer flooding causes

permeability reduction in thief zones by retention of particles and pore volume reduction. The flow equations are solved implicitly to obtain the pressure and the saturation profiles and solved explicitly to obtain the concentration of the polymer by using the IMPSAT finite-difference numerical method because of its high accuracy. To weaken numerical dispersion, the convection-diffusion differential equation of polymer transport is solved by using the fourth-order Runge-Kutta method. The operator-splitting method is used to solve the continuity equation of gel particles. The new numerical method is validated by the experimental and field data and show satisfactory results.

The findings of the above review and evaluation of the theoretical studies are summarized in **Tabe 2-2**.

TABLE 2-2: SUMMARY OF THE THEORETICAL STUDIES

Investigators	Equations	Comments
Zeinijahromi et al(2012)	$-U = -\frac{kk_{rowi}}{\mu(1+\beta_a\sigma_a+\beta_s\sigma_s)}\frac{\partial p}{\partial r} = \frac{q}{2\pi r}$ $-\sigma_s(r,t) = \frac{\lambda_s qt}{2\pi r} c_w \exp\left[-\lambda_s(r-r_w)\right]$ $-Pi(t) = \frac{1}{j(t)} = \frac{\ln\frac{r_e}{r_w}}{\ln\frac{r_e}{r_w}+\beta_s\frac{M}{r_w^2}C_t}$	- Assume small retention concentration. - Can be applied at the early stages of well clogging. - Can not be applied at the late stages of well clogging. - Results show good matching with the field production data.
Goldsztein (2005)	$-\lambda = \frac{3A}{4\pi r^2}$ $-k_{max} = \gamma\lambda$	- Assume incompressible liquid, particle velocity equal to liquid velocity, and uniform flow. - Clogging occurs when k(v)>kmax.

Investigators	Equations	Comments
Civan (2010)	- $\frac{K_o(T)}{K_o(T_{ik})} = \exp\left[A_k\left[\frac{1}{T-T_{ck}} - \frac{1}{T_{ik}-T_{ck}}\right]\right]$ - $\sqrt{\frac{K}{\phi}} = \Gamma\left(\frac{\phi}{1-\phi}\right)^{\beta}, 0 \le \beta \le \infty$	- The model considers temperature variation and particle transport by dispersion and advection. - The model shows that the permeability is affected strongly by the temperature variation because the porous matrix thermal deformation, the filter coefficient, and the pore-throat construction depend on temperature.
Sato et al. (2013)	- $\left[P_q^n + x\left(P_q^{n+1} - P_q^n\right) - P_f\right]^2 = \left(\frac{d_f + d_q}{2}\right)^2$ - $\begin{pmatrix} u'_{qn} \\ u'_{qJ1} \\ u'_{qJ2} \end{pmatrix} = \begin{pmatrix} -e_n & 0 & 0 \\ 0 & e_J & 0 \\ 0 & 0 & e_J \end{pmatrix} \begin{pmatrix} u_{qn} \\ u_{qJ1} \\ u_{qJ2} \end{pmatrix}$	- The effect of the trapping fines particles on the formation damage is numerically studied by using a 3D LBM simulation. - The domain edges are approximately 300 μm length, each edge discretises into 60 lattice nodes.
Tran et al. (2009)	- $\beta = A\left[1 - \exp\left(-BR_{ep}\right)\right] + C$ - $t_d = a\exp\left(\sigma_p^{-b}\right)$ - $t_d = \frac{t}{v\sqrt{D_T D_p}}$	- To avoid plugging, the value of perforation diameter (β) versus Rep should be above the correlated curve. - Showed that the fines particles did not affect the plugging time but after plugging deposited and worked as a membrance.
Feng et at. (2013)	$-\nabla.\left(v_w \nabla c_{gp}\right) + q_w c_{gp} = \frac{\partial \delta_{gp}}{\partial t} + \frac{\partial\left(\phi S_w c_{gp}\right)}{\partial t}$ - $\phi = \phi_o - \delta_{gp}.SHR_{gp}.SWR_{gp}$ - $\left(\frac{K}{K_o}\right) = \left(\frac{\phi}{\phi_o}\right)^3$	- The IMPES method is used to solve the flow equations. - The convection diffusion differential equation of polymer is descreted by using fourth rank Ruge-Kutta method.

where U is the flow velocity, m/s; k is the absolute permeability, md; K_{rowi} is the oil relative permeability at initial water saturation, md; P is the differential pressure, kPa; q is the injection flow rate, cm^3/h; μ is the viscosity, Pa.s; β_a is the formation damage coefficient for attachment, dimensionless; σ_a is the volumetric concentration of attached fines, %; β_s is the formation damage coefficient for straining, dimensionless; σ_s is the volumetric concentration of strained fines, %; r is the radius, μm; t is the time, min; λ_s is the filtration coefficient for size exclusion fines capture, m^{-1}; c_w is produced fines concentration, %; r_w is the well radius, m; pi is the productivity index, dimensionless; j is the impedance, dimensionless; r_e is the drainage radius, m; r_w is well radius, m; M = skin growth coefficient, dimensionless; C_t = total amount of produced fines per unit well length, m^2; λ is the ratio of volume of dashed cylinder and volume of a particle, dimensionless; A is the cross sectional area of the sand pack, cm^2; k_{max} is threshold number of particles for the first time, dimensionless; γ is the empirical material parameter, dimensionless; K_o is initial permeability, md; T is the temperature, $^{\circ}C$; T_{ik} is the reference absolute temperature, K; A_k is the fitting constant (E/Rg), K; T_{ck} is the characteristic-limit absolute temperature, K; K is the permeability, md, Ø is the porosity, dimensionless; β is the empirical parameter, dimensionless; P_q is the position vector for a fine particle, μm; P_f is the position vector for a frame sand grain, μm; d_f is the diameter of a frame sand grain, μm; d_q is the diameter of a fine particle, μm; x is the ratio of the distance, dimensionless; u_q is the particle velocity before the collision, m/s; β is the pore throat to- particle diameter ratio, dimensionless; A is the empirical parameter, dimensionless; B is the empirical parameter, dimensionless; R_{ep} is the particle Reynolds number, dimensionless; C is the empirical parameter, dimensionless;

t_d is the dimensionless plugging time, dimensionless; a is the empirical parameter, dimensionless; b is the empirical parameter, dimensionless; σ_p is the fraction of particle, %; ν is the velocity , cm/s; D_T is the pore throat diameter, μm; D_P is the particle diameter, μm; ν_w is the water flow velocity, m/s; c_{gp} is the gel particles mass concentration, mg/L; q_w is the water flow rate, cm^3/h; δ_{gp} is the retention coefficient of gel particles, dimensionless; $Ø_o$ is the initial porosity, dimensionless; S_w is the water saturation, %; SHR_{gp} is the gel particle shear breaking ratio, dimensionless; SWR_{gp} is the gel particle swelling ratio in polymer solution, dimensionless.

Chapter 3: Factors Affecting the Near-Wellbore Formation Treatment by Gel Particles

Part of this chapter has been previously published as ‘‘Experimental Study of Gel Particles Transport Through Porous Media’’ in the SPE Latin American and Caribbean Petroleum Engineering Conference, Mexico City, Mexico, 16-18 April, 2012 and is used here by permission.

Part of this chapter has been previously published as ‘‘Experimental Investigation and Correlation of Treatment in Weak and High- Permeability Formations by Gel Particles’’ in Production and Operations Journal, Vol. 28, No. 4, pp. 387-401, 2013 and is used here by permission.

3.1 Introduction

Understanding the plugging mechanisms and the transport behavior of the gel particles through the porous media during the gel particles suspension injection is very important for successful near-wellbore formation treatment by the gel particle suspension. Two plugging mechanisms were investigated and illustrated in details in this study. These two mechanisms are the deposition of the gel particles on the pore-surface and the capture of the particles at the pore-throat.

There are many factors that affect the plugging mechanisms and the transport behavior of the gel particles including gel particle properties, carrier fluid properties, gel particle suspension properties, porous media, and operation conditions. These factors are described and investigated in details in this chapter and this study.

3.2 Gel Particle Properties

There are only a limited amount of studies about the gel particles properties,

as discussed in the following.

3.2.1 Gel particle deformation and break-up

Because of its deformable nature, the gel particle can deform and pass through the pore-throat to deposit on the pore-surface, break-into pieces and pass through the pore-throat to deposit on the pore-surface, or be captured at the pore-throat during injection into porous media (Bai et al. 2007). **Fig. 3.1** illustrates the difference between the rigid and deformable particles passing through a pore throat. The rigid particles cannot pass through the pore throat if their size is greater than the pore- throat size, but the deformable particles can deform and pass through at sizes greater than the pore-throat size.

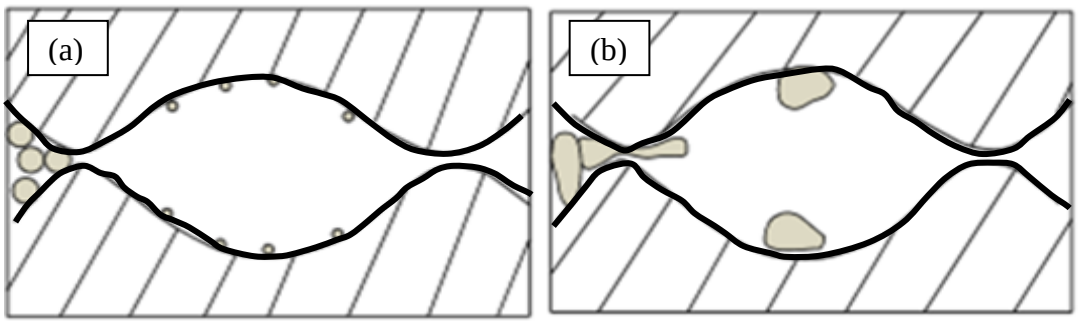

Fig. 3.1: Difference between rigid and deformable particles passing through pore throat: (a) rigid particles (b) deformable particles

Bonet and Wood (2008) describe the motion and the deformation of a particle, as shown in **Fig. 3.2**. The general measure of deformation is the measure of the strain and the strain is the change in the initial elemental vectors dX_1 and dX_2 after they

deform to dx_1 and dx_2. Then, the deformation gradient tensor is given by:

$$F = \frac{dx_1}{dX_1} \quad \text{or} \quad F = \frac{dx_2}{dX_2} \tag{3.1}$$

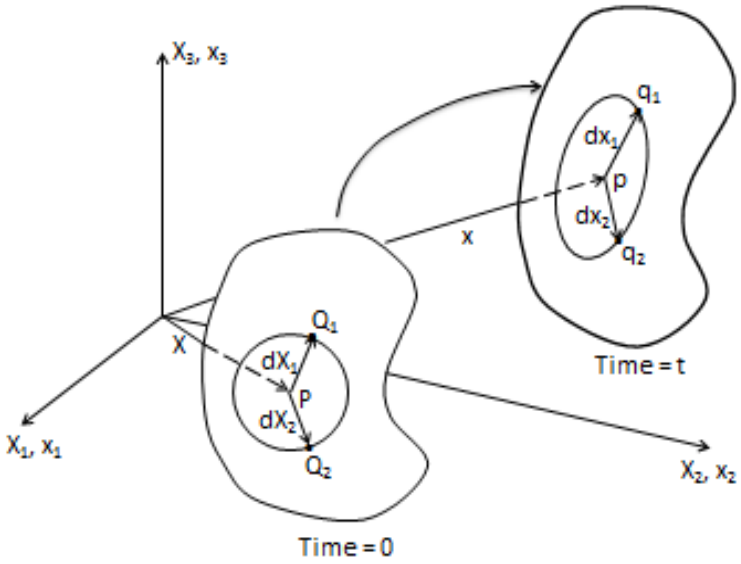

Fig. 3.2: General motion and deformation of a particle (modified after Bonet and Wood 2008)

Gao et al. 2011 describe the deformation of an ellipsoidal elastic particle in a Newtonian viscous fluid in quantitative terms as follows:

$$D = \frac{a-b}{a+b} = \frac{1-w}{1+w} = \frac{G}{\sqrt{1+G^2}} \tag{3.2}$$

where a and b refer to the semi-axes of the ellipsoidal particle, w= b/a and G is the ratio of the viscous forces in the fluid to the elastic forces in the elastic solid particle.

$$G = \frac{\mu_f \dot{\gamma}}{\eta_s} \tag{3.3}$$

where μ_f is the fluid viscosity, η_s is the shear modulus of the elastic solid particle.

$$\eta_s = \frac{\tau_s}{B_s - 1} \tag{3.4}$$

where τ_s is the extra stress tensor, $B_s = F_s F_s^T$ is the Finger or left Cauchy-Green tensor, $\dot{\gamma}$ is the shear rate or the velocity gradient.

$$\dot{\gamma} = \frac{v}{d} \tag{3.5}$$

v is the fluid velocity and d is the distance to the reference surface. As G increases, the D increases, therefore larger elastic deformation of the particle happens at the larger number of G and the elliptical particle become thread-like. Taylor (1932, 1934) studied the break-up of droplets and showed that a droplet can be break-up when the D value is larger than 0.5.

3.2.2 Gel particle coagulation and detachment

The gel particles can stick together to coagulate and form larger aggregates without involving chemical reaction between the particles. The gel particles stickiness (coagulation) was not investigated sufficiently before, but Burya et al. (2001) studied the asphaltene particles stickiness and aggregation in crude oil. The asphaltene particles can stick together with a chemical reaction between them. Burya et al. (2001) showed that the aggregation kinetics of asphaltene particles consist from the diffusion-limited aggregation (DLA) and reaction-limited aggregation (RLA) mechanisms with a crossover behavior between them given by:

$$\frac{dN}{dt} = \frac{N}{\tau_D \dot{\gamma} N + \tau_R} \tag{3.6}$$

where N is the average number of particles forming fractal aggregation, dimensionless, given by:

$$N = \left(\frac{R}{R_o} \right)^{d_f} \tag{3.7}$$

R_o and R are initial particle radius and the instantaneous mean aggregate radius, respectively, μm; d_f is the fractal dimension, dimensionless, γ is a constant, dimensionless, given by:

$$\gamma = \left[\left(\frac{R}{R_o} \right)_D \right]^{d_f} \tag{3.8}$$

τ_D and τ_R represent the characteristics times τ_{char} for the DLA and RLA mechanisms, respectively, dimensionless. Burya et al. (2001) used the analytical solution of Eq. 3.6 to correlate the experimental data of the mean number of asphaltene particle in an aggregate and mean radius of the asphaltene aggregates with the scaled time and obtained a satisfactory matching.

Engel (2000) defined the efficiency of stickiness (coagulation) (α) between two particles as the probability that two particles which collide can stick together with a value ranging from 0 to 1. Thus, the stickiness(α) is defined as the ration of the adhesion rate/collision rate. Kiorboe et al. (1990) determined the stickiness and aggregates of diatom blooms experimentally by use of Couette Chamber system and the following empirical correlation:

$$C_t = C_0 \exp^{-(7.82\ \alpha\ \Phi\ Gm/\pi)t} \tag{3.9}$$

where C_t and C_0 are the particle concentration at times t and 0, respectively, (no. dm^{-3}), Φ is the volume concentration of particles (ppm), and G_m is the mean shear rate of the Coutte Chamber system (s^{-1}) which can be calculated by using the following equation (van Duuren 1968):

$$G_m = 4\,\pi\omega\, r_2\, r_1\, (r_2^2 - r_1^2)^{-1} \qquad (3.10)$$

where ω is the angular velocity (s^{-1}), and r_2 and r_1 are the radii of the outer and the inner cylinders of this system, respectively (cm). Engel (2000) used the Coutte Chamber to determine the variation in the particle stickiness according to the decline of a diatom bloom at low shear rate (G = 0.86 s^{-1}). Engel investigated that the apparent particle stickiness (α) increases with the transparent exopolymer particles (TEP) and can exceed a value of 1, which means the collision rate is underestimated because the stickiness parameter (α) is calculated based on the conventional particle counting only.

The critical shear stress is the minimum shear stress required to detach and lift-off the deposited particles at the pore surface. Civan (1990, 1996) proposed an empirical equation of the critical shear stress (τ_{cr}) as a power-law function of the particle stickiness to the surface according to the particle concentration at pore surface by:

$$\tau_{cr} = k_r C_p^{\alpha} \qquad (3.11)$$

where α is an empirical constant, k_r is a constant and C_p is the particle mass concentration. Potanin and Uriev (1991) developed theoretical equation to calculate the critical shear stress required for detachment of particles.

$$\tau_{cr} = H/24D_p l^2 \qquad (3.12)$$

where H is the Hamaker coefficient of particle and surface interacting through the pore fluid present in between them, J; D_p is the average particle diameter, cm; and l is the separation distance between the particle surfaces in filter cake.

The plugging probability of the pores increases by the gel particles stickiness (coagulation) on the pore-surface and pore-throat. Thus, the efficiency of the near-wellbore formation treatments by the gel particles increases by the gel particles stickiness (coagulation) and decreases by the detachment of the deposited particles at the pore-surface.

3.3 Carrier Fluid Properties

The main functions of the carrier fluid are to suspend and carry the gel particles and prevent the particles from settling. The carrier fluid consists from water and Xanthan and the important properties of the carrier fluid are the viscosity and the density. In the present study, for example, 0.25 gm of Xanthan powder was mixed with 500 ml of water to get the proper viscosity and density that prevent the settling of gel particles.

3.4 Gel Particle Suspension Properties

The gel particle suspension is used for the near-wellbore formation treatment. In the present study, the gel particle suspension was prepared by mixing a predetermined weight of polyacralamide gel, consisting of acrylamide (< 0.2%), sodium azide (0.02%) and water (balance), with carrier fluid using a commercial blender to obtain the desired concentration of the suspension and the desired gel-particles size. The

gel-particle suspension was colored with red by using a liquid color for clear visual observation of the progress of the suspension through the proppant pack. The properties of importance for using the suspension for treatment are the following.

3.4.1 Viscosity

There is a direct relationship between the suspension viscosity and the gel particle deformation. The ratio of the viscous forces in the fluid to the elastic forces in the elastic solid particle increases by the suspension viscosity, as shown in eq. 3.3, and thus the deformation of the gel particle increases, as shown in eq. 3.2. The gel particle suspension viscosities were measured at ambient temperature 23.5°C with a Chann 35 viscometer at shear rate of 511 s^{-1}. The suspension rheology was studied by using six speeds of viscometer to obtain the shear-rate/shear-stress graphs. These graphs demonstrate the pseudoplastic characteristics of the gel-particle suspensions. **Fig. 3.3** shows the shear-rate/shear-stress graph of a 3-vol% suspension.

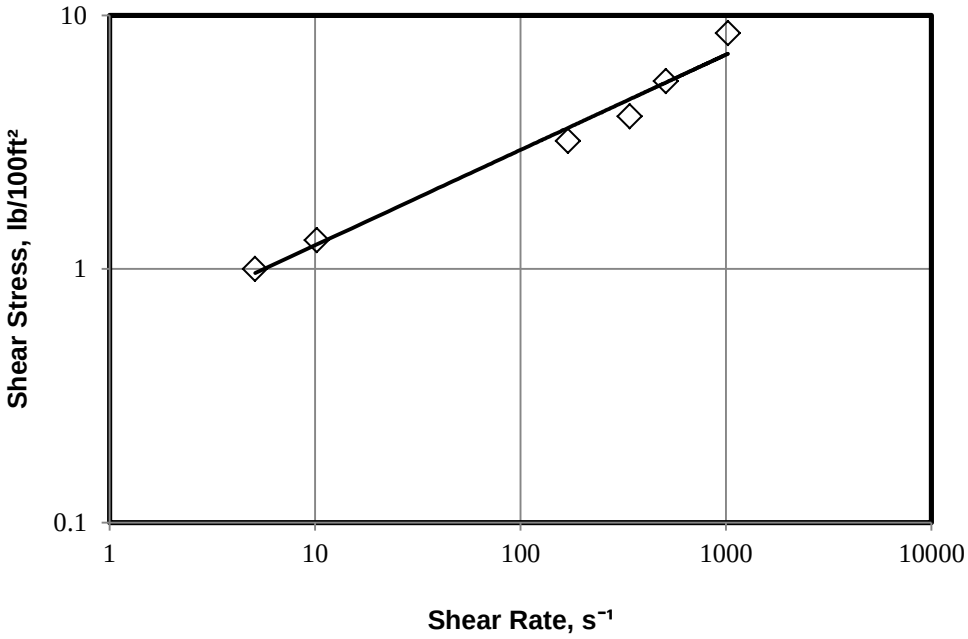

Fig. 3.3: Pseudoplastic behavior of 3 vol% suspension at T= 23.5 °C (exponent n = 0.38)

3.4.2 Gel particle diameter

There is a direct relationship between the plugging of pore throats or capture of gel particles in porous media and the ratio of particle/pore-throat size because plugging occurs when gel particles block the pore throats (Civan 2000, 2007a, and 2010; Iscan and Civan, 2006). Measurement and understanding of the gel-particle size distribution are important in investigation of the mechanism of plugging of porous media by gel particles. The gel particles are irregular shaped and deformable. Thus, the equivalent diameter of a gel particle was calculated by considering the projected area of an irregular particle in two dimensions. This is equal to the projected area of the circular particle with an equivalent diameter (Bai et al. 2007). An optical procedure was used to measure the gel particle size because of the unavailability of an instrument that can be

used to measure the gel particle size distribution like Mastersizer instrument and Elzone analyzer. However, there is no accurate method available for measurement of the actual particle size distribution in a suspension. The optical procedure was applied using a suspension placed under a microscope and digitally photographed by a camera. The dimensions of the irregular gel particles in the photomicrographs were measured in pixels and then converted from pixels to micrometers using a calibration scale. Then, the projected area of a plane of the irregular particle was calculated and converted to the equivalent diameter of a circular particle, and then the following equation was applied (Bai et al. 2007).

$$D_P = \sqrt{\frac{4S}{\pi}} \tag{3.13}$$

Dp indicates the equivalent diameter of a circular particle, *S* is the projected area of a plane of the irregular particle. The gel particles were grouped into chosen ranges according to their diameter values. A particle-size frequency distribution was obtained similar to a normal-size distribution, which represents approximately the gel particle size distribution in the suspension.

3.4.3 Suspension concentration

The concentration of the gel particle in the carrier fluid effects the near-wellbore formation treatment significantly. The permeability reduction increases when the suspension concentration increases because the tendency of plugging increases with the particle concentration and the suspension viscosity increases when the gel particle concentration increases. Properties of the suspensions used in this study are presented in **Table 3-1**.

TABLE 3-1: COMPONENTS AND PROPERTIES OF THE GEL-PARTICLE SUSPENSIONS

Constituent and Properties	Suspension 1	Suspension 2	Suspension 3	Suspension 4
Polymer (vol%, g)	0.5%, 2.63	1%, 5.25	2%, 10.50	3%, 15.75
Water (cm^3)	500	500	500	500
Xanthan powder (g)	0.25	0.25	0.25	0.25
Particles size range (μm)	14- 350	14- 350	14- 350	14- 350
Viscosity at 511 s^{-1} (Pa.s)	0.0035	0.0040	0.0045	0.0055

3.5 Porous Media

The pore-throat size is an important parameter of porous media that effect the near-wellbore formation treatment by gel particles. The permeability reduction increases when the pore-throat size decreases. For the same gel particle diameter, the particle diameter to pore-throat size ratio increases when the pore-throat size decreases and thus the tendency of the pore-throat plugging increases.

The pore-throat size distribution in a core sample is measured typically using the mercury injection capillary pressure method. In this method, the dry core sample is subjected to vacuum and then helium gas is injected at high pressure to indicate even the smaller pore throats that open up at high pressures to obtain the distribution of pore-throat sizes of the core. The core sample used is an unconsolidated proppant pack and the core holder is a cylindrical plastic holder. Therefore, the mercury injection capillary pressure method could not be applied. Instead, the pore throat size had to be estimated

by considering a circular pore throat model of porous media according to Peifeng et al. (2010). D_b indicates the cell body diameter, expressed by:

$$D_b = D_g \sqrt{\frac{\pi}{4(1-\phi)}} \tag{3.14}$$

D_T indicates the pore-throat diameter, given by:

$$D_T = D_b - D_g = D_g \left(\sqrt{\frac{\pi}{4(1-\phi)}} - 1 \right) \tag{3.15}$$

where ϕ is the porosity and Dg is the mean grain diameter of the sieved sample pack.

3.6 Operation Conditions

The important parameters of the operation conditions that effect the near-wellbore treatment by gel particles are described in the following.

3.6.l Flow rate

According to the definition of the particle deformation, the shear rate is an important parameter that can affect the gel particle deformation. The ratio of the viscous forces in the fluid to the elastic forces in the elastic solid particle increases by the shear rate, as shown in eq. 3.3. Thus the deformation of the gel particle increases, as shown in eq. 3.2. The shear rate increases by the flow rate, as shown in eq. 3.5 and thus the deformation and break-up increases by the flow rate. When the gel particles deformation and break-up increase, the transport of the gel particles through the pore-

throat increases and they are not captured at the pore-throat. Thus, the permeability reduction of the high permeability formation decreases at the high deformation and break-up of the gel particles. Baghdikian et al. (1989) determined that the particles deposition over the pore surface decreases when the flow rate increases and the hydrodynamic lift force increases by the flow rate and thus the plugging decreases.

3.6.2 Temperature

There are two effects of temperature on the near-wellbore formation treatment by gel particle suspension. First, the viscosity of the suspension decreases when the temperature increases. The viscosity of the 3 vol% gel particle suspension decreases from 0.0055 Pa.s to 0.0035 Pa.s by increasing the temperature from 23.5 °C to 75 °C, as shown in **Fig. 3.4**. Second, the gel particles are soft and more deformable particles and increased temperature makes them softer and deformable. These two effects make the gel particles less effective because they can pass easily through porous media without causing pore-throat plugging and pore-surface deposition. Therefore, plugging of pores by gel particles becomes less pronounced at high temperatures, as shown in **Fig. 3.5**.

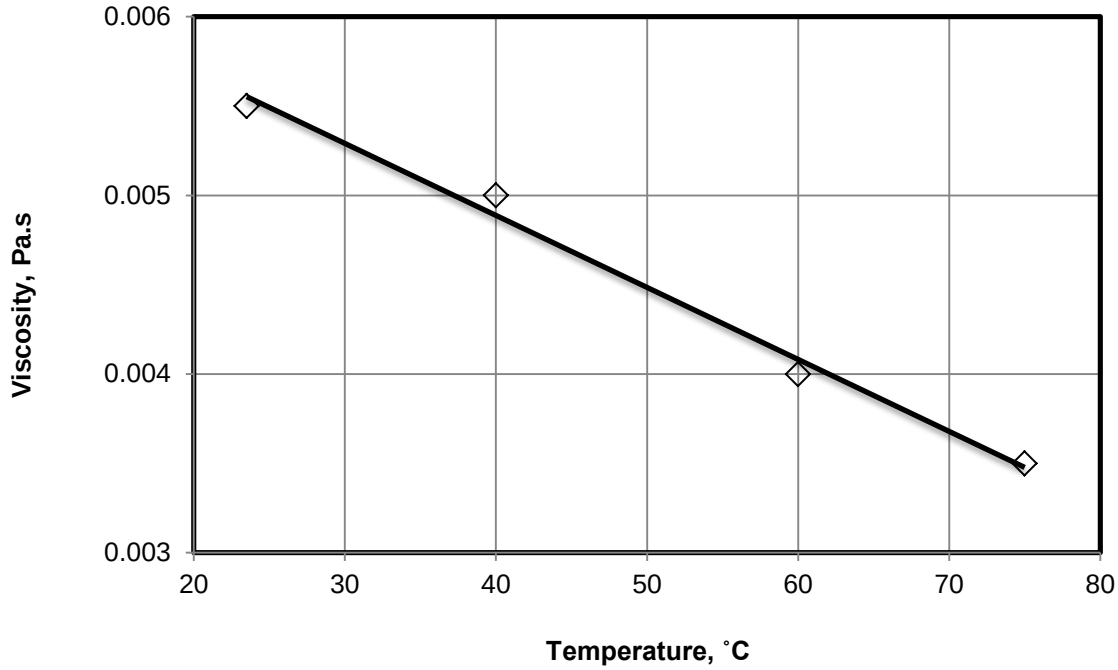

Fig. 3.4: Viscosity of the 3 vol% gel particle suspension with temperature

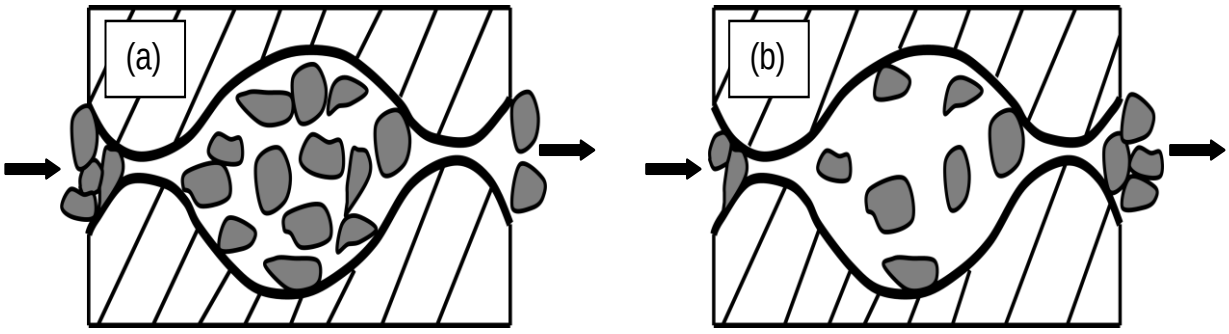

Fig. 3.5: Effect of temperature on gel particles passing through pore
(a) at low temperature (b) at high temperature

Chapter 4: Experimental Studies of Near-Wellbore Formation Treatment

part of this chapter has been previously published as ‘‘Experimental Study of Gel Particles Transport Through Porous Media’’ in the SPE Latin American and Caribbean Petroleum Engineering Conference, Mexico City, Mexico, 16-18 April, 2012 and is used here by permission.

part of this chapter has been previously published as ‘‘Experimental Investigation and Correlation of Treatment in Weak and High- Permeability Formations by Gel Particles’’ in Production and Operations Journal, Vol. 28, No. 4, pp. 387-401, 2013 and is used here by permission.

4.1 Introduction

The following experimental studies were undertaken to investigate the transient behavior of gel particles and silica flour particles during plugging of porous media and the effect of the variation in gel particle and silica flour concentrations, flow rates, ratio of gel particle sizes-to-pore-throat diameter, pore space of the permeable filter disc, sand sizes, and temperatures on the plugging conditions of the high-permeability formations. This is inferred by monitoring the variation of the differential pressure across the proppant pack, the effluent particle size distributions during experiments by flowing deformable gel particles, the filtrate loss and the pressure gradient required to initiate flow across the fluid loss cell. Thus, the conditions for inducing pore plugging by injecting gel particle suspensions and silica flour particle-gel systems into porous media were investigated.

4.2 Experimental Systems and Procedure

4.2.1 Experimental flow apparatus

The experimental studies utilized two separate experimental apparatus as described in the following.

4.2.1.1 Apparatus for gel particle suspensions processes

The schematic experimental flow apparatus (**Fig. 4.1)**; the experimental testing procedure; suspension preparation; and the measurements of viscosity, pore throat size, and gel particle size are described in the following.

A- Tests under isothermal conditions

A Ruska pump was used to flow the gel particle suspension from the accumulator into the proppant pack at a constant rate by the mineral oil. The pump flow rate varies from 5 to 1120 cm^3/hr and the pressure ranges from 0 to 10000 psig. A 500 cm^3 stainless steel accumulator was filled with the particles suspension and contains a steel piston disk to separate the suspension from the mineral oil. An 18.4 cm long and 2.5 cm diameter plastic cylindrical column was used to simulate a core sample . For our study, the sandpack should have sufficiently large and highly connective pores so that we can investigate the conditions for plugging of these pores and reduce the high permeability. Therefore, the ceramic proppant is more suitable than natural sand to create sufficiently large pores and high permeability required in this work. Thus, the plastic column was filled with 16-20 mesh proppant sands. A 30 mesh sieve was used at the inlet and outlet ends of the sand pack to contain the proppant inside the plastic column. Absolute permeability and porosity were measured as 3800 md and 38%, respectively. The properties of the proppant pack are given in **Table 4-1**. Smart Differential Pressure Transmitter ST3000 Series was used to measure the differential

pressure across the sandpack during the tests. A NI SC 2345 Data Acquisition System was used to record the differential pressure during the tests by the Labview software version 7.

The gel-particle suspension was injected at a constant rate at the bottom of the proppant pack at the ambient laboratory temperature of 23.5 $^{\circ}$C using the Ruska pump as a piston-like front from the accumulator and the differential pressure across the sandpack was measured during the experiments by the pressure transducer and recorded by a computer- assisted data-acquisition system. The flow was continued until attaining a constant differential pressure across the proppant pack. The effluent gel particle suspension was collected in a beaker at various times to determine the gel-particles size distribution. The proppant was removed from the plastic cylindrical holder after each run and then washed and dried for reuse again in the next test.

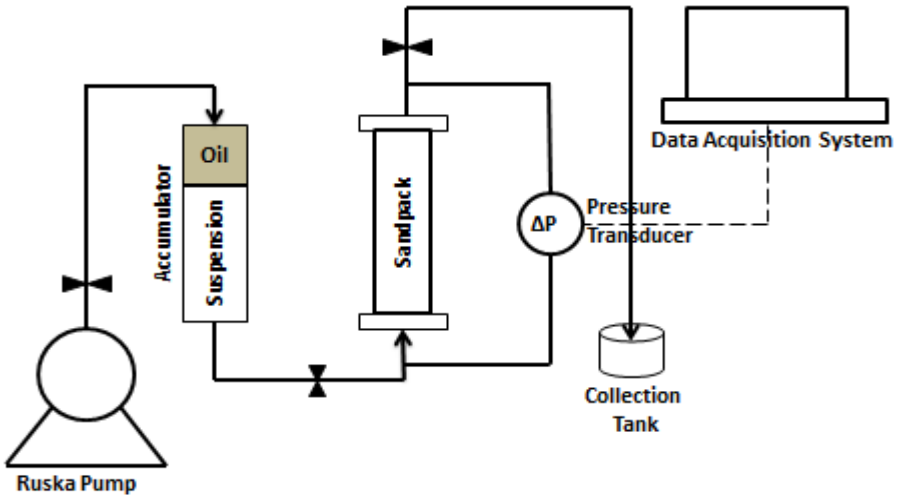

Fig. 4.1: Schematic diagram of the experimental apparatus

TABLE 4-1: PROPERTIES OF THE PROPPANT PACK	
Properties	Data
Porosity (%)	38
Absolute permeability (md)	3800
Grain density (g/cm³)	3.3
Average pore throat diameter (μm)	127
Mesh size	16 – 20

B- Tests under thermal conditions

A glass-made water bath is added to the experimental apparatus as shown in **Fig. 4.2** for purposes of studying the temperature effect on gel particles placement in porous media as described briefly in the following.

The experimental flow apparatus consists of the following major parts: (1) A Ruska pump used to inject the gel particles suspension into the proppant pack at a constant rate using a mineral oil, (2) A 500 cm³ stainless steel accumulator filled with the gel particles suspension, (3) Plastic cylindrical column of 18.4 cm long and 2.5 cm internal diameter filled with 16-20 mesh proppant sands to represent a core sample, the absolute permeability and the porosity of which are 3800 md and 38%, respectively, (4) Smart Differential Pressure Transmitter of ST3000 Series used to measure the differential pressure during the tests, (5) A NI SC 2345 Data Acquisition System equipped with Labview software version 7 used to record the differential pressure during the tests, and (6) Immersion Coiled Heater with Thermostatic Temperature Controller having a sensitivity of ±2°F (±1°C) placed at the bottom of the glass water

vessel used to maintain the proppant pack at the required experiment temperatures, and Pocket-Size K Thermometer of temperature operating range -50 to 750 ˚C using to register the water bath temperature, as shown in **Fig. 4.3.**

A 3 vol% concentration gel particle suspension at different temperatures of 23.5 ˚C, 40 ˚C, 60 ˚C, and 75 ˚C was injected into the proppant pack at a 100 cm³/hr flow rate from an accumulator by using the Ruska pump. The pressure transducer was used to measure the differential pressure across the proppant pack during the experiments by using a computer- assisted data acquisition system and the experiment continued until attaining a final constant differential pressure. Suspension viscosities were measured at different temperatures of 23.5 °C, 40 ˚C, 60 ˚C and 75 ˚C by using a Chann 35 viscometer at shear rate of 511 s^{-1}.

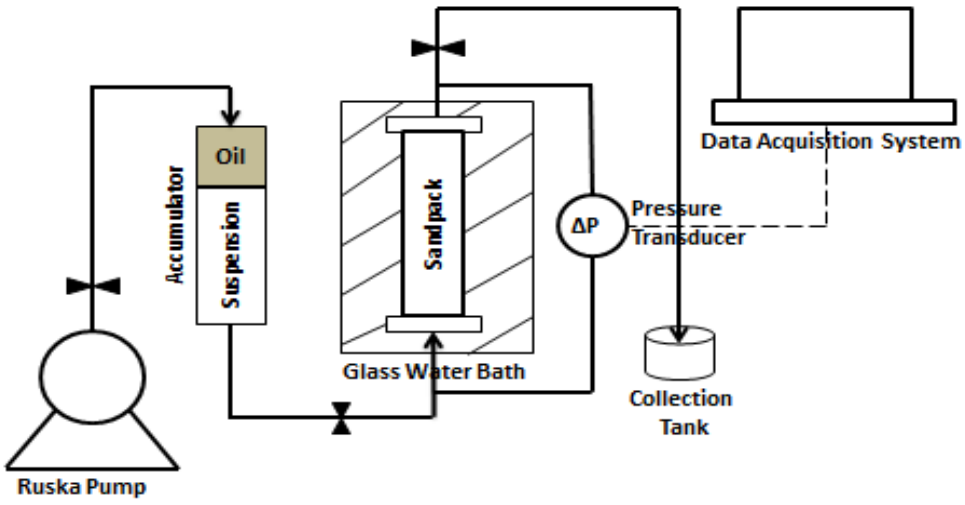

Fig. 4.2: Schematic diagram of the experimental apparatus with heating system

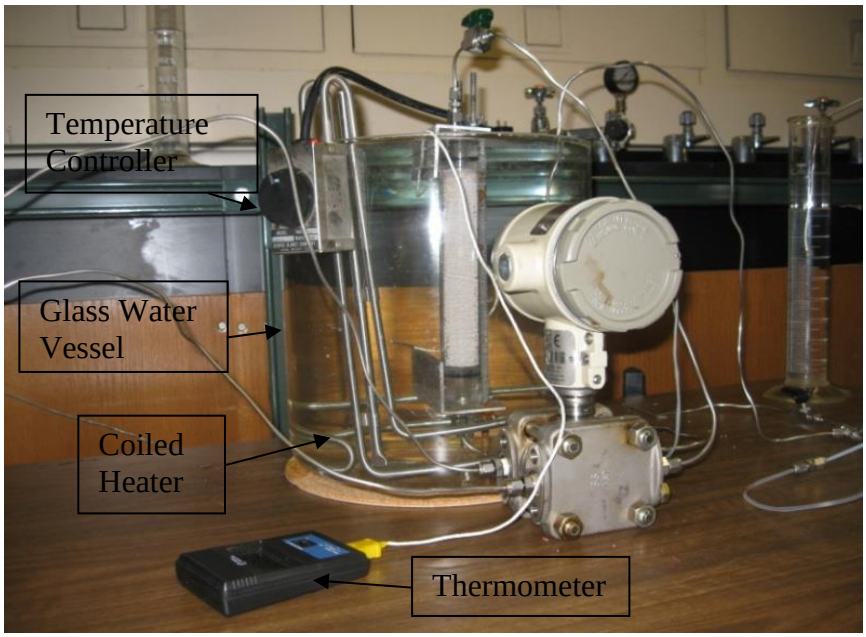

Fig. 4.3: Heating system of the experimental apparatus

4.2.1.2 Apparatus for silica flour particle-gel processes

The following describes the filtrate test apparatus **(Fig. 4.4),** the experimental procedure, and the particle-gel system preparation.

A- Tests under isothermal conditions

A nitrogen tank was used to apply pressure to the particle-gel system in the fluid loss cell at a 3447 kPa pressure. A fluid loss cell with a filter disc at the bottom of the cell and 1-in. column of sand on the filter disc was filled with the particle-gel system. The average pore diameter of the filter discs were 5, 10, and 35 micron, and the sand sizes were 12/20, 20/40, and 40/70 mesh. A graduated glass cylinder was used to measure the filtrate volume during the test.

The particle-gel system was filtered from the fluid loss cell at 3447 kPa pressure using a nitrogen tank and gas pressure regulator at an ambient temperature of 23.5°C,

and the filtrate volume was measured during the test using a graduated glass cylinder. The filtrate test was continued until no gel was filtered or after a 30-minute period of time had elapsed. The remaining particle-gel system was removed from the fluid loss cell and replaced with water to measure the pressure to initiate flow. To measure the value of the pressure to initiate water flow, pressure was applied on the fluid loss cell using the nitrogen tank and the pressure was increased gradually using a gas pressure regulator until the first drop was filtered from the fluid loss cell. The pressure that caused the first filtrate drop was the value of the pressure to initiate water flow.

The particle-gel system was prepared mixing potassium chloride (KCl) with water using a commercial blender and Polymer 1 was added slowly to the water; mixing continued until the polymer was completely hydrated and no lumps or ʻ fish eyes ʼ were present (a minimum of 30-minute mixing time). Polymer 2 was added to the solution and mixed using the blender until homogeneous, and crosslinker was then added to the solution and mixed until homogeneous. Silica flour was added slowly to the solution at the desired concentration and mixed until homogeneous. Components of the particle-gel system are presented in **Table 4-2.**

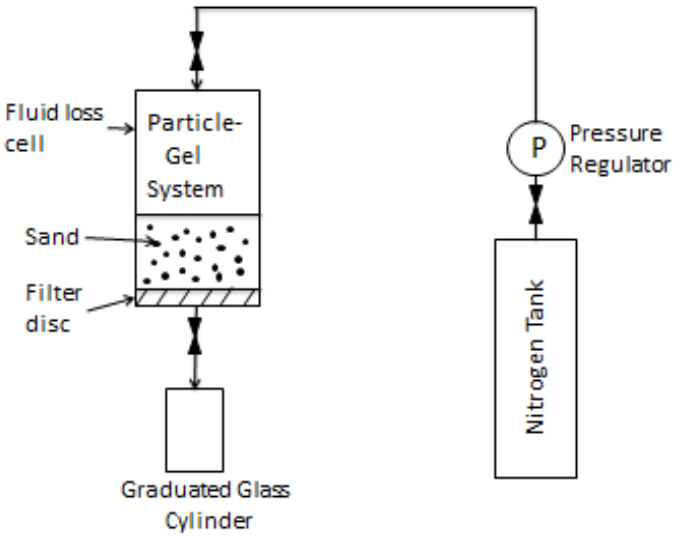

Fig. 4.4- Schematic of the filtrate test apparatus.

TABLE 4-2:COMPONENTS OF THE PARTICLE-GEL SYSTEMS

Constituent	System 1	System 2	System 3	System 4
Water (gm)	78.7	78.7	78.7	78.7
KCl (gm)	9.3	9.3	9.3	9.3
Polymer1 (gm)	0.4	0.4	0.4	0.4
Polymer2 (gm)	46.7	46.7	46.7	46.7
Crosslinker (gm)	8	8	8	8
Silica flour (wt%)	0.56	1.40	2.80	4.20

B- Tests under thermal conditions

Temperature affects the fluid loss of the silica flour particle-gel system and the pressure initiate and thus the thermal effects is an important factor in the near-

wellbore formation treatment by particle-gel system. To study the temperature effect, a heating system was added to the experimental system. The heating system consists from heating tape, temperature controller and thermometer, as shown in **Fig. 4.5**.

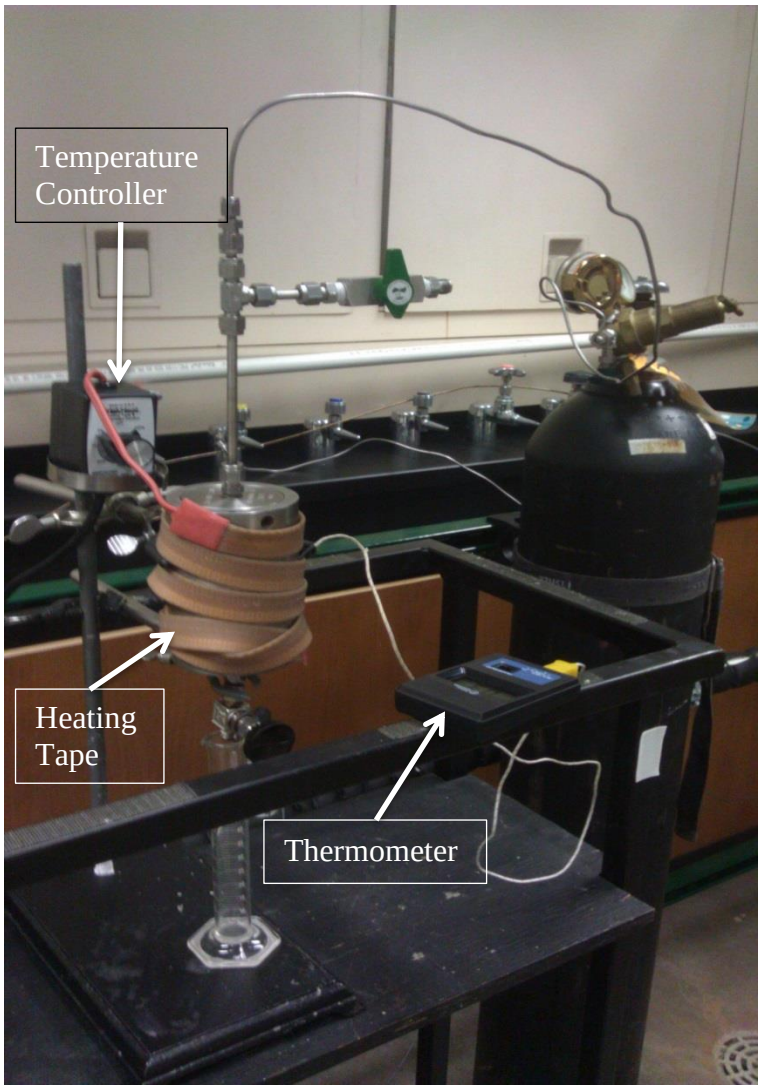

Fig. 4.5: Heating system of the filtrate test apparatus

Chapter 5: Investigation of Treatment in High-Permeability Formations by Gel Particles Suspension

This chapter have been previously published as ‘‘Experimental Study of Gel Particles Transport Through Porous Media’’ in the SPE Latin American and Caribbean Petroleum Engineering Conference, Mexico City, Mexico, 16-18 April, 2012 and is used here by permission.

This chapter has been previously published as ‘‘Experimental Investigation and Correlation of Treatment in Weak and High- Permeability Formations by Gel Particles’’ in Production and Operations Journal, Vol. 28, No. 4, pp. 387-401, 2013 and is used here by permission.

5.1 Introduction

This study investigates the behavior and transport of particle gels through porous media and the conditions favorable for plugging of highly permeable formations and develops useful empirical correlations from the experimental data to assist in controlling of such conditions. These correlations can be used to determine the conditions which induce pore plugging by injecting gel particle suspensions into porous formations.

The diagnostic equations of Wojtanowicz et al. (1987) are applied to investigate the prevailing plugging mechanisms causing permeability reduction under various conditions. The gel particle size distributions are an important part in understanding the mechanism of plugging of porous media, following Civan (2000, 2007a, and 2010), Iscan and Civan (2006), and Iscan et al. (2009). The capture of gel particles in porous media was directly correlated to the ratio of the particle size to the pore throat diameter. The measurements of gel particle sizes of injected and effluent samples were made optically under a microscope equipped with a camera connected to

a computer which can store the photomicrographs. The particle size distribution was studied and useful correlations were developed for the cumulative particle distribution as a function of particle diameter. The experimental study provides an understanding of the transient flow behavior of gel particles through porous media and can assist in choosing suitable parameters for controlling the plugging of the pores and reducing the high permeability of formations to avoid the loss circulation during a drilling operation and control water production in waterflooded mature oil fields. The correlations of experimental data obtained here can be used for determination of the optimal conditions for mitigation and treatment of high permeability formations.

5.2 Experimental Results and Discussion

Because of the deformable nature of the gel particles, the experimental investigation and phenomenological description of the movement and retention of gel particles in porous media is a complicated task. Several transport mechanisms can occur simultaneously during particles transfer through pores and pore throats depending on the local pore and suspension conditions. It is difficult to determine the relative importance of the various particulate mechanisms during the transport process. Hence, an evaluation index was used to determine the dominant mechanism based on the gel particle size distribution of the initial (original) and effluent suspension samples.

5.2.1 Particle size distribution

The total concentration of all particles ranging in the 14- to 350-μm diameter sizes present in the original 3-vol% suspension used in our tests was

determined approximately as $1.7*10^4$ particles/mL of suspension. Particles with diameter sizes smaller than 14 μm cannot be counted with the present equipment. However, such extremely small particles (significantly smaller than pore throats in high-permeability zones) can be ignored because they cannot really contribute to the plugging process unless without having a sufficient time to coagulate. The particle size distribution of the original sample indicates that 30% of these gel particles are larger than the average pore-throat size of 127 μm.

Figs. 5.1 to **5.5** show comparison of the particle size distributions of the collected effluent samples and the 3-vol% original injected sample for the gel-particle suspension at different flow rates after 1 and 5 pore volumes injected (PVI), respectively. The particle size distribution of the original sample shows that 30 % of the gel particles are larger than the average pore throat size. At 1 PVI most of the larger particles are trapped at the pore throat or are first deformed and then captured at the pore surface. There is also a possibility that some smaller particles are captured at the pore surface or some larger particles are broken into pieces and then pass through the pore throats. For 50 cm^3/hr all particles greater than 150 μm, for 100 cm^3/hr the particles greater than 110 μm, for 200 cm^3/hr the particles greater than 130 μm, for 280 cm^3/hr the particles greater than 150 μm, and for 400 cm^3/hr the particles greater than 210 μm are trapped in porous media. These results indicate that at low flow rates the percentage of larger particles trapped at the pore throat or deformed and then captured at the pore surface increases by the flow rate but at high flow rates the percentage of larger particles trapped at the pore throat or deformed and then captured at the pore surface decreases by the flow rate. At 5 PVI, the effluent particle size distribution is

approximately the same as the original. This indicates that all the particles pass through the pore throats of the non- plugging pores without entrapment or deposition. **Fig. 5.6** shows samples of photomicrographs indicating the difference in size and concentration of the particles at 1 PVI and 5 PVI, respectively.

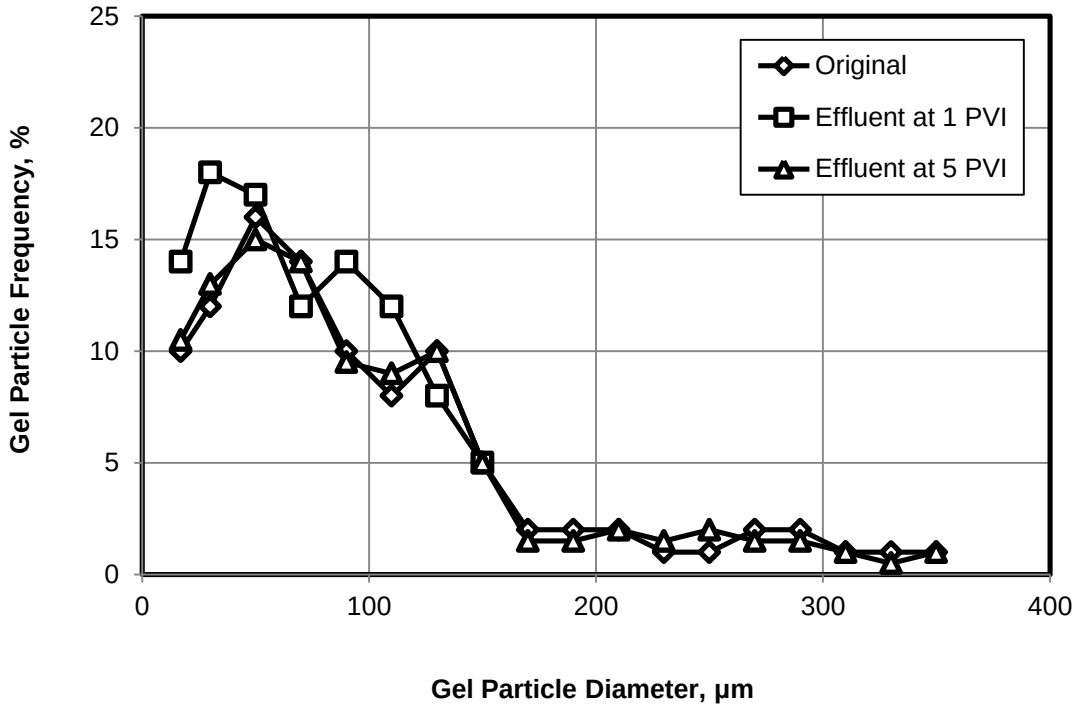

Fig. 5.1: Particles distribution of 3 vol% original & effluent sample at 50cm³/hr after 1 and 5 PVI

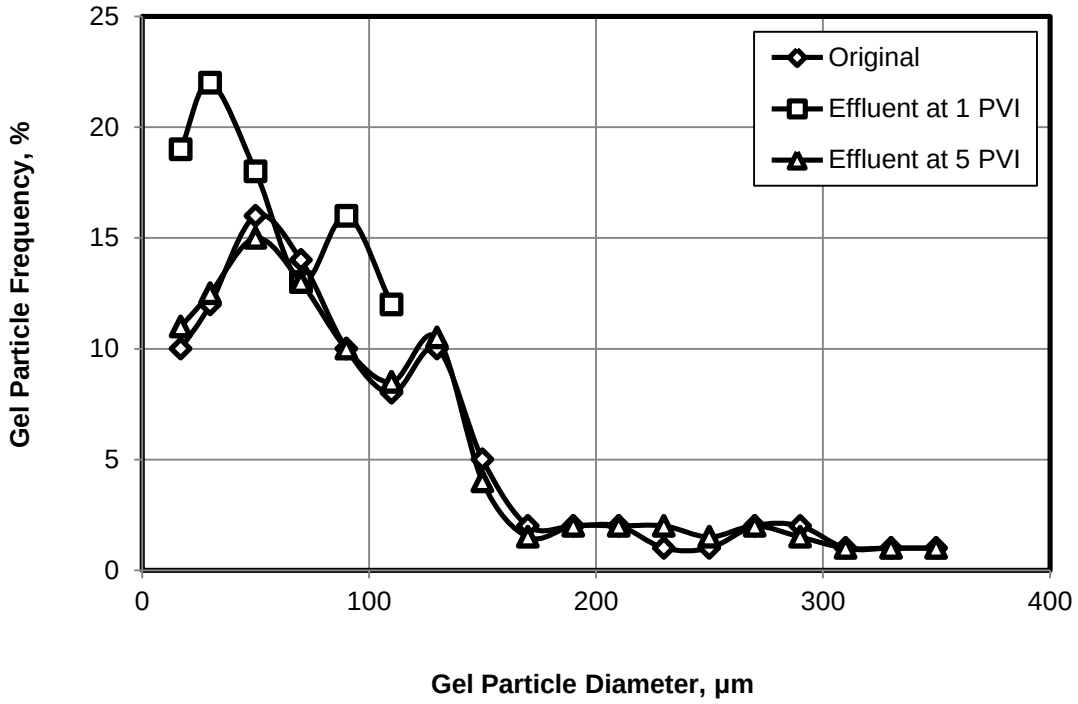

Fig. 5.2: Particles distribution of 3-vol% original & effluent sample at 100cm³/hr after 1 and 5 PVI

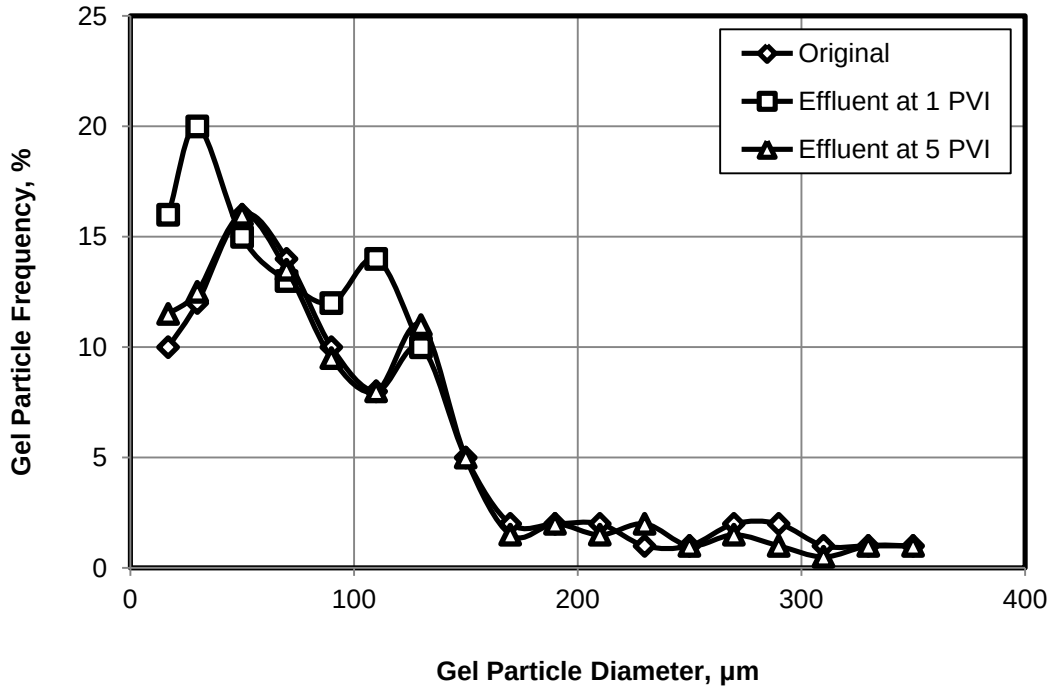

Fig. 5.3: Particles distribution of 3-vol% original & effluent sample at 200 cm³/hr after 1 and 5 PVI

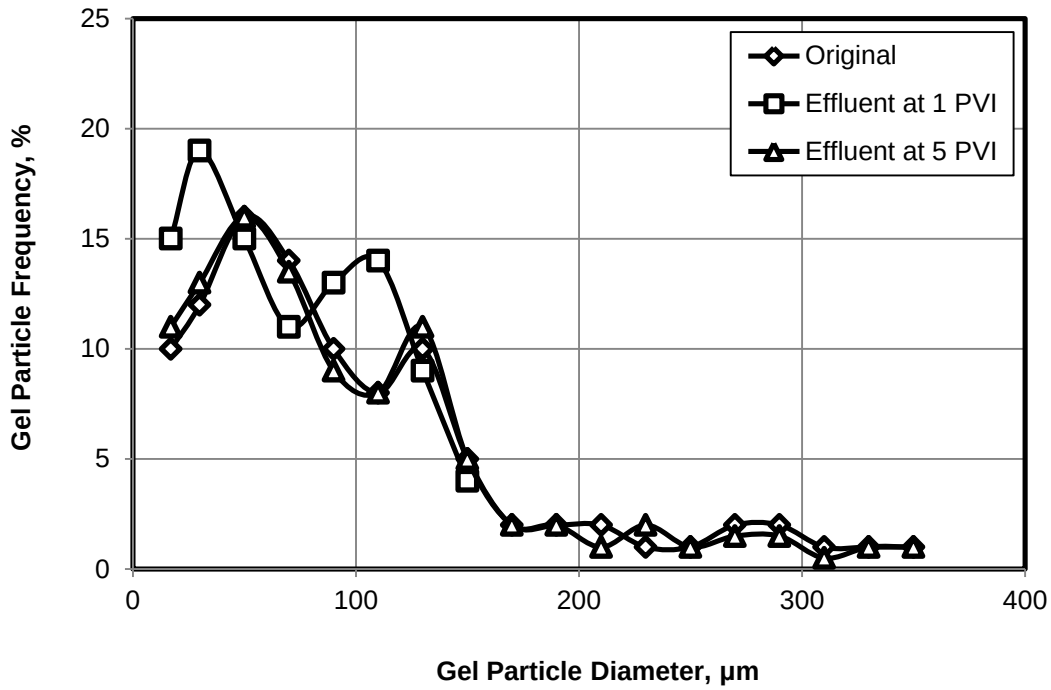

Fig. 5.4: Particles distribution of 3-vol% original & effluent sample at 280 cm³/hr after 1 and 5 PVI

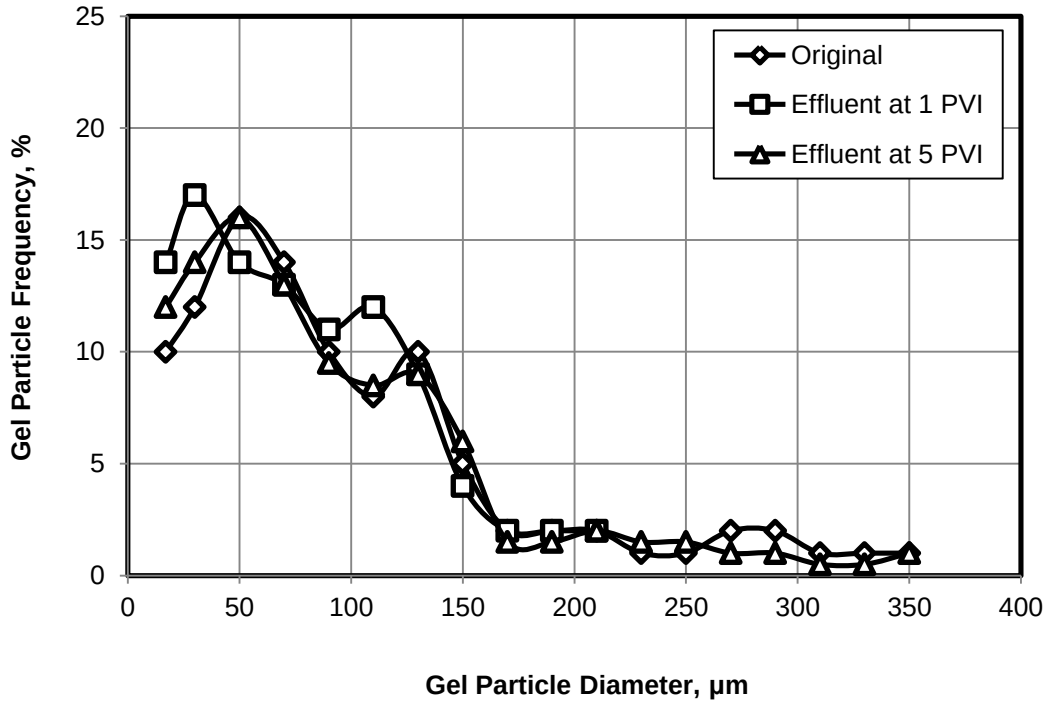

Fig. 5.5: Particles distribution of 3-vol% original & effluent sample at 400cm³/hr after 1 and 5 PVI

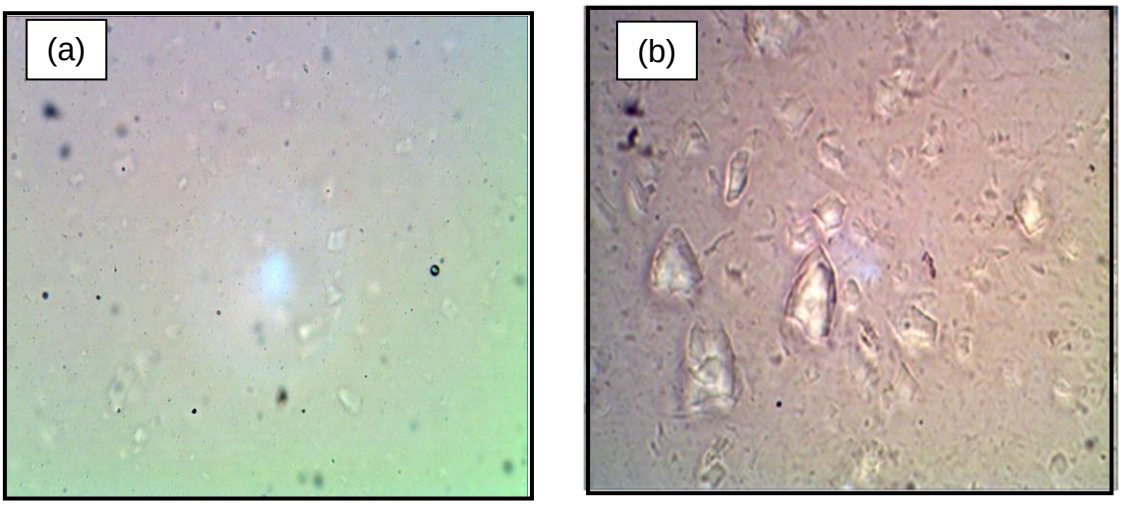

Fig. 5.6: Photomicrographs of effluent samples at 100 cm³/hr: (a) after 1 pore volume injection (PVI) (b) after 5 pore volume injection (PVI)

5.2.2 Effect of suspension concentration

The effect of the concentration of gel particle in the carrier fluid on the differential pressure and permeability reduction during proppant pack flow tests was investigated by conducting several tests in which the flow rate of the injected suspension was kept constant but the concentration of gel particles in the injected suspension was varied. In these tests, a constant flow rate of 100cm³/hr was used to inject suspension with particle concentrations of 0.5, 1, 2, and 3 vol% into the sandpack.

As previously demonstrated by Gruesbeck and Collins (1982), plugging of pathways in porous media occurs mainly when large particles form bridges across pore throats and cause a significant permeability reduction. However, particles smaller than pore throats can pass through, which, under favorable conditions only, can deposit over the pore surface, and cause a negligible

permeability-reduction effect. **Fig. 5.7** shows the variation of the permeability-reduction ratio across the sandpack with PVI for different suspension concentrations at a constant 100-cm3/h flow rate. By injecting the gel particles, differential pressure is built up by particles trapped at the entrance of the pore throats, causing the suspension particles to deform and pass through the pore throats or to be captured at the pore surface. However, a constant steady pressure is established as the injection continues.

The results of the particle size distribution of the effluent samples at 1 PVI show that the particles with different diameters were retained inside the sandpacks, with consequences of the plugging caused essentially by gel particles with sizes comparable to or larger than the pore-throat sizes, while the larger pores serving as nonplugging flow paths were only slightly impaired by surface deposition. Fig. 5.7 shows that the permeability-reduction ratio changes from 0.81 to 0.36 by increasing the concentration of the gel particles from 0.5 to 3 vol%. This happened because the plugging of pores occurs more rapidly as the amount of particles trapped at the pore throats or deformed and then captured at the pore surface increases by concentration increase. Also, as shown in **Fig. 5.8**, for a constant flow rate, the suspension viscosity increases from 0.0035 to 0.0055 Pa.s when the gel-particle concentration increases from 0.5 to 3 vol%. This causes an increase in the differential pressure and permeability reduction.

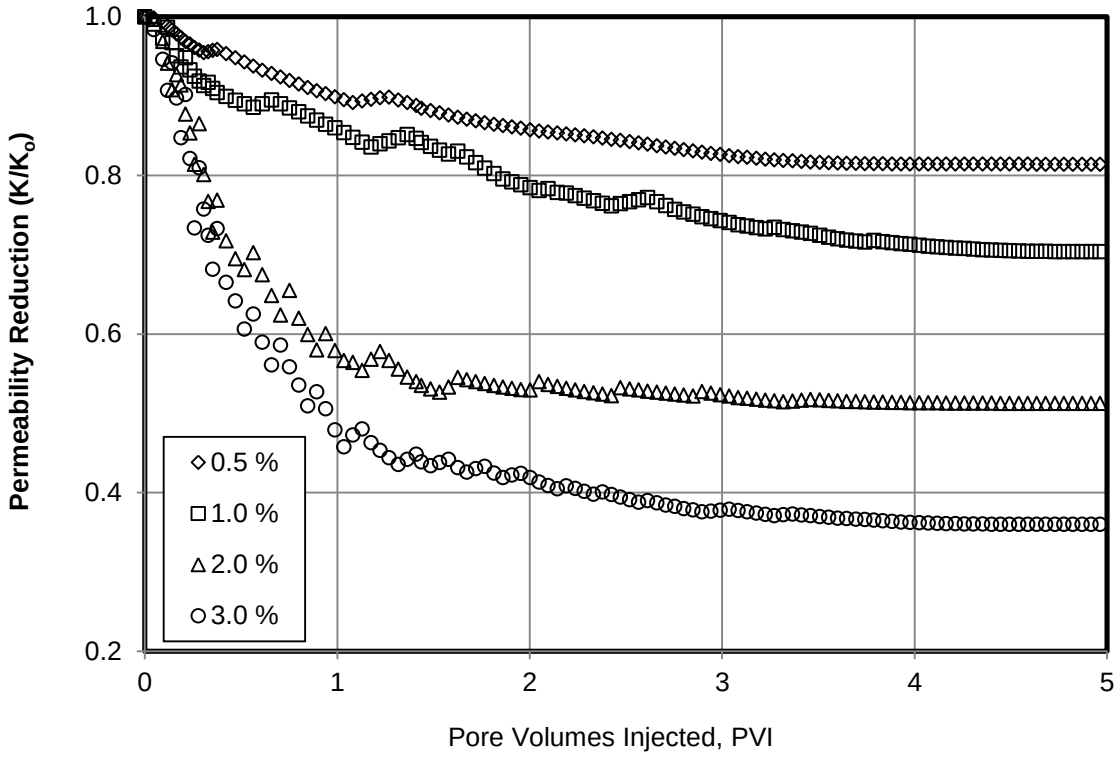

Fig. 5.7: Permeability reduction at 100 cm³/hr for different volume suspension concentrations at T = 23.5 °C

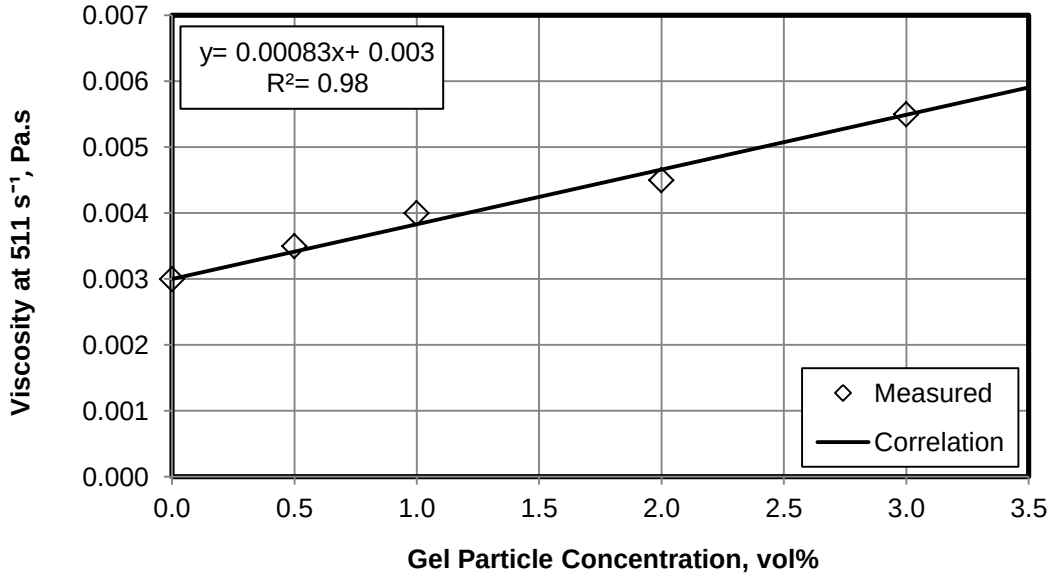

Fig. 5.8: Suspension viscosity at 100 cm³/hr for different particle volume concentrations at T= 23.5 °C

5.2.3 Effect of flow rate

The effect of the suspension injection flow rate on the pressure drop and permeability reduction in the sand pack was investigated by several experiments at a constant 3 vol% concentration for the flow rates of 50 cm^3/hr, 100 cm^3/hr, 200 cm^3/hr, 280 cm^3/hr, and 400 cm^3/hr. **Fig. 5.9** shows the permeability-reduction with pore volumes injected at different flow rates and constant concentration. The permeability reduction increased from 0.46 to 0.36 when the flow rate increased from 50 cm^3/hr to 100 cm^3/hr but the permeability reduction decreased from 0.36 to 0.60 when the flow rate increased from 100 cm^3/hr to 400 cm^3/hr. This is because at the low flow rate the differential pressure increased as much as the injection flow rate (the differential pressure increased from 16.13 kPa to 41.15 kPa when the flow rate increased from 50 cm^3/hr to 100 cm^3/hr), but at the high flow rate, the differential pressure did not increase as much as the injection flow rate (the differential pressure only increased from 41.15 kPa to 98.19 kPa when the flow rate was increased four times from 100cm^3/hr to 400 cm^3/hr). This indicates that the gel particles were able to pass through the pore throats easily at the high flow rate, as we shown from the previous results of the particle size distribution of the effluent sample at 1 PVI for different flow rates. Thus, plugging of pores becomes less pronounced by increasing flow rates.

Baghdikian et al. (1989) investigated the hydrodynamic lift force acting on the rate of particle deposition over and mobilization of particles from pore surfaces. They showed that an increase in the hydrodynamic force with flow rate decreased the particles deposition and increased the particles mobilization, and thus decreased the plugging effect and therefore permeability reduction in porous media. Consequently,

increase of differential pressure and reduction of permeability with increase of flow rate become less pronounced.

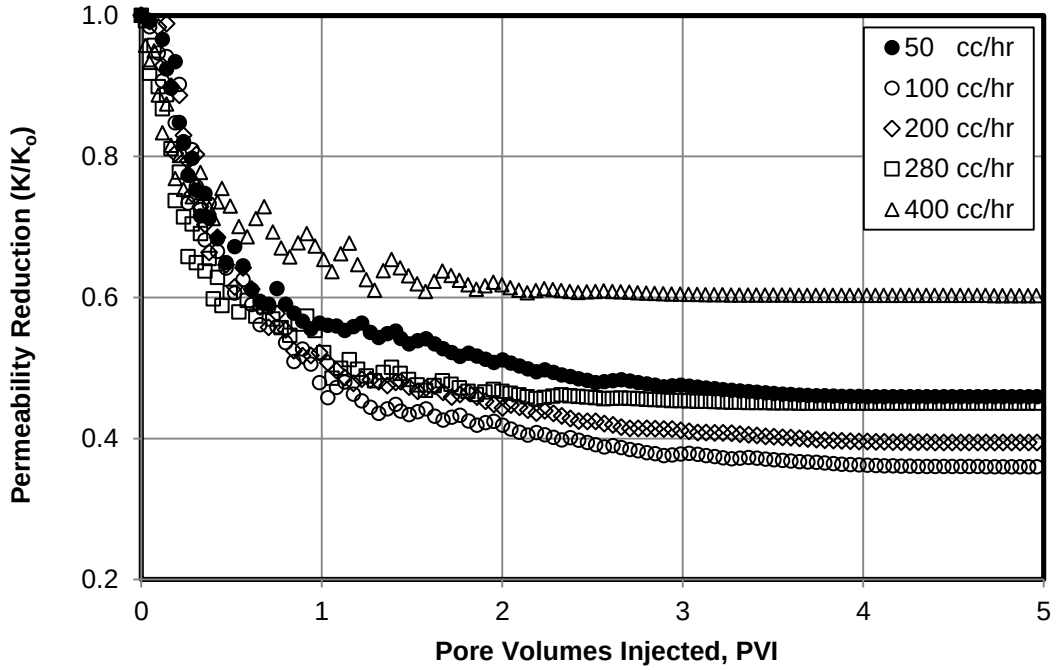

Fig. 5.9: Permeability reduction at 3-vol% concentration for different flow rates at T= 23.5 °C

5.2.4 Effect of particle size

The effect of gel- particle size on the differential pressure and permeability reduction was investigated a number of experiments at a constant 3-vol% suspension concentration and 100-cm³/hr constant flow rate using average particle diameters of 50 µm, 75 µm, 100 µm, 125 µm, and 140 µm, respectively. **Fig. 5.10** shows the permeability reduction with pore volumes injected at different particle sizes, and constant flow rate and concentration. The permeability reduction changes from 0.54 to 0.30 with the average particle size increasing from 50 µm to 140 µm. This indicates that the amount of pores being plugging by the gel particles can be increases by increasing particle size.

It is difficult to determine exactly the prevailing particular processes of gel-particle transport through porous media during the tests because the gel particles are deformable and not rigid. We can consider that the particle will pass through the pore throat if the particle diameter is less than pore-throat size, and the particle will deform and pass through the pore throat to deposit on the pore surface if the particle diameter is larger than the pore-throat size. The rigid particles in diameters larger than the pore-throat size cannot pass through the pore throat. The analysis of the effluent samples at 1 PVI for 100 cm^3/hr showed that the effluent samples contain only small particles because almost all the particles larger than pore throat size are captured in porous media. In this case, the pore surface deposition is the relevant process of the gel-particles transport through porous media.

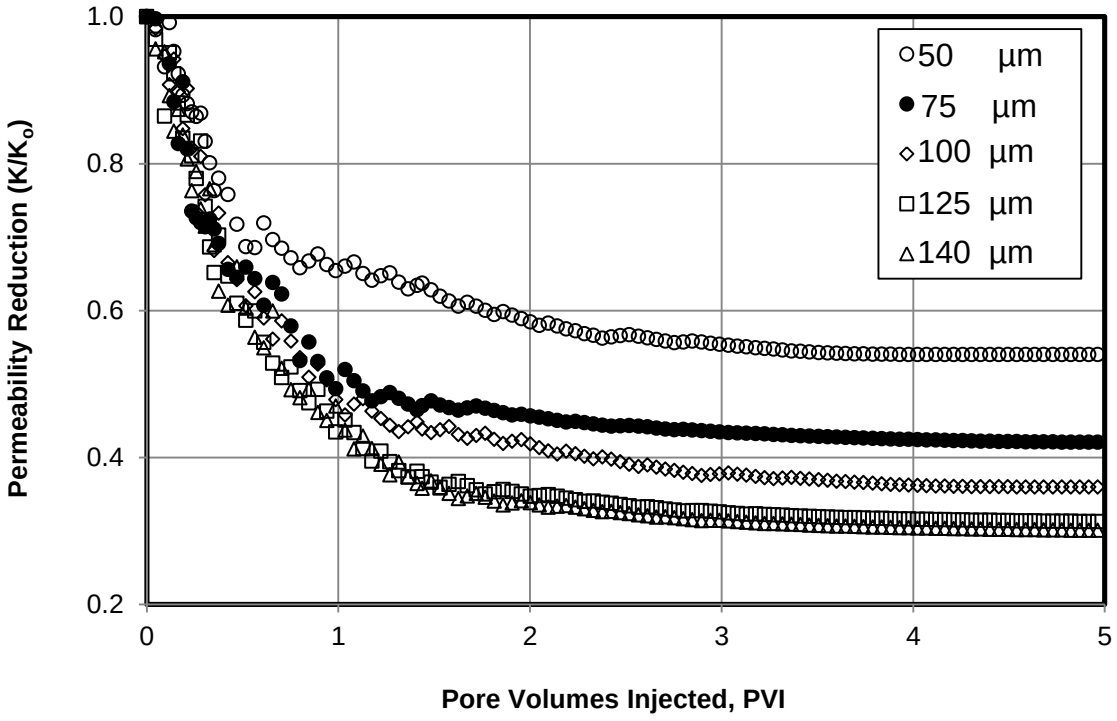

Fig. 5.10: Permeability reduction at 100 cm^3/hr for different particle sizes at T= 23.5 °C

5.3 Development of Empirical Correlations

Empirical correlations were developed from the experimental data by using the relevant parameters of flow rate, concentration, and particle diameter leading to plugging of pores by suspended particles. Instead of resorting to ordinary polynomial regressions which are prone to various limitations (Civan, 2011), special correlation equations were developed and implemented, as described in the Appendix B. It is demonstrated by the correlations presented in this section that these equations can represent the experimental data satisfactorily over the full range of the experimental conditions. The advantage of the particular equations of correlations described in Appendix B that are used here is the elimination of any problems inherent to polynomial regression, such as polynomial oscillations causing inaccurate interpolation values for conditions between measured data.

5.3.1 Suspended particle size distribution before and after flow

The normal size distribution of the suspended particles of the original suspension with minimum particle diameter of 14 micrometer and maximum particle diameter of 350 micrometer and the effluent suspensions at different flow rates were showed in **Fig. 5.11**. Approximately 30 % of the particles have size greater than the pore-throat size (127 micrometer). For the effluent suspensions, Fig. 5.11 shows that at 50 cm^3/hr 18 % of the particles are about 30 micrometer in diameter , while the largest particles (at 150 micrometer) are 5 %; at 100 cm^3/hr, 22 % of the particles are approximately 30 micrometer in diameter, while the largest particles (at 110 micrometer) are 12 %; at 200 cm^3/hr, 20 % of the particles are approximately 30

micrometer in diameter, while the largest particles (at 130 micrometer) are 10 %; at 280 cm^3/hr, 19 % of the particles are approximately 30 micrometer in diameter, while the largest particles (at 150 micrometer) are 4 %; and at 400 cm^3/hr, 17 % of the particles are approximately 30 micrometer in diameter, while the largest particles (at 210 micrometer) are 2 %. These results indicate that at the high flow rate, the percentage of the largest particles that are trapped at the pore throat or deposited at the pore surfaces decreases by the flow rate, and thus, the permeability reduction is less.

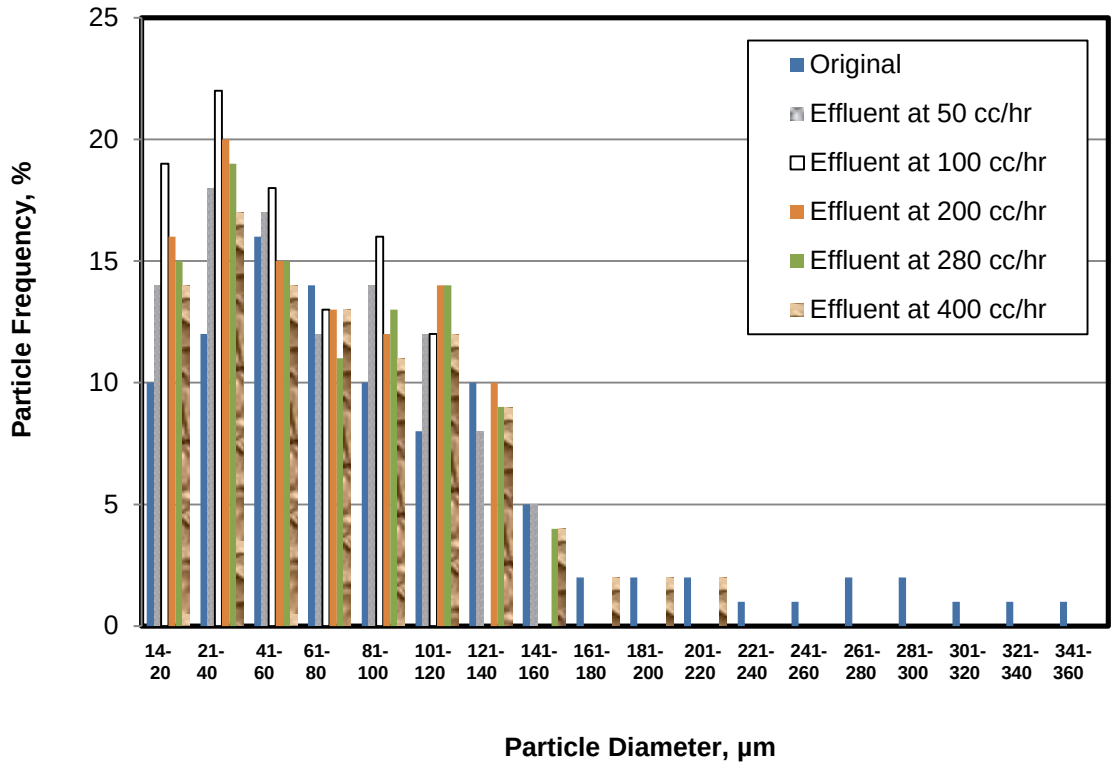

Fig. 5.11: Particle size distribution for the original and effluent suspensions at 1 PVI for different flow rates

Empirical correlations were developed from the histogram of the particle size distribution for the original suspension and the effluent samples at different flow rates, as shown in **Fig. 5.12**. These correlations show an exponential relationship between the

cumulative particle distribution and the particle diameter with high regression coefficient (R^2) so that we can use it to predict the cumulative particle distribution at any diameter of the suspended particles for these flow rates, and, from the cumulative particle distribution we can know the percentage of the particles that are trapped and deposited in the porous media, which can demonstrate the permeability reduction. Note F(x) represents the cumulative particle distribution, %; and the normalized particle diameter is given by X = (Dp - Dpmin)/(Dpmax - Dpmin).

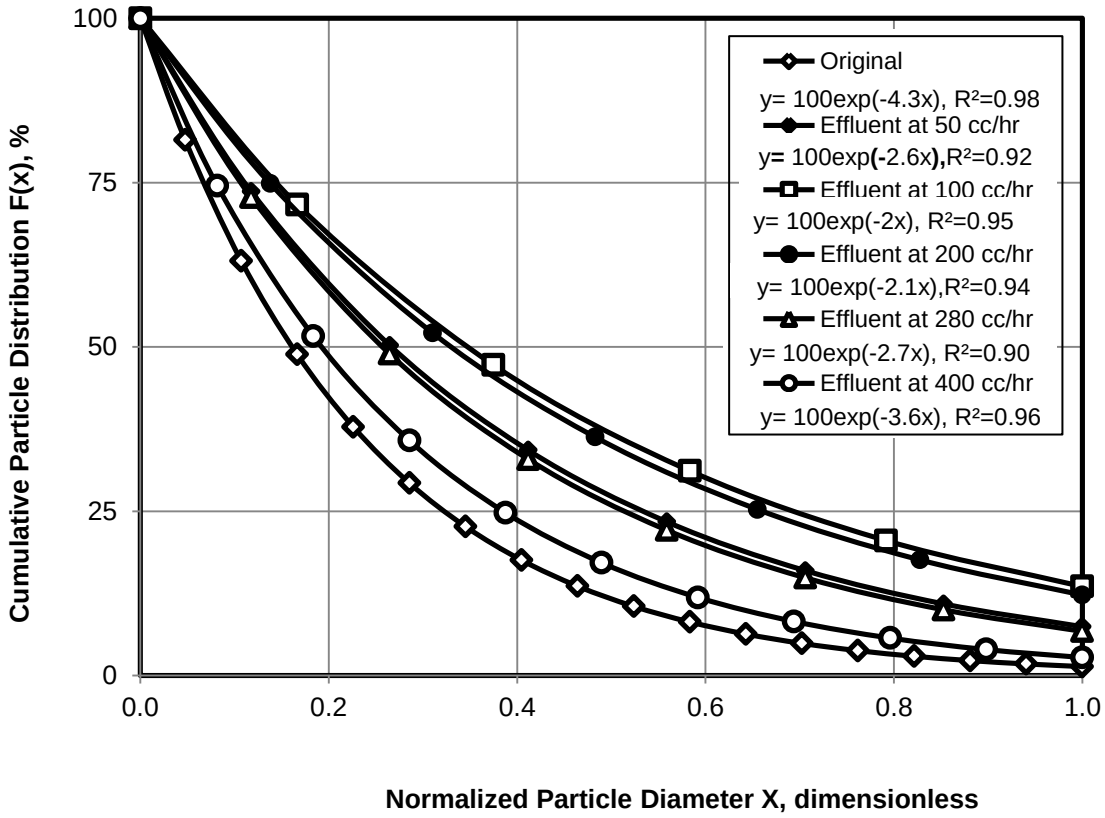

Fig. 5.12: Calculated particle size distribution for the original and effluent suspensions at 1 PVI for different flow rates

5.3.2 Differential pressure across proppant pack

The experimental results show that differential pressure increases from 11.58 to

41.15 kPa when increasing the gel- particle- suspension concentration from 0.5 to 3 vol% because the amount of particles that deform and deposit at the pore surface increases when the concentration increases. Also, the viscosity of the suspension increases from 0.0035 to 0.0055 kPa.s when increasing the concentration from 0.5 to 3 vol%, which leads to an increase in the differential pressure. **Fig. 5.13** shows an exponential relationship between the gel-particle concentration and differential pressure across the proppant pack. The following relationship correlates the experimental data satisfactorily:

$$\Delta P = 8.07 \exp\left(0.55 C_P\right), R^2 = 0.99 \qquad (5.1)$$

where ΔP indicates differential pressure across proppant pack, kPa; and C_P is gel-particle concentration, vol%.

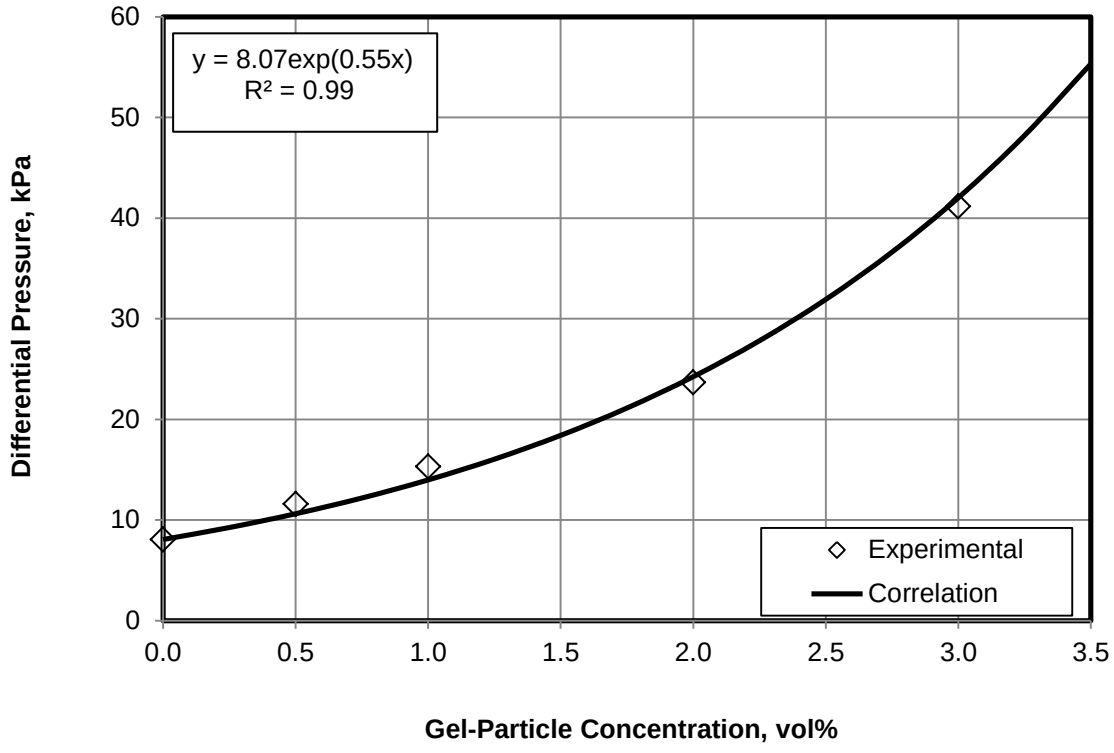

Fig. 5.13: Exponential relationship between gel particle concentration and differential pressure at 100 cm³/hr and 23.5 °C

For low flow rate, the differential pressure increases from 0 to 16.13 kPa by increasing the flow rate from 0 to 50 cm3/h and from 16.13 to 41.15 kPa by increasing the flow rate from 50 to 100 cm3/h. For high flow rate, the differential pressure increases from 41.15 to 75.10 kPa, 75.10 to 92.10 kPa, and 92.10 to 98.19 kPa by increasing the flow rate from 100 to 200 cm3/h, 200 to 280 cm3/h, 280 to 400 cm3/h, respectively. These results show that for the high flow rate, the differential pressure does not increase as much as the injection flow rate. Increasing the flow rate leads to an increase in the hydrodynamic lift force, which causes a decrease in the particles deposition over the pore surface and an enhancement in the release of particles from the pore surface; consequently, plugging decreases and the increase in the differential pressure decreases (Baghdikian et al., 1989). For the high flow rate, the percentage of larger particles that are trapped at the pore throat or deformed and then captured at the pore surface decreases as the flow rate increases. **Fig. 5.14** shows the relationship between injection flow rate and differential pressure across the proppant pack. The following relationship correlates the experimental data satisfactorily:

$$\Delta P = 6.65 - 6.65\exp(0.0001q) + 115\left(\frac{q^{1.80}}{q^{1.80} + 7136}\right), R^2 = 1 \qquad (5.2)$$

where ΔP indicates differential pressure across proppant pack, in kPa, and q is injection flow rate, in cm³/hr. The empirical parameters -6.65 and 0.0001 were determined first by applying Eq. B-1, given in Appendix B, and then the empirical parameters 1.80, 115, and 7136 were determined by applying Eq. B-2 given in Appendix B, as shown in **Figs. C.1** and **C.2** in Appendix C.

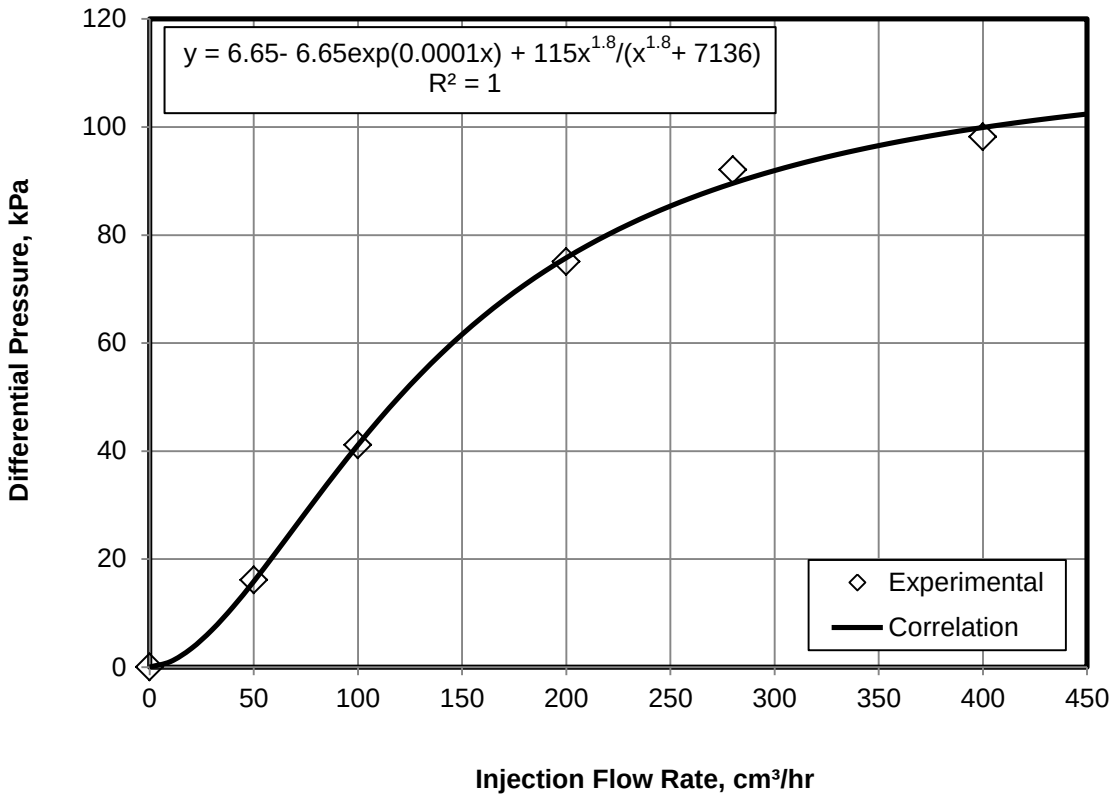

Fig. 5.14: The relationship between injection flow rate and differential pressure at 3 vol% and 23.5 °C

The differential pressure increases from 27.40 kPa to 50.01 kPa by increasing the average particle size from 50 µm to 140 µm because the amount of the pores that are plugging by the gel particles increases with increase in particle size. **Fig. 5.15** shows the relationship between the gel-particle diameter and differential pressure across the proppant pack. The following relationship correlates the experimental data satisfactory.

$$\Delta P = 122\left(\frac{D_p}{D_p + 265}\right) + 8.07, R^2 = 1 \qquad (5.3)$$

where ΔP indicates differential pressure across proppant pack, in kPa, and D_p is the gel-particle diameter, in µm. The empirical parameters 122 and 265 were determined by

applying Eq. B-3, given in Appendix B, as shown in **Fig. C.3** in Appendix C.

These simple empirical correlations can be used to predict the differential pressure across the proppant pack for a similar material and operation conditions at any gel particle concentration, flow rate, or gel-particle diameter because the regression coefficients (R^2) of these relationships are high (0.99- 1).

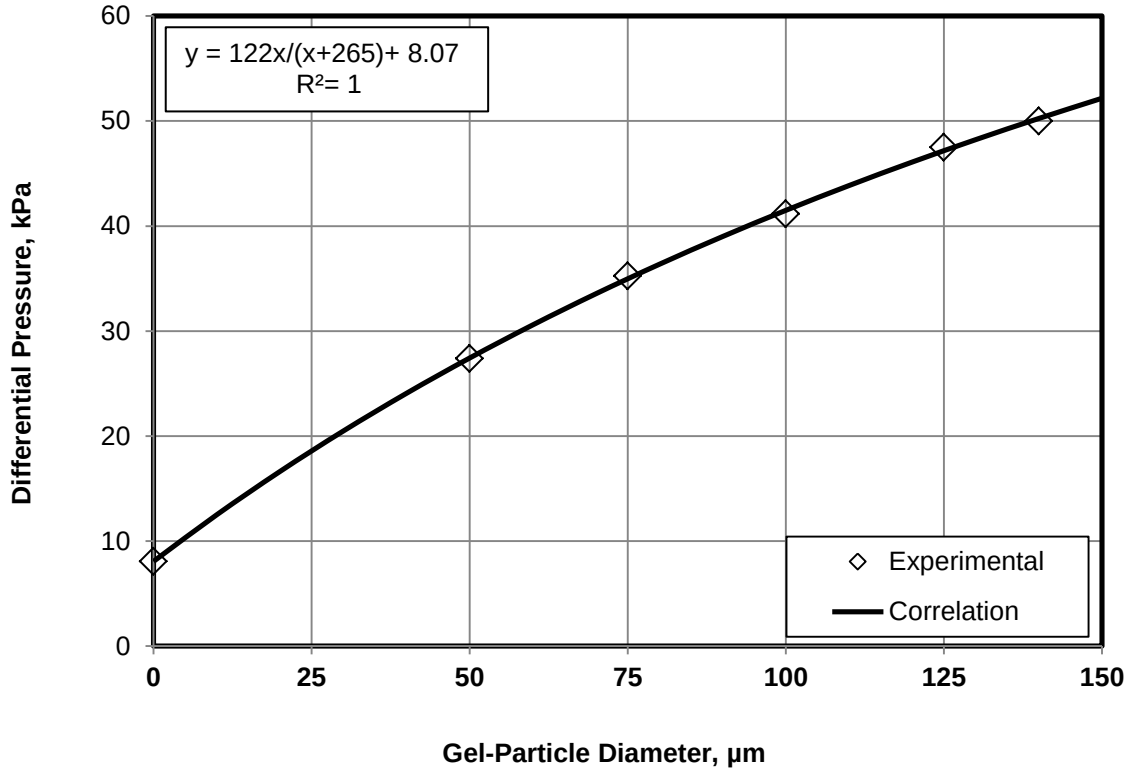

Fig. 5.15: The relationship between gel-particle diameter and differential pressure at 100 cm³/hr and 23.5 °C

It is very important to know the change in the differential pressure during the gel-particle-suspension injection because the differential pressure was built up by the plugging of the pores, thus reducing the high permeability of porous media. Therefore, the parameters that give higher differential pressure should be used to achieve a successful field applications of gel-particle-suspension injection for treating the

reservoir permeability heterogeneity to avoid the loss of circulation during a drilling operation and control water production in mature waterflooded oil fields.

5.3.3 Permeability impairment (reduction)

The permeability reduction increased from 0.81 at 0.5-vol% suspension concentration to 0.36 at 3-vol% suspension concentration because the tendency of plugging increased with particle concentration**. Fig. 5.16** shows the relationship between gel-particle concentration and permeability reduction at 100-cm³/hr flow rate and ambient temperature of 23.5 °C. The following relationship correlates the experimental data satisfactorily:

$$\frac{K}{K_o} = 1 + 5.55\left(\frac{C_p^{0.64}}{C_p^{0.64} - 19.42}\right), R^2 = 1 \qquad (5.4)$$

where (K/K_o) indicates the permeability reduction (dimensionless) and C_p is gel-particle concentration, vol%. The empirical parameters 0.64, 5.55 and -19.42 were determined by applying Eq. B-4 given in Appendix B, as shown in **Fig. C.4** in Appendix C.

Fig. 5.17 shows the exponential relationship between the injection flow rate of 3-vol% suspension and the permeability reduction at ambient temperature of 23.4 °C. The permeability reduction increases for the low flow rate and decreases for the high flow because of the hydrodynamic force and the viscosity. The following exponential relationship correlates the experimental data satisfactorily.

$$\frac{K}{K_o} = 0.80\exp(-0.022q) + 0.20\exp(0.0028q), R^2 = 0.98 \qquad (5.5)$$

where (K/Ko) indicates permeability reduction (dimensionless) and q is injection flow rate, in cm^3/hr.

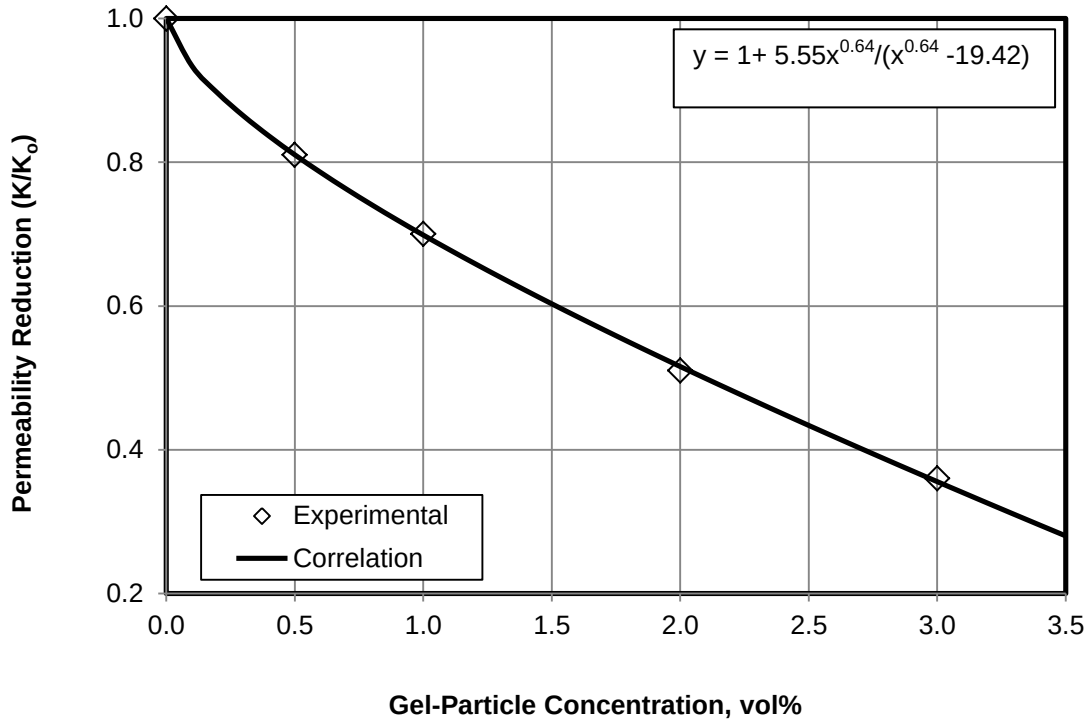

Fig. 5.16: The relationship between gel particle concentration and permeability reduction at 100 cm^3/hr and 23.5 ˚C

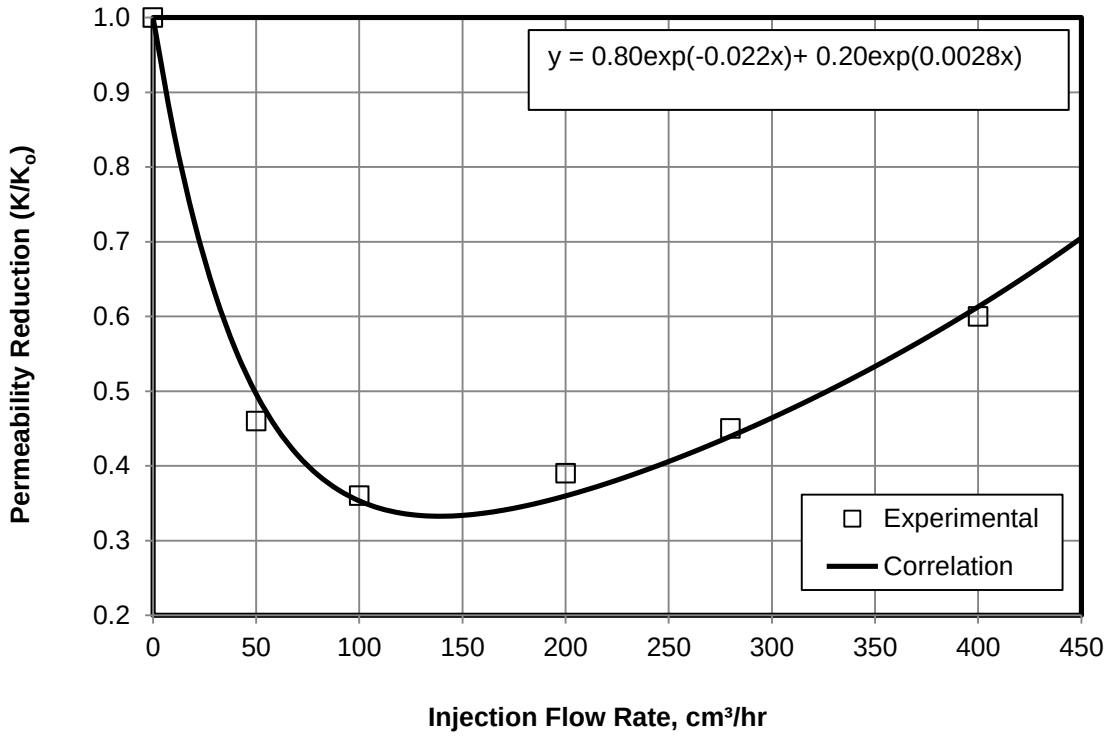

Fig. 5.17: Exponential relationship between injection flow rate of 3 vol% suspension and permeability reduction at T= 23.5 °C

The permeability reduction increases from 0.54 to 0.30 with increasing average particle size from 50 µm to 140 µm because the amount of pores that are plugging by the gel particles increases with increase in particle sizes. **Fig. 5.18** shows the relationship between the gel particle diameter and the permeability reduction at 100 cm³/hr flow rate and ambient temperature of 23.5 °C. The following relationship correlates the experimental data satisfactory.

$$\frac{K}{K_o} = 1 - 0.80\left(\frac{D_p^{1.60}}{D_p^{1.60} + 389}\right), R^2 = 1 \qquad (5.6)$$

where K/K_o indicates permeability reduction (dimensionless) and D_p is gel-particle diameter, in µm. The values of the empirical parameters were determined by applying Eq. B-4 given in Appendix A, as shown in **Fig. C.5** in Appendix C.

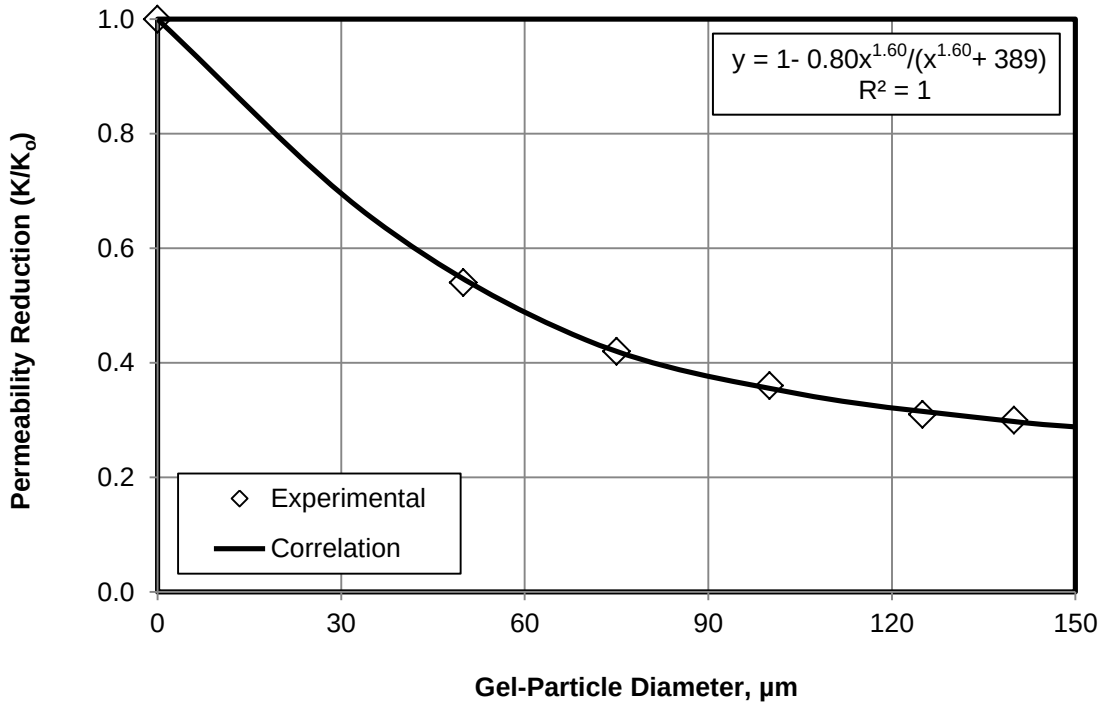

Fig. 5.:18 The relationship between gel particle diameter and permeability reduction at 100 cm³/hr and 23.5 °C

Another proppant pack with 3600-md permeability, 34% porosity, and 59 µm pore- throat size was used to study the variation of permeability reduction with particle diameter/pore-throat size for different suspensions. **Fig. 5.19** shows the relationship between particle diameter /pore-throat size and the permeability reduction at 100 cm³/hr flow rate and ambient temperature 23.5 °C. The following relationship correlates the experimental data satisfactory:

$$\frac{K}{K_o} = 1 - 0.77\left(\frac{\left(D_P / D_T\right)^{1.80}}{\left(D_p / D_T\right)^{1.80} + 0.126}\right), R^2 = 1 \qquad (5.7)$$

where (K/Ko) indicates permeability reduction (dimensionless) and D_p/D_T particle diameter /pore-throat size (dimensionless). The values of the empirical parameters were

determined by applying Eq. B-4 given in Appendix B, as shown in **Fig. C.6** in Appendix C.

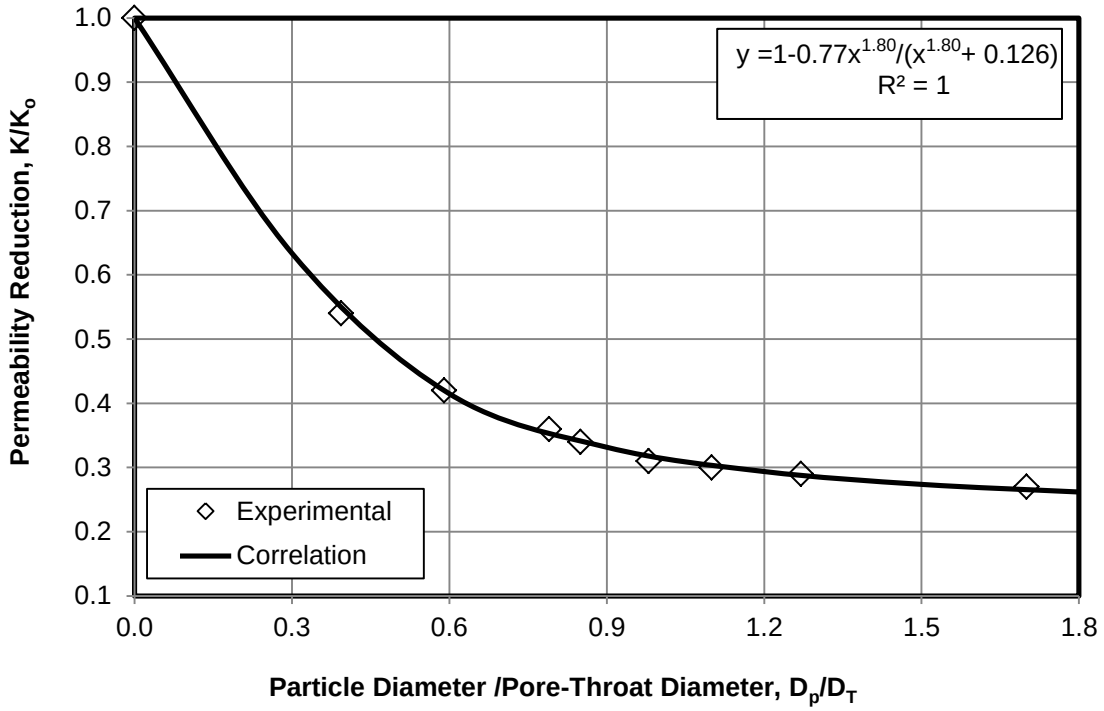

Fig. 5.19: Variation of permeability reduction with particle diameter to pore-throat size for different suspensions at 100 cm³/hr

These empirical correlations can be used to predict the permeability reduction across the proppant pack for a similar material and the operation conditions at any gel-particle concentration, flow rate, gel-particle diameter or particle diameter/pore-throat size because the regression coefficients (R^2) of these correlations are high (0.98- 1). The permeability reduction of the porous media was caused from the plugging of the pores by the gel particles. Therefore, the parameters that lead to the best plugging of the pores and the best reducing of the high permeability of the formations should be used for successful field applications of treating the reservoir permeability heterogeneity to avoid the loss of circulation during a drilling operation and control water production in

mature waterflooded oil fields having highly permeable zones.

5.3.4 Resistance factor

Fig. 5.20 shows the relationship between the gel-particle concentration and resistance factor. The resistance factor is the ratio of the water mobility (K_w/μ_w) before suspension injection to the suspension mobility (K/μ) during suspension injection at the same flow rate (Littmann 1988):

$$F_r = (K_w / \mu_w)/(K / \mu) \tag{5.8}$$

Where F_r indicates the resistance factor (dimensionless); K_w is the effective water permeability, in md; μ_w is the water viscosity, in Pa.s; K is the suspension permeability, in md; and μ is the suspension viscosity, in Pa.s. The resistance factor increased from 4.3 at suspension concentration of 0.5 vol% to 15.3 at suspension concentration of 3 vol%. This means that an increase in plugging of the pores occurs when the suspension concentration increases. The following relationship correlates the experimental data satisfactory.

$$F_r = 0.62 + 8\left(\frac{C_p}{C_p + 0.80}\right) + 0.38\exp\left(0.66C_p{}^{1.40}\right), R^2 = 1 \tag{5.9}$$

where F_r indicates resistance factor (dimensionless) and C_p is gel-particle concentration, vol%. This correlation was obtained by regression of a weighted-sum combination of Eqs. B-5 and B-6, both given in Appendix B, as shown in **Figs. C.7** and **C.8** in Appendix C.

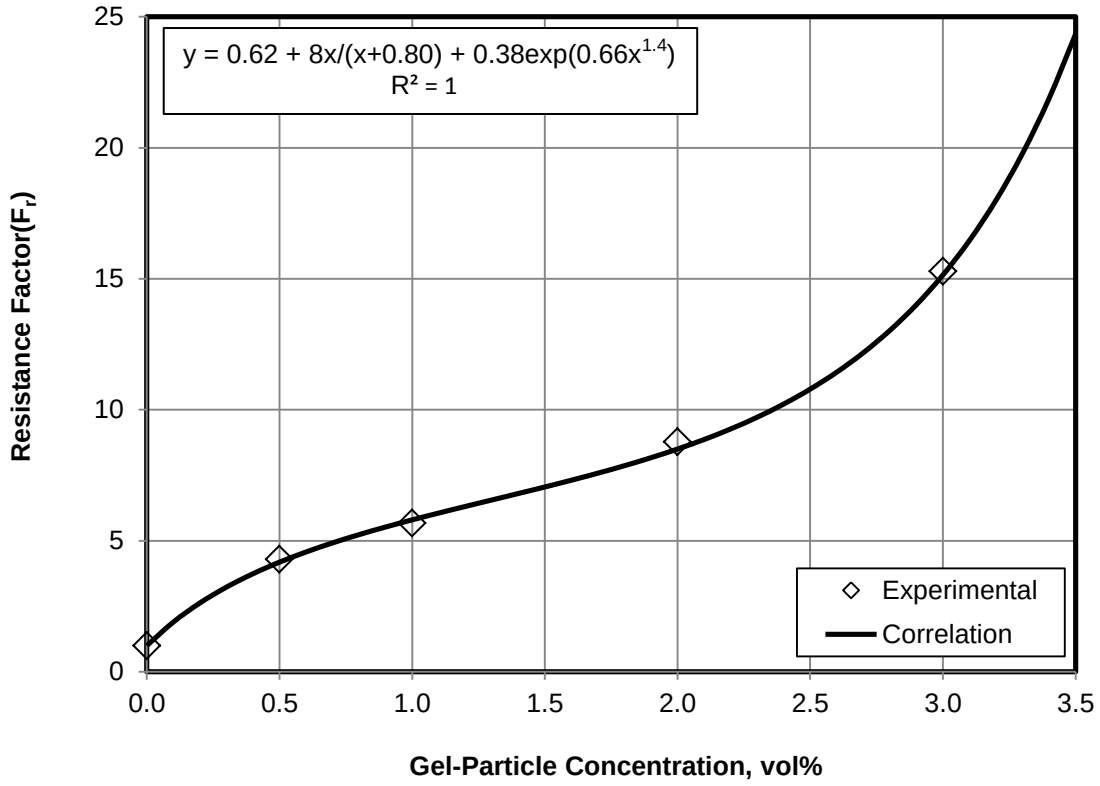

Fig. 5.20: Polynomial relationship between gel-particle concentration and resistance factor at 100 cm³/hr and 23.5 °C

Fig. 5.21 shows the relationship between injection flow rate and resistance factor. The resistance factor increases for the low flow rate and decreases for the high flow rate because of the hydrodynamic force and the viscosity, the resistance factor increased from 12.01 to 15.29 when the flow rate increased from 50 cm³/hr to 100 cm³/hr and the resistance factor decreased from 15.3 to 9.1 when the flow rate increased from 100cm³/hr to 400cm³/hr. The following relationship correlates the experimental data satisfactorily.

$$F_r = -16 + 22\left(\frac{q}{q+38}\right) + 16\exp\left(-75E-07q^2\right), R^2 = 0.99 \qquad (5.10)$$

where F_r indicates resistance factor (dimensionless) and q is injection flow rate, in

cm³/hr. This correlation was obtained by regression of a weighted-sum combination of Eqs. B-6 and B-7, both given in Appendix B, as shown in **Figs. C.9** and **C.10** in Appendix C.

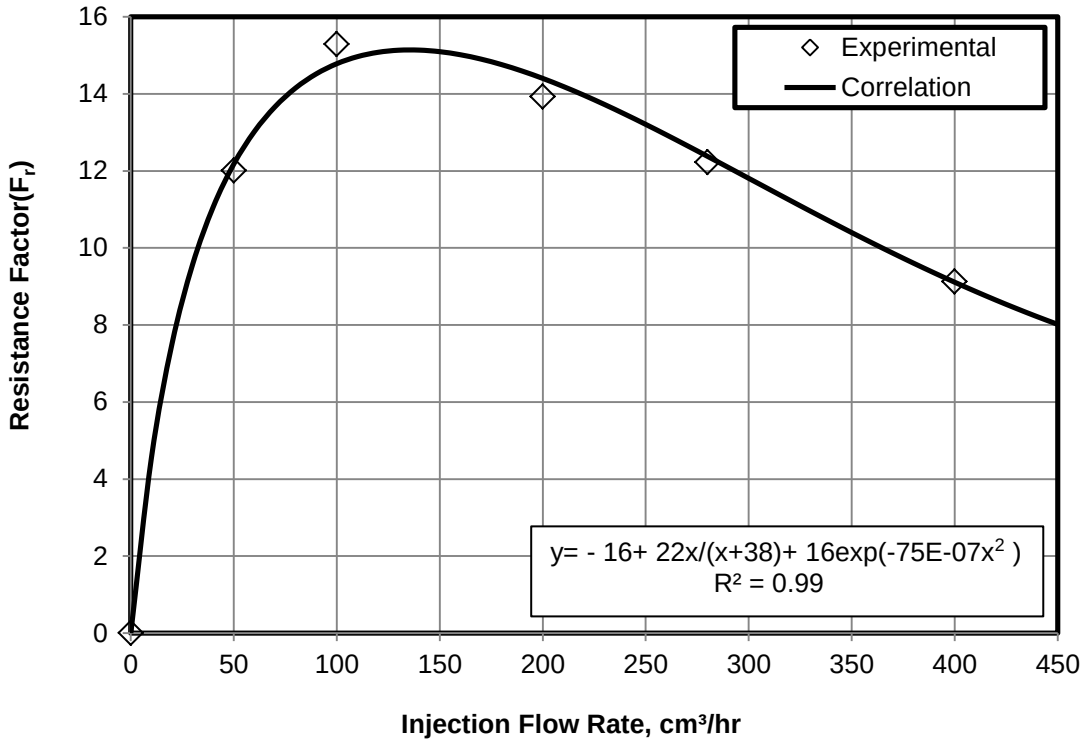

Fig. 5.21: The relationship between injection flow rate and resistance factor at 3 vol% and 23.5 °C

Fig. 5.22 shows the relationship between gel-particle diameter and resistance factor. The resistance factor increases from 15.3 to 17.7 by increasing the gel particle diameter from 100 µm to 125 µm because the plugging of the pores increases as the gel-particle diameter increases. The following relationship correlates the experimental data satisfactory.

$$F_r = 1 + 35.09\left(\frac{D_p}{D_p + 141.62}\right), R^2 = 1 \qquad (5.11)$$

where F_r indicates resistance factor (dimensionless) and D_p is gel-particle diameter, in μm. The empirical parameters of this correlation were determined by applying Eq. B-5 given in Appendix B, as shown in **Fig. C.11** in Appendix C.

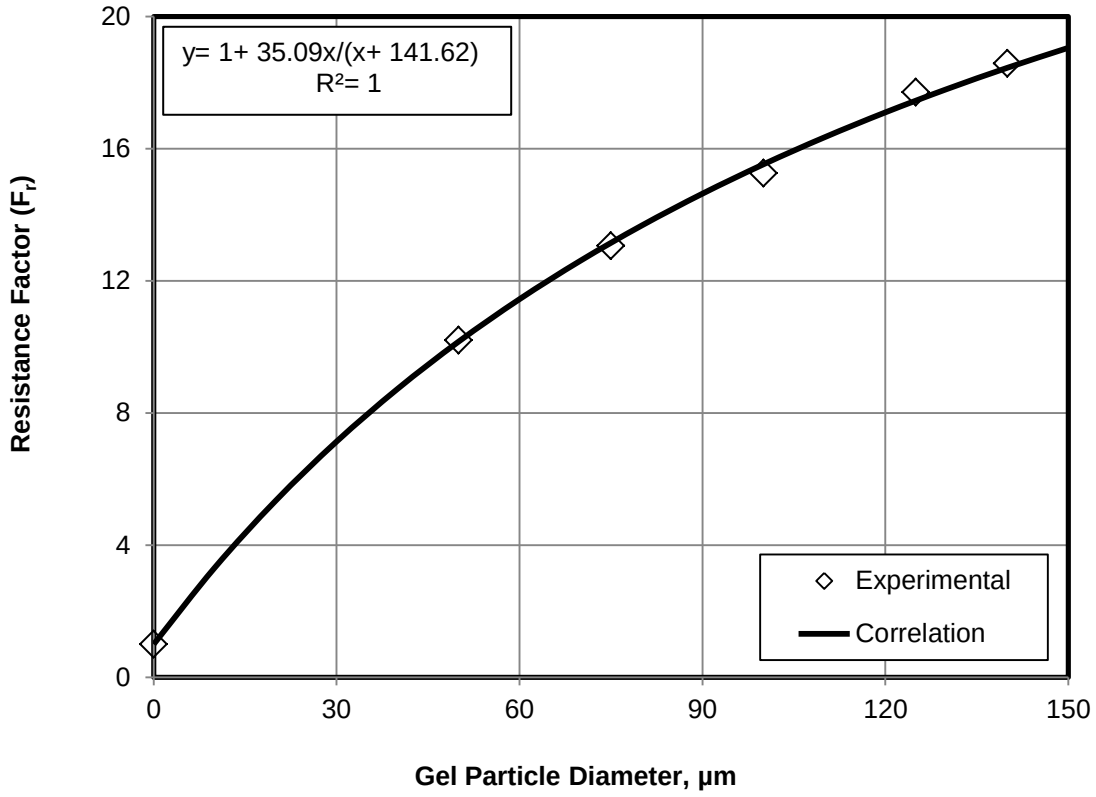

Fig. 5.22: The relationship between gel particle diameter and resistance factor at 100 cm³/hr and 23.5 °C

These correlations can be used to predict the resistance factor across the proppant pack for a similar material and the operation conditions at any gel-particle concentration, flow rate, or gel-particle diameter because the regression coefficients (R^2) of these correlations are high (0.99- 1). According to the definition of the resistance factor, high resistance factor means that there was a high reduction in the permeability of the porous media. Therefore, the parameters that lead to higher resistance factor should be chosen to achieve successful application of gel-particle-suspension injection

for field applications to avoid the loss of circulation during a drilling operation and control water production in mature waterflooded oil fields having highly permeable zones.

5.4 Plugging Criteria Correlated by Use of Dimensionless Groups

The experimental data generated in this study illustrate the effect of particle concentration, flow rate, and pore-throat/particle size ratio on the plugging mechanisms. To determine the conditions that lead to pore plugging (i.e., the plugging criteria), two dimensionless variables and the power- law and exponential-law equations presented by Civan (2000, 2007a) were applied to correlate the measured data:

$$\beta = D_T / D_P \tag{5.12}$$

$$R_{ep} = C_P \nu D_P / \mu \tag{5.13}$$

$$\beta = A_1 R_{ep}^{B_1} + C_1 \tag{5.14}$$

$$\beta = A_2 \left[1 - \exp\left(-B_2 R_{ep}^{\lambda}\right)\right] + C_2 \tag{5.15}$$

Eq. 5.15 is a modified form of the exponential- law equation presented by Civan (2000, 2007a). Here, β indicates the pore-throat/particle-diameter ratio, which is the first dimensionless variable; R_{ep} is the particle Reynolds number which is the second dimensionless group of variables; C_p is the particle concentration in the suspension; μ is the viscosity of the suspension; ν is the velocity of the particles (assuming the particle velocity is equal to the suspension velocity); λ is an empirical exponent; A_1, A_2, B_1,

B_2, C_1, and C_2 are the empirical fitting parameters; D_T is the average pore-throat diameter; and D_p is the average particle diameter calculated as:

$$(D_P)_{avg} = \frac{\sum_{i=1}^{n} \sigma_i (D_P)_i}{\sum_{i=1}^{n} \sigma_i} \tag{5.16}$$

where σ_i is the volume fraction of particle i; and $(D_p)i$ is the diameter of particle i.

Eqs. 5.14 and 5.15 describe the occurrence of pore plugging with certain fluid/ particle conditions such as the particle concentration, fluid viscosity, pore-throat/ particle diameter ratio, and fluid velocity. Applying the power- law and exponential-law correlations of the two dimensionless groups, a correlation curve can be developed with two regions. The region above the curve represents the non-plugging conditions, and region below the curve represents the plugging conditions. The physical meaning of the coefficient C is that the plugging always occurs when $0<D_T/D_p<1$ (the particle size equal to or greater than pore-throat size), so C in Eqs. 5.14 and 5.15 assumes a value of unity. However, this physical interpretation is not always valid because the deformable gel particles with diameter greater than pore-throat size may be able to squeeze and move through a pore throat. The empirical parameters A_1, B_1, C_1, A_2, B_2 and C_2 and the empirical exponent λ were determined by using the linearized forms of Eqs. B-8 and B-9 given in Appendix B. The best straight- line that matches the experimental data was obtained by the method of least squares, and the values of the fitting parameters were determined as the highest coefficient of regression of this straight line, as shown in **Table 5-1** and **Figs. D.1** and **D.2** in Appendix D. **Figs. 5.23** and 5.**24** present the successful power- law and exponential correlations, respectively, of the experimental data by use of the gel suspensions of different particle concentrations and different

average particles diameter. The regression coefficients of the experimental data are 0.97 for the power- law and 0.96 for the exponential- law. The power- law and exponential correlations curves, given in Figs. 5.23 and 5.24, respectively, indicate that no plugging occurs if $\beta > 1.35$ at any value of R_{ep} because all the points are above the curve. Pore plugging occurs at low particle concentration when β is close to 1.0. Thus, the condition can change from non-plugging to plugging position by a small increase in particle concentration in the range of $1<\beta<1.35$. According to the correlations of the dimensionless groups, the plugging occurs under certain conditions of particles concentration, flow rate, and pore-throat/ particle diameter ratio. Pore plugging induces permeability reduction, thus the dimensional analysis can assist in determining the functional trends of the correlations of the present experimental data, such as the differential pressure, the permeability reduction, and the resistance factor.

TABLE 5-1: BEST- ESTIMATE FITTING PARAMETERS

Model	Parameters (dimensionless)				
Power- Law	$A_1 = 54$	$B_1 = 0.511$	$C_1 = 1.00$		$R^2 = 0.97$
Exponential- Law	$A_2 = 690$	$B_2 = -0.07$	$C_2 = 1.00$	$\lambda = 0.50$	$R^2 = 0.96$

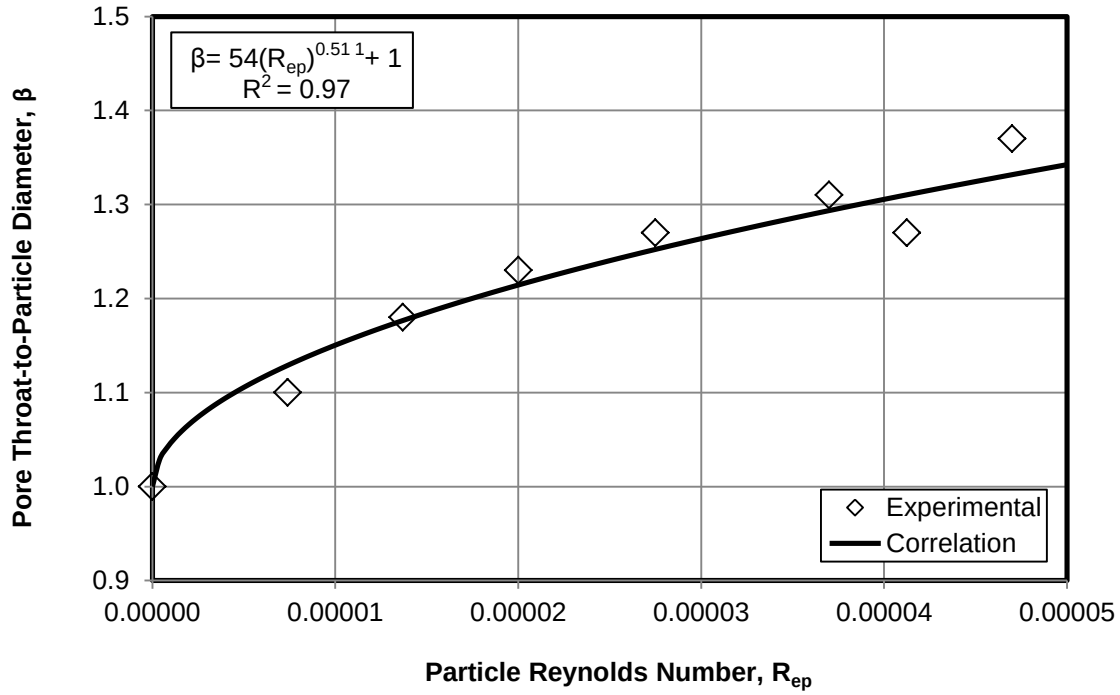

Fig. 5.23: Experimental and correlation results from power- law model as a function of particle Reynolds number

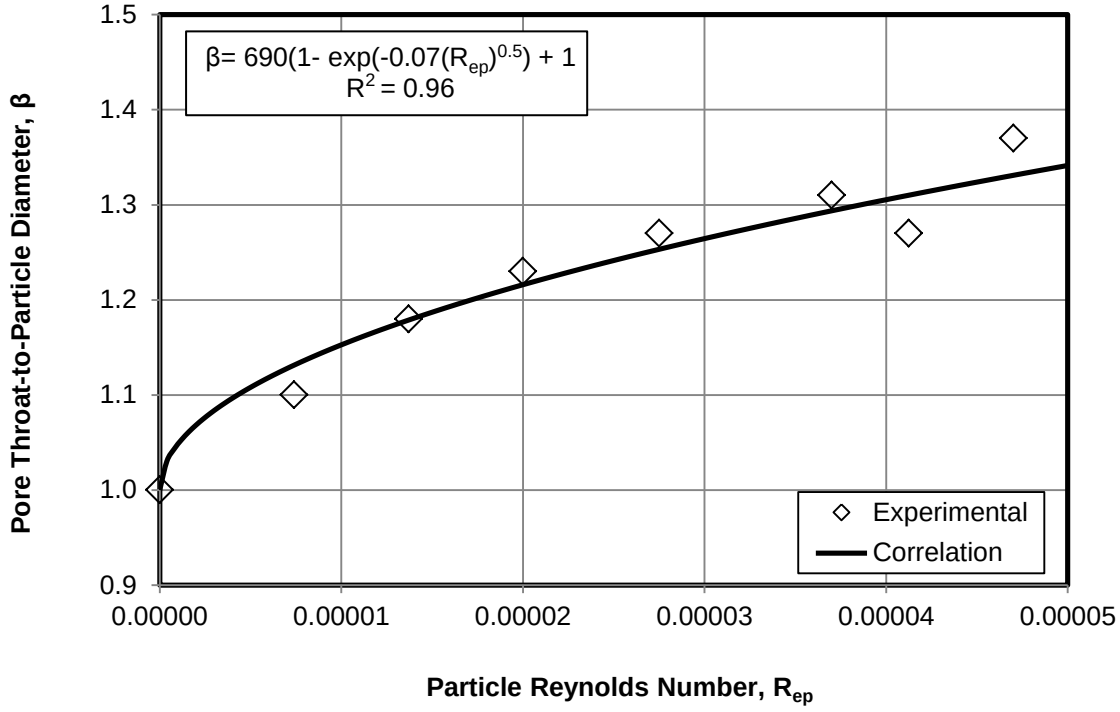

Fig. 5.24: Experimental and correlation results from exponential- law model as a function of particle Reynolds number

5.5 Identification of Particle Retention Mechanisms

Wojtanowicz et al. (1987) proposed a quantitative approach for analyzing the single-fluid phase formation-permeability-reduction trends because of fine-particles invasion and deposition. Three different mechanisms of particulate injection processes were recognized, and the corresponding diagnostic equations were derived for these mechanisms by assuming that one mechanism dominates at a time of suspension injection, as summarized in **Table 5-2**. These three mechanisms are (a) pore-surface deposition in which gradual pore reduction occurs when particle size smaller than pore-throat size; (b) pore-throat plugging in which single pore blocking occurs when the particle size is comparable or larger than the average size of the pore throat; and (c) pore filling, which occurs as a result of internal filter cake (neglecting the external cake) (Civan 2007a). The fundamental assumptions of the method of Wojtanowicz et al. (1987) are homogeneous formation and constant flow rate, low solid concentration, and pore-volume reduction caused by particle capture, but neglecting the gravity effect.

TABLE 5-2: WOJTANOWICZ ET AL. (1987) DIAGNOSTIC EQUATIONS

Permeability Reduction Mechanisms	Diagnostic Equations	Straight Line Plotting Scheme
Pore surface deposition	$(K/K_o)^{½} = 1- C_3t$	$(K/K_o)^{½}$ vs. t
Pore throat plugging	$K/K_o = 1- C_4t$	K/K_o vs. t
Pore filling	$K_o/K = 1+ C_5t$	K_o/K vs. t

Figs. 5.25 and **5.26** present the permeability-change tendency during the injection of gel particles into the proppant pack. These figures show a wavy-shape trend

for alteration of permeability observed during the experiments, indicating the occurrence of consecutive plugging and unplugging phenomena. Thus, the gel particles in the suspension tend to be captured at the small pore throats initially, then the gel particles with diameter larger than the pore-throat sizes are diverted to the larger unplugged pore throats and accumulate behind them, leading to generation and building up of high differential pressure. This differential pressure causes deformation of the gel particles captured at some pore throats and induces them to pass through these pores. After the deformation and passing of these gel particles, the process of pressure build up by particle accumulation begins again until the gel particles deform and pass through the pore throat once more. The frequent plugging and unplugging processes continue until a steady flow at a constant differential-pressure and permeability reduction level is attained, at which the gel-particle-suspension injection process should be terminated.

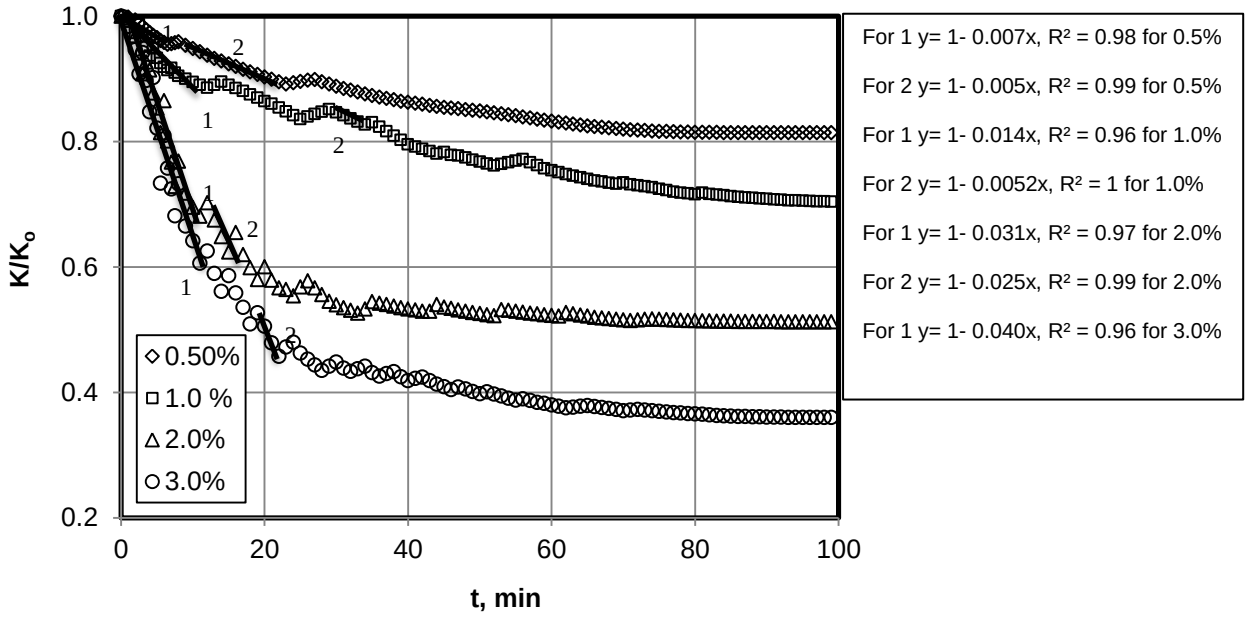

Fig. 5.25: Pore-throat-plugging mechanism for different particle concentrations at 100 cm³/hr and 23.5 °C

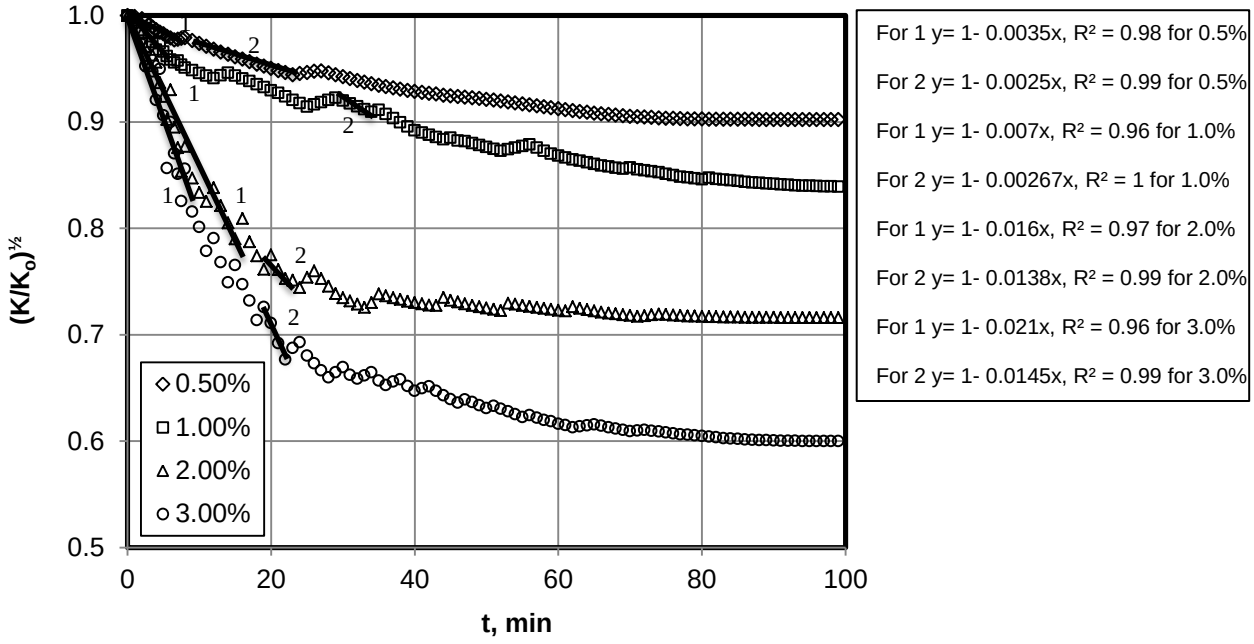

Fig. 5.26: Pore-surface-deposition mechanism for different particle concentrations at 100 cm³/hr and 23.5 °C

The diagnostic equations of Wojtanowicz et al. (1987) consider an initial condition that $K/K_o = 1.0$ at $t = 0$. Therefore, they can be applied over various regions only after shifting the time so that the initial reference time considered in our data analysis becomes zero for each consecutive period. Figs. 5.25 and 5.26 represent the straight- line plotting of the diagnostic equations of the pore-throat-plugging mechanism and the pore-surface-deposit mechanism for regions 1 and 2 for different gel-particle-suspension concentrations (0.5 , 1, 2, and 3 vol%) at a constant flow rate of 100 cm³/hr and ambient temperature of 23.5 °C. These figures indicate that the pore-throat-plugging mechanism and the pore-surface-deposition mechanism are dominant, indicated with high regression coefficients. **Tables 5-3 and 5-4** show that the values of the rate-constants of the plugging regions increase with particle concentration because the amount of particles that are trapped at the pore throats or deformed and then captured at

the pore surface increases when the concentration increases. The pore filling dose not occur because an internal filter cake cannot be formed in the proppant pack.

TABLE 5-3: RATE CONSTANTS OF PLUGGING REGIONS FOR PORE-THROAT- PLUGGING MECHANISM AT DIFFERENT PARTICLE CONCENTRATIONS

Particle Concentrations (vol%)	Regions	Rate Constants (min ⁻¹)	R^2
0.5	1	0.0070	0.98
0.5	2	0.0050	0.99
1.0	1	0.0140	0.96
1.0	2	0.0052	1.00
2.0	1	0.0310	0.97
2.0	2	0.0250	0.99
3.0	1	0.0400	0.96
3.0	2	0.0248	0.99

TABLE 5-4: RATE CONSTANTS OF PLUGGING REGIONS FOR PORE-SURFACE -DEPOSITION MECHANISM AT DIFFERENT PARTICLE CONCENTRATIONS

Particle Concentrations (vol%)	Regions	Rate Constants (min ⁻¹)	R^2
0.5	1	0.0035	0.98
0.5	2	0.0025	0.99
1.0	1	0.0070	0.96
1.0	2	0.0026	1.00
2.0	1	0.0160	0.97
2.0	2	0.0138	0.99
3.0	1	0.0210	0.96
3.0	2	0.0145	0.99

5.6 Conclusions

The main findings of the present flow tests conducted using 3800- md, 16- to 20-mesh sand packs can be summarized as the following:

- This is a relatively new technology, and, therefore, quantitative evaluation the effect of various factors on the performance of gel-particle applications presented in this study is significant for practical applications of gel-particle-suspension injection. Therefore, important correlations were developed that can assist in controlling plugging in highly permeable formations and treating these formations by reducing the high permeability to avoid loss of circulation during drilling operations and to control water production in mature waterflooded oil fields containing highly permeable zones.

- Consecutive plugging and unplugging phenomena occur during gel-particle injection into proppant packs. Accumulation of the particles behind the pore throats leads to a differential pressure buildup, and the particles can pass through other pores because of the ability of the gel particles to deform or break, which causes a subsequent reduction in the differential pressure.

- The plugging and unplugging processes continue until a steady flow is attained in which the differential-pressure level and permeability reduction approach constant limit values, at which time the gel-particle-suspension-injection process should be stopped. The values of the rate constants of the plugging regions increase with particle volume concentration because the amount of particles that are trapped at the pore throats or deformed and then captured at the pore surface increases with the gel-particle concentration.

- The gel-particle distribution of the suspensions before and after injection was studied to determine which particles can be trapped and deposited inside the sandpacks, to determine the percentage of these particles, and to demonstrate the permeability reduction effect. Empirical correlations were developed from the gel-particle distribution to predict the cumulative particle distribution at any diameter of the suspended particles for certain conditions.

- Conditions leading to pore plugging in highly permeable formations can be quantified in terms of the relevant dimensionless groups, such as the particle Reynolds number (R_{ep}) and pore-throat/particle size ratio (β). Plugging occurs if the R_{ep} vs. β is in the region indicated below the curve obtained by plotting of the developed empirical correlations.

- The diagnostic equations of Wojtanowicz et al. (1987) can be used for identification of the relevant governing mechanisms of impairment of porous media during the injection of gel-particle suspensions into the sandpacks at different conditions.

Chapter 6: Thermal Effects on Near-Wellbore Formation Treatment by Gel Particles Suspension

This Chapter has been previously published as ‘‘Experimental Investigation and Correlation of Thermal Effects on Near-Wellbore Formation Treatment by Gel Particles’’ in the SPE International Symposium on Oilfield Chemistry, Woodland, TX, 8-10 April, 2013 and is used here by permission.

6.1 Introduction

Temperature plays an important factor in suspended gel particles treatment of high permeability near-wellbore zones because temperature affects the gel particles properties. Thus, temperature is affect the transient behavior of gel particles through porous media by influencing the plugging mechanisms and their rates. Practically, there are no correlations reported that can be used for designing of suspended gel particles placement for near-well bore formation treatment by considering the effect of near-wellbore zone temperatures. For this purpose, an experimental study of thermal effects on conditioning and reducing the high permeability of formations is undertaken to investigate the relevant processes and correlate the experimental results for successful gel particles applications in oil fields.

The effect of temperature on plugging of highly permeable near-wellbore formations is investigated by injection of suspension of gel particles into proppant packs at different temperatures and useful correlations are developed for field applications. The effect of temperature on permeability impairment at various temperatures (23.5 ˚C, 40 ˚C, 60 ˚C, and 75 ˚C) is investigated at a constant 100 cm^3/hr flow rate and a 3 vol% gel particles concentration. Experiments are conducted using unconsolidated plastic

glass proppant packs. The resulting pressure differentials across the proppant pack are measured during the experiments and the permeability reductions and resistance factors are inferred by the variation of differential pressures with time. Further, we investigate the mechanisms of plugging and unplugging phenomena during the injection of gel particles into the proppant pack at various temperatures. The permeability reduction increases during plugging and decreases during unplugging. The plugging and unplugging processes occur repetitively over consecutive periods of times. The frequency of the plugging and unplugging regions decreases by increase in temperature. The rate constants of plugging and unplugging processes are determined at various temperatures. The experimental data of the differential pressure, permeability reduction, and resistance factor, and the rate constants determined at various temperatures are correlated by using Vogel-Tammann- Fulcher (VTF) - type equations similar to Civan (2008, 2011a). Excellent agreement is observed between the experimental data and the correlations. Hence, these correlations can be used to predict the effect of temperature on conditioning of the high permeability formations by means of injection of suspension of gel particles.

6.2 Experimental Results, Data Analyses, and Discussion

Differential pressure build up is a key issue during the gel particle suspension injection by plugging of the pores and thus reducing the high permeability and increasing the resistance factor of porous media. Therefore, it is very important to study the effect of temperature on the differential pressure during the gel particle suspension injection because higher differential pressure should be attained to achieve a successful

field applications of the gel particle suspension injection to treat the reservoir permeability heterogeneity and thus prevent the loss circulation during a drilling operation and control the water production in waterflooded mature oil fields. The empirical correlations for the viscosity, differential pressure, and permeability reduction and resistance factor across proppant pack are developed from the experimentally measured data at different temperatures. It is demonstrated that these equations can represent the measured and experimental data satisfactorily over the range of the experimental conditions.

Several tests were carried out in which the flow rate of the injected suspension and the concentration of gel particles in the injected suspension were kept constant at 100 cm^3/hr and 3 vol%, respectively, but the temperature of the proppant pack was varied at 23.5 ˚C, 40 ˚C, 60 ˚C, and 75 ˚C in each experiment in order to investigate the effect of temperature on the differential pressure and permeability reduction of the proppant pack. **Fig. 6.1** shows the variation permeability reduction across the proppant pack with pore volumes injected for different temperatures of 23.5 ˚C, 40 ˚C, 60 ˚C, and 75 ˚C at a constant 100 cm^3/hr flow rate and a constant 3 vol% gel concentration. Differential pressure is build up during the injection of the gel particles suspension when particles are trapped at the pore throats causing the gel particles to deform and pass through the pore throats or to be captured across the pores and the injection continues until a constant steady pressure is attained. Fig. 6.1 shows that the permeability reduction decreased from 0.36 to 0.42 by increasing the temperature of the sand pack from 23.5 ˚C to 75 ˚C. This happened because the gel particles became softer and deformable by temperature and the degree of pore-throat plugging and pore-

surface deposition decreased. Consequently, the gel particles were able to pass through the pore easily at high temperature and plugging of pores becomes less pronounced at increasing temperatures. Thus, the differential pressure decreased from 41.15 kPa to 22.68 kPa when the temperature increased from 23.5 ˚C to 75 ˚C. Also, for a constant flow rate and concentration, the suspension viscosity decreases from 0.0055 Pa.s to 0.0035 Pa.s when the temperature increased from 23.5 ˚C to 75 ˚C. This causes a decrease in the differential pressure and permeability reduction.

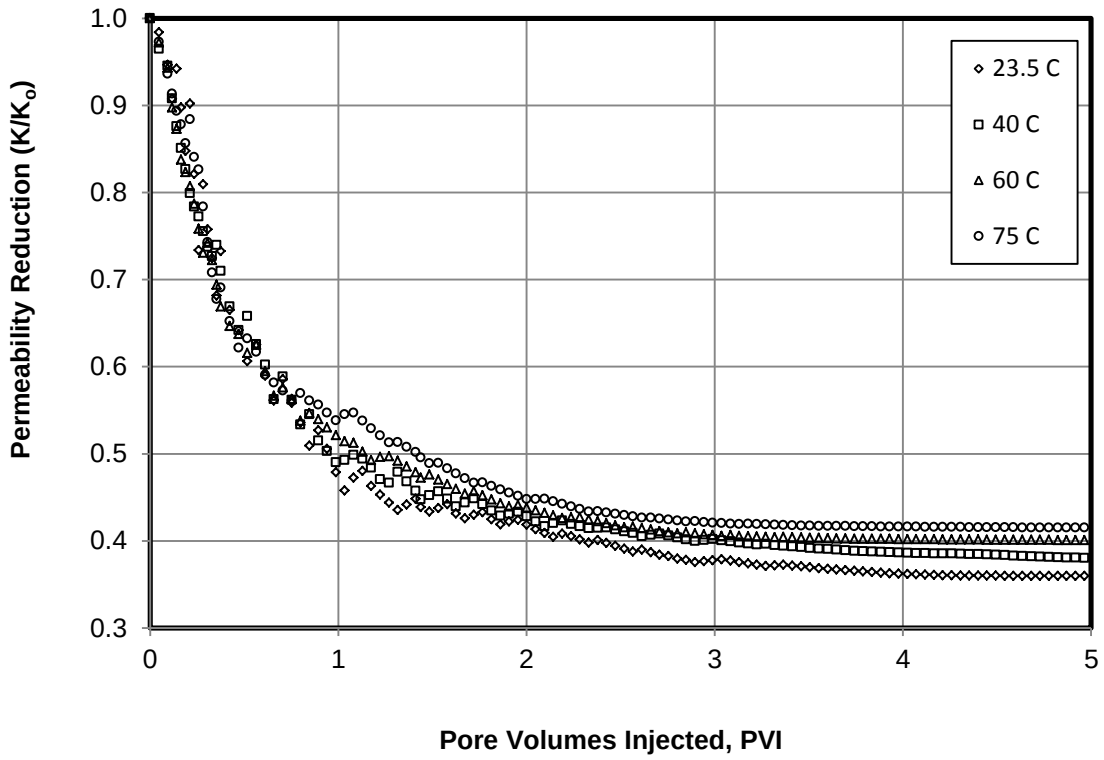

Fig. 6.1: Permeability reduction at 3 vol% concentration for different temperatures at 100 cm^3/hr

6.3 Correlation of Measurements

Several empirical correlations of practical importance are developed from the experimental data at different temperatures for effective design of the suspended gel particles treatment in weak and highly permeable near- wellbore formations. The empirical correlations will be developed by using a VTF- type equation. The results are compared to measured and experimental data to determine the reliably for design of treatment of highly permeable formations by gel particles under different temperature

The Vogel- Tammann- Fulcher-type equations (VTF) are widely used to correlate the experimental data for the temperature dependent parameters (Vogel 1921; Tammann and Hesse 1926; Fulcher 1925). Civan (2004, 2005, 2006a and b, 2007b and c, and 2008, 2010) described the VTF equation as an asymptotic exponential function in the following general form:

$$\ln f = \ln f_c - \frac{C}{T - T_c} \qquad (6.1)$$

where f is a temperature dependent parameter (unit determined by the type of property); f_c is a pre- exponential coefficient (unit determined by the type of property); T is the actual temperature, K; T_c is the critical temperature, K; and C is defined as E/Rg, where E is the activation energy (J/kmol), and R_g is the universal gas constant (J/kmol- K). f_c, T_c, and C are the fitting constants and are determined by using the special least- squares method developed by Monkos (2003) and then trial and error method of T_c is used in the straight- line VTF plot of the experimental data until get the best regression coefficient (R^2) value. The applications of this equation are illustrated in the following. The viscosity of the 3 vol % gel particles suspension decreases from 0.0055 Pa.s to

0.0035 Pa.s by increasing the temperature from 23.5 ˚C to 75 ˚C. The measured data of a 3 vol% concentration gel suspension viscosity is correlated by using the VTF equation, given by:

$$\ln \mu = \ln \mu_c - \frac{C}{T - T_c} \qquad (6.2)$$

where μ is the suspension viscosity, Pa.s; and μ_c is the pre- exponential coefficient of viscosity is 0.03484 Pa.s. The fitting constants T_c and C are 550 K and -465 K, respectively. **Fig. 6.2** shows the straight- line VTF plot of the measured data for the 3 vol% suspension viscosity. **Fig. 6.3** shows comparison between the suspension viscosity values obtained from VTF equation and the measured data.

The differential pressure across the proppant pack decreases from 41.15 kPa to 22.68 kPa by increasing the temperature of the sand pack from 23.5 ˚C to 75 ˚C because the gel particles were able to deform and then pass through the pore throats easily at high temperatures and hence, the amount of particles that deformed and deposited at the pore surface decreases when the temperature increases. Also, the viscosity of the suspension decreases from 0.0055 Pa.s to 0.0035 Pa.s by increasing the temperature from 23.5 ˚C to 75 ˚C which leads to a decrease in the differential pressure. The experimental data of the differential pressure across the proppant pack is correlated by using the VTF equation, given by:

$$\ln \Delta P = \ln \Delta P_c - \frac{C}{T - T_c} \qquad (6.3)$$

where ΔP is the differential pressure across proppant pack, kPa; and ΔP_c is the pre-

exponential coefficient of differential pressure is 2703 kPa. The fitting constants T_c and C are 700 K and -1685 K, respectively. **Fig. 6.4** shows the straight- line VTF plot of the experimental data for the differential pressure across proppant pack. **Fig. 6.6** shows comparison between the differential pressure values obtained from VTF equation and the experimental data.

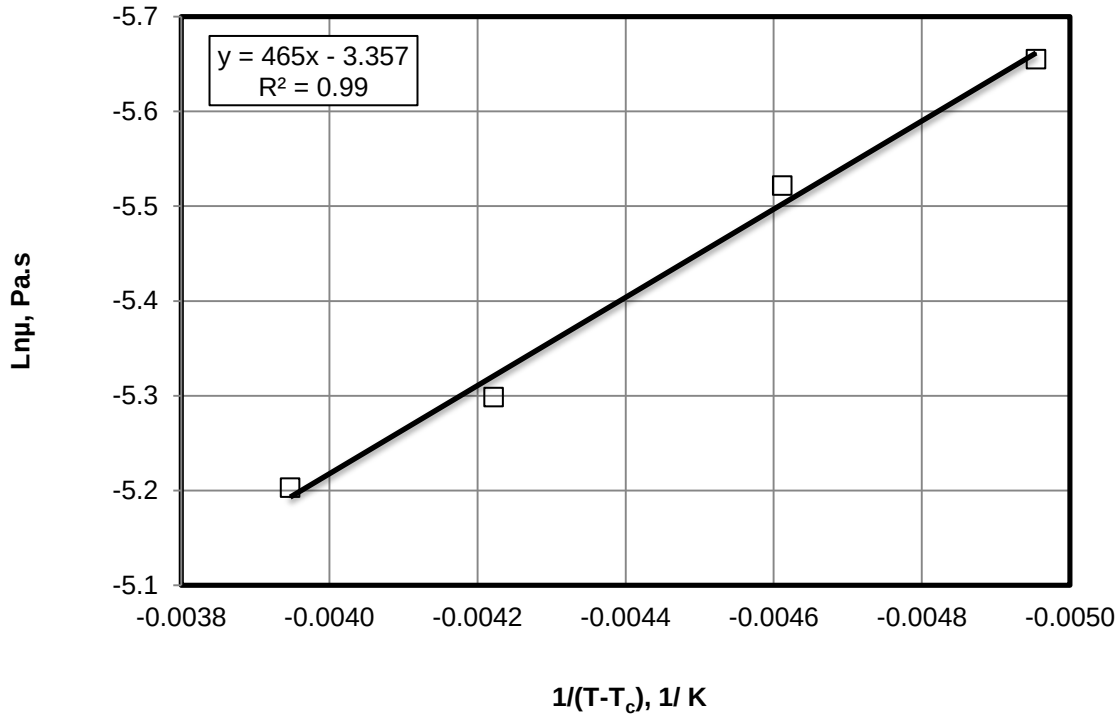

Fig. 6.2: Straight- line VTF plot for the 3 vol% suspension viscosity

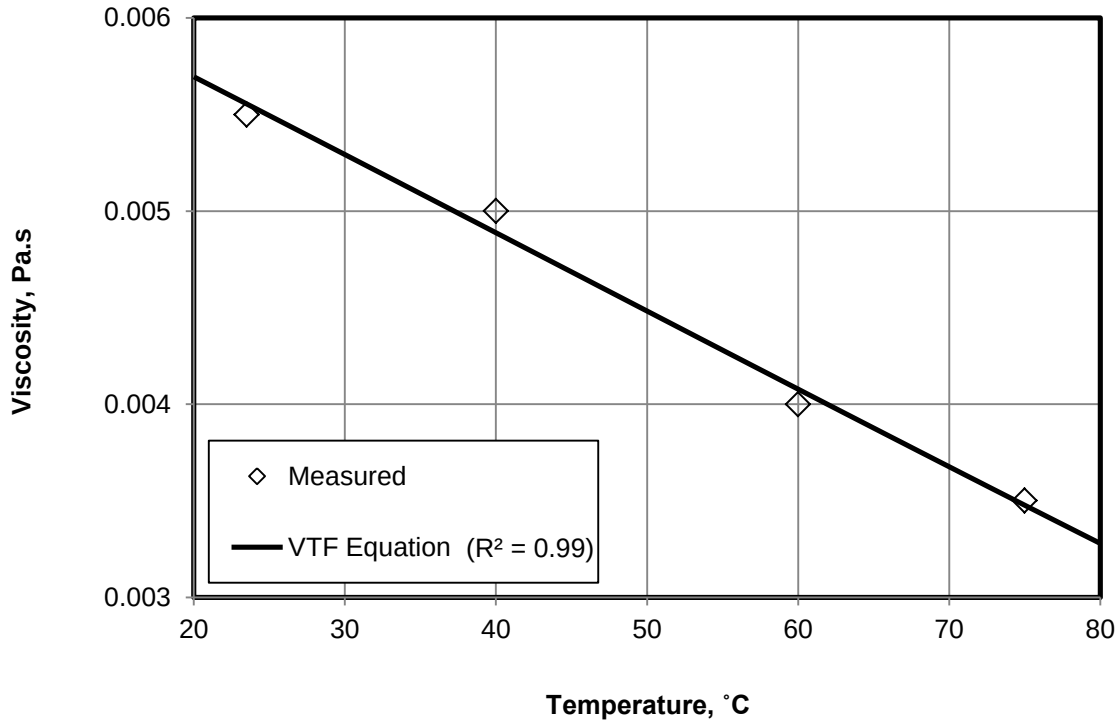

Fig. 6.3: Comparison between suspension viscosity obtained from the VTF equation and the measured data

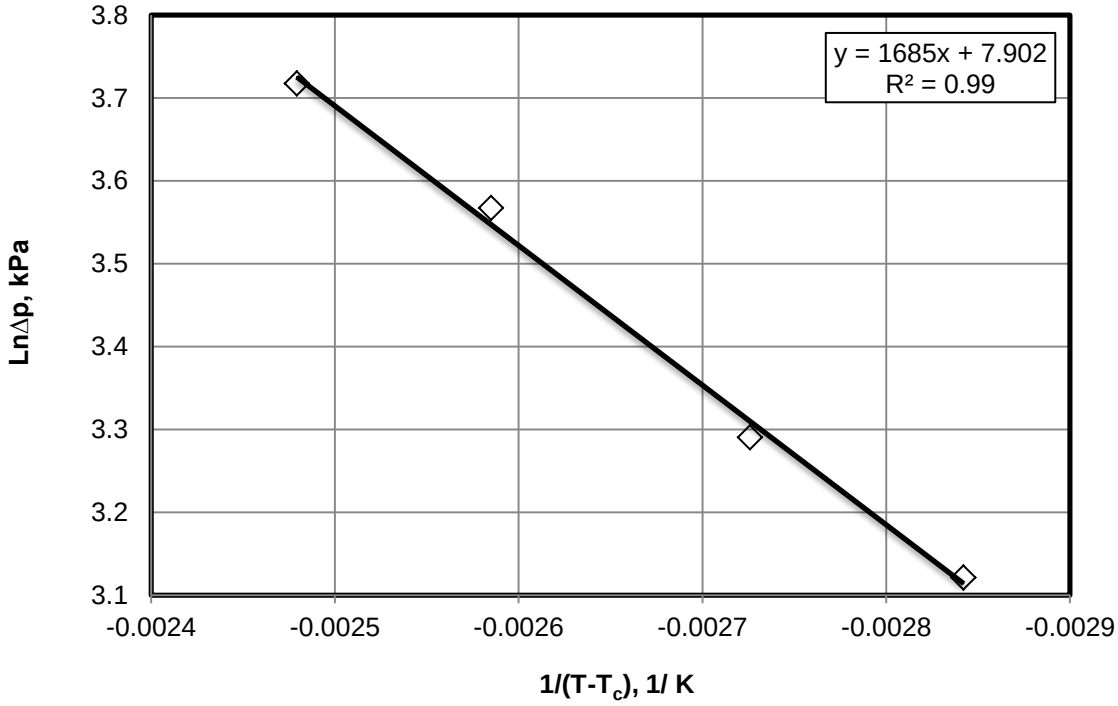

Fig. 6.4: Straight- line VTF plot for the differential pressure

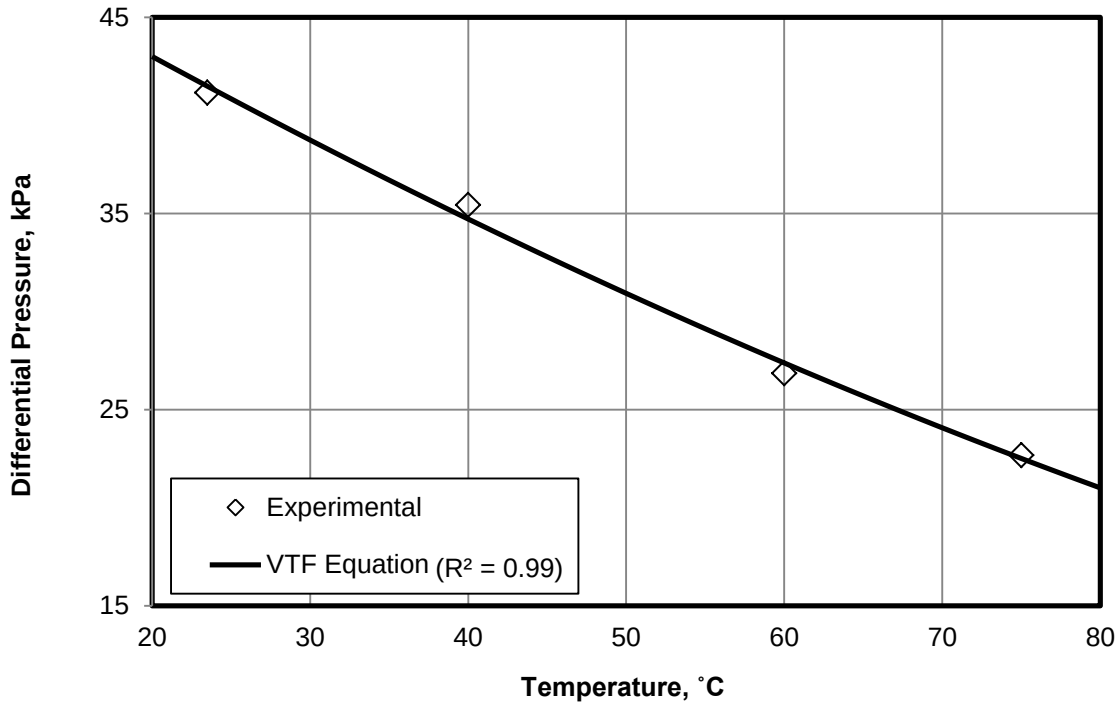

Fig. 6.5: Comparison between differential pressure obtained from the VTF equation and the experimental data

The permeability reduction decreased from 0.36 at 23.5 ˚C temperature to 0.42 at 75 ˚C temperature because the tendency of plugging decreased with increasing temperature**.** The experimental data of the permeability impairment (reduction) is correlated by using the VTF equation, given by:

$$\ln \frac{K}{K_o} = \ln\left(\frac{K}{K_o}\right)_c - \frac{C}{T - T_c} \qquad (6.4)$$

where (K/Ko) is the permeability impairment (reduction), dimensionless; and $(K/Ko)_c$ is the pre- exponential coefficient of permeability impairment (reduction) is 0.711. The fitting constants T_c and C are 100 K and 134 K, respectively. **Fig. 6.6** shows the straight- line VTF plot of the experimental data for the permeability impairment

(reduction). **Fig. 6.7** shows comparison between the permeability impairment (reduction) values obtained from VTF equation and the experimental data.

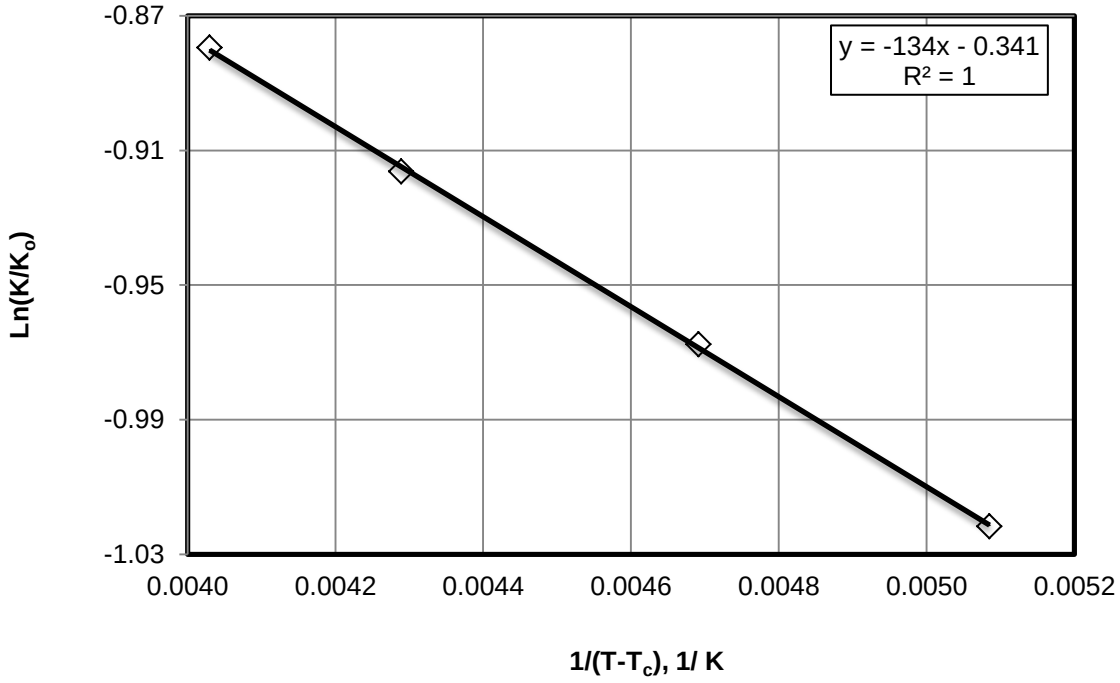

Fig. 6.6: Straight- line VTF plot for the permeability reduction

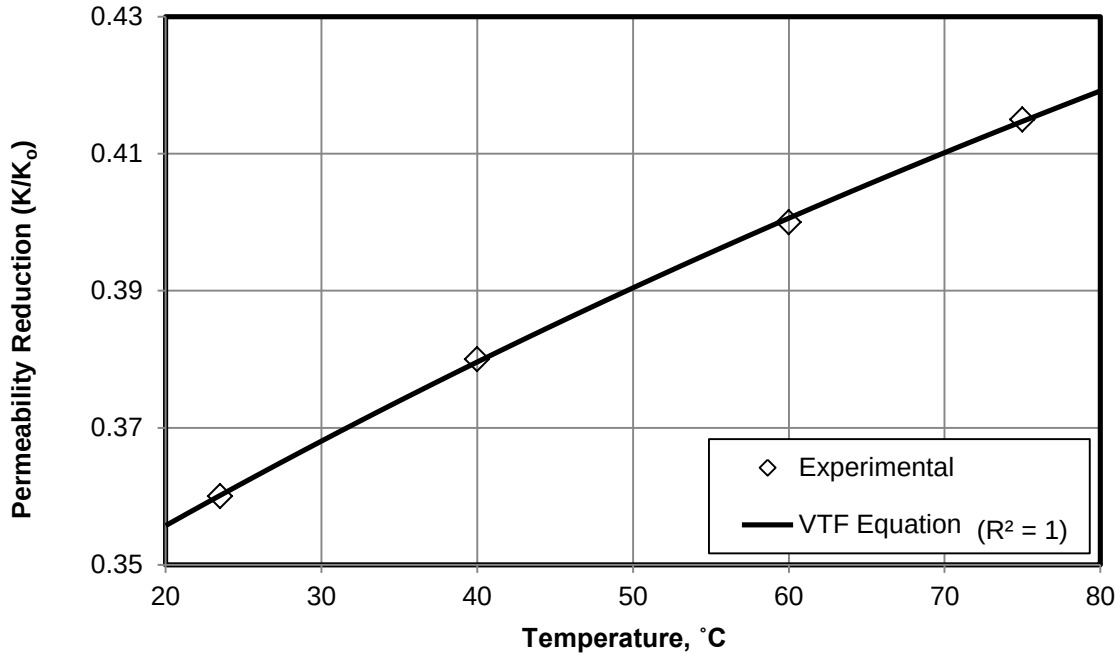

Fig. 6.7: Comparison between permeability reduction obtained from the VTF equation and the experimental data

The resistance factor is defined as the ratio of the water mobility before suspension injection to the suspension mobility during suspension injection at the same flow rate (Littmann 1988):

$$F_r = (K_w / \mu_w)/(K / \mu) \qquad (6.5)$$

F_r indicates the resistance factor, dimensionless; K_w is the effective water permeability, md; μ_w is the water viscosity, Pa.s; K is the suspension permeability, md, and μ is the suspension viscosity, Pa.s. The resistance factor decreased from 15.3 at temperature of 23.5 ˚C to 8.43 at temperature of 75 ˚C. This indicates a decreasing in plugging of the pores occurs when increasing the temperature. The experimental data of the permeability impairment (reduction) is correlated by using the VTF equation, given by:

$$\ln F_r = \ln(F_r)_c - \frac{C}{T - T_c} \qquad (6.6)$$

where F_r is the resistance factor, dimensionless; $(F_r)_c$ is the pre- exponential coefficient of resistance factor = 0.000223. The fitting constants T_c and C are -600 K and -10000 K, respectively. **Fig. 6.8** shows the straight- line VTF plot of the experimental data for the resistance factor. **Fig. 6.9** shows comparison between the resistance factor values obtained from VTF equation and the experimental data. As can be seen, the VTF correlation values of viscosity, differential pressure, and permeability reduction and resistance factor are close to the experimental data because of the high regression coefficients (R^2) of these relationships, around the unity. Thus, we can use the VTF equation to predict the viscosity, differential pressure across the proppant pack, permeability impairment (reduction) and resistance factor for a similar material and operation conditions at any temperature.

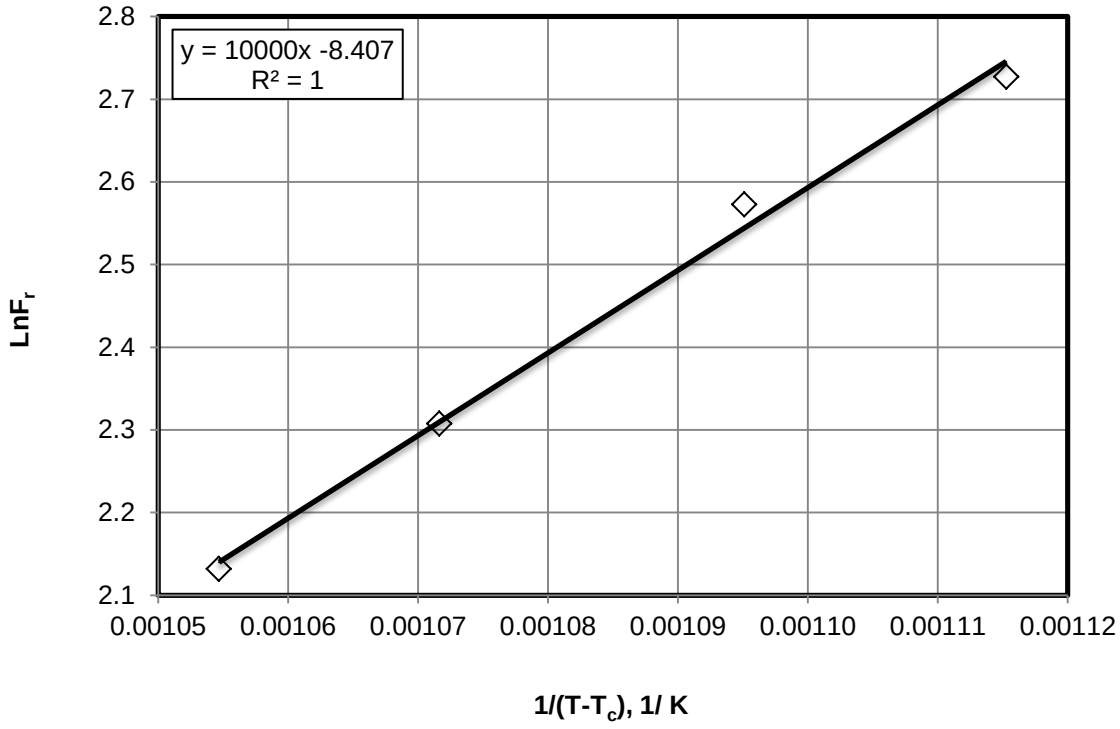

Fig. 6.8: Straight- line VTF plot for the resistance factors

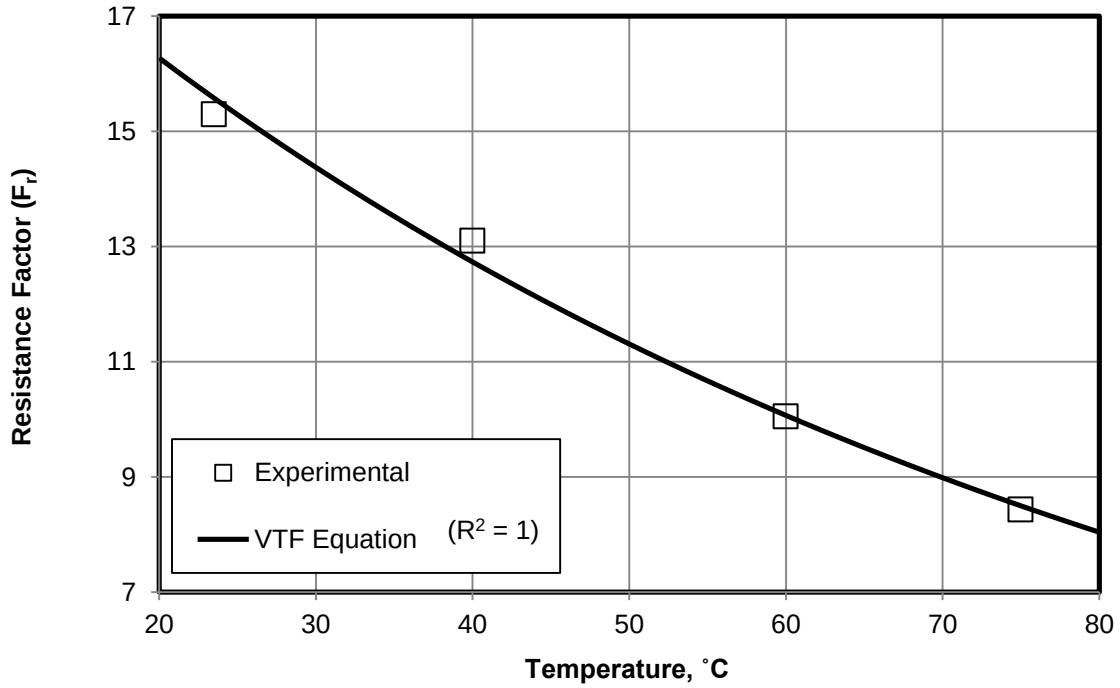

Fig. 6.9: Comparison between resistance factor obtained from the VTF equation and the experimental data

6.4 Correlation of Thermal Effect on Plugging/Unplugging Processes

A consecutive plugging and unplugging phenomena is observed during the injection of gel particles into the proppant pack at various temperatures as seen in **Fig. 6.10**. The permeability reduction increases during plugging and decreases during unplugging. The plugging event occurs when the gel is captured and accumulated behind the pore throats, causing a buildup of differential pressure. The unplugging event occurs when the differential pressure leads to a deformation of the gel particles captured and accumulated at some pore throats and then pass through these pores, decreasing the differential pressure (Al- Ibadi and Civan 2012 and 2013a). A series of plugging and unplugging processes occurs repetitively over consecutive periods of times and continues until attaining a steady flow at a constant differential pressure and permeability reduction level.

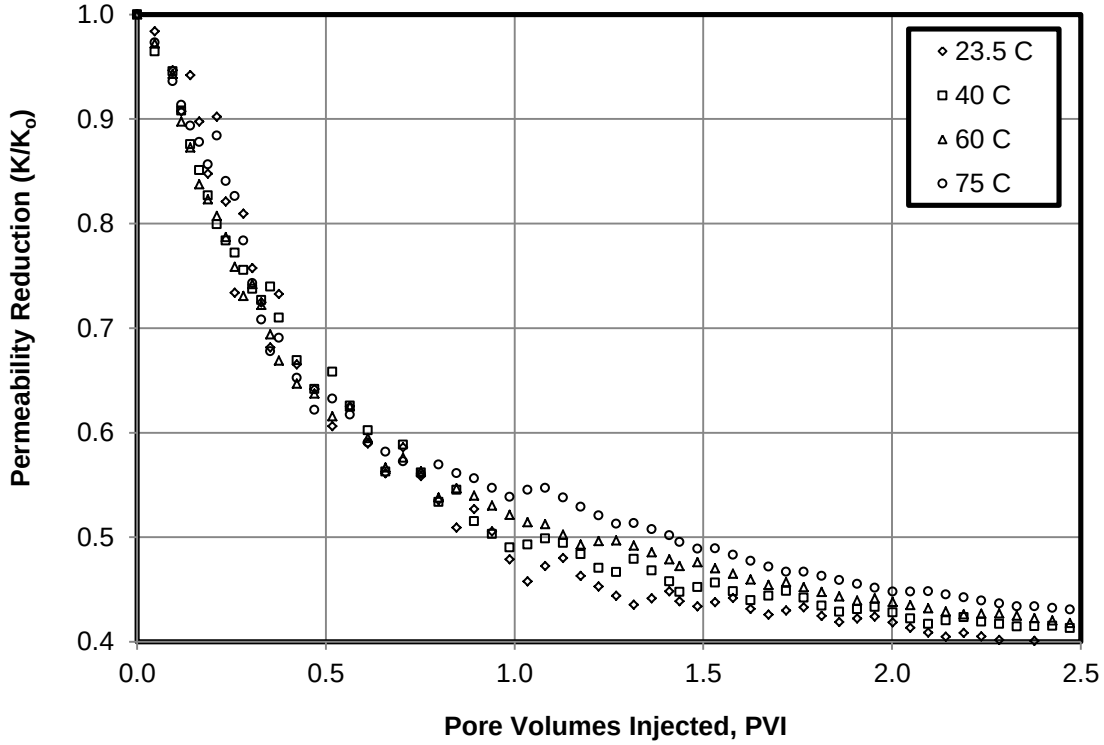

Fig. 6.10: Permeability reduction at 3 vol% concentration for different temperatures at 100 cm^3/hr

Figs. 6.11 to **6.18** show the plugging and unplugging events occurring during the injection of gel particles into the proppant pack at various temperatures. The number of plugging and unplugging regions decreases by increase in temperature. The plugging and unplugging events can be modeled and represented as straight line plots shown in Figs. 6.11 to 6.18. The straight lines are not parallel because they have different slopes and not horizontal because the slopes are not equal zero. The slopes of the straight lines represent the rate constant values for the plugging and unplugging processes. **Tables 6-1** to **6-8** show the rate and intercept constants values for plugging and unplugging processes at various temperatures. The values of the rate constants decrease by the pore volume injected, indicating that first the gel particles are captured at the small pore throat and then the gel particles of diameter larger than the pore throat size are diverted toward the larger unplugging pore throats and accumulate behind them, as described by Civan and Nguyen (2005). Thus, the rate constants of plugging and unplugging regions are determined and correlated for the rate of plugging and unplugging at various temperatures. **Figs. E.1** and **E.2** show the relationship between the rate constants of plugging and unplugging regions and the pore volumes injected for 3 vol% particles suspension at various temperatures. The rate constant of plugging and unplugging regions are correlated by using Eq. B-6 given in appendix B, as shown in **Figs. E.3** and **E.4** in Appendix E. Further, the intercept of the plugging and unplugging regions are determined and correlated with the pore volumes injected at various temperatures as shown in **Figs. E.5** and **E.6.** The intercept of the plugging regions are correlated by using equation B-4 given in Appendix B and the intercept of the unplugging regions are correlated by applying equation B-2 given in appendix B, as shown in **Figs. E.7** and **E.8** in appendix E.

The values of the rate constants and the intercepts of the plugging and unplugging regions were correlated by used of Eqs. 6.7 and 6.8, respectively, as shown in Figs. E.1, E.2, E.5, and E.6:

$$y = A\exp\left(-Bx^{\beta}\right) \tag{6.7}$$

$$y = A\left[\frac{x^{\beta}}{x^{\beta} - B}\right] \tag{6.8}$$

where y represent the rate constants of the plugging and unplugging regions, dimensionless or the intercept of the plugging and unplugging regions, dimensionless; x represents the pore volume injected, dimensionless; A, B, and β are empirical parameters, dimensionless.

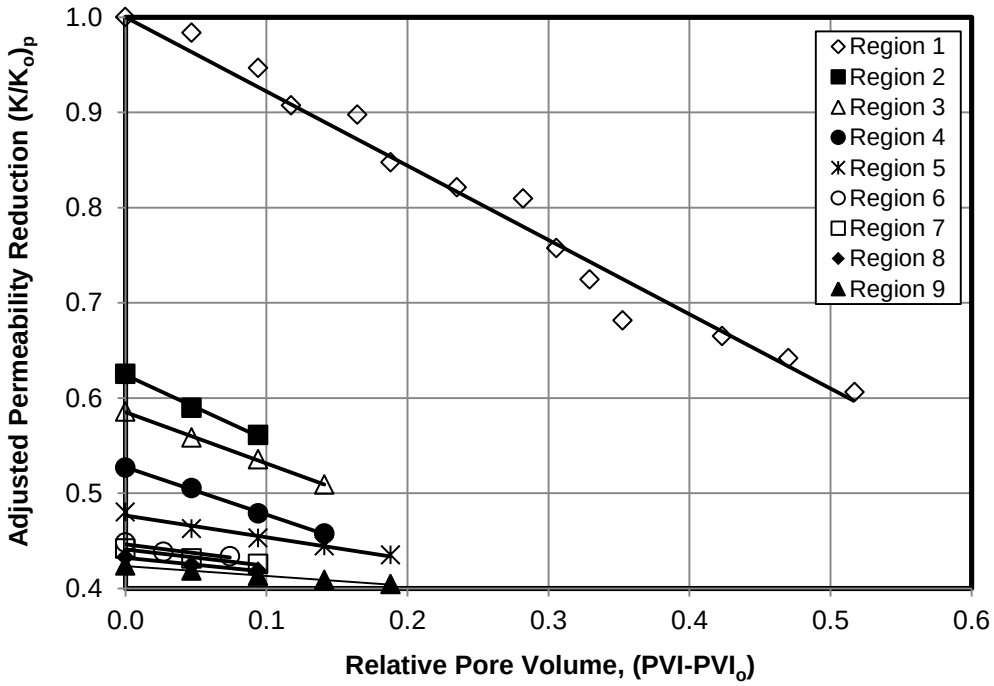

Fig. 6.11: Plugging events trends at T= 23.5 ˚C

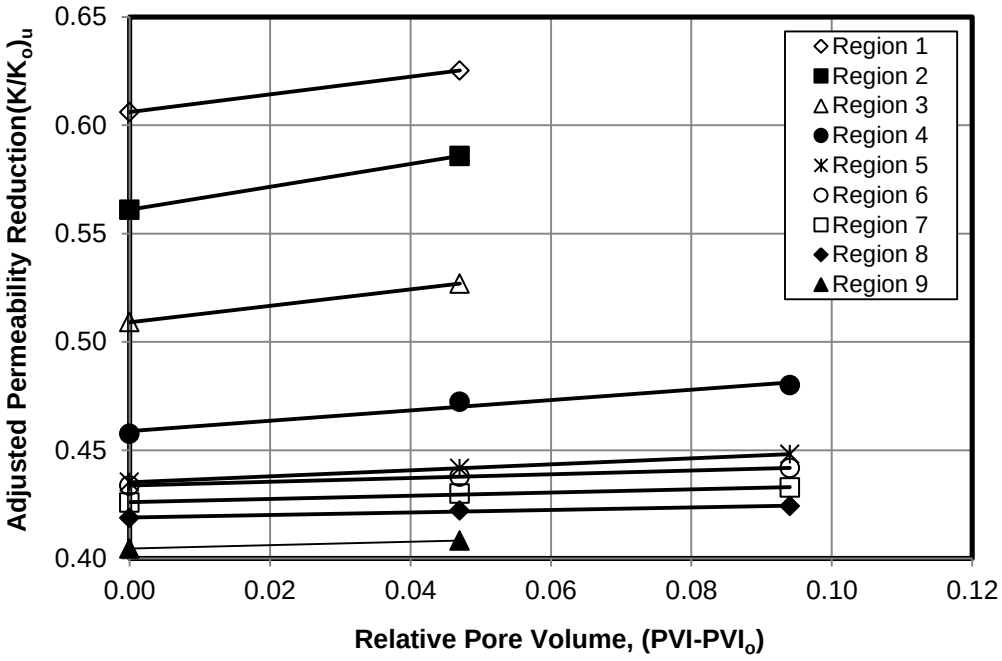

Fig. 6.12: Unplugging events trends at T= 23.5 ˚C

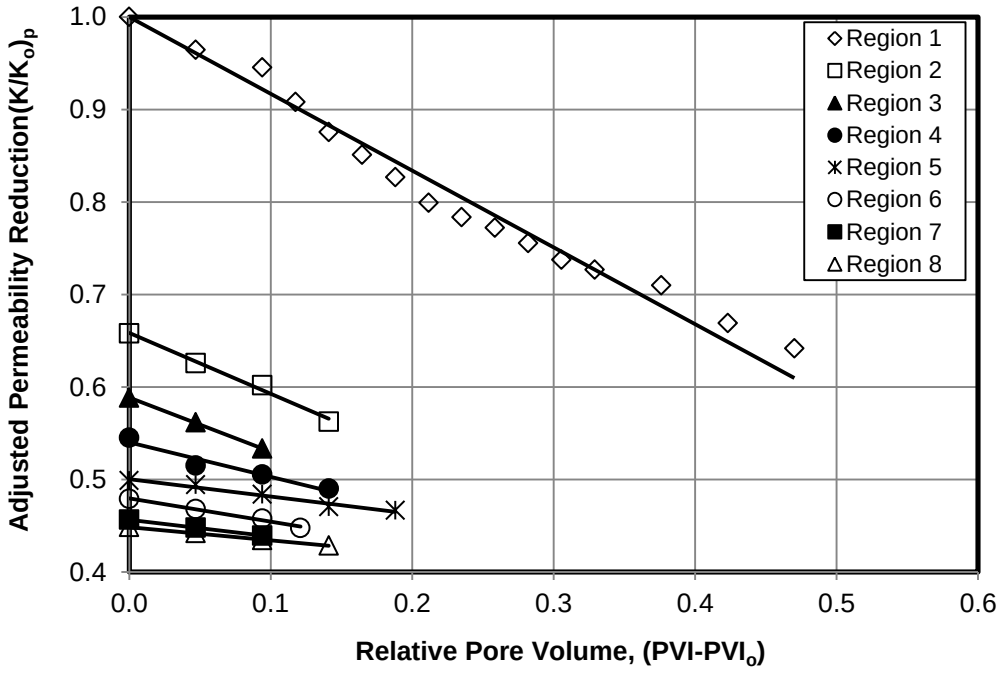

Fig. 6.13: Plugging events trends at T= 40 ˚C

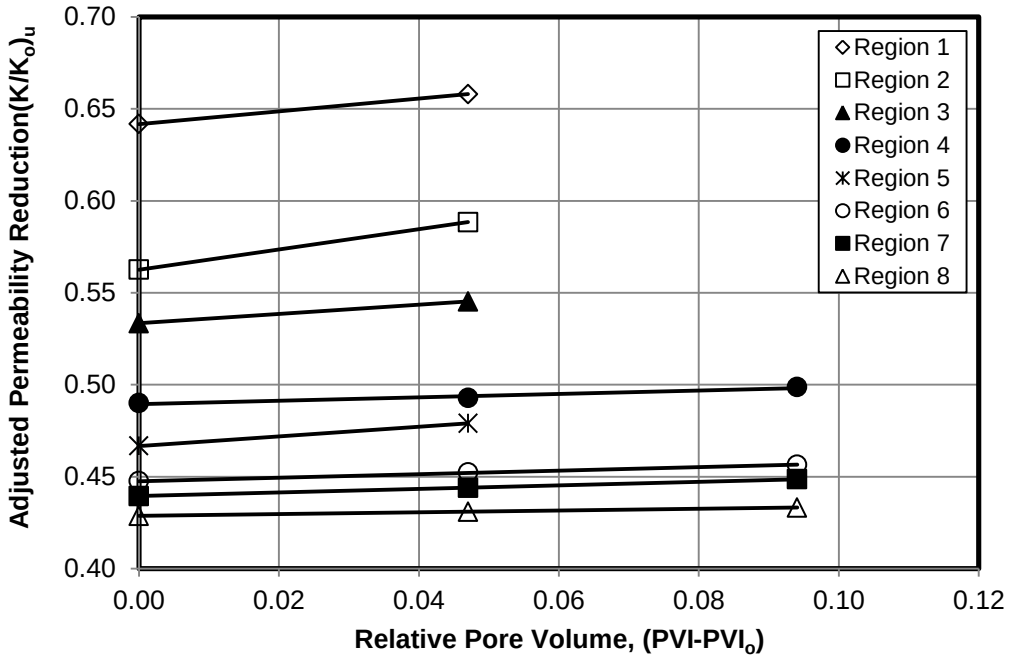

Fig. 6.14: Unplugging events trends at T= 40 ˚C

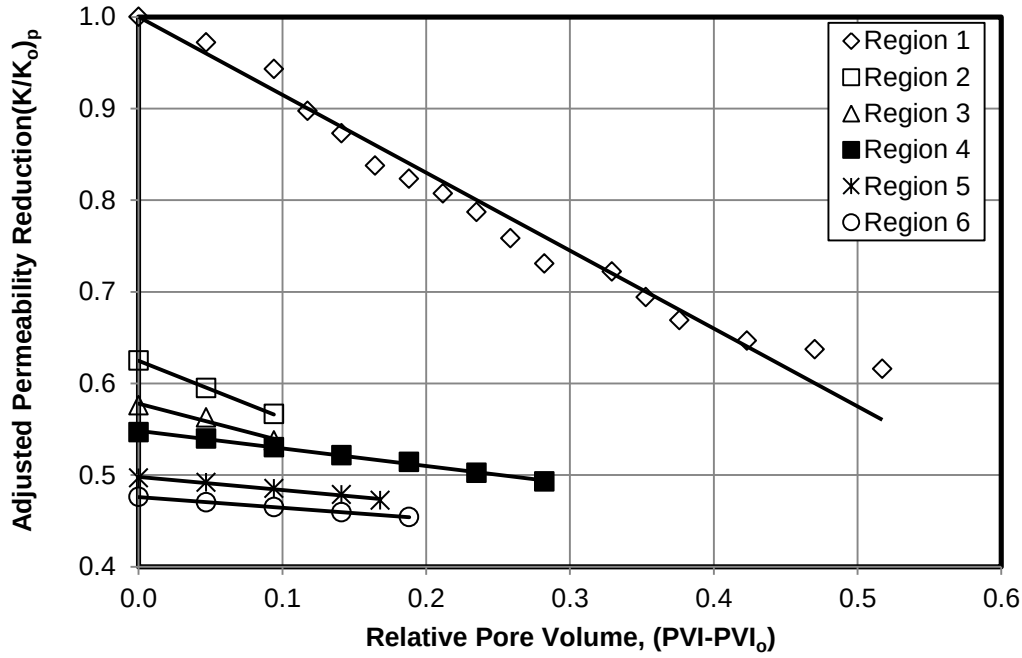

Fig. 6.15: Plugging events trends at T= 60 ˚C

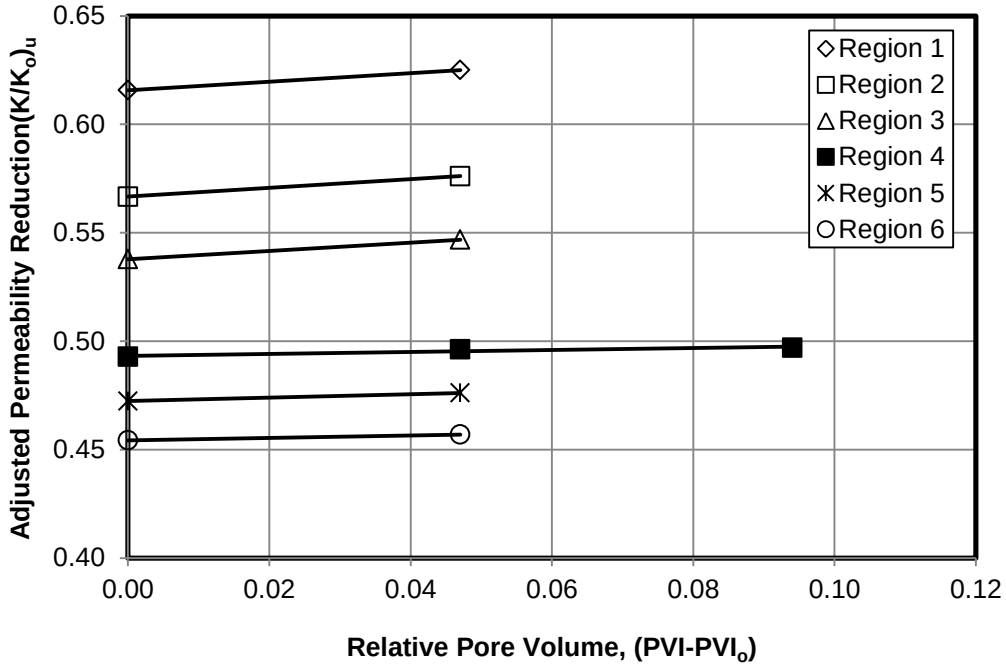

Fig. 6.16: Unplugging events trends at T= 60 ˚C

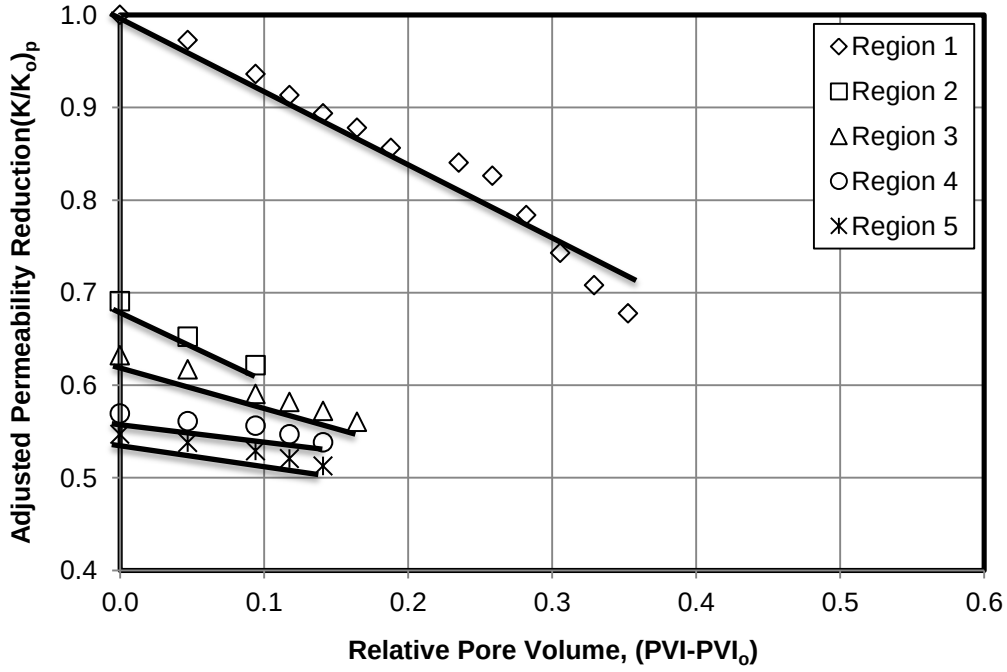

Fig. 6.17: Plugging events trends at T= 75 ˚

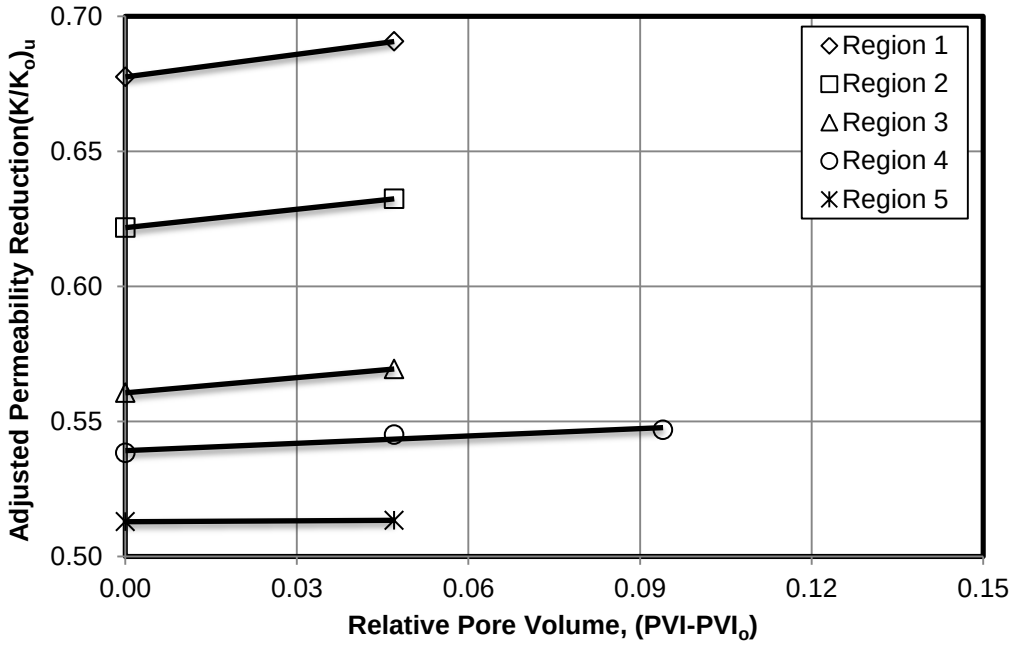

Fig. 6.18: Unplugging events trends at T= 75 ˚C

TABLE 6-1: RATE AND INTERCEPT CONSTANTS OF PLUGGING REGIONS AT T=23.5 ˚C

Regions	Rate Constants (dimensionless)	Intercept Constants (dimensionless)	R^2
1	0.78	1	0.98
2	0.68	0.62	1
3	0.54	0.59	1
4	0.50	0.53	1
5	0.23	0.48	0.98
6	0.19	0.45	0.89
7	0.17	0.44	0.97
8	0.15	0.43	0.99
9	0.10	0.42	1

TABLE 6-2: RATE AND INTERCEPT CONSTANTS OF UNPLUGGING REGIONS AT T=23.5 ˚C

Regions	Rate Constants (dimensionless)	Intercept Constants (dimensionless)	R^2
1	0.45	0.61	1
2	0.50	0.56	1
3	0.38	0.51	1
4	0.24	0.46	0.97
5	0.14	0.44	1
6	0.09	0.43	1
7	0.07	0.42	0.99
8	0.06	0.41	0.98
9	0.07	0.40	1

TABLE 6-3: RATE AND INTERCEPT CONSTANTS OF PLUGGING REGIONS AT T=40 ˚C

Regions	Rate Constants (dimensionless)	Intercept Constants (dimensionless)	R^2
1	0.83	1	0.98
2	0.66	0.66	0.99
3	0.58	0.59	1
4	0.37	0.54	0.95
5	0.18	0.50	0.97
6	0.25	0.48	0.99
7	0.18	0.46	1
8	0.13	0.45	1

TABLE 6-4: RATE AND INTERCEPT CONSTANTS OF UNPLUGGING REGIONS AT T=40 ˚C

Regions	Rate Constants (dimensionless)	Intercept Constants (dimensionless)	R^2
1	0.35	0.64	1
2	0.55	0.56	1
3	0.25	0.53	1
4	0.09	0.49	0.96
5	0.26	0.47	1
6	0.10	0.45	1
7	0.09	0.44	1
8	0.05	0.43	1

TABLE 6-5: RATE AND INTERCEPT CONSTANTS OF PLUGGING REGIONS AT T=60 ˚C

Regions	Rate Constants (dimensionless)	Intercept Constants (dimensionless)	R^2
1	0.85	1	0.97
2	0.62	0.62	1
3	0.41	0.58	0.97
4	0.19	0.55	1
5	0.14	0.50	0.99
6	0.11	0.48	1

TABLE 6-6: RATE AND INTERCEPT CONSTANTS OF UNPLUGGING REGIONS AT T=60 ˚C

Regions	Rate Constants (dimensionless)	Intercept Constants (dimensionless)	R^2
1	0.30	0.62	1
2	0.20	0.57	1
3	0.19	0.54	1
4	0.05	0.49	0.89
5	0.07	0.47	1
6	0.05	0.45	1

TABLE 6-7: RATE AND INTERCEPT CONSTANTS OF PLUGGING REGIONS AT T=75 ˚C

Regions	Rate Constants (dimensionless)	Intercept Constants (dimensionless)	R^2
1	0.86	1	0.95
2	0.73	0.69	1
3	0.44	0.63	0.99
4	0.22	0.57	0.94
5	0.22	0.55	0.98

TABLE 6-8: RATE AND INTERCEPT CONSTANTS OF UNPLUGGING REGIONS AT T=75 ˚C			
Regions	Rate Constants (dimensionless)	Intercept Constants (dimensionless)	R^2
1	0.28	0.68	1
2	0.23	0.62	1
3	0.19	0.56	1
4	0.09	0.54	0.95
5	0.01	0.51	1

The effect of temperature on the plugging mechanism is observed from the number of the plugging regions and the permeability reduction at various temperatures. The number of the plugging regions decreases by the temperature increases, the number of the plugging regions decreases from 9 to 5 when the temperature increases from 23.5 ˚C to 75 ˚C. Hence, the permeability reduction decreases from 0.36 to 0.42 when the temperature increases from 23.5 ˚C to 75 ˚C. This occurs because the gel particles become more deforming and pass easily through the pore throats at the high temperature. Therefore, plugging of pores by gel particles is less pronounced by increasing temperature and hence, permeability reduction decreases, as shown in Fig. 6.1.

6.4.1 Simultaneous fitting of correlation

Simultaneous fitting of correlations is developed by collecting the values of

A, B, and β from the exponential correlations of the thermal effects and plotted against temperatures, as shown in **Figs. E.9** to **E.19** given in Appendix E. The plotted A, B, and β were correlated as linear functions ($y = a_i + b_i x$) where y represents A, B, and β; x represents temperatures; a_i and b_i represents initial guesses of parameters (See figures E.9 to E.19). By substituting the linear functions of A, B, and β in the relationships of the rate constants of plugging and unplugging and intercepts of plugging and unplugging regions, as shown in Eqs. 6.9 and 6.10, empirical correlations of the thermal effect on the rate and intercept constants of plugging and unplugging were developed which can be used for practical applications, as shown in **Figs. 6.19** to **6.22**. The rate constants of plugging and unplugging regions represent the slopes of the straight lines and not represent the permeability impairment (reduction), therefore the initial values of the curves are not 1, as shown in Figs. 6.19 and 6.20. The first region of the plugging starts from value 1 of the permeability impairment (reduction), therefore the curves of the intercept of plugging regions start from 1, as shown in Fig. 6.21.

$$y = (a_1 T + b_1)\exp\left[-(a_2 T + b_2)x^{(a_3 T + b_3)}\right] \tag{6.9}$$

$$y = (a_1 T + b_1)\left[\frac{x^{(a_3 T + b_3)}}{x^{(a_3 T + b_3)} - (a_2 T + b_2)}\right] \tag{6.10}$$

where y represent the rate constants of the plugging and unplugging regions, dimensionless or the intercept of the plugging and unplugging regions, dimensionless; x represents the pore volume injected, dimensionless; T represents the temperature, °C; and a_1, b_1, a_2, b_2, a_3, and b_3 represent initial guesses, dimensionless.

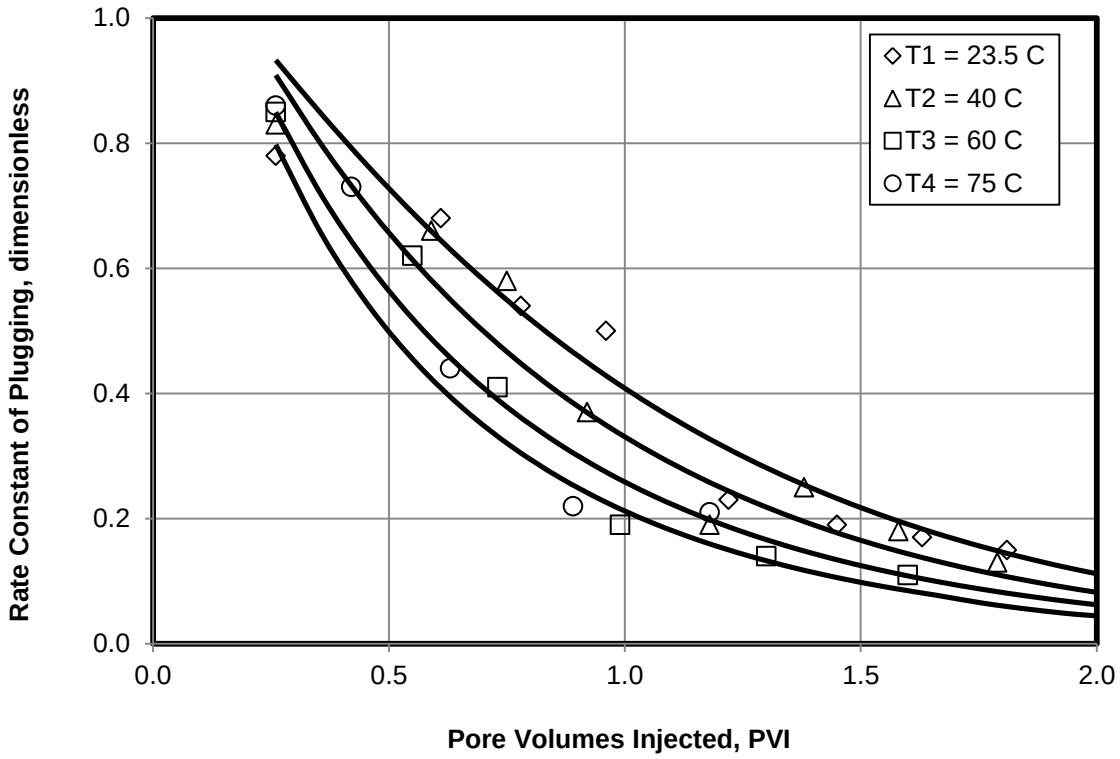

Fig. 6.19: Rate constant of plugging at different pore volumes injected and different temperatures

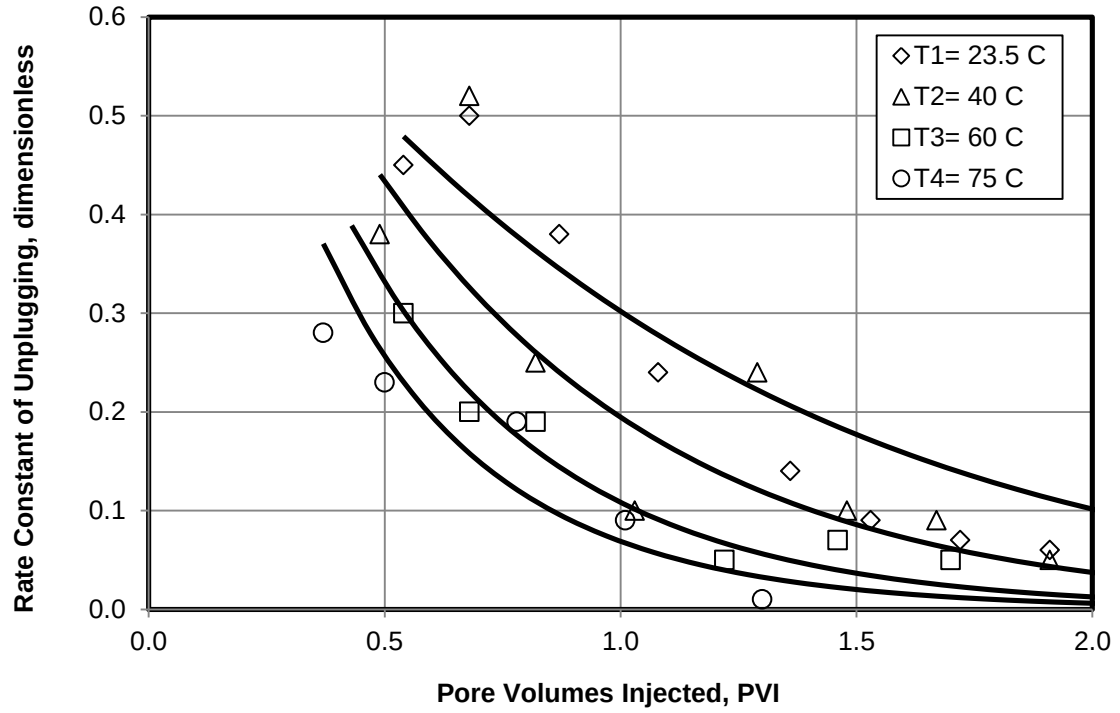

Fig. 6.20: Rate constant of unplugging at different pore volumes injected and different temperatures

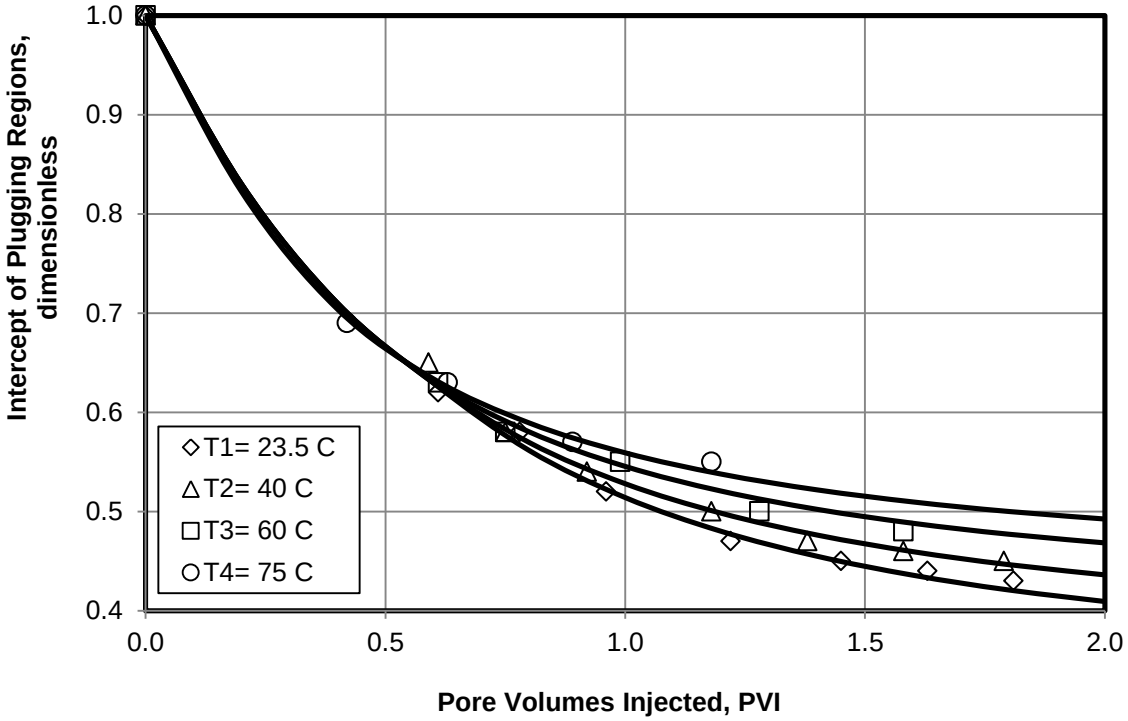

Fig. 6.21: Intercept of plugging regions at different pore volumes injected and different temperatures

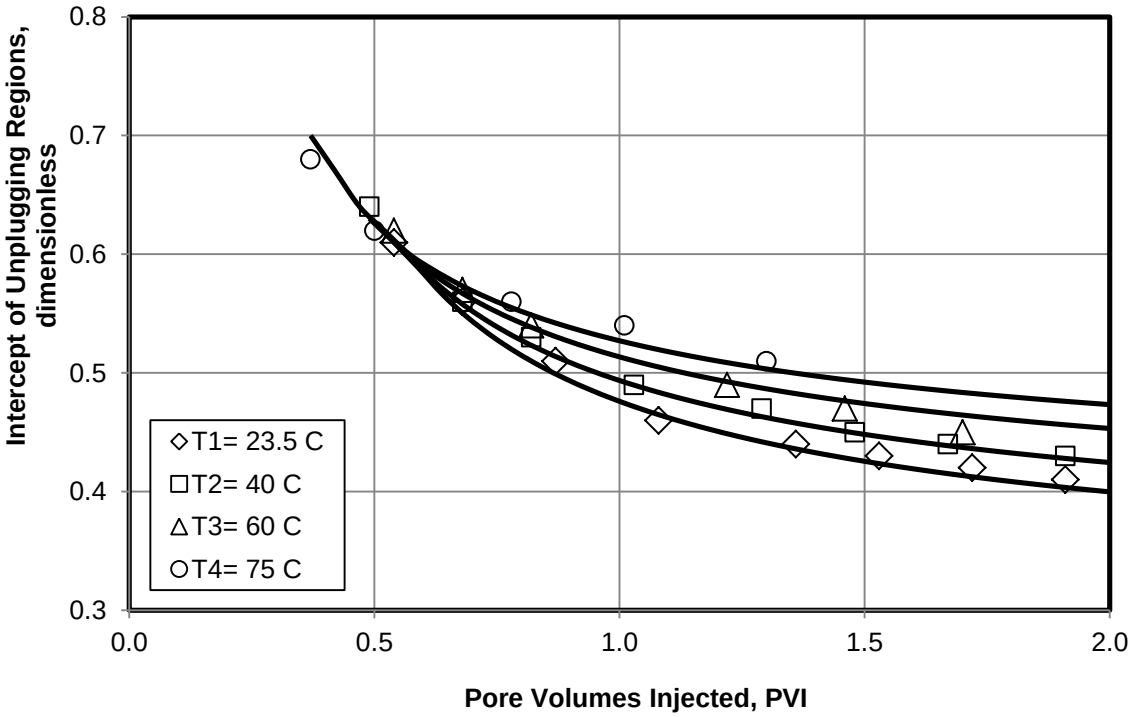

Fig. 6.22: Intercept of unplugging regions at different pore volumes injected and different temperatures

6.5 Conclusions

The main findings of this experimental study can be summarized as the following:

- Quantitative evaluation of the thermal effect on the performance of gel particles applications was study for successful field applications of gel particle suspension injection. Thus, important empirical correlations for thermal effect were developed which can be used for controlling plugging in highly permeable formations and conditioning of these formations by reducing the high permeability. Hence, we can prevent loss circulation during drilling operations in formations having high permeability zones and control water production in waterflooded mature oil fields.
- The Vogel-Tammann- Fulcher (VTF) - type equation is used to correlate the experimentally measured data of the viscosity, differential pressure, permeability reduction, and resistance factor at various temperatures and an excellent agreement is observed between the experimental data and the correlations. Hence, these correlations can be used to predict the effect of temperature on conditioning and reducing the high permeability of the formations by injection of a suspension of gel particles.
- The effect of temperature on plugging and unplugging phenomena which occurred during the injection of gel particles into the proppant pack was investigated and a decrease in the number of plugging and unplugging regions by increasing in temperature was observed. This occurs because the gel particles become more deforming and pass easily through the pore throats at high temperatures. Therefore, plugging of pores by gel particles becomes less pronounced by increasing temperature and permeability reduction decreases. The rate constants of the plugging and

unplugging regions were determined and correlated successfully with temperature.

Chapter 7: Dimensional Analysis of Near-Wellbore Formation Treatment by Gel Particles Suspension

This Chapter has been previously published as ‘‘Evaluation of Near- Wellbore Formation Treatment by Gel Particles Using Dimensional Analysis’’ in the SPE Production and Operations Symposium, Oklahoma City, Ok, 23-26 March, 2013 and is used here by permission.

7.1 Introduction

Several important factors affect the gel particles transport through porous media and hence the near-wellbore formation treatment by gel particles, including flow rate, gel particles concentration, gel particle diameter, pore-throat size, and temperature. However, concerning the transport of soft-gel particles through narrow pore throats in porous media, the deformation property is a particularly important factor that causes the oscillation phenomenon observed of the measured pressure differential and hence in the resulting permeability reduction trends. In fact, the dimensional analysis of the gel particles injection data presented in the following proves the importance of the deformation property of the gel particles. Because the overall phenomena of gel particles transport and entrapment in porous media involve many complicated processes, the difficulty of analyzing the experimental data is alleviated by developing dimensionless correlations which can assist in evaluating the near-wellbore formation treatment by gel particles.

The relevant dimensionless correlations of experimental data of gel particles plugging of porous media are developed based on the dimensional analysis method which can be used for effective design and monitoring of treatment of high-permeability

near-wellbore formation by gel particles suspension. The dimensionless groups are developed from the primary variables of the sand packs, gel particles suspension, and operation conditions. Step-by-step procedure of elimination of the basic dimensions was used for combination of variables into relevant dimensionless groups. The normalized dimensionless groups were used to correlate the measured permeability reduction by gel particles at different temperatures, concentrations, flow rates, and gel particles diameters. Comparison between correlated and measured permeability reduction indicates satisfactory results, especially for the limit value of the final permeability reduction. Hence, the effect of the ratio of the particle-diameter to pore-throat size on permeability reduction under various conditions is correlated successfully.

7.2 Relevant Dimensionless Groups

The permeability reduction data obtained from the tests of Al-Ibadi and Civan (2012, 2013a and 2013b) by gel particles suspension injection into sand packs at different temperatures, flow rates, gel particles diameters, and gel particles concentrations are now correlated by dimensional analysis. The dimensionless correlations of the experimental data are developed from dimensionless groups in normalized forms to accommodate for differences in the final limit values of permeability reduction attained under different conditions.

The actual variables used in this study are summarized in **Table 7-1** and all the variables and their units are summarized in **Table 7-2**. The basic dimensions involved in this study are mass M, length L, time T, and temperature θ. Step-by-step procedure applied for derivation of the relevant dimensionless groups involves the first step to

eliminate M, the second step to eliminate L, the third step to eliminate T, and the fourth step to eliminate K, as illustrated in Table 7-2. The variables are grouped into several groups according to the initial system such as the porous media group, the gel particle suspension group, and the operation conditions group.

The dimensionless groups are obtained from the variables by means of the combination of variables method (Churchill 1997) and the number of dimensionless groups is equal to the number of the variables minus the number of the basic dimensions (Van Driest 1946). We have 14 variables and 4 basic dimensions as shown in Table 7-2. Therefore, the number of the dimensionless groups obtained from these variables is 10 as follows:

$$\Pi_1 = \frac{K}{z^2}\ ,\ \Pi_2 = \frac{D_p}{D_T}\ ,\ \Pi_3 = \frac{A}{z^2}\quad ,\quad \Pi_4 = \frac{\mu t}{\rho z^2}\ ,\ \Pi_5 = \frac{\mu t}{\rho D_p^2}\ ,\quad \Pi_6 = \frac{tv}{z}$$

$$\Pi_7 = \frac{tv}{D_p}\quad ,\ \Pi_8 = \frac{t^2\Delta p}{\rho z^2}\ ,\ \Pi_9 = \frac{t^2 c\theta}{z^2}\quad ,\quad \Pi_{10} = \frac{t^2 c\theta}{D_p^2} \qquad (7.1)$$

The dimensionless groups are manipulated to obtain conventional dimensionless group as the following, for example:

$$\Pi_{10}{}' = \frac{\Pi_1\Pi_8}{\Pi_6\Pi_4} = \frac{K\Delta p}{\mu v z} \qquad (7.2)$$

Table 7-1: Summary of Primary Variables

Variable Group	Variable	Unit	Values				
Sand Pack	D_g	μm	1015	650			
Gel	D_p	μm	50	75	100	125	140
	C_p	vol%	0.5%	1%	2%	3%	
Test Conditions	v	cm/s	0.0072	0.0144	0.0288	0.0403	0.0576
	θ	K	296.5	313	333	348	

Table 7-2: Step-by-Step Elimination of the Fundamental Dimensions

Initial System	Dimensions	Step1 Eliminate M		Step 2 Eliminate L		Step 3 Eliminate T		Step 4 Eliminate K
Variables		Vari.	Dimen.	Vari.	Dimen.	Vari.	Dimen.	Dimen.
Porous Media								
K	L^2	K	L^2	K/z^2:dim. group	1			
D_T	L	D_T	L	D_p/D_T: dim. group	1			
A	L^2	A	L^2	A/z^2: dim. group	1			
z	L	z	L	z: scaling variable	L			
ϕ	L^3/L^3	ϕ	L^3/L^3	ϕ	L^3/L^3			
Gel Particle Suspension								
μ	M/LT	μ/ρ	L^2/T	$\mu/\rho/z^2$	1/T	$t\mu/\rho/z^2$: dim. group	1	
				$\mu/\rho/D_p^2$	1/T	$t\mu/\rho/D_p^2$: dim. group	1	
ρ	M/L^3	ρ:scaling variable	M/L^3					
D_p	L	D_p	L	D_p: scaling variable	L			
C_p	L^3/L^3	C_p	L^3/L^3	C_p	L^3/L^3			
Operation Conditions								
v	L/T	v	L/T	v/z	1/T	tv/z: dim. group	1	
				v/D_p	1/T	tv/D_p: dim. group	1	

t	T	t	T	t	T	t: scaling variable	T		
Δp	M/LT^2	Δp/ρ	L^2/T^2	$\Delta p/\rho/z^2$	$1/T^2$	$t^2\Delta p/\rho/z^2$: dim. group	1		
θ	K	θ	K	θ	K	θ	K	θ: scaling variable	K
c	L^2/T^2K	c	L^2/T^2K	c/z^2	$1/T^2K$	t^2c/z^2	1/K	$\theta t^2c/z^2$	1
				c/D_p^2	$1/T^2K$	t^2c/D_p^2	1/K	$\theta t^2c/D_p^2$	1

7.3. Data Analysis and Correlation

The correlations of dimensionless groups, plots of data and correlations after normalization, and permeability obtained from dimensionless correlations are presented in the following.

7.3.1 Dimensionless groups selected for correlations

Although we determined 10 dimensionless groups, we only used 7 dimensionless groups to correlate the measure data obtained from the gel particle suspension injection into the sand pack at different concentrations, flow rates, gel particle diameter, and temperatures (Al-Ibadi and Civan 2012, 2013a, and 2013b). Dimensionless group Π_2 combining D_p with D_T show the effect of the ratio of the particle diameter (D_p) to the pore throat size (D_T) (produced from the grain diameter (D_g) of the sand pack) on the permeability reduction (K/K_o). Dimensionless group Π_4 combining μ, t, ρ and z variables show the effect of the suspension viscosity μ change with the gel particle concentration (C_p) on the permeability reduction. Dimensionless

group Π_5 combining μ, t, ρ and *Dp* variables show the effect of the particle diameter (D_p) on the permeability reduction. Dimensionless group Π_6 combining v, t, and z variables show the effect of the suspension velocity (v) on the permeability reduction. Dimensionless group Π_7 combining v, t, and D_p variables show the effect of the particle diameter (D_p) on the permeability reduction. Dimensionless group Π_9 combining t, c, θ and z variables show the effect of the temperature (θ) on the permeability reduction. Dimensionless group Π_{10} combining t, c, θ and D_p variables show the effect of the particle diameter (D_p) on the permeability reduction. The following combined dimensionless group was also used to represent the permeability reduction (K/K_o):

$$\Pi_{10}'' = \frac{\Pi_{10}'}{\Pi_{10\,o}'} = \frac{K\Delta p \,/\, \mu v z}{K_o \Delta p_o \,/\, \mu_o v_o z_o} = \frac{K\Delta p \mu_o v_o z_o}{K_o \Delta p_o \mu v z} \qquad (7.3)$$

To develop dimensionless correlations of the thermal effect on near well- bore formation treatment by gel particles, we used Π_4 dimensionless group because it contains suspension viscosity (μ) affected by temperature and used Π_9 dimensionless group because it contains the temperature (θ). The dimensionless correlation of the effect of the gel particle concentration on near well-bore formation treatment by gel particles is developed using Π_4 dimensionless group because it contains suspension viscosity (μ) that increases by the gel concentration. To develop dimensionless correlation of the effect of the flow rate on near well-bore formation treatment by gel particles, we used Π_6 dimensionless group because it contains suspension velocity (v). The dimensionless correlation of the effect of the gel particle diameter on near well-bore formation treatment by gel particles is developed using Π_5, Π_7, and Π_{10}

dimensionless groups because they contain the particle diameter (D_p).

7.3.2 Dimensionless plots of experimental data

Figs. 7.1 and 7.2 show the Π_4 and Π_9 dimensionless groups for the permeability reduction at 3 vol% concentration for different temperatures at 100 cm³/h. These figures show that the maximum values of the dimensionless groups at 5 PVI different by the temperature. The values of the Π_4 dimensionless group are 1.04 at 23.5 ˚C, 0.95 at 40 ˚C, 0.76 at 60 ˚C, and 0.66 at 75 ˚C and for the Π_9 dimensionless group are 1.50E+15 at 23.5 ˚C, 1.59E+15 at 40 ˚C, 1.69E+15 at 60 ˚C, and 1.77E+15 at 75 ˚C. **Fig. 7.3** shows the Π_4 dimensionless group for the permeability reduction at 100 cm³/hr for different concentrations at T= 23.5 ˚C. Fig. 7.3 shows that the maximum values of the Π_4 dimensionless group at 5 PVI different by the gel particles concentration, 0.66 at 0.5% concentration, 0.76 at 1.0% concentration, 0.85 at 2.0% concentration, and 1.04 at 3.0% concentration. **Fig. 7.4** shows the Π_6 dimensionless group for the permeability reduction at 3 vol% concentration and 23.5 ˚C for different flow rates. The figure shows that the maximum values of the dimensionless group at 5 PVI different by the flow rate, 2.5 at 50 cm³/hr, 5 at 100 cm³/hr, 10 at 200 cm³/hr, 14 at 280 cm³/hr, and 20 at 400 cm³/hr. **Figs. 7.5** to **7.7** show the Π_5, Π_7, and Π_{10} dimensionless groups for the permeability reduction at 100 cm³/hr and 23.5 ˚C for different particle sizes for the sand pack of 1015 µm grain diameter. The maximum values of the Π_5, Π_7, and Π_{10} dimensionless groups at 5 PVI different by the particle diameters are shown in Figs. 7.5 to 6.7. **Figs. 7.8** to **7.10** show the Π_5, Π_7, and Π_{10} dimensionless groups for the permeability reduction at 100 cm³/hr and 23.5 ˚C for different particle sizes for the sand

pack of 650 µm grain diameter and the maximum values of the dimensionless groups at 5 PVI different by the particle diameter.

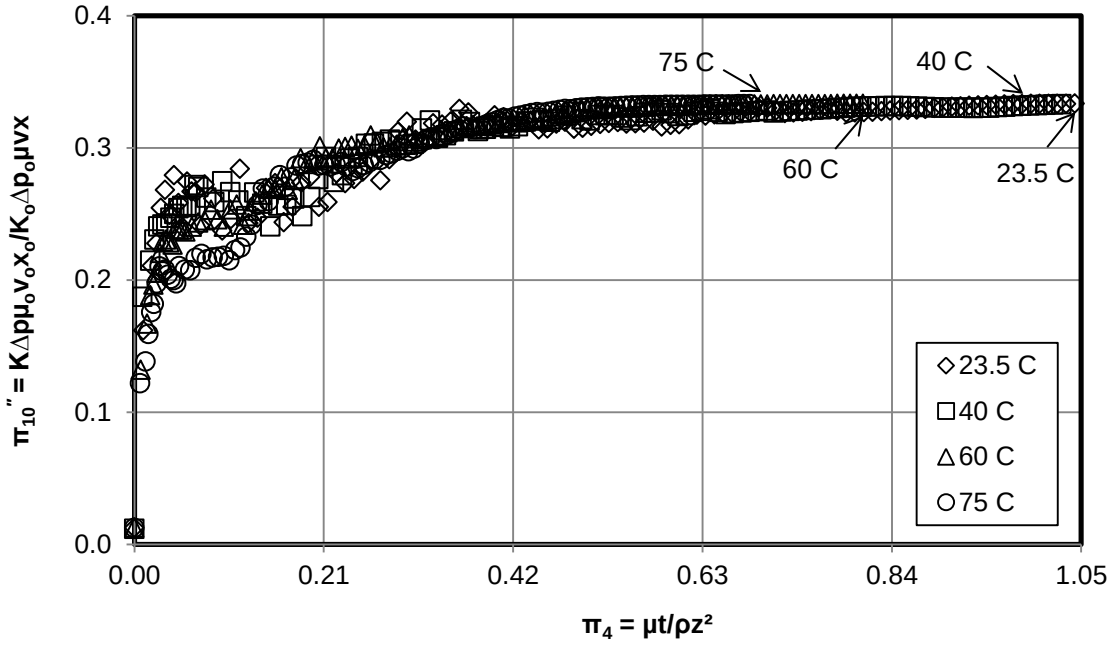

Fig. 7.1: The dimensionless groups for permeability reduction at 3 vol% concentration for different temperatures at 100 cm³/h

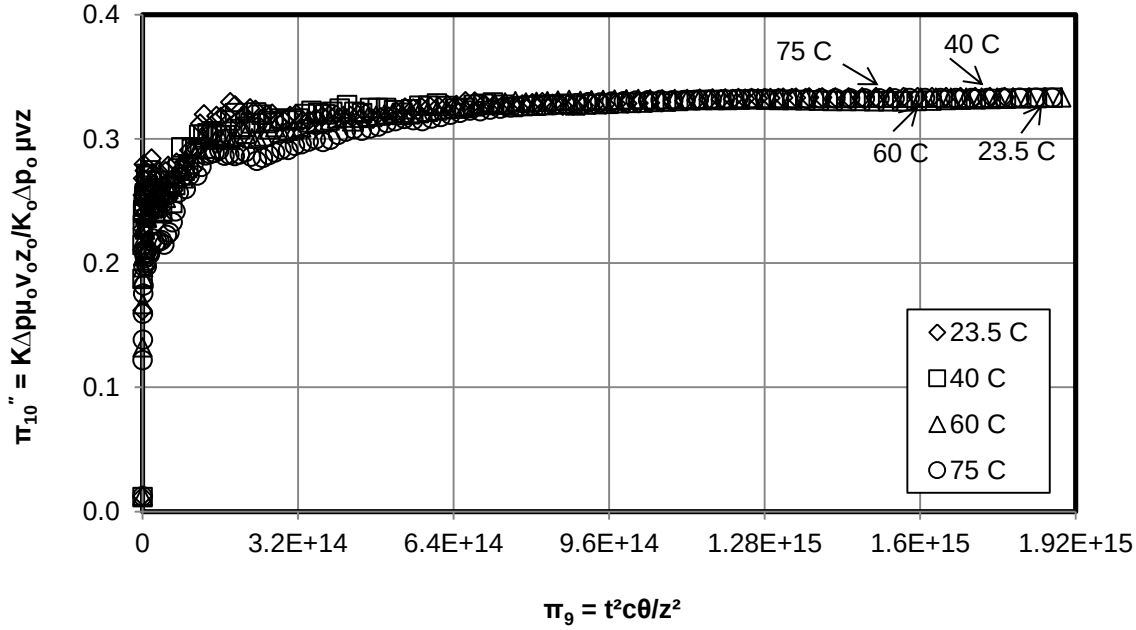

Fig. 7.2: The dimensionless groups for permeability reduction at 3 vol% concentration for different temperatures at 100 cm³/h

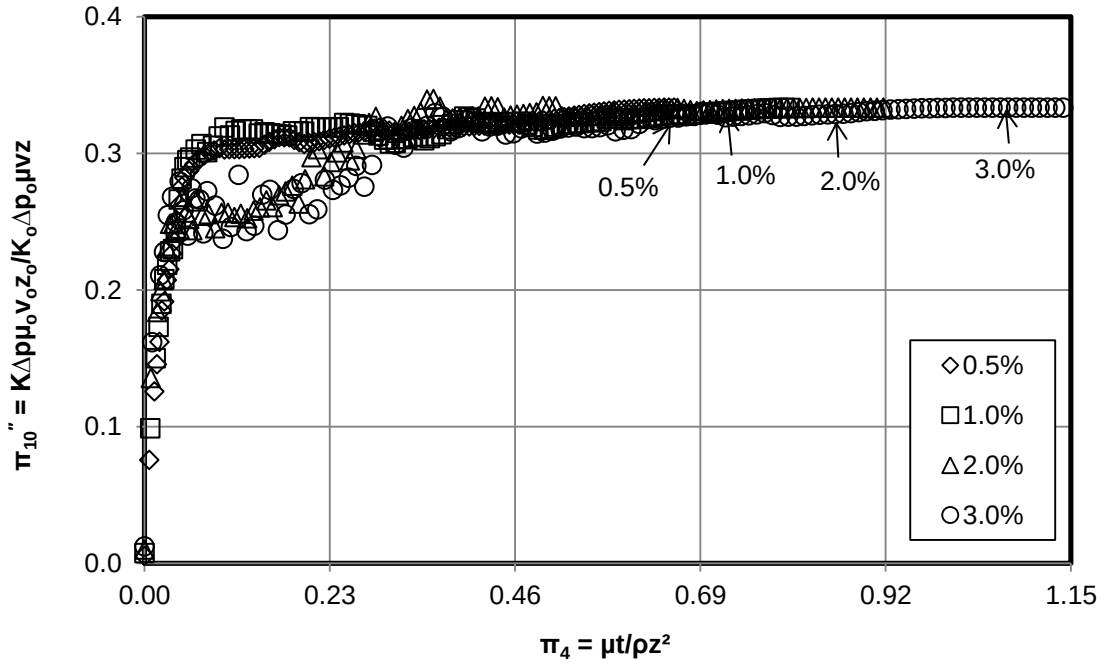

Fig. 7.3: The dimensionless groups for permeability reduction at 100 cm³/h for different concentrations at T= 23.5 ˚C

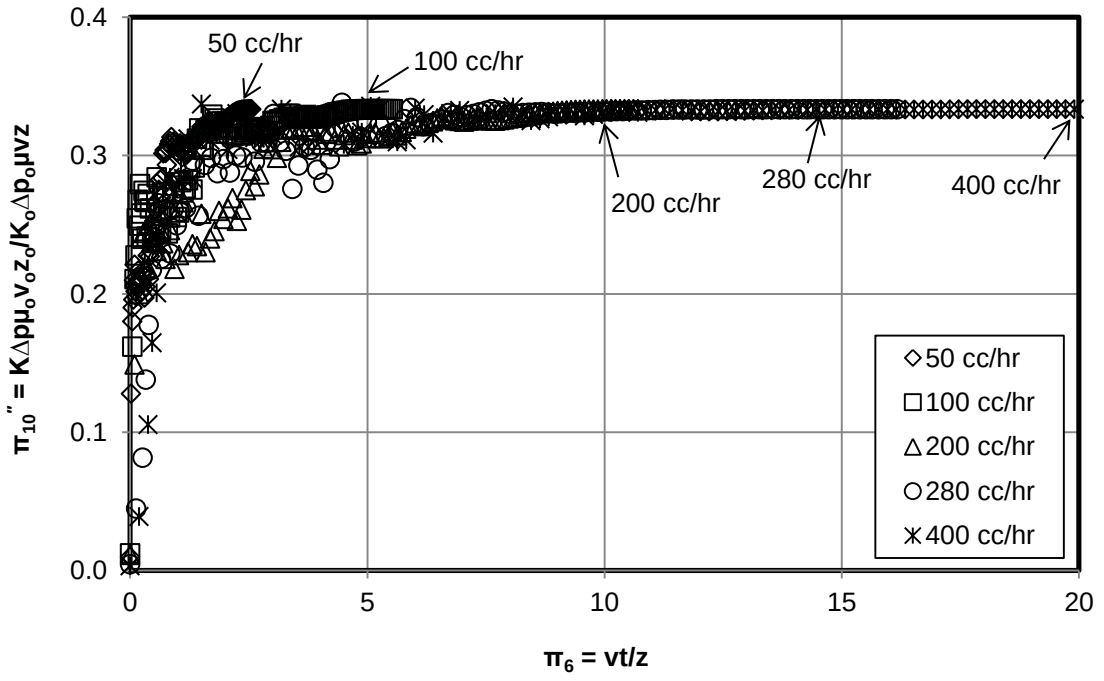

Fig. 7.4: The dimensionless groups for permeability reduction at 3 vol% concentration for different flow rates at T= 23.5 ˚C

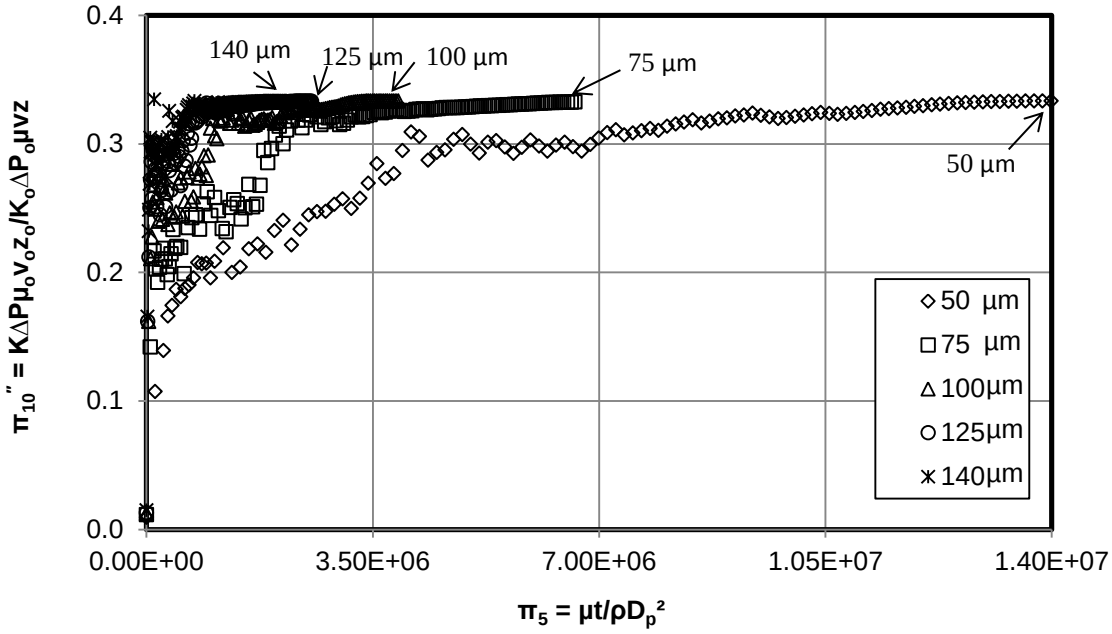

Fig. 7.5: The dimensionless groups for permeability reduction at 100 cm³/hr for diameter different gel particle sizes at T= 23.5 ˚C for the sand pack of 1015 µm grain

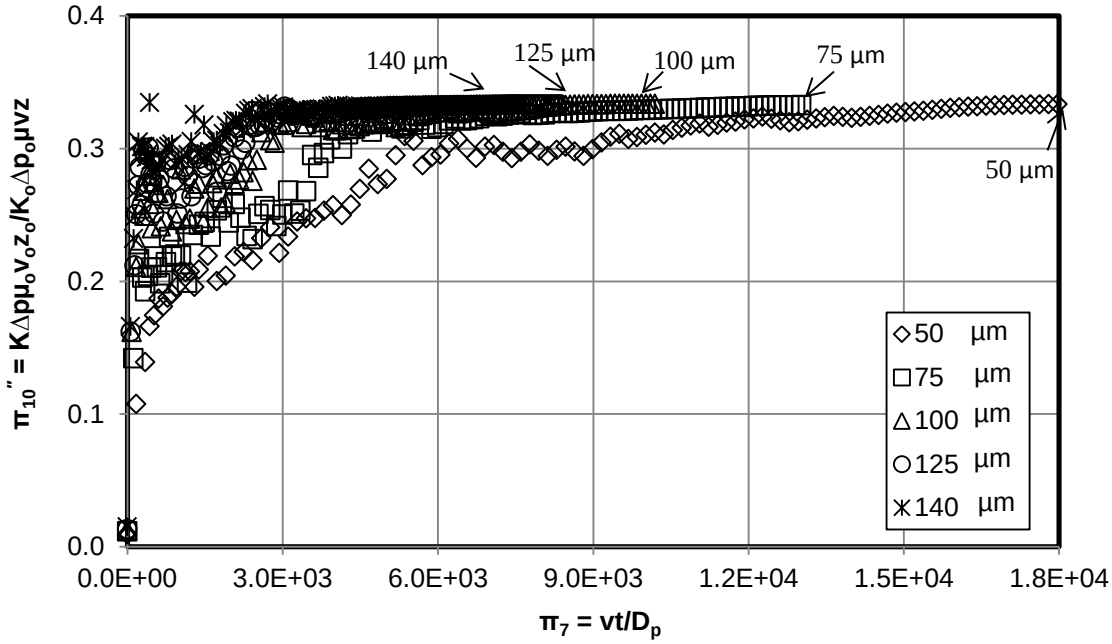

Fig. 7.6: The dimensionless groups for permeability reduction at 100 cm³/hr for different gel particle sizes at T= 23.5 ˚C for the sand pack of 1015 µm grain diameter

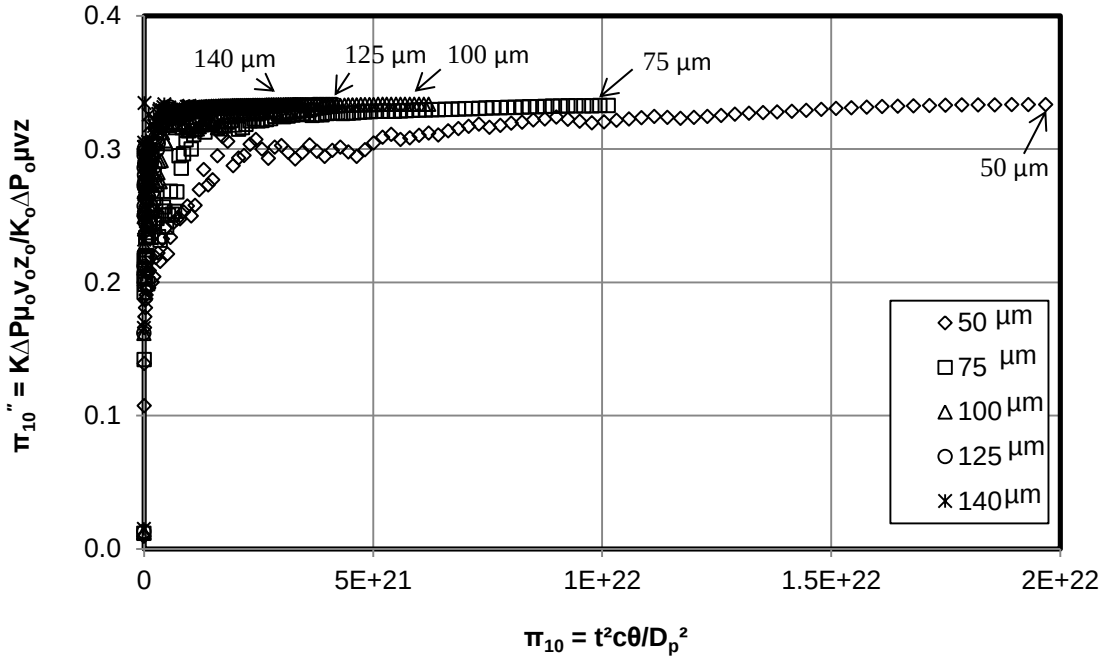

Fig. 7.7: The dimensionless groups for permeability reduction at 100 cm³/h for different gel particle sizes at T= 23.5 ˚C for the sand pack of 1015 µm grain diameter

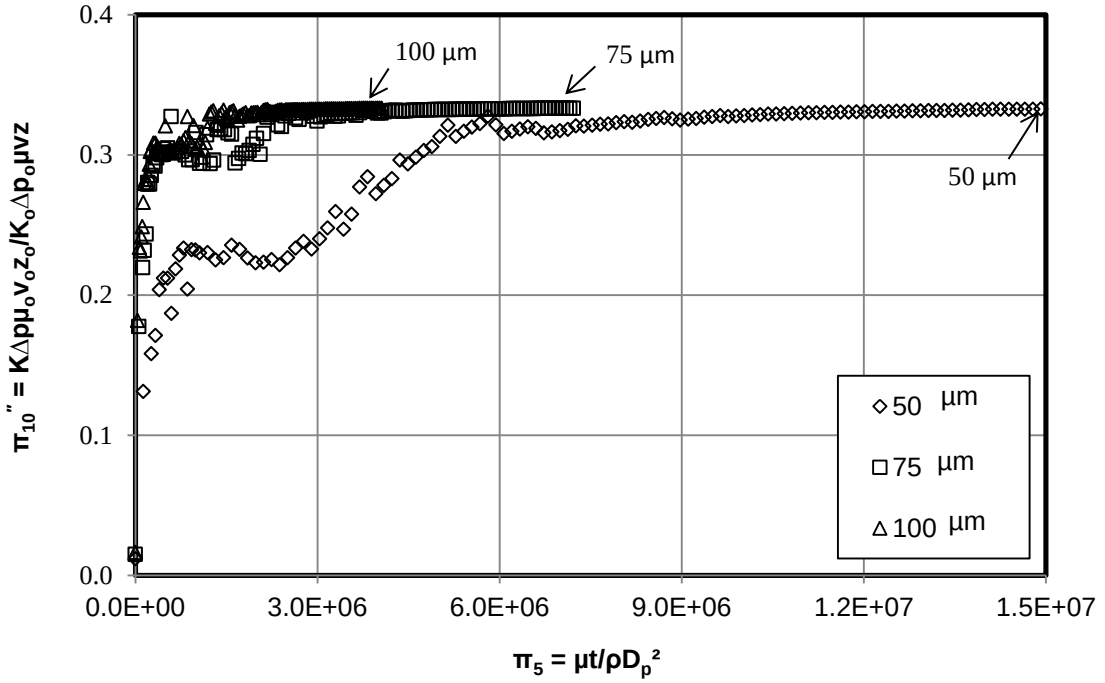

Fig. 7.8: The dimensionless groups for permeability reduction at 100 cm³/h for different gel particle sizes at T= 23.5 ˚C for the sand pack of 650 µm grain diameter

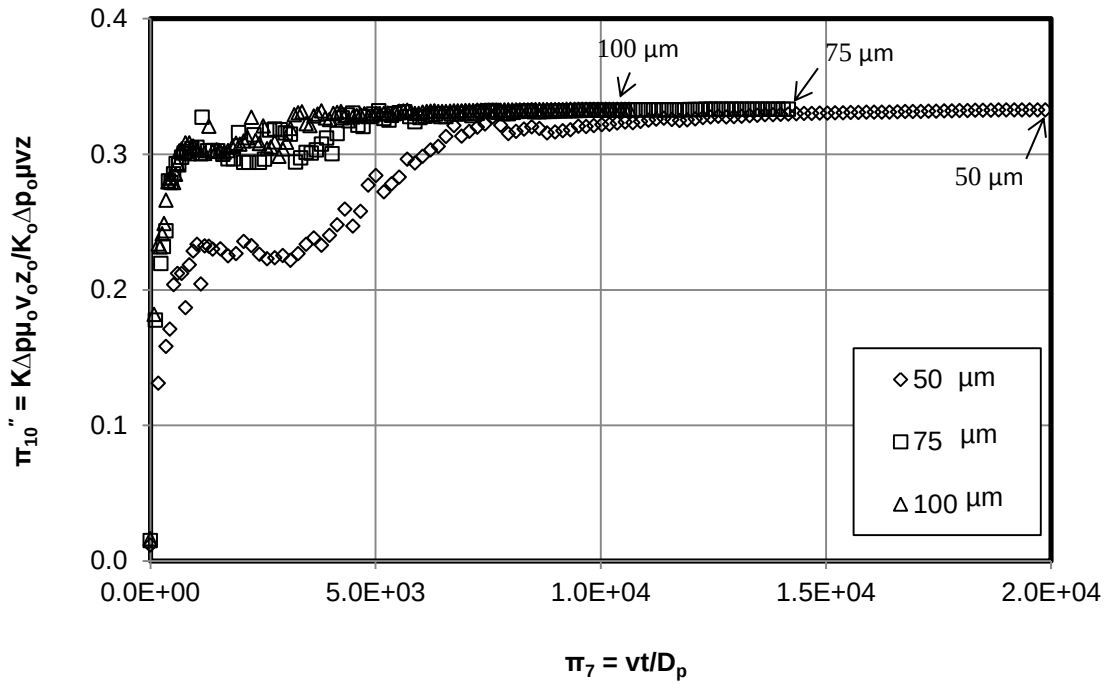

Fig. 7.9: The dimensionless groups for permeability reduction at 100 cm³/h for different gel particle sizes at T= 23.5 ˚C for the sand pack of 650 µm grain diameter

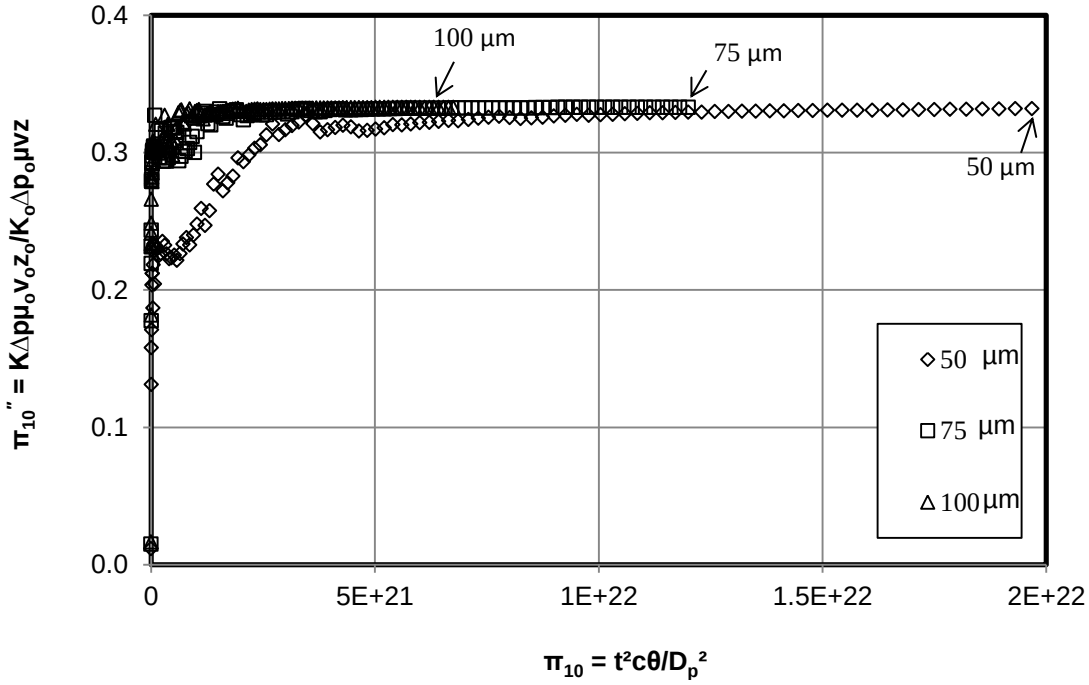

Fig. 7.10: The dimensionless groups for permeability reduction at 100 cm³/h for different gel particle sizes at T= 23.5 ˚C for the sand pack of 650 µm grain diameter

7.3.3 Normalized experimental data

The above direct plotting of the dimensionless groups revealed that the maximum limit values of the various dimensionless groups are different by their final limit values. Thus, it is inconvenient to correlate with the dimensionless groups directly. We resort to the following normalized values method in order to avoid this problem according to Civan (2011b).

$$x^* = \frac{x - x_{\min}}{x_{\max} - x_{\min}} \tag{7.4}$$

where x is the value of the actual dimensionless group; x^* is the normalized value of the dimensionless group; x_{min} is the minimum value of the dimensionless group; and x_{max} is the maximum value of the dimensionless group.

Figs. 7.11 and **7.12** show the normalized Π_4 and Π_9 dimensionless groups for the permeability reduction at 3 vol% concentration for different temperatures at 100 cm³/h and the correlation curves obtained by applying equation B-2 given in Appendix B on the normalized dimensionless groups data, as shown in **Figs. F.1** and **F.2** in Appendix F. **Fig. 7.13** shows the normalized Π_4 dimensionless group for the permeability reduction at 100 cm³/h for different concentrations at T= 23.5 ˚C and the correlation curve obtained by applying equation B-7 given in Appendix B on the normalized dimensionless group data, as shown in **Fig. F.3** in Appendix F. **Fig. 7.14** shows the normalized Π_6 dimensionless group for the permeability reduction at 3 vol% concentration and 23.5 ˚C for different flow rates and the correlation curve obtained by applying equation B-7 given in Appendix B on the normalized dimensionless group data, as shown in **Fig. F.4** in Appendix F. For the permeability reduction at 100 cm³/h

and 23.5 ˚C for different particle sizes for the sand pack of 1015 µm grain diameter, we obtained same values of the normalized dimensionless groups of Π_5 , Π_7 , and Π_{10} and same correlation curves by applying equation B-2 on the normalized dimensionless group data. Therefore, we used only Π_5 dimensionless group to correlate the data as shown in **Fig. 7.15** for the sand pack of 1015 µm grain diameter and in **Fig. 7.16** for the sand pack of 650 µm grain diameter, as shown in **Figs. F.5** and **F.6** in Appendix F.

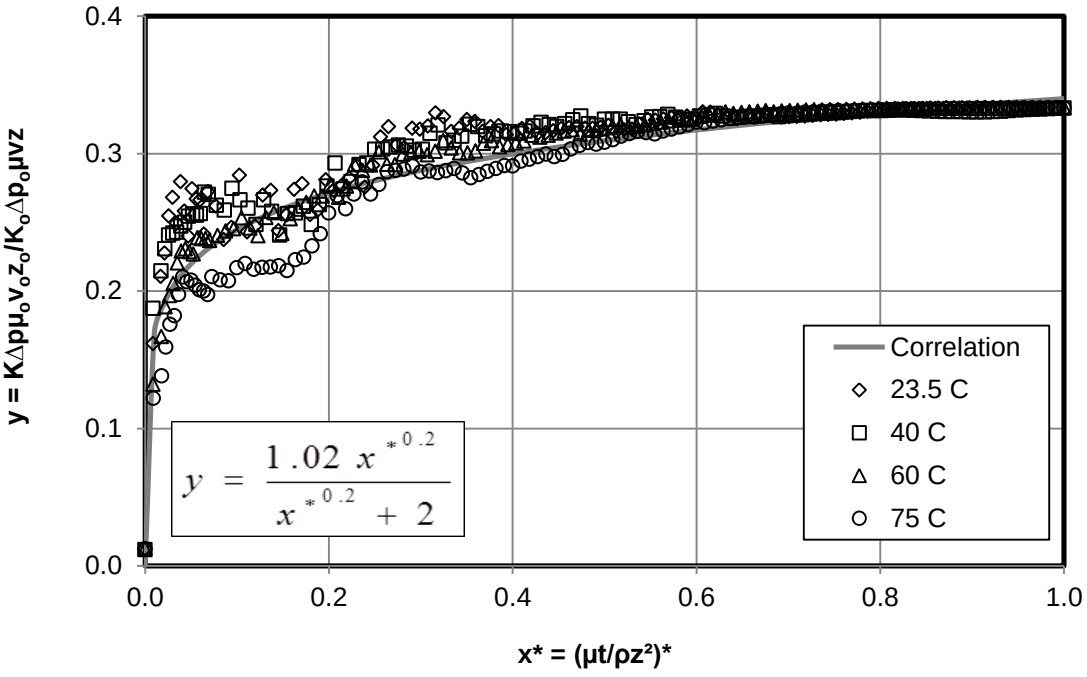

Fig. 7.11: Correlation of the normalized dimensionless groups for permeability reduction at 3 vol% concentration for different temperatures at 100 cm³/h

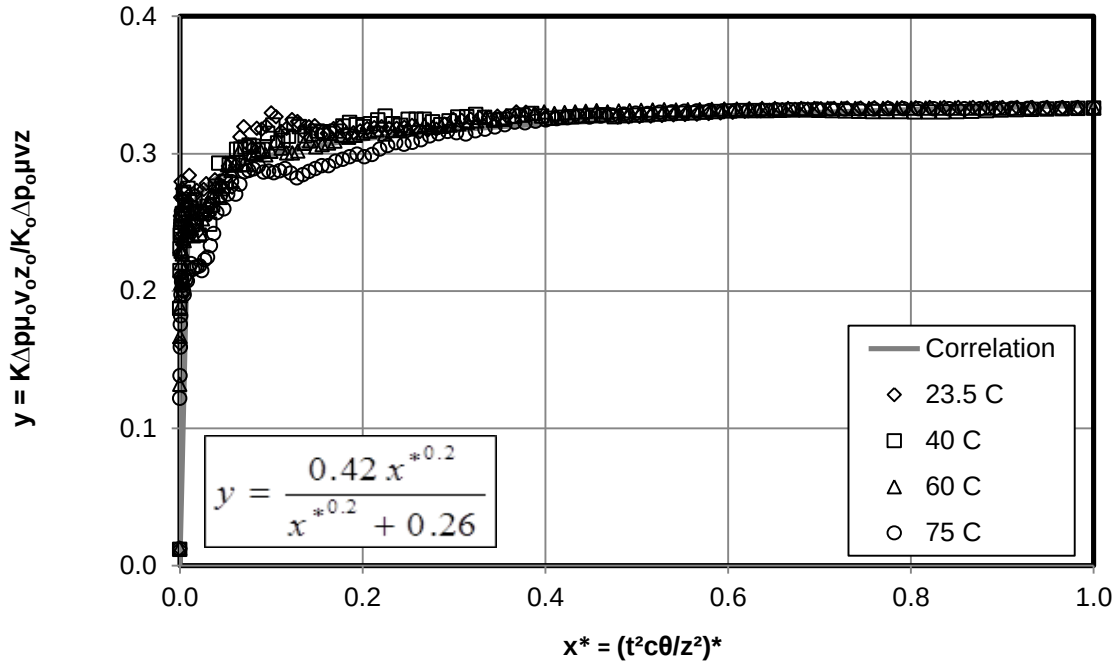

Fig. 7.12: Correlation of the normalized dimensionless groups for permeability reduction at 3 vol% concentration for different temperatures at 100 cm³/h

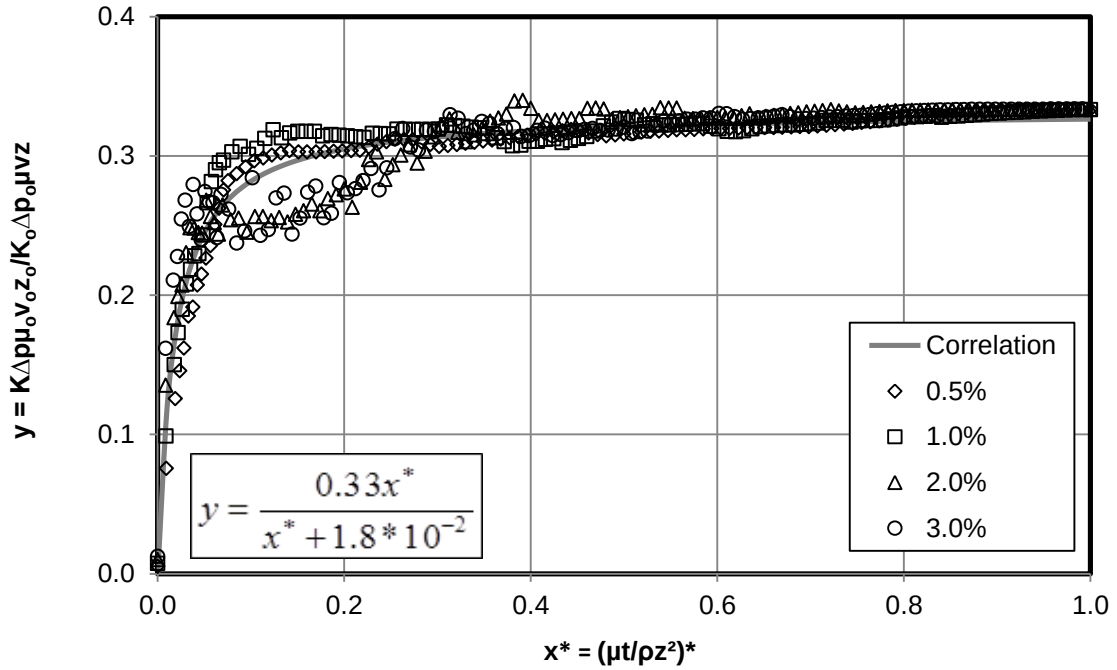

Fig. 7.13: Correlation of the normalized dimensionless groups for permeability reduction at 100 cm³/h for different concentrations at T= 23.5 ˚C

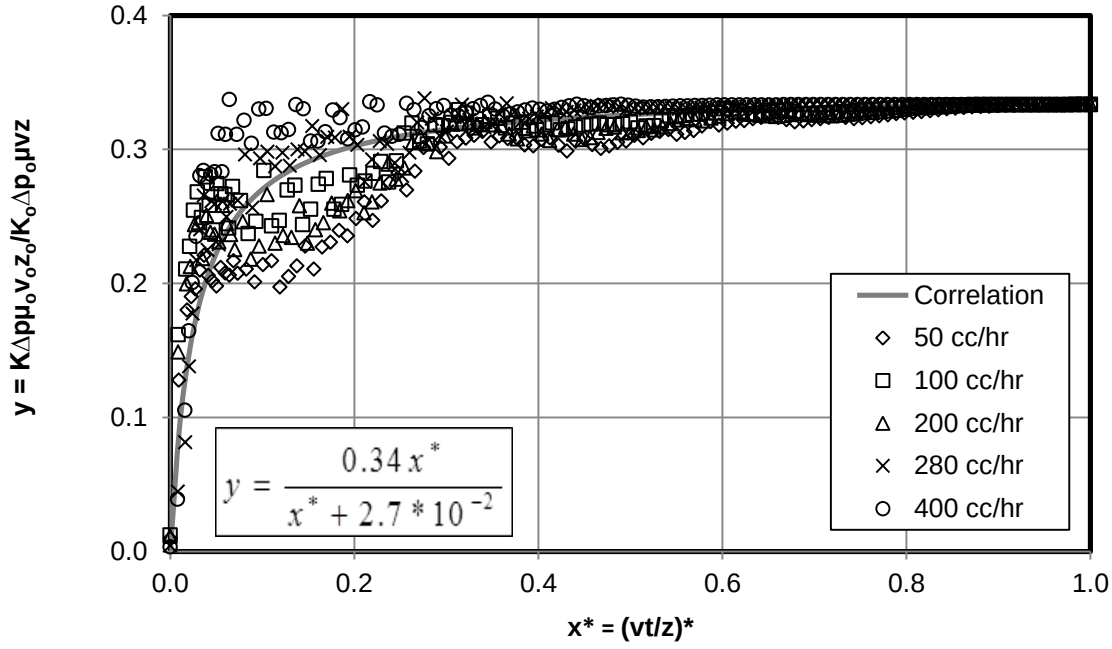

Fig. 7.14: Correlation of the normalized dimensionless groups for permeability reduction at 3 vol% concentration for different flow rates at T= 23.5 ˚C diameter at different gel particles sizes

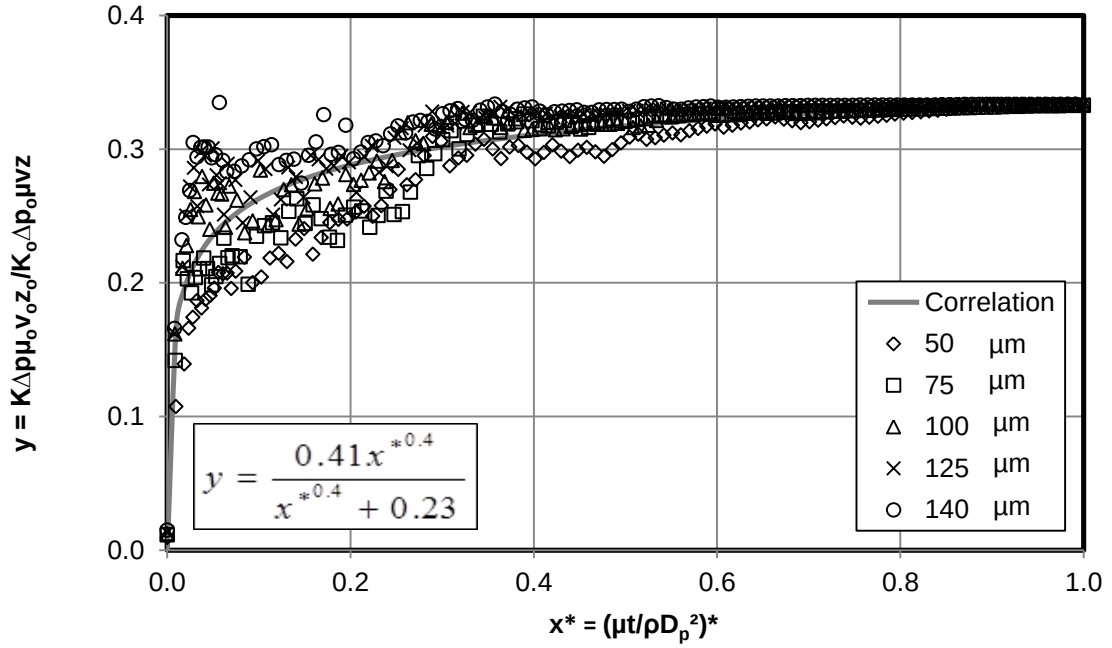

Fig. 7.15: Correlation of the normalized dimensionless groups for permeability reduction at 100 cm³/hr for different gel particle sizes at T= 23.5 ˚C for the sand pack of 1015 μm grain diameter

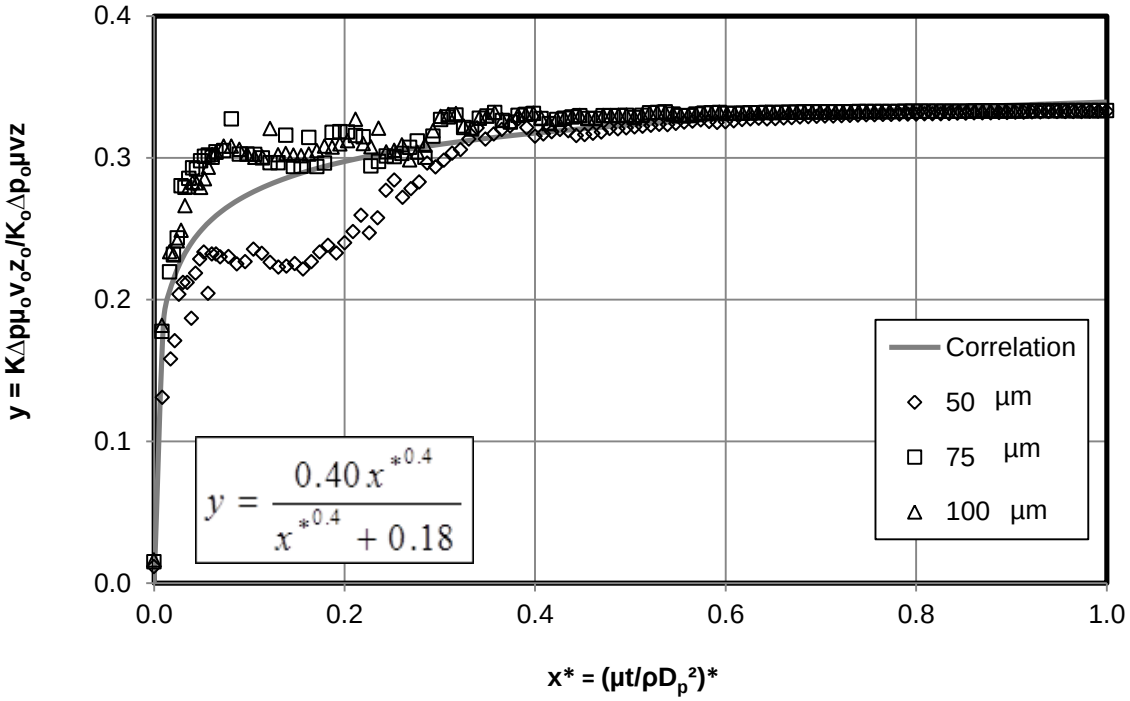

Fig. 7.16: Correlation of the normalized dimensionless groups for permeability reduction at 100 cm³/hr for different gel particle sizes at T= 23.5 ˚C for the sand pack of 650 μm grain diameter

7.3.4 Permeability Reduction Correlations

Figs. 7.17 and **7.18** show the measured permeability reduction *(K/K_o)* and the correlated permeability reduction obtained from the dimensionless correlations of the normalized Π_4 and Π_9 dimensionless groups for permeability reduction at 3 vol% concentration for different temperatures at 100 cm³/h. The measured data show permeability reduction from 0.36 to 0.415 by increasing the temperature from 23.5 ˚C to 75 ˚C. This means that the plugging of pores and pore- throats decreases by the temperature because the gel particles became more soft and deformable by temperature. The correlated data of the normalized Π_4 dimensionless group show permeability reduction from 0.366 to 0.427 and the normalized Π_9 dimensionless group show

permeability reduction from 0.358 to 0.417 by increasing the temperature from 23.5 ˚C to 75 ˚C.

Fig. 7.19 shows the measured permeability reduction and the correlated permeability reduction obtained from the dimensionless correlations of the normalized Π_4 dimensionless group for permeability reduction at 100 cm^3/h for different concentrations at T = 23.5 ˚C. The measured data show permeability reduction from 0.81 to 0.36 by increasing the gel particles concentration from 0.5% to 3.0% because the amount of particles plugging the pores increases by concentration. The correlated data of the normalized Π_4 dimensionless group show permeability reduction from 0.80 to 0.354 by increasing the gel particles concentration from 0.5% to 3.0%.

Fig. 7.20 shows the measured permeability reduction and the correlated permeability reduction obtained from the dimensionless correlations of the normalized Π_6 dimensionless group for permeability reduction at 3 vol% concentration and 23.5 ˚C for different flow rates. The measured data show permeability reduction increasing from 0.0.46 to 0.36 by increasing the flow rate from 50 cc/h to 100 cc/h and decreasing from 0.36 to 0.60 by increasing the flow rate from 100 cc/h to 400 cc/h because at the high flow rate the particles can pass easily through the pore throats and the plugging of pores decreases. The correlated data of the normalized Π_6 dimensionless group show the same values of the measured permeability reduction when the flow rate increases from 50 cc/h to 100 cc/h and from 100cc/h to 400 cc/h.

Fig. 7.21 shows the measured permeability reduction and the correlated permeability reduction obtained from the dimensionless correlations of the normalized Π_5 dimensionless group for permeability reduction at 100 cm^3/h and 23.5 ˚C for

different particle sizes for the sand pack of 1015 µm grain diameter. The measured data show permeability reduction from 0.54 to 0.30 by increasing the particle diameter from 50 µm to 400 µm because the plugging of pores increases by gel particle size. The correlated data of the normalized Π_5 dimensionless group show permeability reduction from 0.544 to 0.30 by increasing the particle size from 50 µm to 140 µm.

Fig. 7.22 shows the measured permeability reduction and the correlated permeability reduction obtained from the dimensionless correlations of the normalized Π_5 dimensionless group for permeability reduction at 100 cm³/hr and 23.5 ˚C for different particle sizes for the sand pack of 650 µm grain diameter. The measured data show permeability reduction from 0.34 to 0.27 by increasing the particle diameter from 50 µm to 100 µm and the correlated data of the normalized Π_5 dimensionless group show permeability reduction from 0.346 to 0.273 by increasing the particle size from 50 µm to 75 µm.

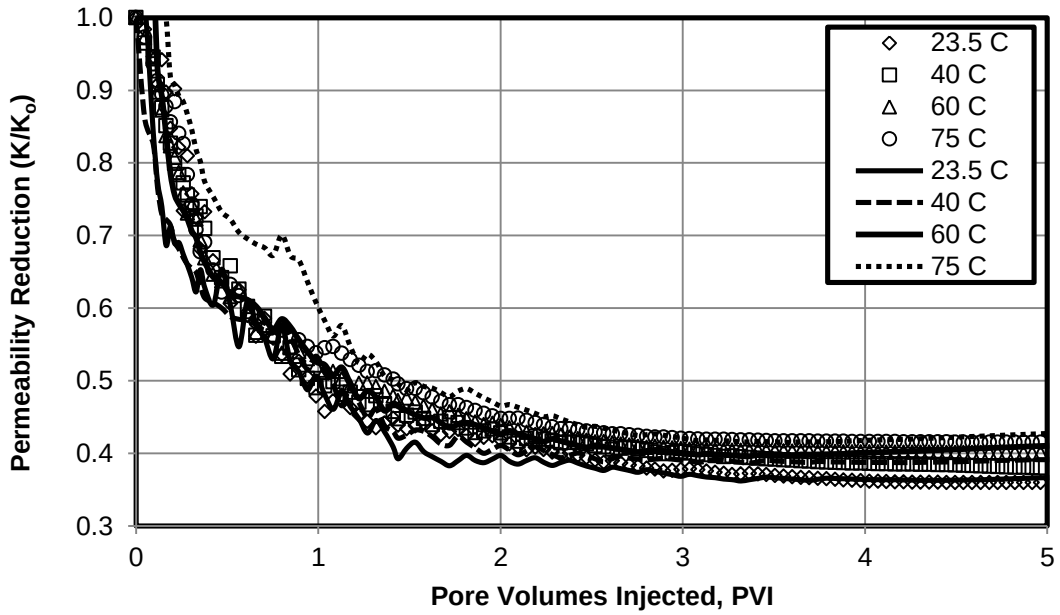

Fig. 7.17: Measured permeability reduction and correlated permeability reduction (from $K\Delta p\mu_o v_o z_o/K_o\Delta p_o\mu vz$ and $(\mu t/\rho z^2)$* correlation) at 3 vol% concentration for different temperatures at 100 cm³/h

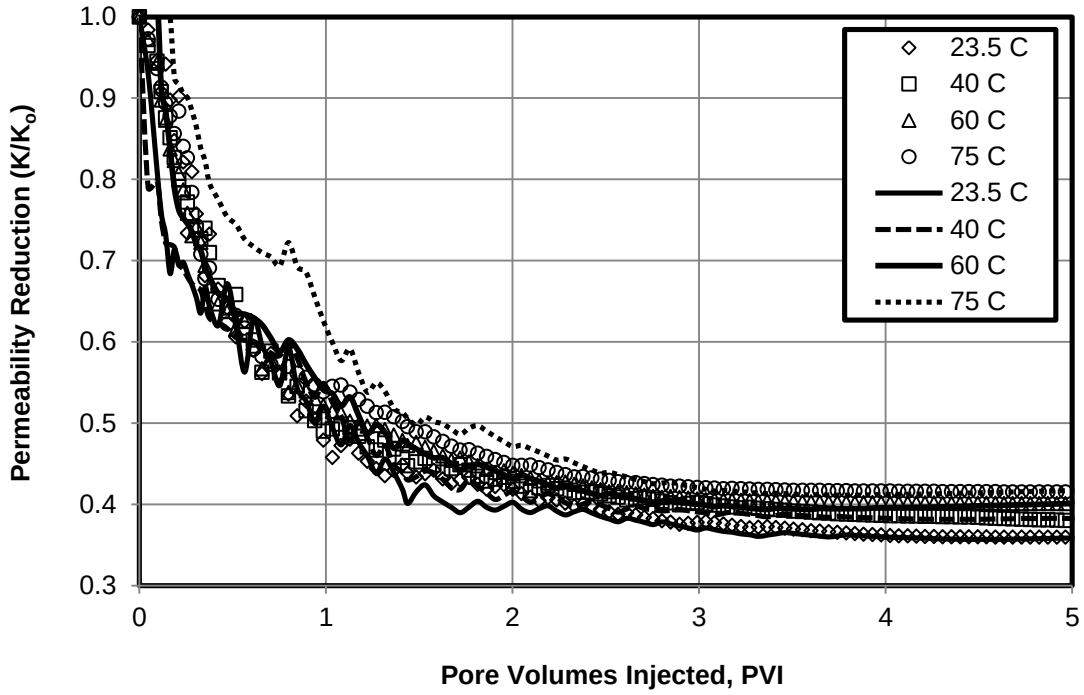

Fig. 7.18: Measured permeability reduction and correlated permeability reduction (from $K\Delta p\mu_o v_o z_o/K_o\Delta p_o\mu vz$ and $(t^2c\theta/z^2)$* correlation) at 3 vol% concentration for different temperatures at 100 cm^3/h

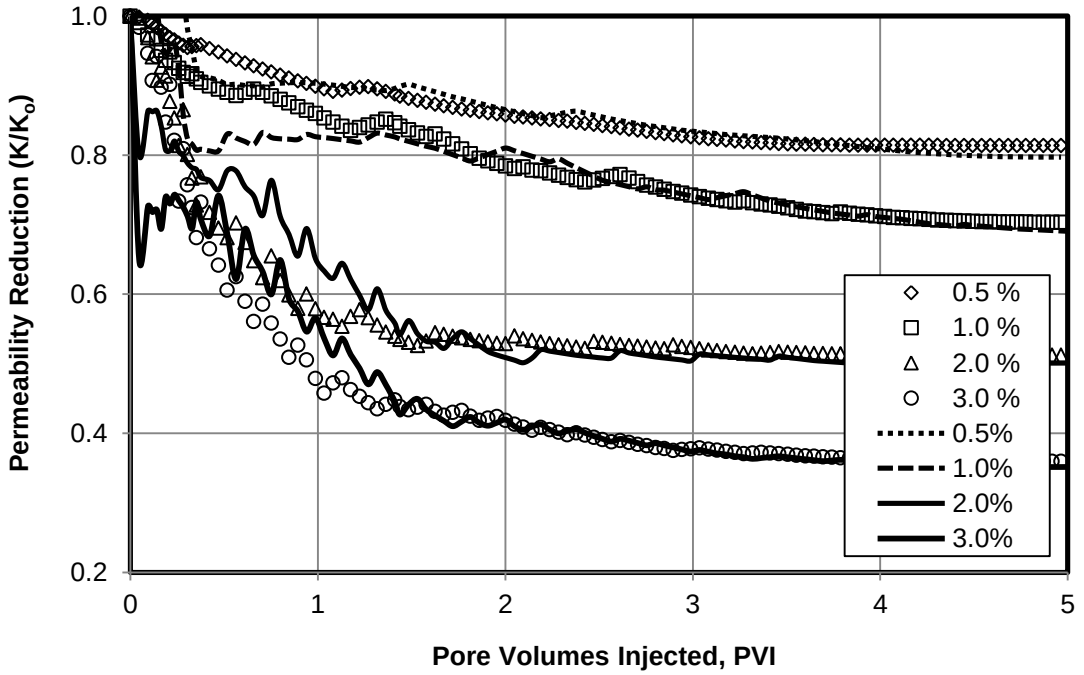

Figure 7.19: Measured permeability reduction and correlated permeability reduction (from $K\Delta p\mu_o v_o z_o/K_o\Delta p_o\mu vz$ and $(\mu t/\rho z^2)$* correlation) at 100 cm^3/h for different concentrations at T=23.5˚C

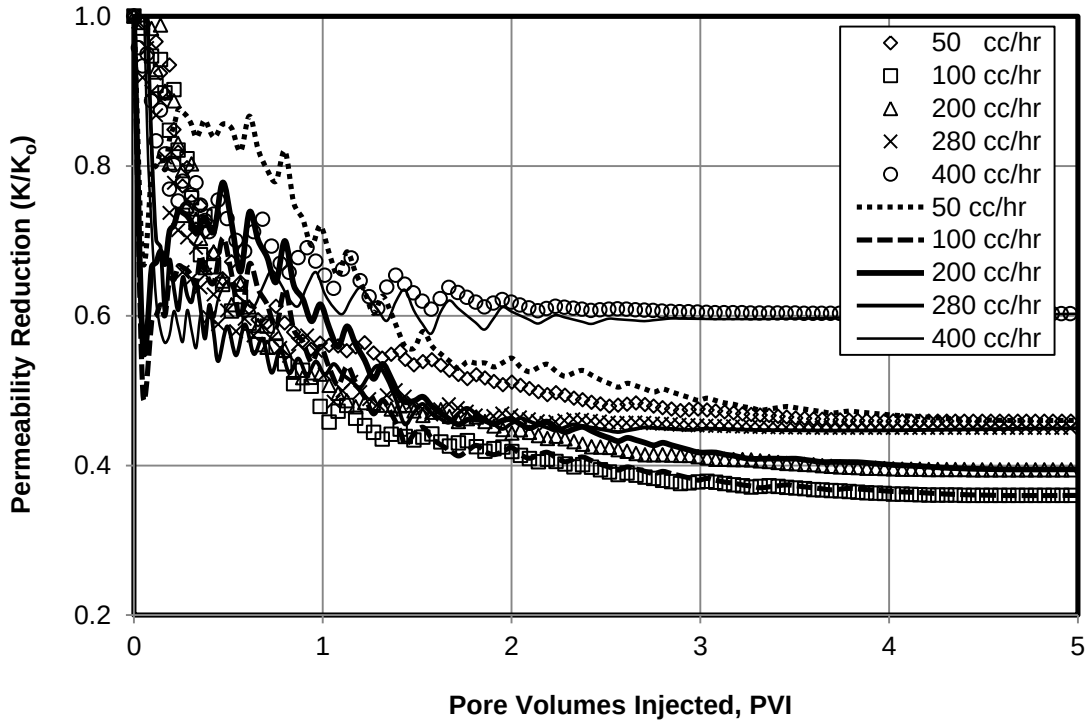

Figure 7.20: Measured permeability reduction and correlated permeability reduction (from $K\Delta p\mu_o v_o z_o/K_o\Delta p_o\mu vz$ and $(vt/z)^*$ correlation) at 3 vol% concentration for different flow rates at T= 23.5 ˚C

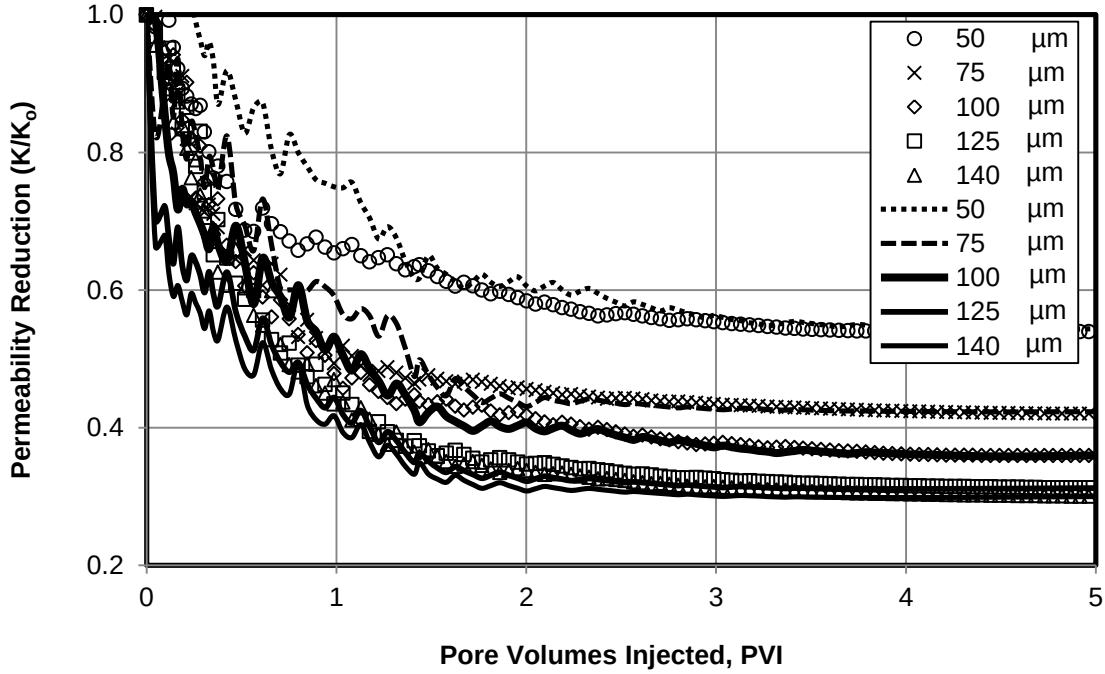

Figure 7.21: Measured permeability reduction and correlated permeability reduction (from $K\Delta p\mu_o v_o z_o/K_o\Delta p_o\mu vz$ and $(\mu t/\rho D_p^2)^*$ correlation) at 100 cm³/h for different gel particle sizes at T= 23.5 ˚C for the sand pack of 1015 µm grain diameter

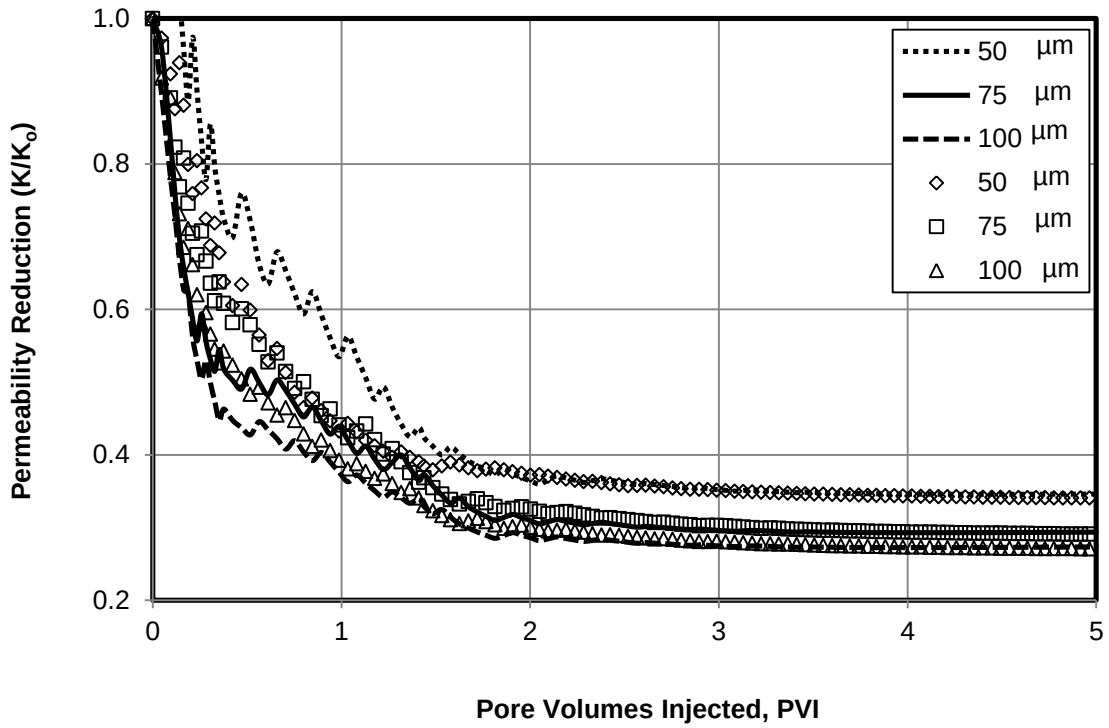

Figure 7.22: Measured permeability reduction and correlated permeability reduction (from $K\Delta p\mu_o v_o z_o/K_o\Delta p_o\mu vz$ and $(\mu t/\rho D_p^2)$* correlation) at 100 cm^3/h for different gel particle sizes at T= 23.5 ˚C for the sand pack of 650 µm grain diameter

7.4 Correlated Versus Measured Permeability Reduction

The correlated data of all the normalized dimensionless groups presented above show satisfactory results in comparison with the measured data of the permeability reduction. Thus, the dimensionless correlations can be used to predict the permeability reduction across the sand pack during the gel particles injection at any temperature, particle concentration, flow rate, and particle diameter. **Figs. 7.23** to **7.28** show comparison between the measured permeability reduction and the correlated permeability reduction obtained from all the dimensionless correlations of all the normalized dimensionless groups for the permeability reduction at different

temperatures, particle concentrations, flow rates, and particle diameters. The plot of the correlated versus measured permeability reduction clusters close the diagonal-line indicating that the dimensional correlations represent the data satisfactory. Also, the accuracy is lower during the early injection period but improves rapidly as more pore volumes of suspension injected, as shown in the **Figs. 7.29** to **7.34** of the steady limit value of correlated versus measured permeability reduction at 5 pore volumes injected (PVI). The reason of the scatter of the points and the lower accuracy during the early injection period is the consecutively occurring plugging and unplugging phenomena that were demonstrated in our previous studies (Al-Ibadi and Civan 2012, 2013a and 2013b). At the beginning of the gel particles injection, the particles are trapped at the entrance of the pore-throats causing a buildup in the differential pressure which subsequently leads to deformation and passing of the trapped particles through the pore-throats decreases the differential pressure. The plugging and unplugging processes induced by suspension injection repeat continuously until attaining a constant steady differential pressure and the permeability reduction reaches approximately a constant limit value.

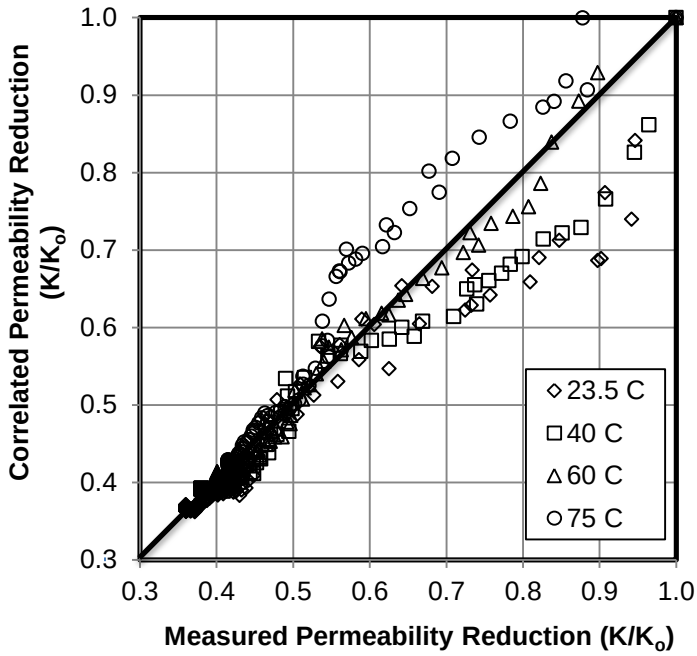

Fig. 7.23: Comparison between measured permeability reduction and correlated permeability reduction at 3 vol% concentration for different temperatures at 100 cm³/h

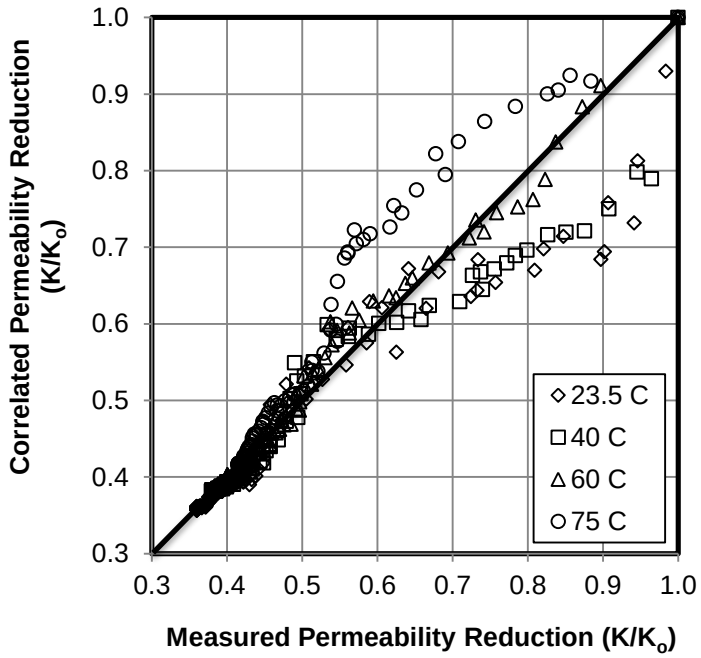

Fig. 7.24: Comparison between measured permeability reduction and correlated permeability reduction at 3 vol% concentration for different temperatures at 100 cm³/h

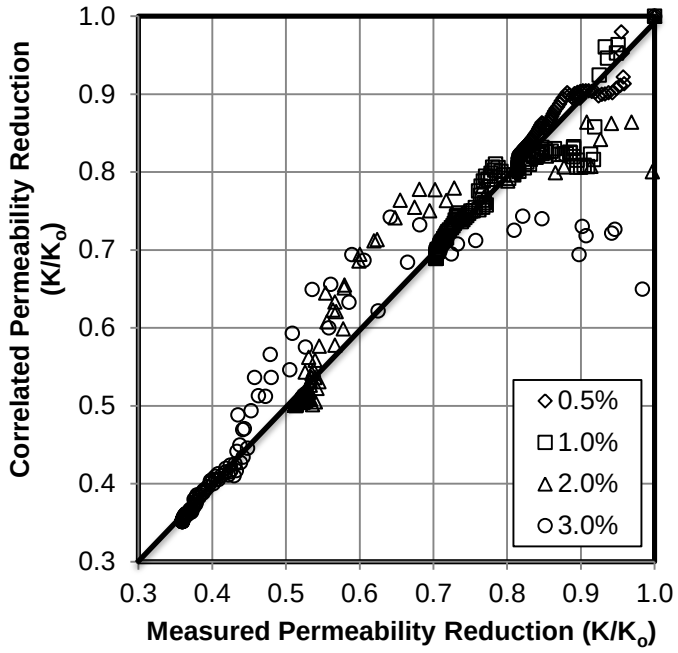

Fig. 7.25: Comparison between measured permeability reduction and correlated permeability reduction at 100 cm³/h for different concentrations at T= 23.5 ˚C

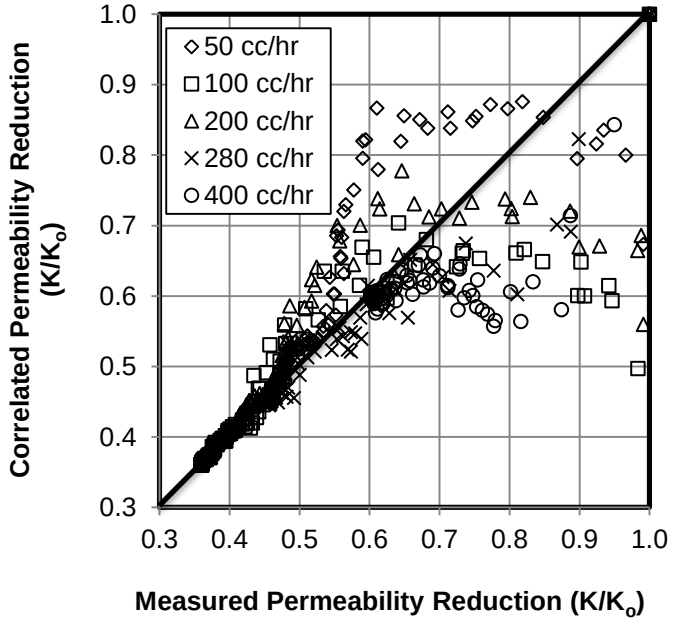

Fig. 7.26: Comparison between measured permeability reduction and correlated permeability reduction at 3 vol% concentration for different flow rates at T= 23.5 ˚C

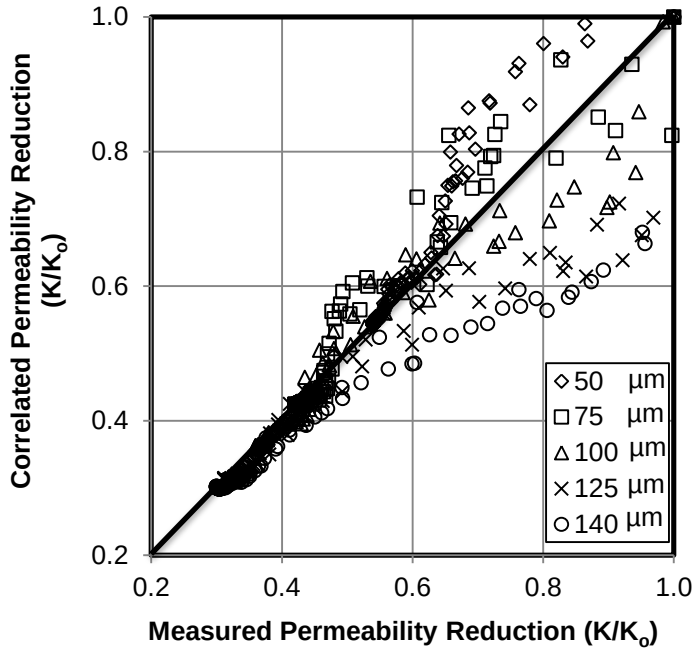

Fig. 7.27: Comparison between measured permeability reduction and correlated permeability reduction at 100 cc/h for different gel particle sizes at T= 23.5 ˚C for the sand pack of 1015 µm grain diameter

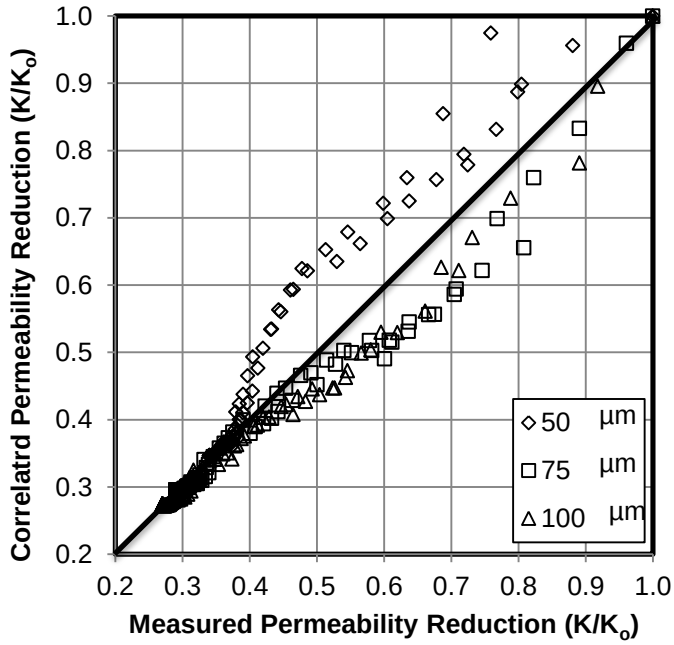

Fig. 7.28: Comparison between measured permeability reduction and correlated permeability reduction at 100 cc/h for different gel particle sizes at T= 23.5 ˚C for the sand pack of 650 µm grain diameter

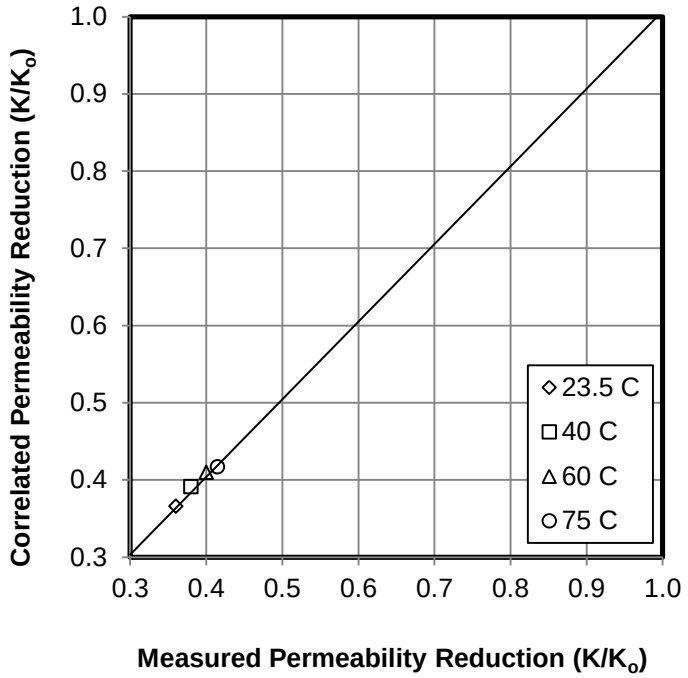

Fig. 7.29: Comparison between constant limit value of steady measured permeability reduction and correlated permeability reduction at 5 PVI for different temperatures

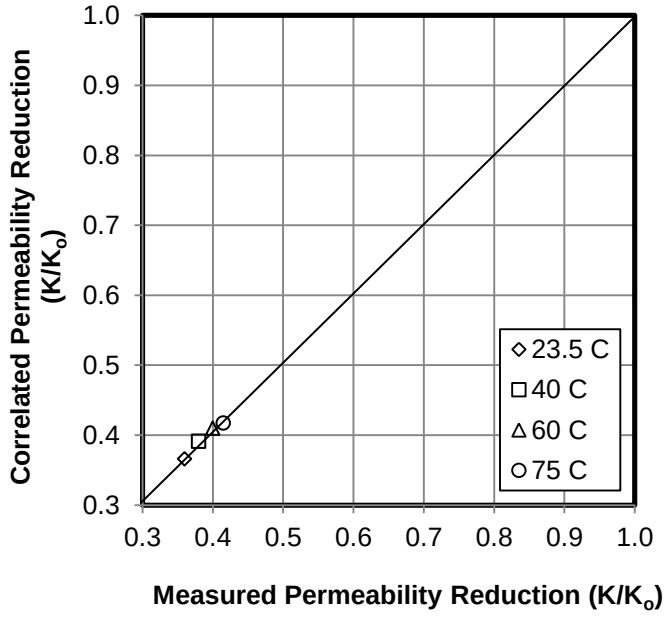

Fig. 7.30: Comparison between constant limit value of steady measured permeability reduction and correlated permeability reduction at 5 PVI for different temperatures

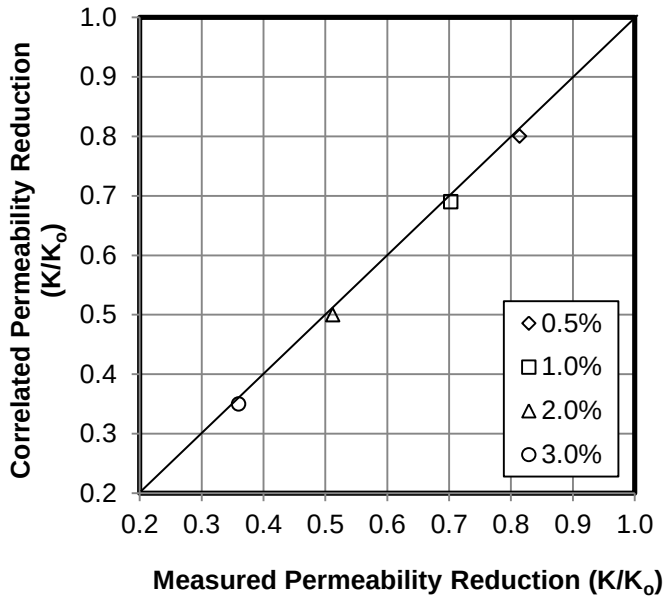

Fig. 7.31: Comparison between constant limit value of steady measured permeability reduction and correlated permeability reduction at 5 PVI for different concentrations

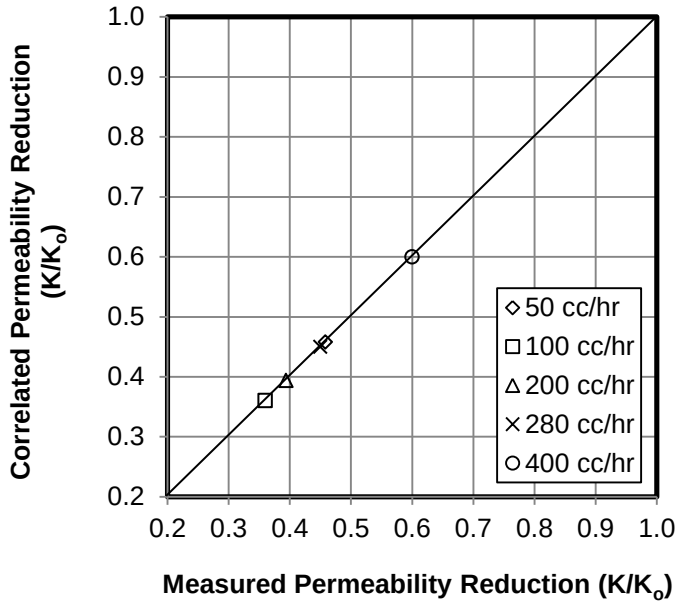

Fig. 7.32: Comparison between constant limit value of steady measured permeability reduction and correlated permeability reduction at 5 PVI for different flow rates

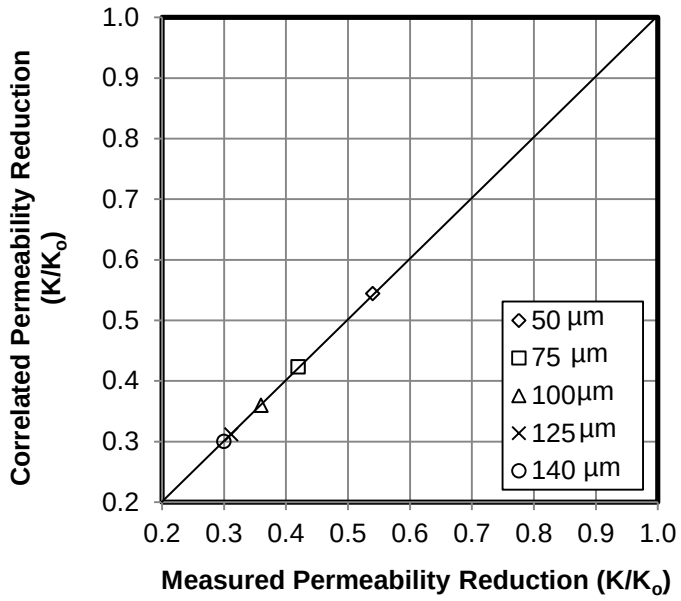

Fig. 7.33: Comparison between constant limit value of steady measured permeability reduction and correlated permeability reduction at 5 PVI for different gel particle sizes for the sand pack of 1015 µm grain diameter

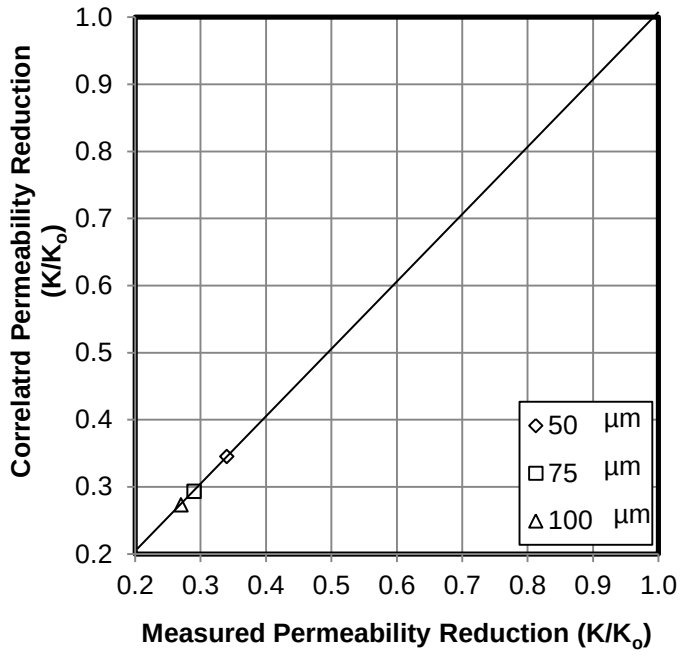

Fig. 7.34: Comparison between constant limit value of steady measured permeability reduction and correlated permeability reduction at 5 PVI for different gel particle sizes for the sand pack of 650 µm grain diameter

7.5 Effect of Particle-Diameter to Pore-Throat Size Ratio on Permeability Reduction

The limit value of the steady measured permeability reduction at 100 cm^3/h for 3 vol% concentration at T = 23.5 ˚C for different particle-diameter to pore-throat size ratios was correlated satisfactory in our previous studies (Al-Ibadi and Civan 2012 and 2013a) as shown in **Fig. 7.35**. The experimental data show a permeability reduction from 0.54 to 0.27 by increasing the ratio of particle-diameter to pore-throat size from 0.40 to 1.7 because pore plugging is enhanced by increase in the particle-diameter to pore-throat size ratio.

To correlate the effect of the ratio of the gel particle-diameter to the pore-throat size on the permeability reduction by gel particles, we used the Π_2 dimensionless group that represents (D_p/D_T). **Figs. 7.36** and **7.37** show the limit value of steady measured and correlated dimensionless group and permeability reduction, respectively, at 100 cm^3/h for 3 vol% concentration at T = 23.5 ˚C for different particle-diameter to pore-throat size ratios. The correlated data of the dimensionless group show satisfactory results compared with the measured data. **Fig. 7.38** shows a comparison and satisfactory correlation between the constant limit values of the measured and correlated permeability reductions at 100 cc/h for 3 vol% concentration at T = 23.5 ˚C for different particle-diameter to pore-throat size ratios.

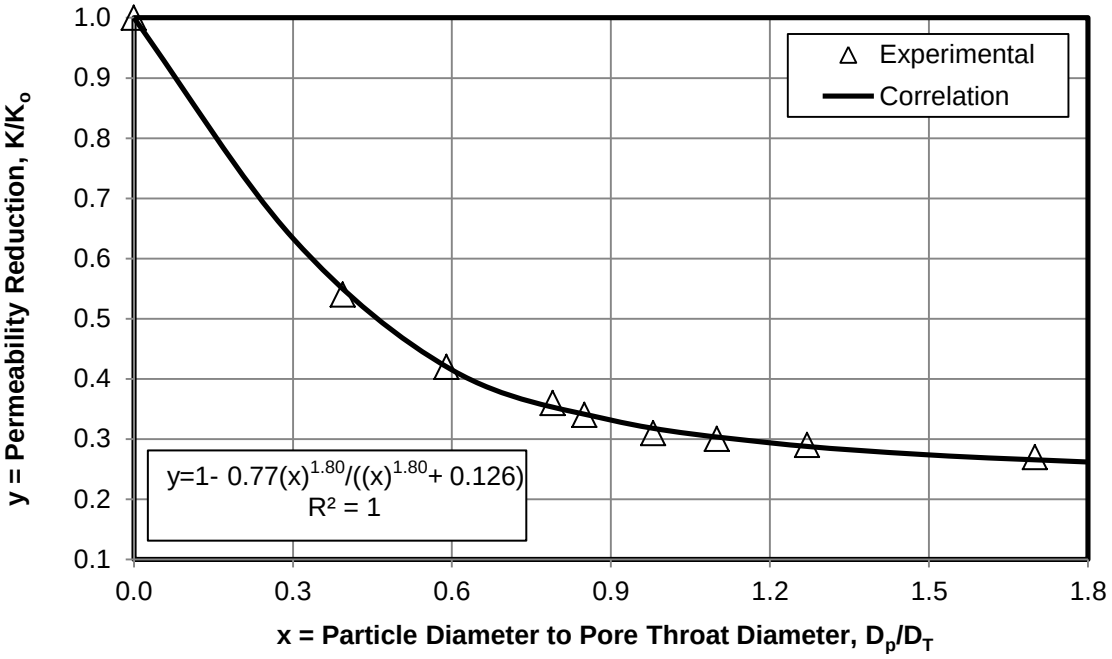

Fig. 7.35: Limit value of steady measured permeability reduction and correlated permeability reduction at 100 cm³/h for 3 vol% concentration at T= 23.5 ˚C for different particle diameter to pore-throat size ratios (Al-Ibadi and Civan 2012 and 2013a)

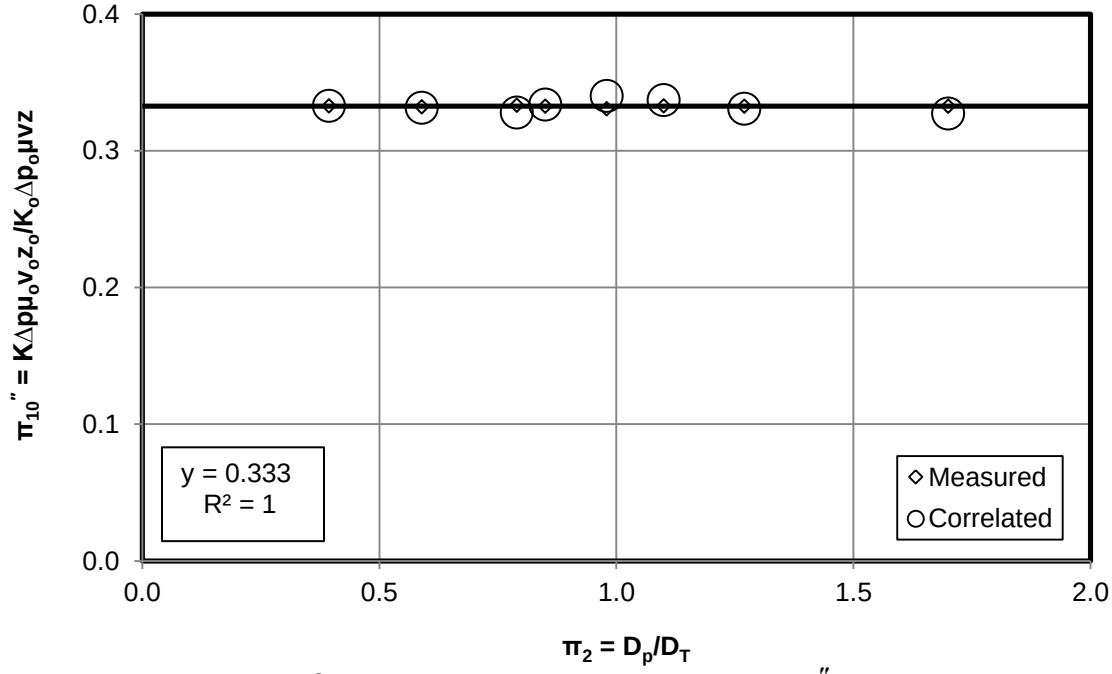

Fig. 7.36: Limit value of steady measured and correlated π_{10}'' and π_2 dimensionless groups for permeability reduction at 100 cm³/h for 3 vol% concentration at T= 23.5 ˚C for different particle diameter to pore-throat size ratios

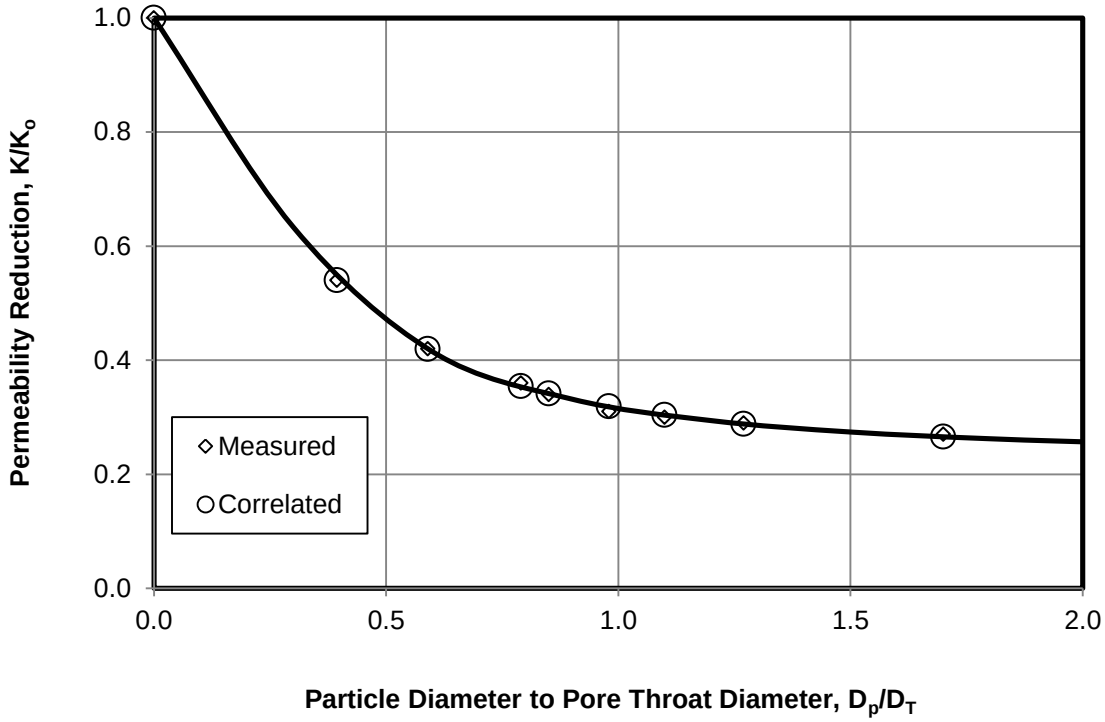

Figure 7.37: Measured permeability reduction and correlated permeability reduction (from $K\Delta p\mu_o v_o z_o/K_o\Delta p_o\mu vz$ and D_p/D_T dimensionless groups) at 100 cm³/h for 3 vol% at T= 23.5 ˚C for different particle diameter to pore-throat size ratios

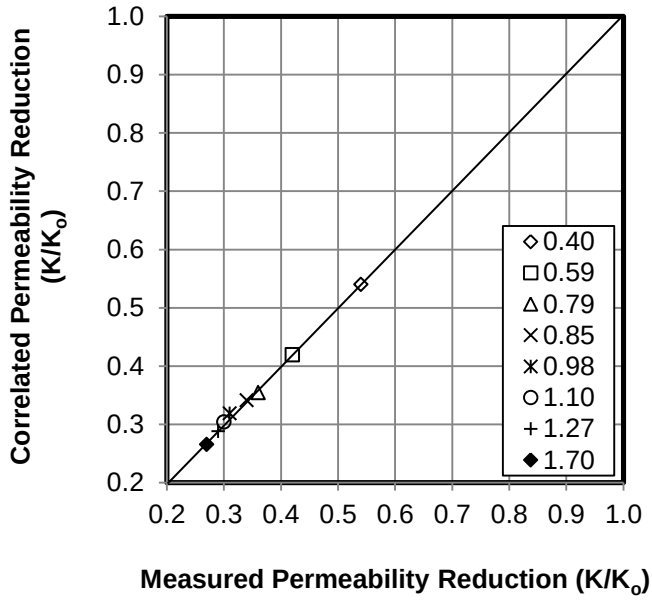

Fig. 7.38: Comparison between constant limit value of measured permeability reduction and correlated permeability reduction at 100 cm^3/h for 3 vol% concentration at T= 23.5 ˚C for different particle diameter to pore-throat size ratios

7.6 Discussion and Conclusions

The dimensional analysis of the gel particles injection into the sand packs provided the following results and conclusions of practical importance:

- The evaluation of the near well-bore formation treatment by gel particles using dimensionless correlations was presented and various important dimensionless correlations were developed which can assist in designing for conditioning of the high permeability formations with gel particles.
- The original 14 variables of the sand packs, gel particles suspensions, and the operation conditions, were reduced to 10 dimensionless groups by means of the method of dimensional analysis. However, only 7 out of these 10 dimensionless groups were sufficient to obtain meaningful correlations of our experimental data.
- The maximum limit values of the dimensionless groups were observed to be different for different experimental conditions. This problem was alleviated conveniently by using the normalized dimensionless groups to obtain an effective correlation of the permeability reduction of the sand packs at different temperatures, concentrations, flow rates, and gel particles diameters.
- Comparison between the measured and correlated permeability reduction obtained from the normalized dimensionless groups was shown to yield a satisfactory match, especially at the steady limit values of permeability reduction.
- The effect of the ratio of the gel-particle to pore-throat size ratio on the permeability reduction by gel particles was correlated successfully using the dimensionless group involving the ratio of the gel-particle to pore-throat size.

- The outstanding advantage of using the normalized dimensionless groups rather than the actual variables is to be able to develop empirical correlations which are applicable also at field conditions which are different than the laboratory test conditions.
- The present dimensionless correlations can predict the evolving permeability reduction under the varying conditions of gel particles suspension injection processes. In contrast, the previous empirical correlations of gel particles injection can only provide an estimate of the final permeability reduction attained at the end of treatment.
- The particles trapped across the pore throats initially cause a pressure build-up (and permeability decrease) which eventually leads to deformation and passing of the particles through pore-throats resulting in a subsequent reduction of the differential pressure (and permeability increase). Thus, the measured and correlated permeability reduction show consecutively decreasing and increasing permeability trends (oscillation phenomenon) caused by the plugging and unplugging phenomena.

Chapter 8: Experimental Investigation and Correlation of Particle-Gel Systems for Near-Wellbore Water Shutoff Treatments

8.1 Introduction

The particle- gel system was used as a method of near-wellbore formation treatment to prevent or control water production in waterfloooded mature oil fields. This system consists from a polymer/crosslinker as the gel and a silica flour as the particles to provide leak off control and act as a diverting filter cake (Dalrymple et al. 2008; Ali et al. 2008; van Eijden et al. 2005). The gel squeezes into the matrix, developing a shallow matrix seal. One application of this system has been in wells where the water producing zones were identified and separated from the oil producing zones, wherein zonal isolation was not an option. The entire interval was treated and, following a shut-in period to allow the system to crosslink, the wellbore was cleaned with coiled tubing (CT) and the hydrocarbon zone could then be re-perforated. Dalrymple et al. (2008) applied 50 wt% silica flour concentration to achieve sufficient fluid loss control of the gel but it is desirable to lower this concentration.

Optimization particulate concentration, leak off, and threshold pressure are studied qualitatively and quantitatively by laboratory testing. To study the leak off, fluid loss tests are performed at constant pressure and the volume of the filtrate water is measured during the test. Effects of silica flour concentration, pore space of the permeable filter disk, sand size and temperature on the leak off and the pressure initiate flow are studied by adding different amount of silica flour to special gel system using

permeable filter disks of different pore spaces and sand of varying sizes and temperatures. The sand represents a gravel pack and the filter disc represents the formation. To study the threshold pressures, the pressures that initiate water flow are measured after the fluid loss tests.

In the present study Empirical correlations and charts are developed from the experimental data which can be used to predict the fluid loss, the pressure necessary to initiate flow, and the filtrate volume at any silica flour concentration, pore diameter of formation, sand size, and temperature. Additionally, correlations for the critical silica flour concentration are developed which can be used to predict the critical silica flour concentration at any pore diameter of filter disc and sand size. The critical silica flour concentration is the concentration below which there is no effect on the filtrate volume and the pressure to initiate flow and above which the filtrate volume can decreases and the pressure initiate flow can increase. This study can aid the successful design to achieve optimal conformance control for reducing high permeability and controlling water production in waterflooded mature oil fields. Rather than correlating the individual data set, correlating the data in groups for similar tests to develop general correlations is preferred. This can help ensure the similar trends in correlations of all the data points of the measurement in a consistent manner so that the trends of correlations will be similar. Therefore, correlating data in groups is advantageous to obtain the best meaningful generalized correlations, which can aid the design of field scale applications at any conditions which could differ from conditions of the experimental study or measurements.

8.2 Analysis and Investigation of Experimental Results

Described next are the experimental investigation and phenomenological description of the filtrate loss and the pressure to initiate flow. The silica flour-gel system during fluid loss testing was passed through sand (gravel pack) similarly to filtration through a disc (formation), as shown in **Fig. 8.1**. Silica flour concentration in the system that reached the filtration disc was an important factor affecting filtrate loss and pressure to initiate flow because the silica flour became trapped in the pores of the filtrate disc, forming a filter cake.

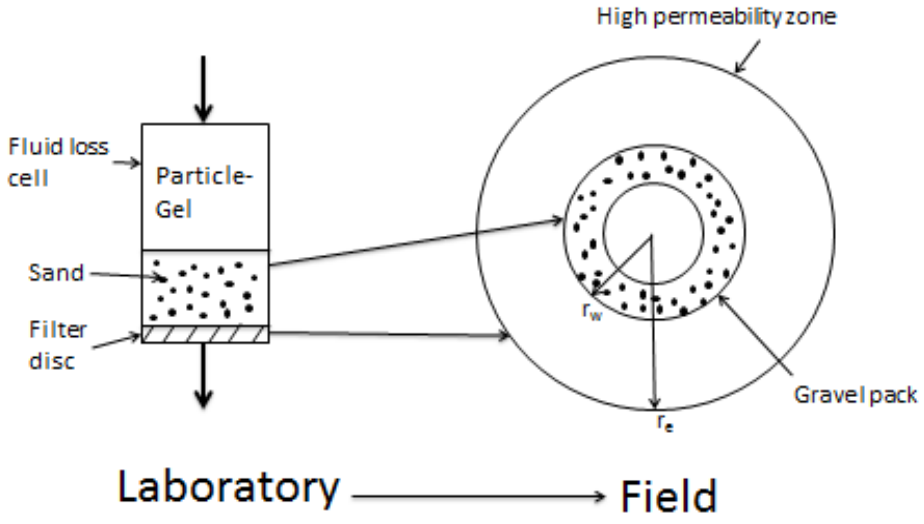

Fig. 8.1- Convert the filtrate test from laboratory scale to field scale

For the same filter disc and silica flour concentration, the fluid loss of the silica flour-gel system were increased and the pressure to initiate flow was decreased by increasing the sand mesh because the sand and pore sizes were decreased. This leads to silica flour entrapment in the pores of the sand, causing the filter disc to have low

concentration of silica flour, which caused low silica flour to be trapped in the pores of the filter disc and low filter cake formation on the filter disc, as shown in **Fig. 8.2**.

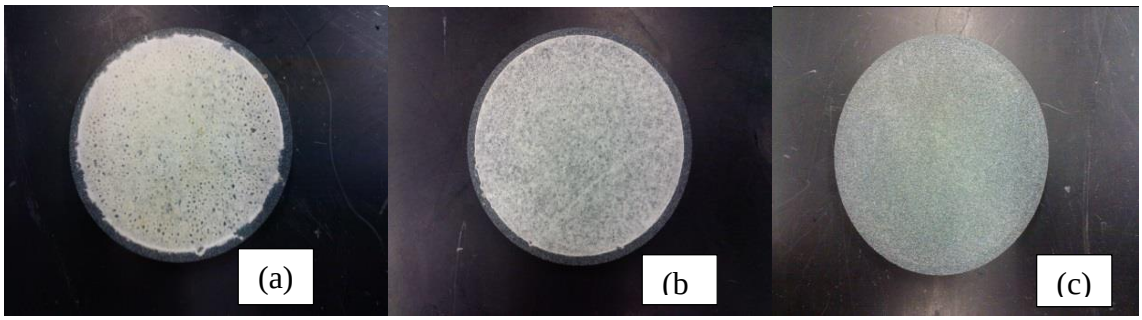

Fig. 8.2: The filtrate cake for same filter disc and same silica flour concentration and different sand sizes (a) 12/20 mesh (b) 20/40 sand (c) 40/70 mesh

8.3 Development of Empirical Correlations

8.3.1 Fluid Loss

Empirical correlations from the experimental data were developed by considering several relevant parameters, such as silica flour concentration, sand size, and pore size of filter disc that effect fluid loss. Charts for practical applications of fluid loss were constructed by performing the following steps:

1- Develop a relationship which correlates the experimental data of fluid loss percent with silica flour concentration.

2- Determine the critical silica flour concentration for all experimental conditions.

3- Correlate the experimental data at various conditions with the critical silica flour concentration.

4- Apply the correlations of the experimental data developed above to construct charts of fluid loss that can be used for practical applications at other conditions.

1- Correlation of the Experimental Data of Fluid Loss

Experimental data were correlated by the following exponential relationship.

$$y = A\exp\left(-Bx^{\alpha}\right) \qquad (8.1)$$

where y represents the fluid loss of the particle-gel system (%); x is the silica flour concentration (wt%); A, B, and α are empirical parameters (dimensionless), determined by applying Eq. B-6, given in Appendix B. For the same filter disc and different sand sizes, **Figs. G.1** to **G.3** show an exponential relationship between the fluid loss and silica flour concentration for 35, 10, and 5 micron average pore diameter of filter disc at different sand sizes. **Figs. G.4** to **G.6** show straight line plot of Eq. B-6 for 35, 10, and 5 micron pore diameter of filter disc at different sand sizes, given in Appendix G.

2- Determination of the Critical Silica Flour Concentrations

The critical silica flour concentration is the concentration below which there is no effect on the fluid loss% and the pressure initiate flow and above which the fluid loss will decreases and the pressure initiate flow increases. The critical silica flour concentration represents the minimum value at which the fluid loss equal 100%. The critical silica flour concentrations were determined from the correlations developed in the following section at 100% fluid loss for all the experimental conditions, as shown in **Table 8-1**.

Table 8-1: CRITICAL SILICA FLOUR CONCENTRATIONS		
Pore diameter of filter disc (micron)	Sand size (mesh)	Critical silica flour concentration wt%
35	12/20	0.60
35	20/40	0.70
35	40/70	0.84
10	12/20	0.28
10	20/40	0.32
10	40/70	0.38
5	12/20	0. 08
5	20/40	0.15
5	40/70	0.20

3- Correlation of the experimental data with the critical silica flour concentration

The experimental data were correlated with the critical silica flour concentration as a minimum value by used of the following exponential relationship.

$$y = 100 \exp\left[- B(x - x_{cr})^{\alpha} \right] \qquad (8.2)$$

where y represents the fluid loss of the particle-gel system (%); x is the silica flour concentration (wt%); x_{cr} is the critical silica flour concentration (wt%); B, and α are empirical parameters, dimensionless, determined by applying Eq. B-10, given in

Appendix B. For the same filter disc and different sand sizes, **Figs. G.7** to **G.9** show an exponential relationship between the fluid loss and silica flour concentration for 35, 10, and 5 micron average pore diameter of filter disc at different sand sizes. **Figs. G.10** to **G.12** show straight line plot of Eq. B-10 for 35, 10, and 5 micron pore diameter of filter disc at different sand sizes, given in Appendix G.

4- Development of charts for fluid loss

Charts of fluid loss were developed based on the exponential relationships of the experimental data with the critical silica flour concentrations which can be used to estimate the fluid loss of the particle-gel system at any silica flour concentration, pore diameter of filter disc, and sand size. The values of B, α, and x_{cr} were collected from the exponential relationships of same pore diameter of filter disc and different sand sizes and plotted against sand sizes, as shown in **Fig. G.13** to **G.21**. The plotted B, α, and x_{cr} were correlated as linear functions ($y = a_i x + b_i$) where y represents B, α, or x_{cr}; x represents sand size; and a_i and b_i represent initial guesses of parameters (Figs. G.13 to G.21). By substituting the linear functions of B, α, and x_{cr} in the exponential relationship, as shown in Eq. 8.3, empirical correlations were developed and used to construct charts of fluid loss at 35, 10, and 5 micron pore diameter of filter disc and different sand mesh, and different silica flour concentrations, as shown in **Figs. 8.3** to **8.5**.

$$F.L. = 100 \exp\left[-\left(a_1 D_s + b_1\right)\left(C_s - \left(a_2 D_s + b_2\right)\right)^{\left(a_3 D_s + b_3\right)}\right] \qquad (8.3)$$

where F.L. represents the fluid loss (vol%); D_s represents the sand diameter (micron); C_s represents the silica flour concentration (wt%); and a_1, b_1, a_2, b_2, a_3, and b_3 represent initial guesses (dimensionless). The values of the initial guesses of a_1, b_1, a_2, b_2, a_3, and b_3 in Eq. 8.3 were collected from the linear functions of 35, 10, and 5 micron pore diameter of filter disc and plotted against pore diameter of filter disc, as shown in **Figs. G.22** to **G.27** given in Appendix G. The parameters of a_1, b_1, a_2, b_2, a_3, and b_3 were correlated as linear functions ($y = a_i x + b_i$) where y represents a_1, b_1, a_2, b_2, a_3, or b_3; x represents pore diameter of filter disc; and a_i and b_i represent initial guesses of parameters (Figs. G.22 to G.27). The linear functions of a_1, b_1, a_2, b_2, a_3, and b_3 were substituted in Eq. 8.3 and general empirical correlation of the fluid loss was developed which can be used at any pore diameter of filter disc, sand mesh, and silica flour concentration.

$$F.L. = 100\exp\left[-\left(\left(66E-07D_F+33E-05\right)D_s+\left(-0.04D_F+2.06\right)\right)\left(C_s-\left(5E-06D_F+6E-05\right)D_s+\left(0.02D_F+0.16\right)\right)^{\left(-6E-06D_F+2E-05\right)D_s+\left(0.012D_F+0.474\right)}\right] \quad (8.4)$$

where D_F represents pore diameter of filter disc, micron. **Fig. 8.6** shows the chart of fluid loss at 12/20 sand mesh and different pore diameters of filter disc and different silica flour concentrations which was developed by the general empirical correlation (Eq.8.4). Fig. 8.6 shows that for the same sand mesh and same silica flour concentration, the filtration volume of the silica flour-gel system increased by increasing the pore diameter of the filter disc because the silica flour was passed through the large pores of the filter disc and low silica flour was trapped in the pores and low filtrate cake was formed on the filtrate disc, as shown in **Fig. 8.7**.

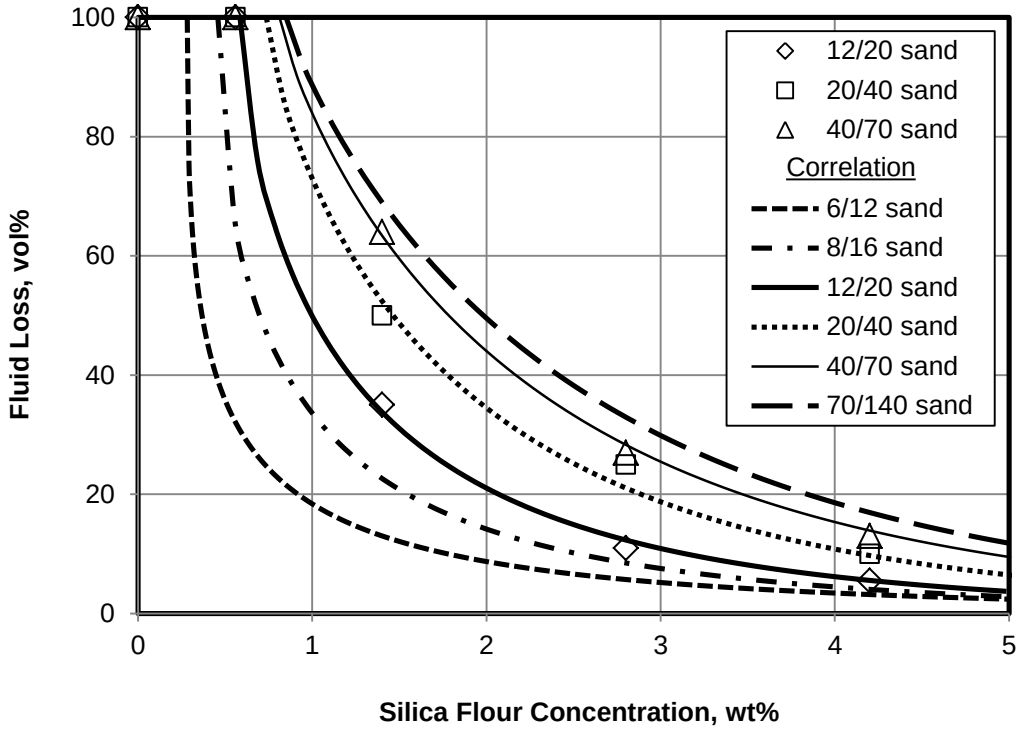

Fig. 8.3: Experimental and correlated fluid loss at different silica flour concentrations and different sand sizes for 35 micron pore diameter of filter disc (Plot of Eq. 8.3)

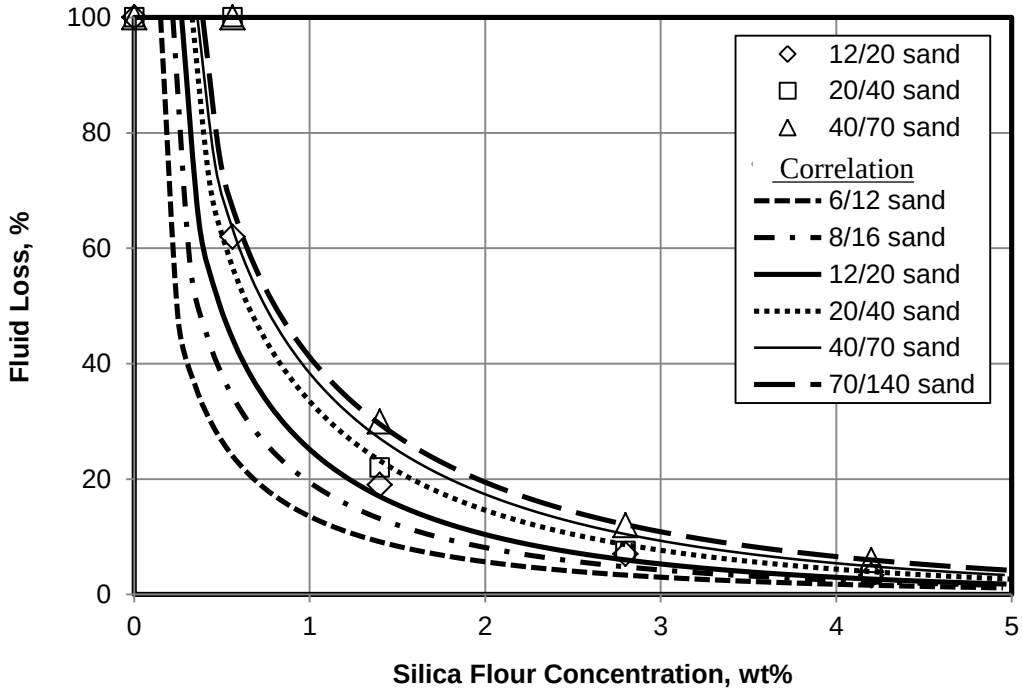

Fig. 8.4: Experimental and correlated fluid loss at different silica flour concentrations and different sand sizes for 10 micron pore diameter of filter disc (Plot of Eq. 8.3)

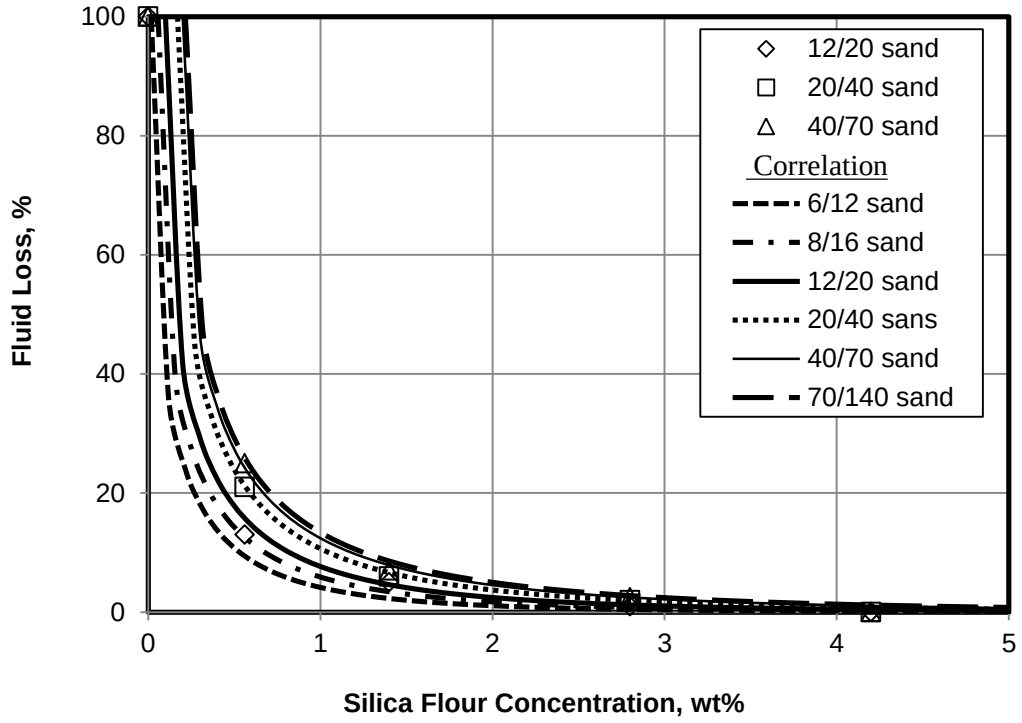

Fig. 8.5: Experimental and correlated fluid loss at different silica flour concentrations and different sand sizes for 5 micron pore diameter of filter disc (Plot of Eq. 8.3)

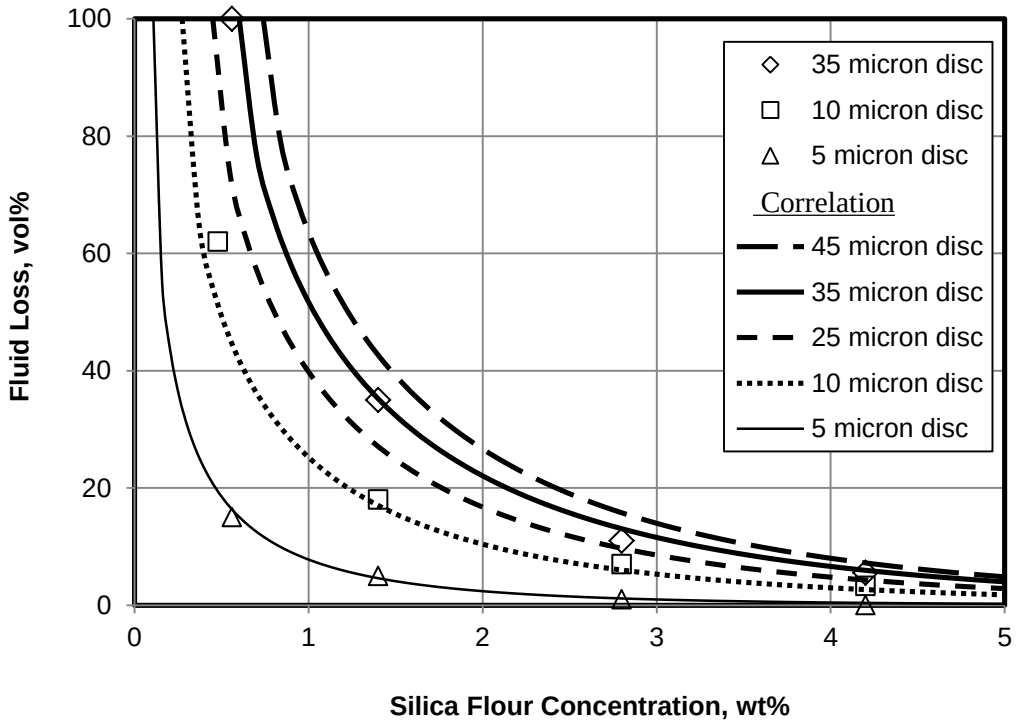

Fig. 8.6: Experimental and correlated fluid loss at different silica flour concentration and different pore diameters of filter discs for 12/20 sand mesh (Plot of Eq. 8.4)

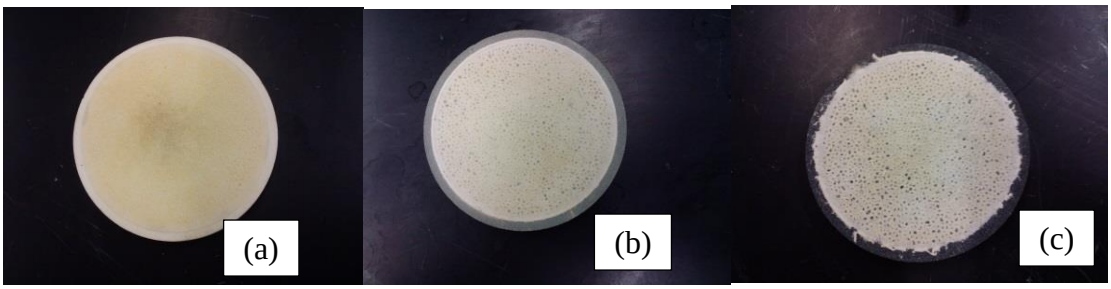

Fig. 8.7: The filtrate cake for same sand mesh and same silica flour concentration and different pore diameters of filter discs (a) 5 micron (b) 10 micron (c) 35 micron

8.3.2 Critical Silica Flour Concentration

The critical silica flour concentration represents the value of concentration at which the fluid loss and the pressure initiate flow change. The determination of the critical silica flour concentration is very important because it represents the initial condition of the empirical correlation for practical application. Charts of critical silica flour concentration were developed from the experimental data which can be used to estimate the critical silica flour concentration at any pore diameter of filter disc and sand size. The values of x_{cr} of same pore diameter of filter disc and different sand sizes were calculated from the linear functions of figures G. 15, G.18, and G. 21 and plotted against sand sizes, as shown in **Fig. H.1**. The plotted x_{cr} in Fig. H.1were correlated as linear functions and the values of A, and B were collected from the linear functions and plotted against sand size, as shown in **Figs. H.2** and **H.3**. The plotted As and Bs were correlated again as linear functions ($y = a_i x + b_i$) where y represents A, or B; x represents sand size, and a_i and b_i represent initial guesses of parameters (Figs. H.2 and H.3). The empirical correlation was developed by substituting the linear functions of A, and B in the critical silica flour concentration relationship, as shown in Eq. 8.5. This

empirical correlation was used to construct chart of critical silica flour concentration which can be used for practical applications, as shown in **Fig. 8.8**.

$$x_{cr} = -(4E-06D_F + 7E-05)Ds + (0.0214D_F + 0.1415) \qquad (8.5)$$

where x_{cr} represents critical silica flour concentration (wt%); D_s represents sand diameter (micron); and D_F represents pore diameter of filter disc (micron).

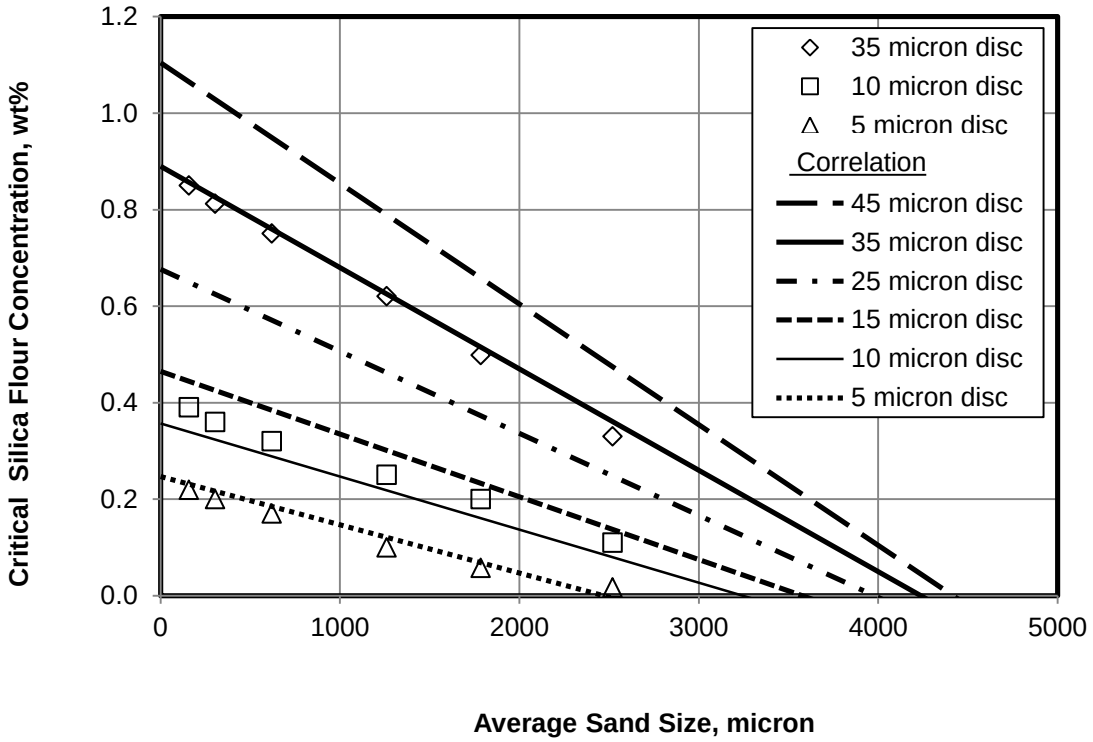

Fig. 8.8: Experimental and correlated critical silica flour concentration at different sand sizes and different pore diameter of filter discs (Plot of Eq. 8.5)

Fig. 8.8 shows that the critical silica flour concentration increased by increasing the pore diameter of filter disc because the silica flour passed through the

large pores of the filter disc and low silica flour trapped in the pores of the filter disc. The maximum value of the critical silica flour concentration is determine at the sand size equal zero. The maximum value of the critical silica flour concentration for 5, 10, 15, 25, 35, and 45 micron pore diameter of filter disc are 0.25, 0.36, 0.47, 0.68, 0.89, and 1.10 wt%, respectively. Fig. 8.8 shows that the critical silica flour concentration was decreased by increasing the sand size because the silica flour passed through the pores of the sand and the gel-particle system reached the filter disc at a high concentration of the silica flour. The minimum value of the critical silica flour concentration is zero and for 5, 10, 15, 25, 35, and 45 micron pore diameter of filter disc the minimum value of the critical silica flour concentration is determined at the sand size 2400, 3200, 3500, 3900, 4200, and 4400 micron, respectively.

8.3.3 Pressure Initiate Flow

Charts and empirical correlations were developed from the experimental data of several relevant parameters, such as pore size of filter disc, silica flour concentration, and sand size that effect pressure initiate flow. The experimental data of the pressure initiate flow were correlated with the critical silica flour concentration as an initial condition by the following relationship.

$$y = \frac{A(x - x_{cr})^{\alpha}}{(x - x_{cr})^{\alpha} + B} \tag{8.6}$$

where y represents the pressure initiate flow (kPa); x is the silica flour concentration (wt%); x_{cr} is the critical silica flour concentration (wt%), were determined by applying Eq. 8.5; A, B, and α are empirical parameters (dimensionless), were determined by

applying Eq. B-11, given in Appendix B. For the same filter disc and different sand sizes, **Figs. I.1** to **I.3** show the relationship between the pressure initiate flow and silica flour concentration for 35, 10, and 5 micron average pore diameter of filter disc at different sand sizes. **Figs. I.4** to **I.6** show straight line plot of Eq. B-11 at different sand sizes for 35, 10, and 5 micron pore diameters of filter disc.

To develop charts of pressure to initiate flow of same pore diameter of filter disc and different silica flour concentration and sand sizes, the values of A, B, and α of the correlations were plotted against sand sizes, as shown in **Figs. I.7** to **I.15**, and correlated as linear functions ($y = a_i x + b_i$) where y represents A, B, and α; x represents sand size, a_i and b_i represent initial guesses of parameters. These linear functions were substituted in Eq. 8.6 to get new empirical correlations used to construct charts of pressure initiate flow at 35, 10, and 5 micron pore diameter of filter disc and different sand sizes and silica flour concentrations, as shown in Figs. 8.9 to 8.11.

$$P = \frac{(a_1 D_s + b_1)(C_s - x_{cr})^{(a_3 D_s + b_3)}}{(C_s - x_{cr})^{(a_3 D_s + b_3)} + (a_2 D_s + b_2)} \qquad (8.7)$$

where P represents the pressure initiate flow (kPa); D_s represents the sand diameter, micron; C_s represents the silica flour concentration (wt%); x_{cr} represents critical silica flour concentration (wt%); and a_1, b_1, a_2, b_2, a_3, and b_3 represent initial guesses (dimensionless). The values of a_1, b_1, a_2, b_2, a_3, and b_3 in Eq. 8.7 were plotted against pore diameter of filter disc and correlated as linear functions, as shown in **Figs. I.16** to **I.21** and substituted in Eq. 8.7 to develop a general empirical correlation of the pressure initiate flow which can be used at any pore diameter of filter disc, silica flour concentration, and sand size.

$$P = \frac{\left[\left(-0.043D_F + 3.278\right)D_s + \left(-161D_F + 8070\right)\right]}{\left(C_s - x_{cr}\right)^{\left(-15E-06D_F+3E-04\right)D_s+\left(0.013D_F+0.686\right)}}$$

$$\frac{\left(C_s - x_{cr}\right)^{\left(-15E-06D_F+3E-04\right)D_s+\left(0.013D_F+686\right)}}{+\left(-0.00016D_s + 0.021D_F + 0.494\right)} \qquad (8.8)$$

Fig. 8.12 shows application of Eq. 8.8 to calculate the pressure initiate flow at 12/20 sand mesh and different pore diameters of filter disc and different silica flour concentrations. Fig. 8.12 demonstrated that the pressure initiate flow for the same sand mesh and same silica flour concentration decreased by increasing the pore diameter of the filter disc because low silica flour was trapped in the large pores and low filtrate cake was formed, as shown in Fig. 8.7.

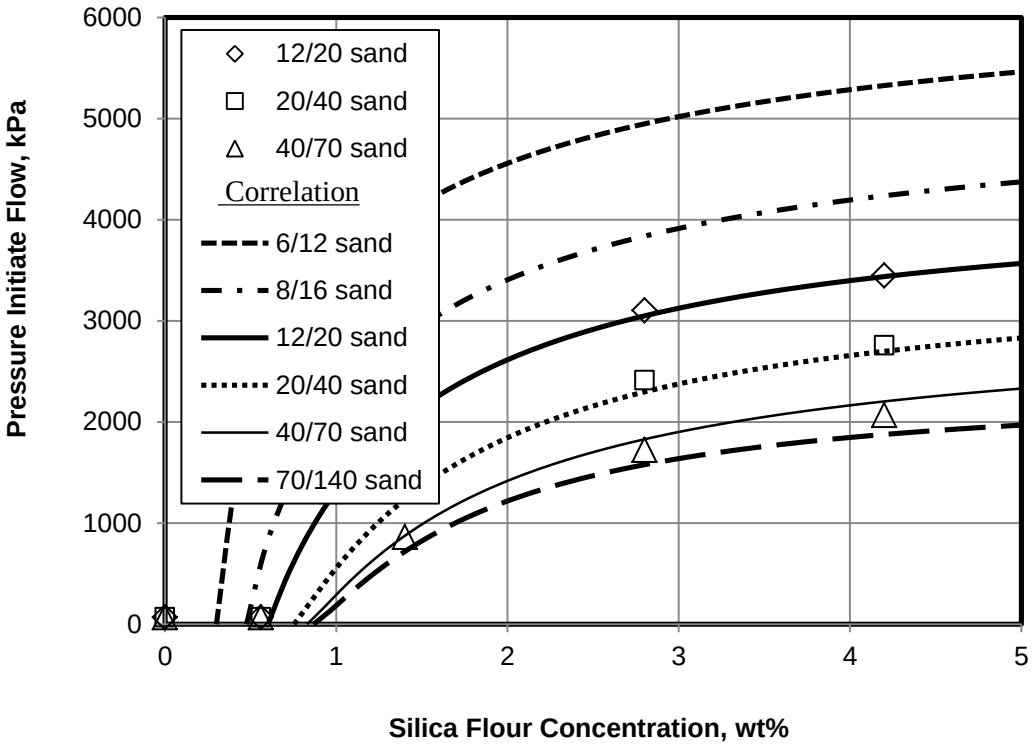

Fig. 8.9: Experimental and correlated pressure initiate flow at different silica flour concentrations and different sand sizes for 35 micron pore diameter of filter disc (Plot of Eq. 8.7)

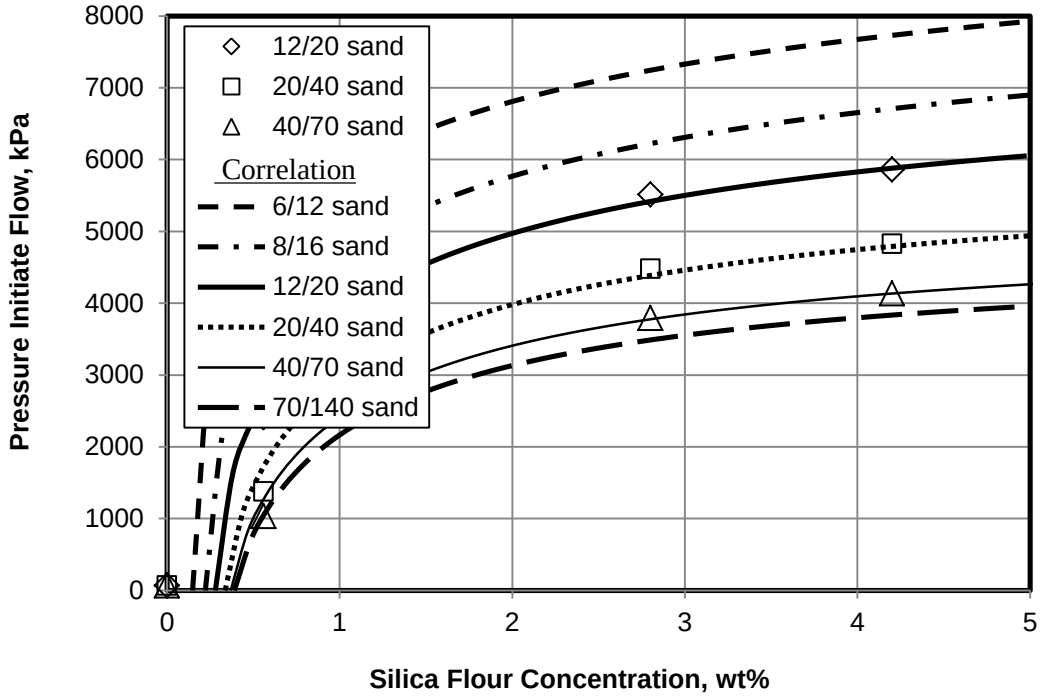

Fig. 8.10: Experimental and correlated pressure initiate flow at different silica flour concentrations and different sand sizes for 10 micron pore diameter of filter disc (Plot of Eq. 8.7)

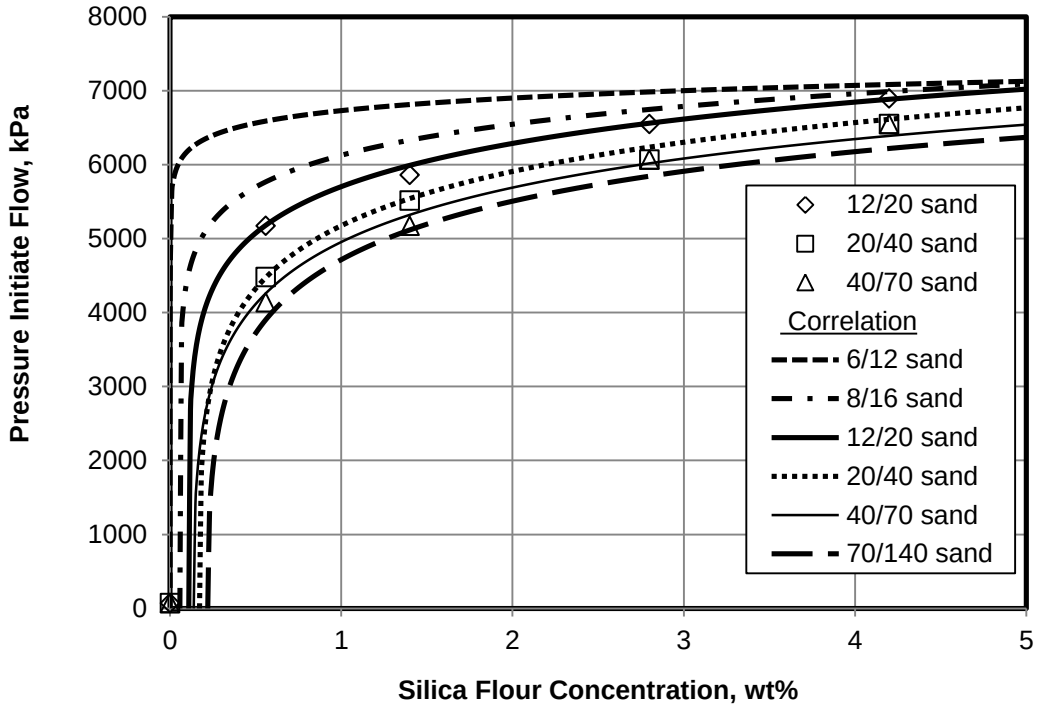

Fig. 8.11: Experimental and correlated pressure initiate flow at different silica flour concentrations and different sand sizes for 5 micron pore diameter of filter disc (Plot of Eq. 8.7)

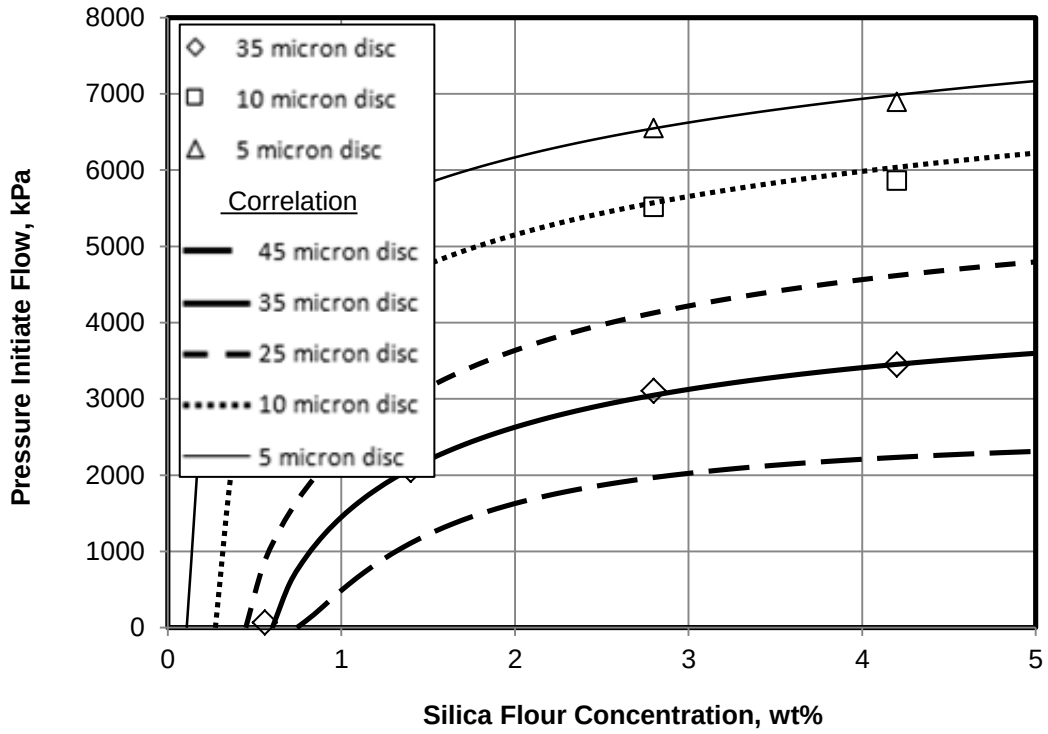

Fig. 8.12: Experimental and correlated pressure initiate flow at different silica flour concentrations and different pore diameters of filter discs for 12/20 sand mesh (Plot of Eq. 8.8)

8.4 Thermal Effects

The fluid loss of the 2.8 wt% silica flour particle-gel system is studied at 35 micron pore diameter filter disc, 12/20 sand mesh and different temperatures of 23.5, 51, 68, and 83 °C. The filtrate tests results show an increase in the fluid loss of the silica flour particle-gel system by increasing the temperature. The fluid loss was increased from 11 to 12.5% by increasing the temperature from 23.5 to 83 °C. This happened because the viscosity of the silica flour particle-gel system decreases by temperature which lead to the particle-gel system pass through the pores easily. The viscosity decreases from 0.059 to 0.027 Pa.s when the temperature increases from 23.5 to 83 °C.

The pressure initiate flow after the filtrate tests of the silica flour particle-gel system is studied at different temperatures of 23.5, 51, 68, and 83 °C. The experimental results show decreases in the pressure initiate flow by increasing the temperature. The pressure initiate flow was decreased from 3100 to 2070 kPa by increasing the temperature from 23.5 to 83 °C. This happened because the degree of pore plugging by the silica flour particle-gel decreased by temperature.

8.4.1 Correlation of Thermal Effects

Empirical correlations of practical importance are developed from the experimental data at different temperatures for effective design of the silica flour particle-gel system application of near-wellbore formation treatment. The Vogel-Tammann- Fulcher (VTF)-type equations (Eq. 6.1) was used to correlate the experimental data for viscosity, the fluid loss, and the pressure initiate flow of the silica flour particle-gel system, as follows:

$$\ln \mu = \ln \mu_c - \frac{C}{T - T_c} \tag{8.9}$$

where μ is the viscosity (Pa.s), T is the actual temperature (K), μ_c is the pre-exponential coefficient of the viscosity = 0.0027 Pa.s, and Tc and C are 120 and -545 K, respectively.

$$\ln(F.L.) = \ln(F.L.)_c - \frac{C}{T - T_c} \tag{8.10}$$

where F.L. is the fluid loss (vol%), T is the actual temperature (K), $(F.L.)_c$ is the pre-exponential coefficient of fluid loss = 8.60 vol%, and Tc and C are 470 and 42.80 K, respectively. Further,

$$\ln P = \ln P_c - \frac{C}{T - T_c} \tag{8.11}$$

where P is the pressure to initiate flow (kPa), T is the actual temperature (K), P_c is the pre-exponential coefficient of pressure to initiate flow = 4824 kPa, and Tc and C are 420 and -54.18 K, respectively.

Figs. 8.13 to **8.15** show the straight- line VTF plots of the experimental data of the 2.8 wt% silica flour particle-gel viscosity, fluid loss, and pressure initiate flow . **Figs. 8.16** to **8.18** show comparisons between the viscosity, fluid loss, and pressure to initiate flow values obtained from VTF equation and the experimental data.

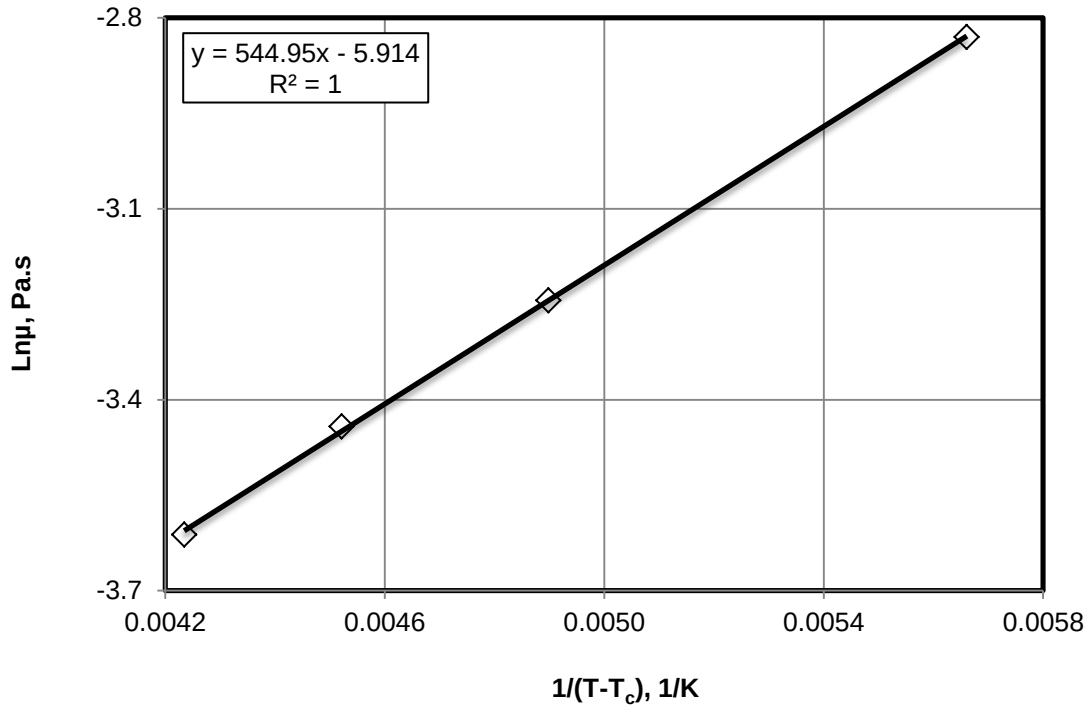

Fig. 8.13: Straight- line VTF plot for the 2.8 wt% particle-gel system viscosity

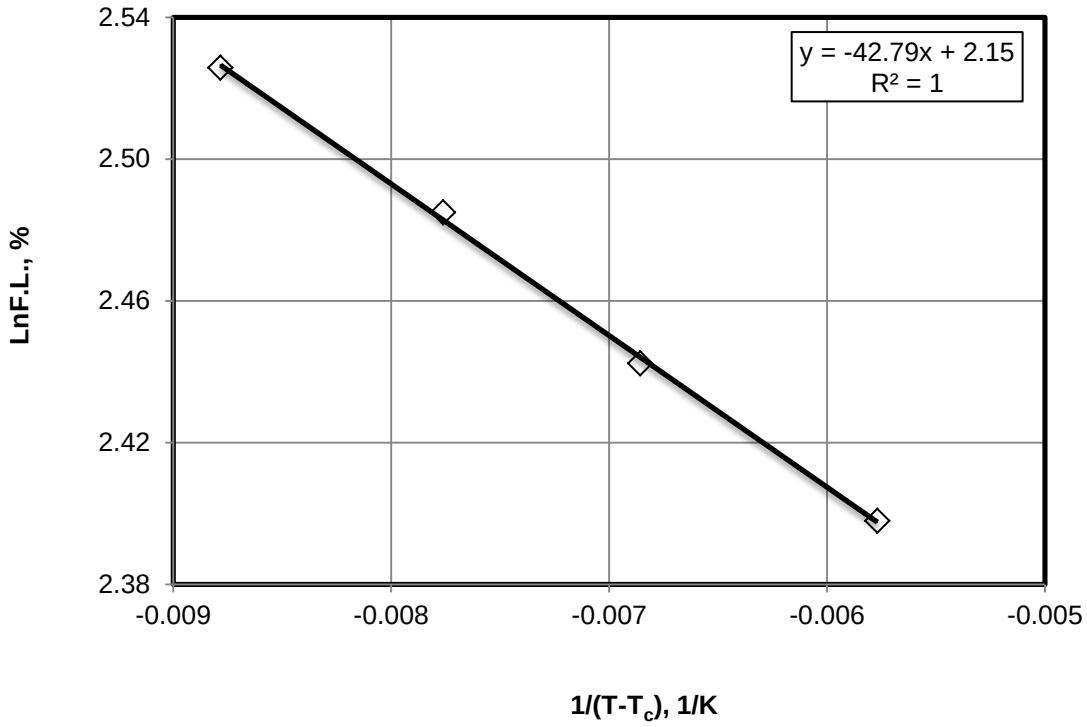

Fig. 8.14: Straight- line VTF plot for the fluid loss

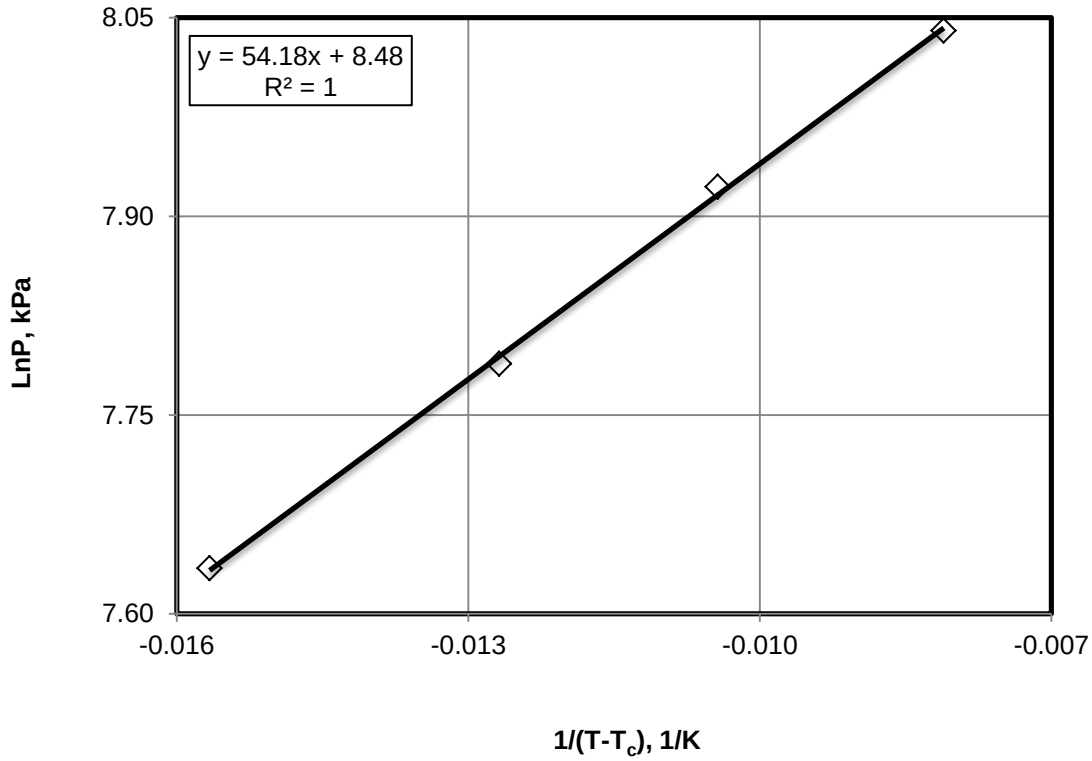

Fig. 8.15: Straight- line VTF plot for the pressure initiate flow

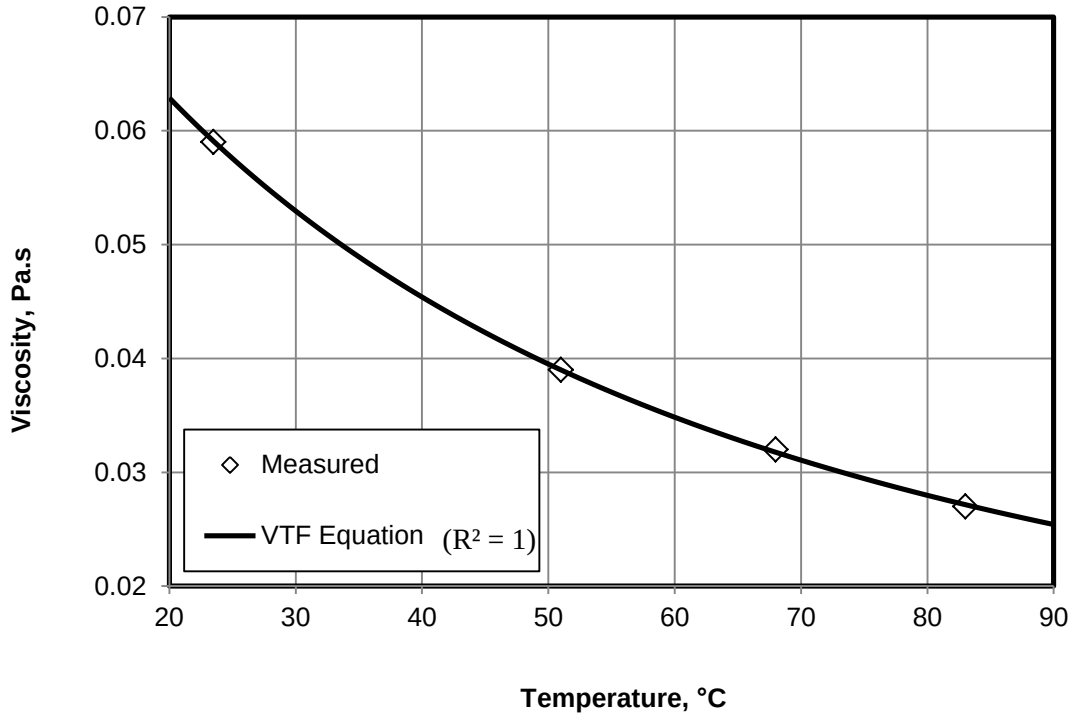

Fig. 8.16: Comparison between silica flour particle-gel system viscosity obtained from the VTF equation and the measured data

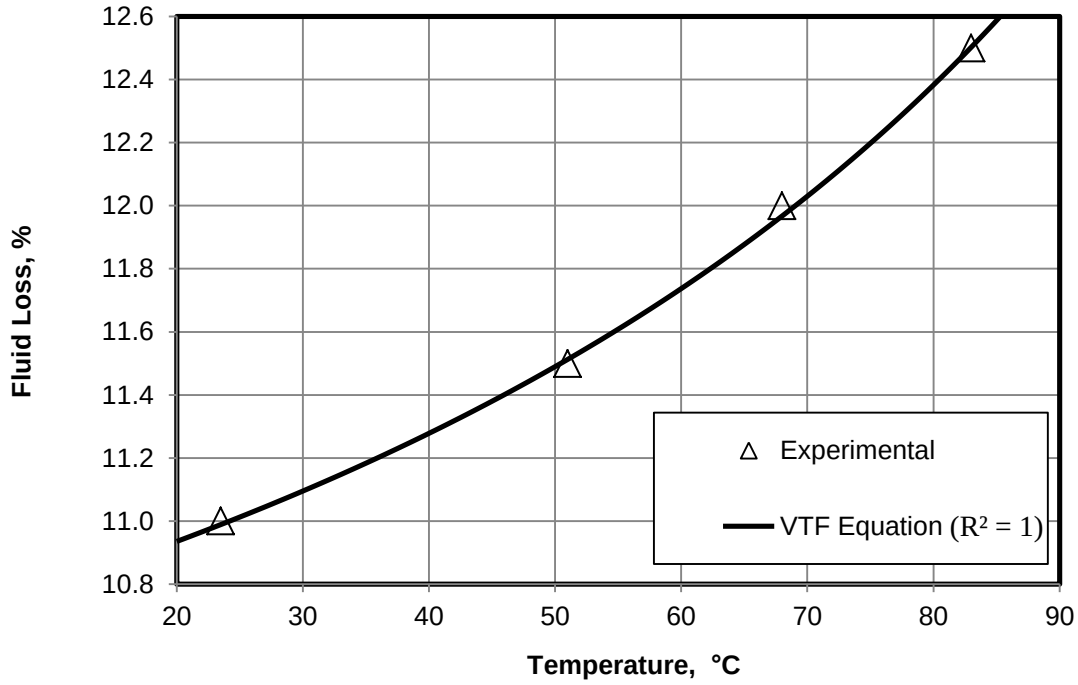

Fig. 8.17: Comparison between fluid loss obtained from the VTF equation and the experimental data

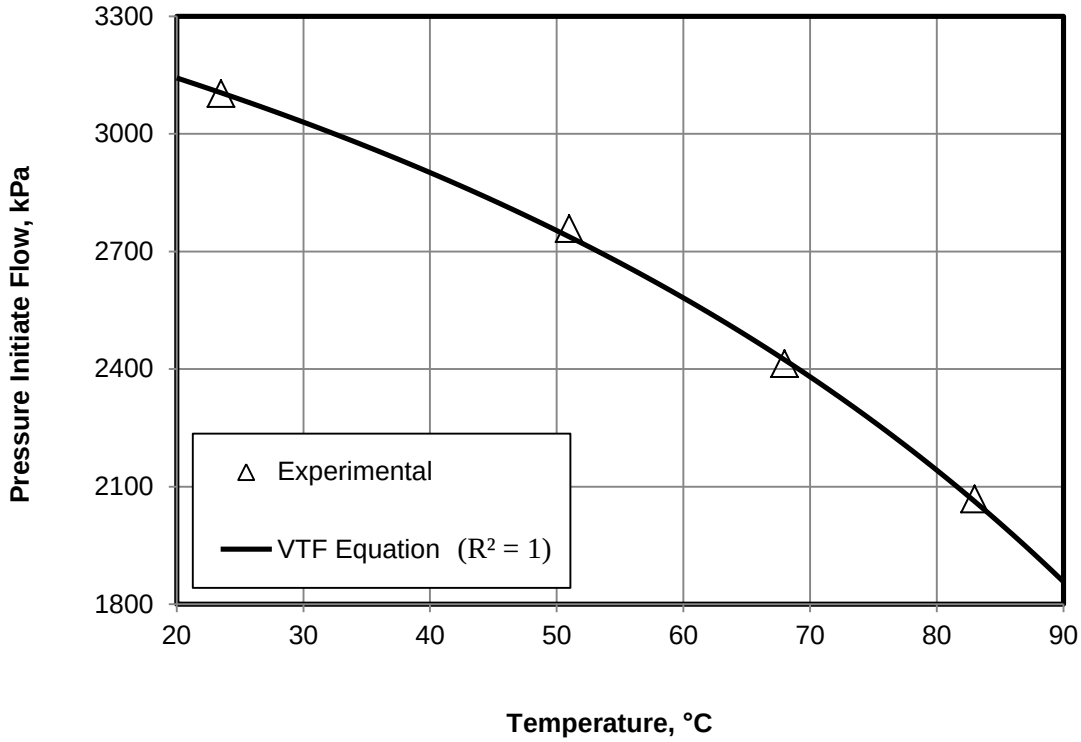

Fig. 8.18: Comparison between pressure initiate flow obtained from the VTF equation and the experimental data

The experimental results show that when the temperature increased from 23.5 to 83°C, the viscosity of the 2.8 wt% silica flour particle-gel system deceased from 0.059 to 0.027 Pa.s, the fluid loss increased from 12.5 to 11%, and the pressure to initiate flow decreased from 3100 to 2070 kPa. The VTF correlations of viscosity, fluid loss, and pressure to initiate flow are close to the experimental data. Thus, the VTF equation can be used to predict viscosity, fluid loss, and pressure to initiate flow for a similar material and operational conditions at any temperature.

8.5 Conclusions

The primary findings of this experimental study can be summarized as follows:

- Quantitative evaluation of various factors affecting the performance of silica flour particle-gel applications was studied for successful field applications of particle-gel system injection. Thus, important empirical correlations were developed which can assist in conditioning of highly permeable formations by reducing the high permeability and increasing the pressure to initiate flow. Hence, operators can treat near-wellbore formations having high permeability zones and prevent or control water production in waterflooded mature oil fields.
- Instead of correlating individual data set, the data was correlated as groups and best meaningful generalized correlations and charts were developed which can help design silica flour particle-gel field trip applications at any operation conditions for near-wellbore formation treatment.
- The effects of temperature on the fluid loss and the pressure to initiate flow of the silica flour particle-gel process were investigated and an increase to fluid loss and a decrease to pressure initiate flow were observed. This occured because the silica flour particle-gel viscosity decreased by temperature which leads to the particle-gel system transport easily through the pores.
- Important empirical correlations for thermal effect with high agreement between the experimental data and correlations were developed using (VTF)- type equations, which can be used for successful design of the silica flour particle-gel system application of near-wellbore formation treatment.

Chapter 9: Filtration Analysis of Particle-Gel Systems for Near-Wellbore Water Shutoff Treatments

9.1 Introduction

The high permeability formations are prone to high water production occurrence in oil or gas producing wells which causes several undesirable problems to the oil industry. Using silica flour particle- gel system is a method to reduce or condition the high permeability of reservoir formation and thus avoid the water production problem. The leak off of the silica flour particle-gel system is studied by fluid loss tests at different silica flour concentrations, pore space of the permeable filter disc, and sand sizes. The rate constant of filtrate and spurt loss volume are determined and correlated with the silica flour concentration at different sand sizes and pore diameters filter discs. Exponential relationship is used to correlate the experimental data of the leak off tests of the silica flour particle-gel system and empirical correlations are developed of the filtrate volume of the silica flour particle-gel system at different sand sizes, pore diameters of the filter disc, and silica flour concentrations. The developed empirical correlations can be used to predict the evolving filtrate volume and thus can assist in effective and successful design of silica flour particle-gel system used for near-wellbore formation treatment under varying conditions.

9.2 Development of Empirical Correlations of Filtrate Volume

The experimental data obtained from the tests of Al-Ibadi et al. (2015) by silica

flour particle- gel system are correlated by exponential relationship. Empirical correlations of filtrate volume of the silica flour particle-gel system were developed from the experimental data of the leak off tests at different silica flour concentrations, pore diameters of filter discs, and sand sizes. The experimental data were correlated by the following exponential relationship.

$$y = A\exp\left(Bx^{\alpha}\right) \tag{9.1}$$

where y represents the filtrate volume of the particle-gel system, cm^3; x is the filtrate time, min; A, B, and α are empirical parameters, dimensionless, were determined by applying Eq. B-6, given in Appendix B. **Figs. 9.1** to **9.3** show the experimental filtrate volume *(V_f)* and the correlated filtrate volume obtained from the exponential relationship at 35 micron pore diameter of filter disc for different sand sizes at 12/20, 20/40, and 40/70 sand mesh and different silica flour concentrations at 0.21, 0.53, 1.06, and 1.60 vol%. **Figs. J.1** to **J.3** show straight line plot of Eq. B-6 for 35 micron pore diameter of filter disc at different sand sizes and different silica flour concentrations. For same filter disc and same sand mesh, the experimental data show filtrate volume reduction by increasing the silica flour concentration, for 35 micron pore diameter of filter disc and 12/20 sand mesh, the filtrate volume deceases from 76 cm^3 to 5.5 cm^3 by increases the silica flour concentration from 0.21 vol% to 1.60 vol%, as shown in Fig. 9.1. This happened because the amount of the silica flour trapped in the pores of the filter disc increased by silica flour concentration and high filtrate cake was formed on the filtrate disc, as shown in **Fig. 9.4**. For same filter disc and same silica flour concentration, the experimental data show filtrate volume increases as the sand mesh

increases. For 35 micron pore diameter of filter disc and 1.06 vol% silica flour concentration, the filtrate volume increases from 11 cm^3 to 25 cm^3 by increase of the sand mesh from 12/20 to 20/40, as shown in Figs. 9.1 and 9.2. This happened because the sand size was decreased and the pores size was decreased which lead to the silica flour entrapment in the pores of the sandpack and the silica flour particle-gel system that reached to the filter disc have low concentration of the silica flour. This causes low silica flour entrapment in the pores of the filter disc and low filtrate cake formation on the filter disc, as shown in **Fig. 9.5**.

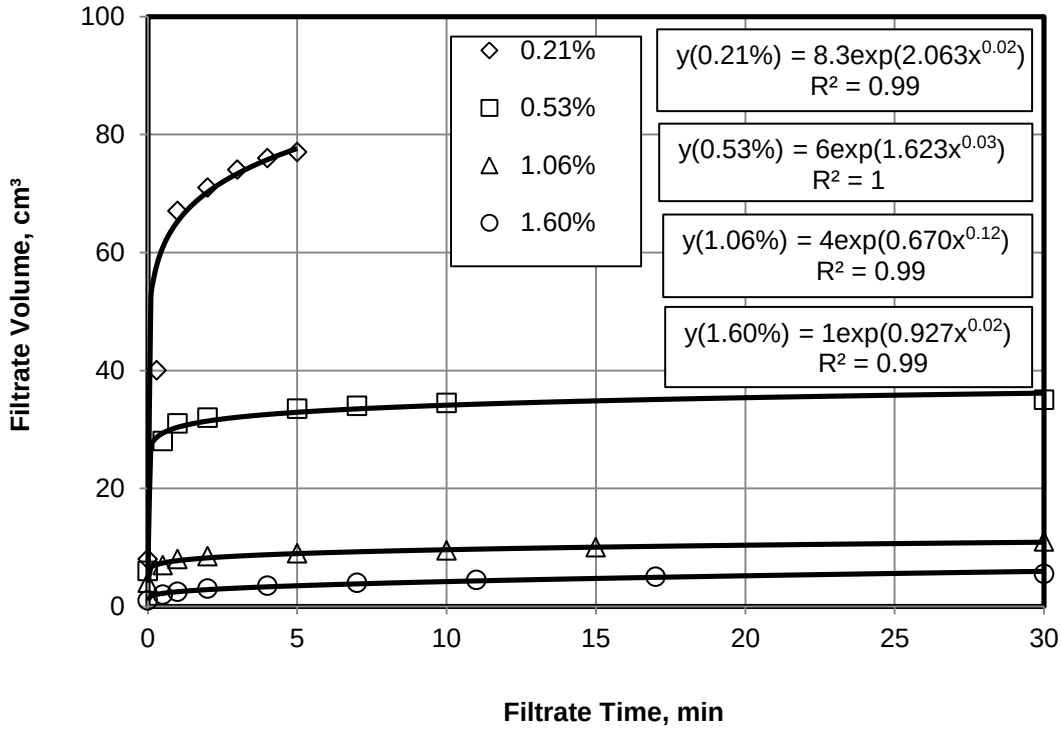

Fig. 9.1: Exponential relationship between filtrate time and filtrate volume at 35 micron pore diameter of filter disc and 12/20 sand mesh for different silica flour concentrations

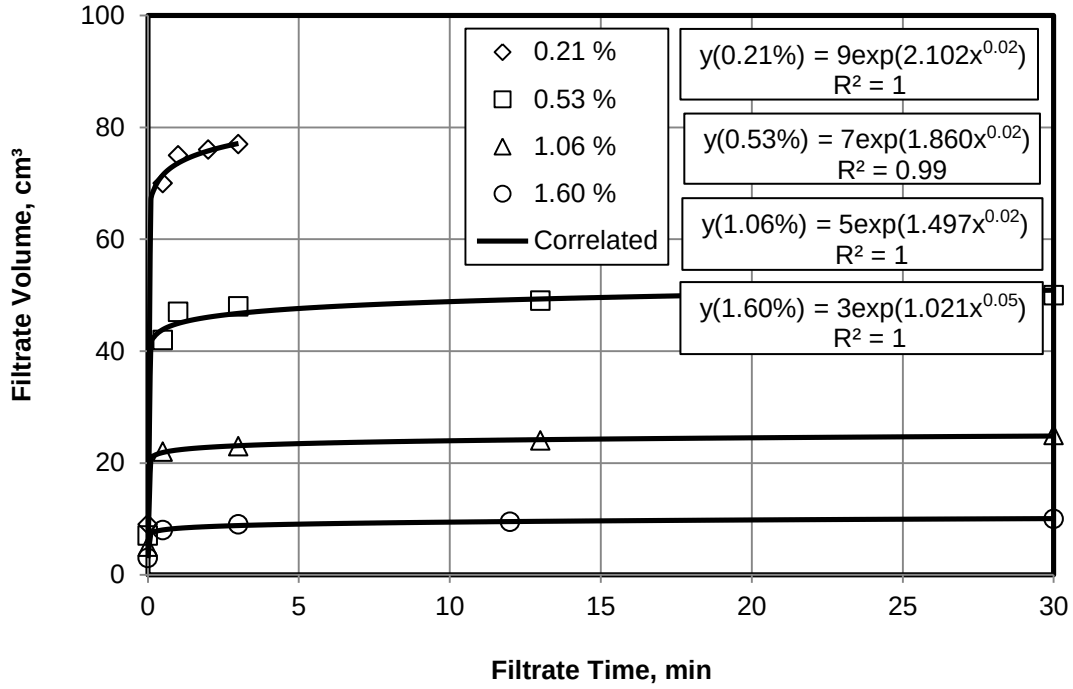

Fig. 9.2: Exponential relationship between filtrate time and filtrate volume at 35 micron pore diameter of filter disc and 20/40 sand mesh for different silica flour concentrations

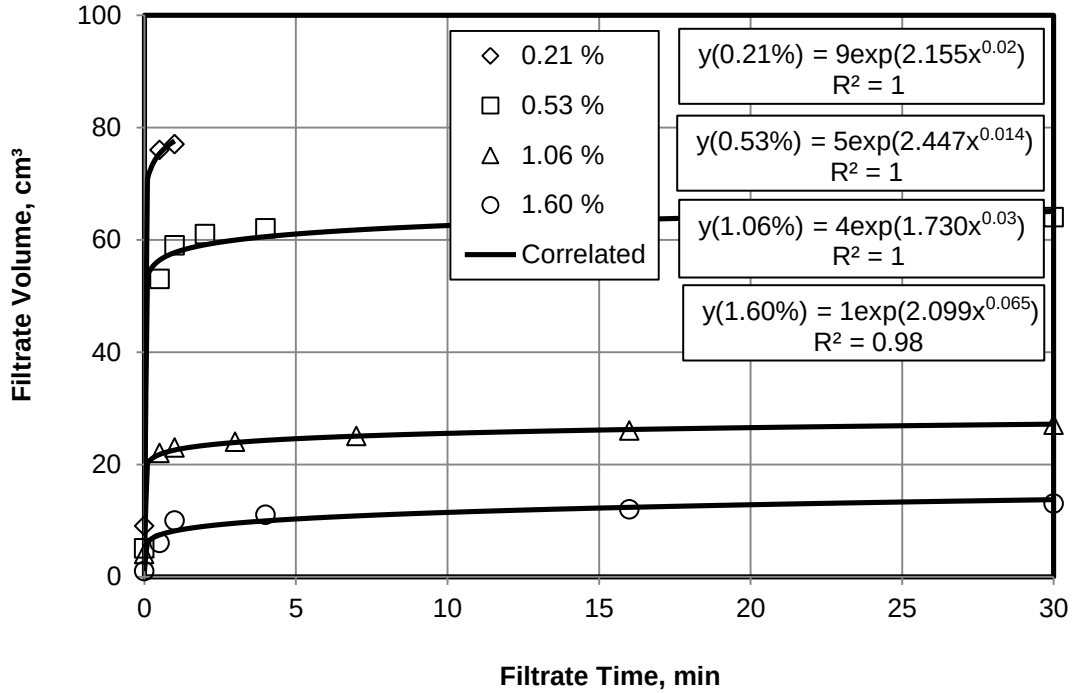

Fig. 9.3: Exponential relationship between filtrate time and filtrate volume at 35 micron pore diameter of filter disc and 40/70 sand mesh for different silica flour concentrations

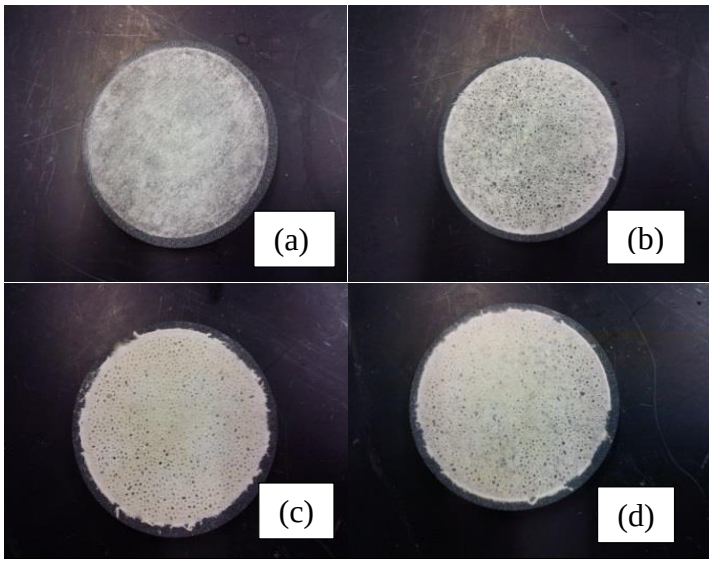

Fig. 9.4: The filtrate cake for same sand mesh and same filter disc and different silica flour concentrations (a) 0.21 vol% (b) 0.53 vol% (c) 1.06 vol% (d) 1.60 vol%

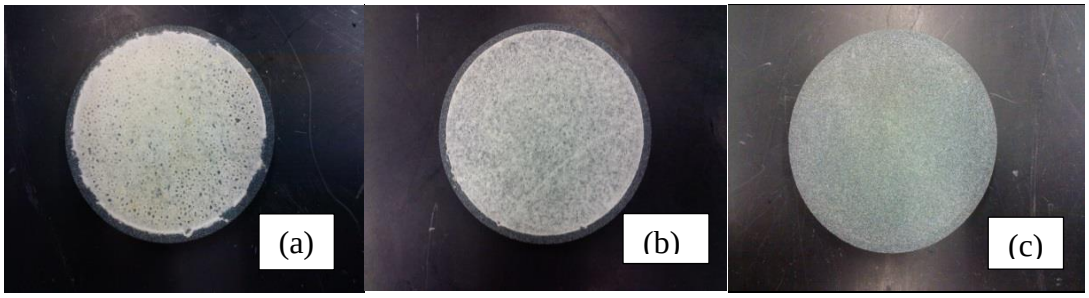

Fig. 9.5: The filtrate cake for same filter disc and same silica flour concentration and different sand sizes (a) 12/20 mesh (b) 20/40 sand (c) 40/70 mesh

Figs. 9.6 to **9.11** show the experimental filtrate volume *(V_f)* and the correlated filtrate volume obtained from the exponential relationship at 10 and 5 micron pore diameters filter discs for different sand sizes at12/20, 20/40, and 40/70 sand mesh and different silica flour concentrations at 0.21, 0.53, 1.06, and 1.60 vol%. **Figs. J.4** to **J.9**

show straight line plot of Eq. B-6 for 10 and 5 micron pore diameters filter disc at different sand sizes and different silica flour concentrations. For the same sand mesh and same silica flour concentration, the experimental data show filtrate volume increases as the pore diameter of the filter disc increases. For 12/20 sand mesh and 1.06 vol% silica flour concentration, the filtrate volume increases from 1 cm^3 to 7 cm^3 by increase of the pore diameter of the filter disc from 5 micron to 10 micron, as shown in Figs. 9.6 and 9.9. This happened because the silica flour passed into the large pores of the filter disc and low silica flour was trapped in the pores and low filtrate cake was formed on the filtrate disc, as shown in **Fig. 9.12**.

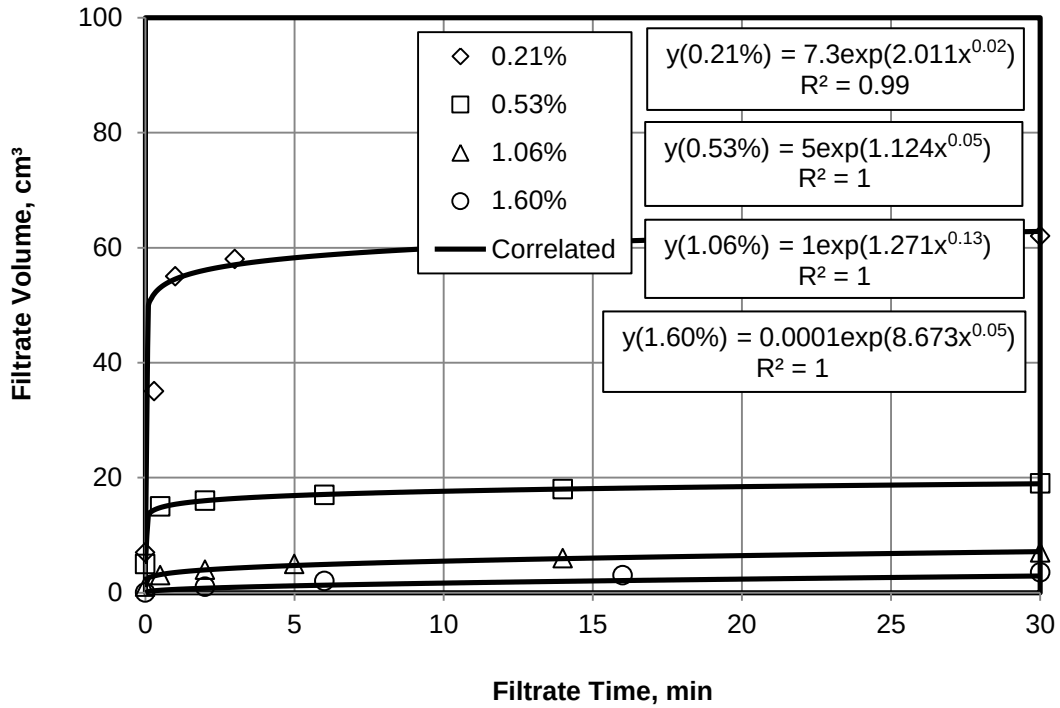

Fig. 9.6: Exponential relationship between filtrate time and filtrate volume at 10 micron pore diameter of filter disc and 12/20 sand mesh for different silica flour concentrations

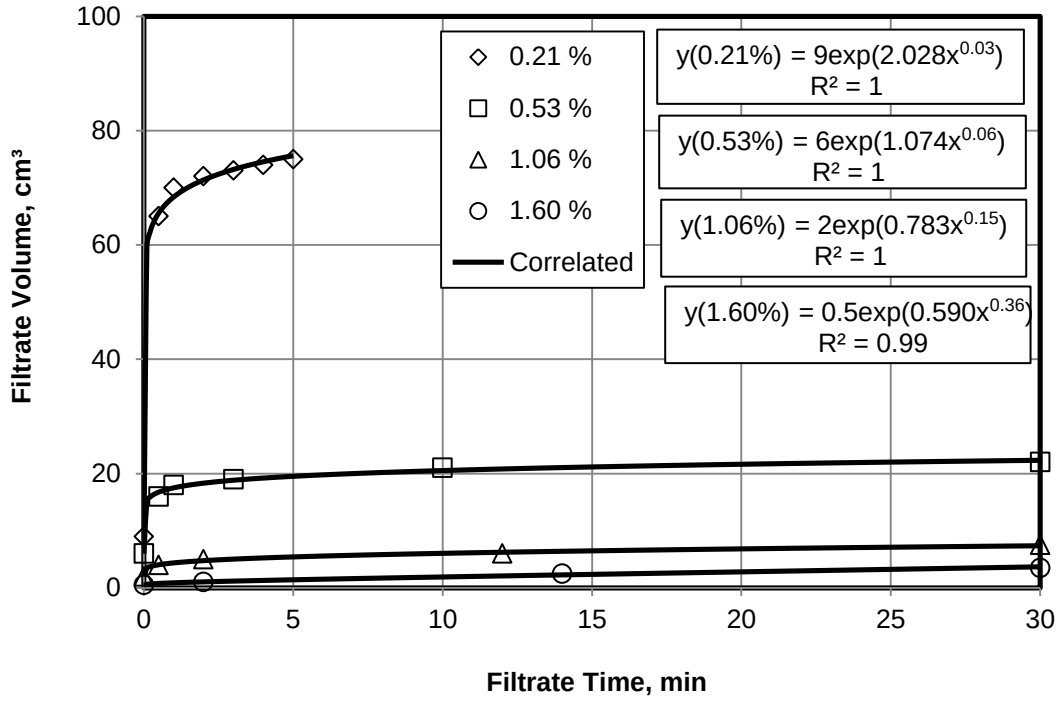

Fig. 9.7: Exponential relationship between filtrate time and filtrate volume at 10 micron pore diameter of filter disc and 20/40 sand mesh for different silica flour concentrations

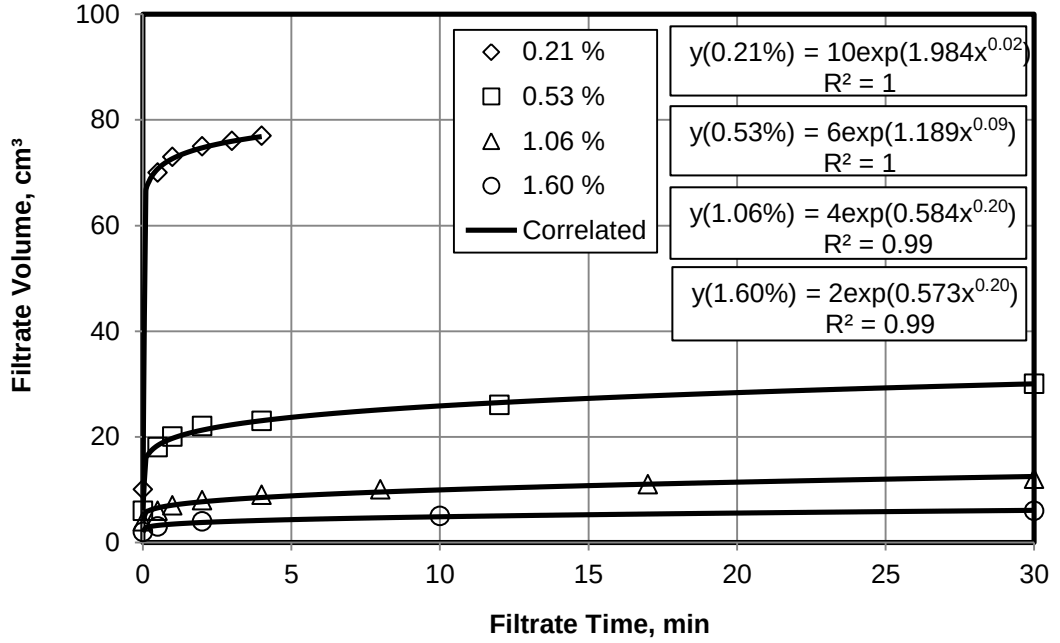

Fig. 9.8: Exponential relationship between filtrate time and filtrate volume at 10 micron pore diameter of filter disc and 40/70 sand mesh for different silica flour concentrations

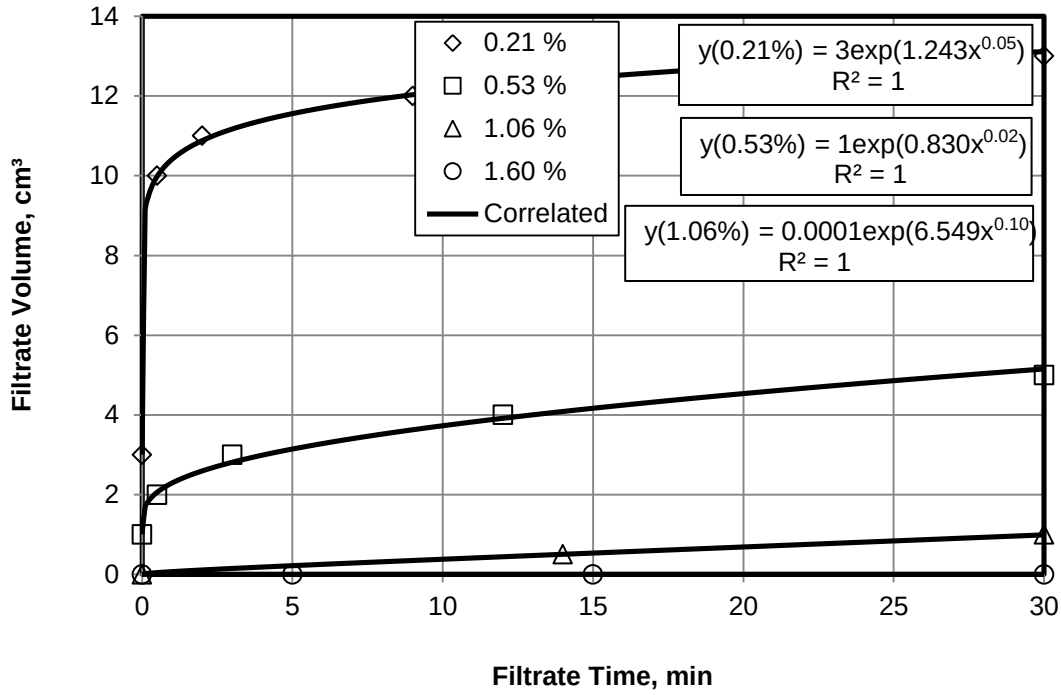

Fig. 9.9: Exponential relationship between filtrate time and filtrate volume at 5 micron pore diameter of filter disc and 12/20 sand mesh for different silica flour concentrations

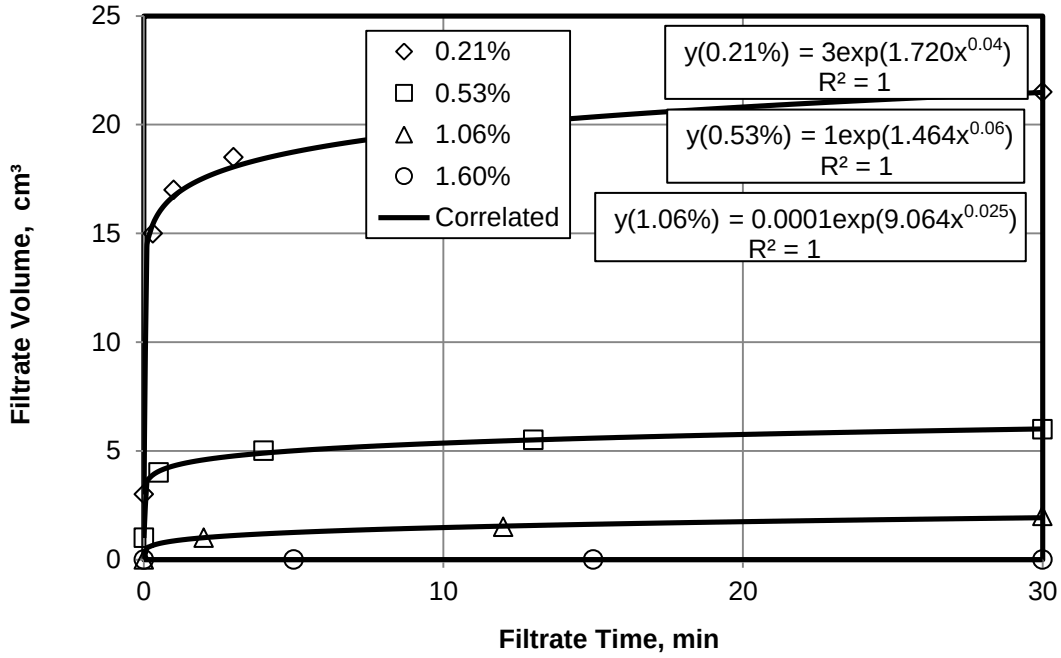

Fig. 9.10: Exponential relationship between filtrate time and filtrate volume at 5 micron pore diameter of filter disc and 20/40 sand mesh for different silica flour concentrations

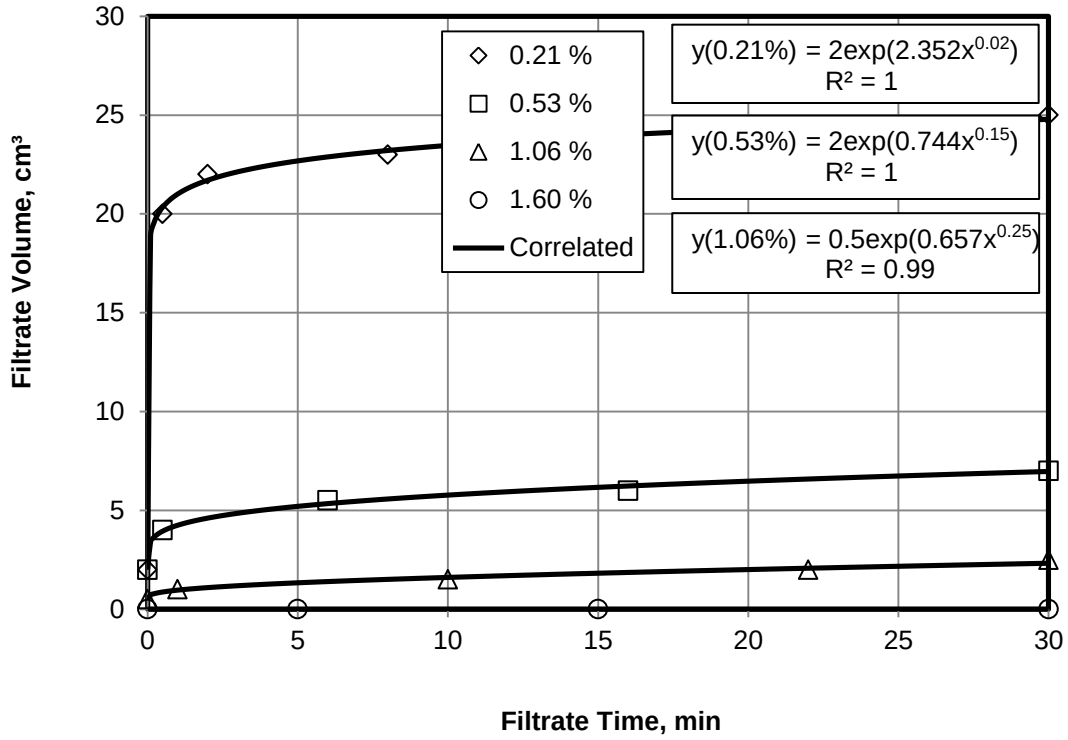

Fig. 9.11: Exponential relationship between filtrate time and filtrate volume at 5 micron pore diameter of filter disc and 40/70 sand mesh for different silica flour concentrations

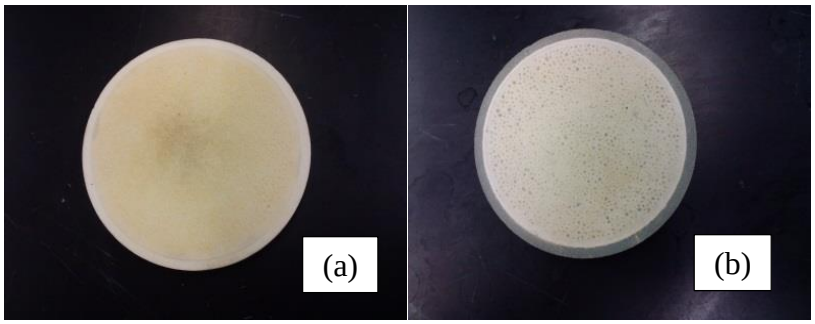

Fig. 9.12: The filtrate cake for same sand mesh and same silica flour concentration and different pore diameter of filter discs (a) 5 micron (b) 10 micron

9.3 Correlations of Rate Constant of Filtrate and Spurt Loss Volume

The experimental results of the fluid loss tests showed a reasonable relationship between the filtrate volume and the silica flour concentration, sand size, and pore diameter of filter disc. The filtrate volume decreased by silica flour concentration and sand size increased and the filtrate volume increased as the pore diameter of the filter disc increased. For the fluid loss test, the rate constant of filtrate and the spurt loss volume are important variables because they give a good idea about the expected filtrate volume during the fluid loss test. **Figs. 9.13** to **9.15** show the filtrate volume of the silica flour particle-gel system during the fluid loss test for different silica flour concentrations, pore diameters filter discs, and sand sizes. The filtrate volume is modeled and represented as straight line plots shown in Figs. 9.19 to 9.21. The slops of the straight lines represent the rate constants of filtrate and the intercepts represent the spurt loss volumes. **Table 9-1** shows the rate constants of filtrate and the spurts loss volumes of the silica flour particle-gel system at different sand sizes, pore diameters of the filter discs, and silica flour concentrations. The rate constants of the filtrate and spurt loss volumes decreased by silica flour concentrations and sand sizes because the pores plugging increased and increased by pore diameters of the filter discs because the pores plugging decreased. **Figs. K.1** and **K.2** in Appendix K show the relationship between the rate constants of filtrate and spurt loss volumes and the silica flour concentrations of the particle-gel system at different sand sizes and pore diameters of the filter discs. The rate constant of the filtrate and the spurt loss volumes are correlated by using Eq. B-6 given in Appendix B, as shown in **Figs. K.3 to K.8**. The rate constants of the filtrate and the spurt loss volumes were correlated using the

exponential relationship shown in Eq. 6.7. The correlations showed intersection between them because of the individual data correlation, as shown in Figs. K.1 and K.2. The correlations are simultaneously fitted by collecting the empirical parameters values from the correlations and plotted against the sand sizes and pore diameters of the filter discs correlated as linear functions, as shown in **Figs. K.9** to **K.14**. The linear functions of A, B, and β are substituted in the exponential relationships of the rate constants of the filtrate and spurt loss volumes and the empirical correlations are developed which can be used to predict the filtrate volume of the silica flour particle-gel system at any conditions, as shown in **Figs. 9.16** and **9.17**.

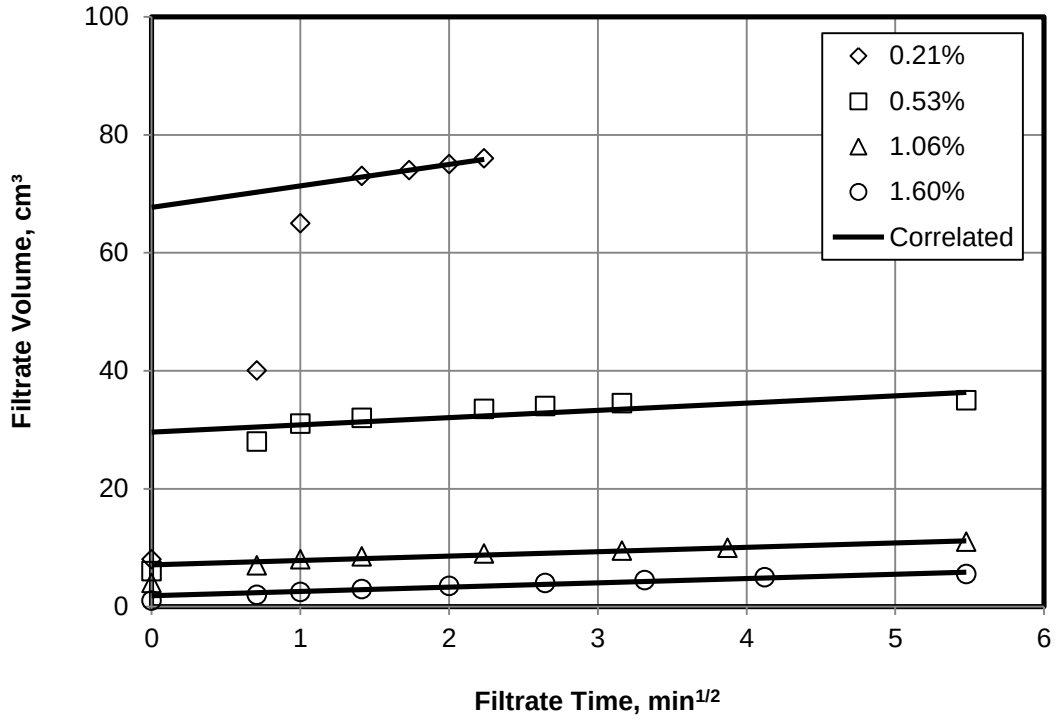

Fig. 9.13: Experimental and correlated filtrate volume of 35 micron pore diameter filter disc and 12/20 sand mesh for different silica flour concentrations

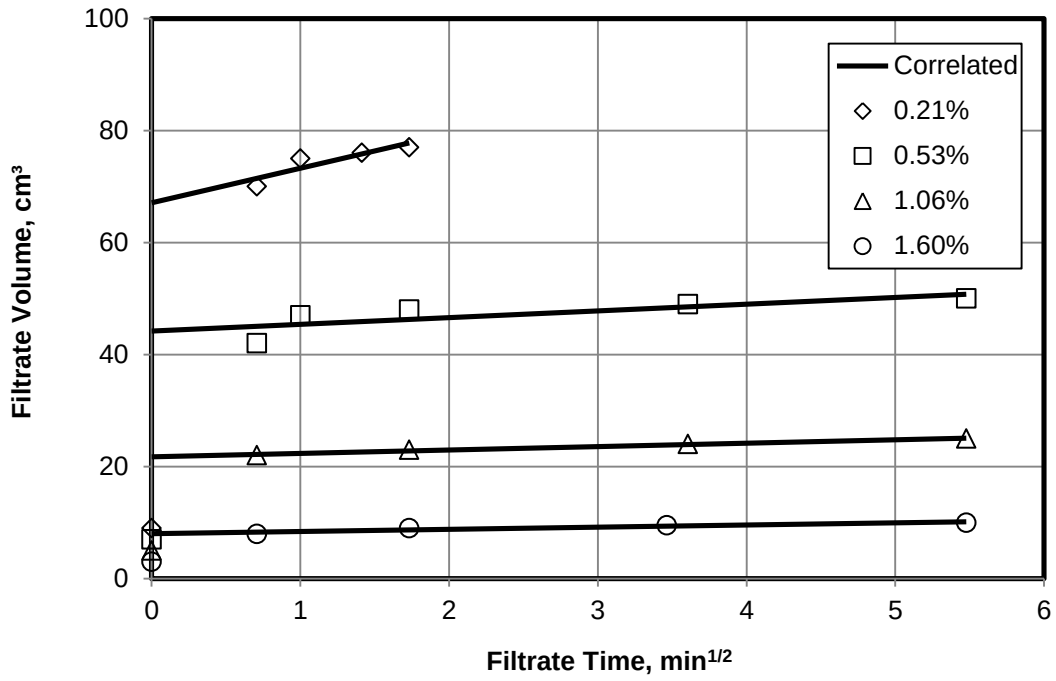

Fig. 9.14: Experimental and correlated filtrate volume of 35 micron pore diameter filter disc and 20/40 sand mesh for different silica flour concentrations

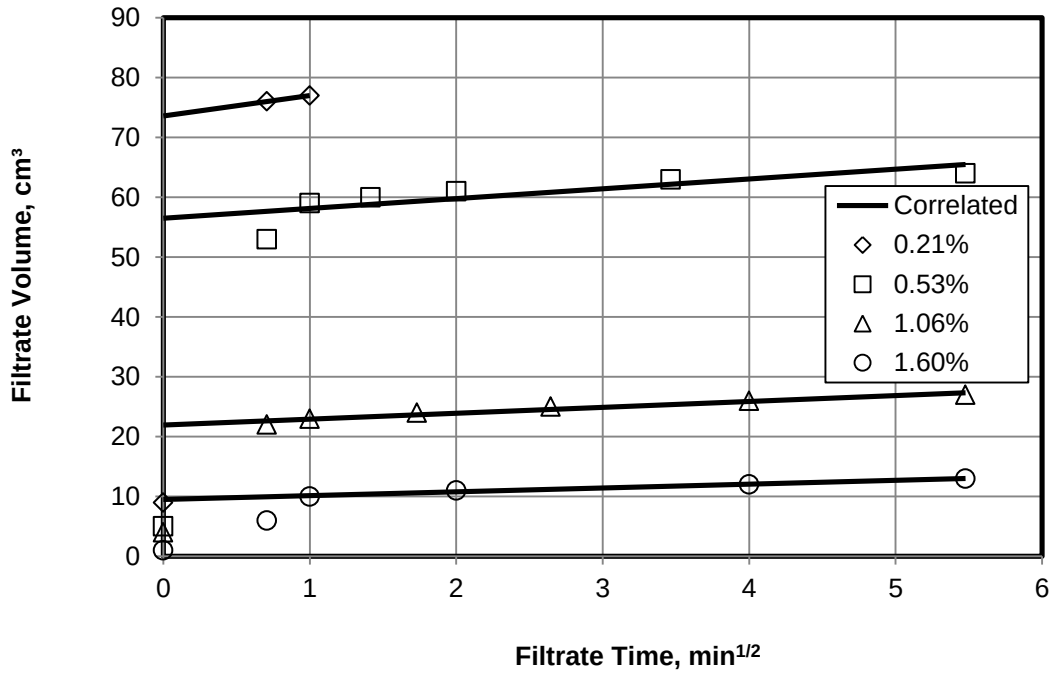

Fig. 9.15: Experimental and correlated filtrate volume of 35 micron pore diameter filter disc and 40/70 sand mesh for different silica flour concentrations

TABLE 9-1: RATE CONSTANTS OF FILTRATE AND SPURT LOSS VOLUME OF 35 MICRON PORE DIAMETER FILTER DISC AT DIFFERENT SAND SIZES AND DIFFERENT SILICA FLOUR CONCENTRATIONS

Sand size (mesh)	Silica Flour Concentration (vol%)	Rate Constant ($cm^3/min^{1/2}$)	Spurt Loss Volume (cm^3)	R^2
12/20	0.21	3.64	67.80	0.99
	0.53	1.23	29.64	0.67
	1.06	0.74	7.10	0.94
	1.60	0.67	2.08	0.97
20/40	0.21	6.17	67.10	0.81
	0.53	1.20	44.20	0.60
	1.06	0.61	21.70	0.98
	1.60	0.39	8.00	0.90
40/70	0.21	3.42	73.00	1
	0.53	1.64	56.00	0.60
	1.06	0.99	21.95	0.95
	1.60	0.64	9.51	0.99

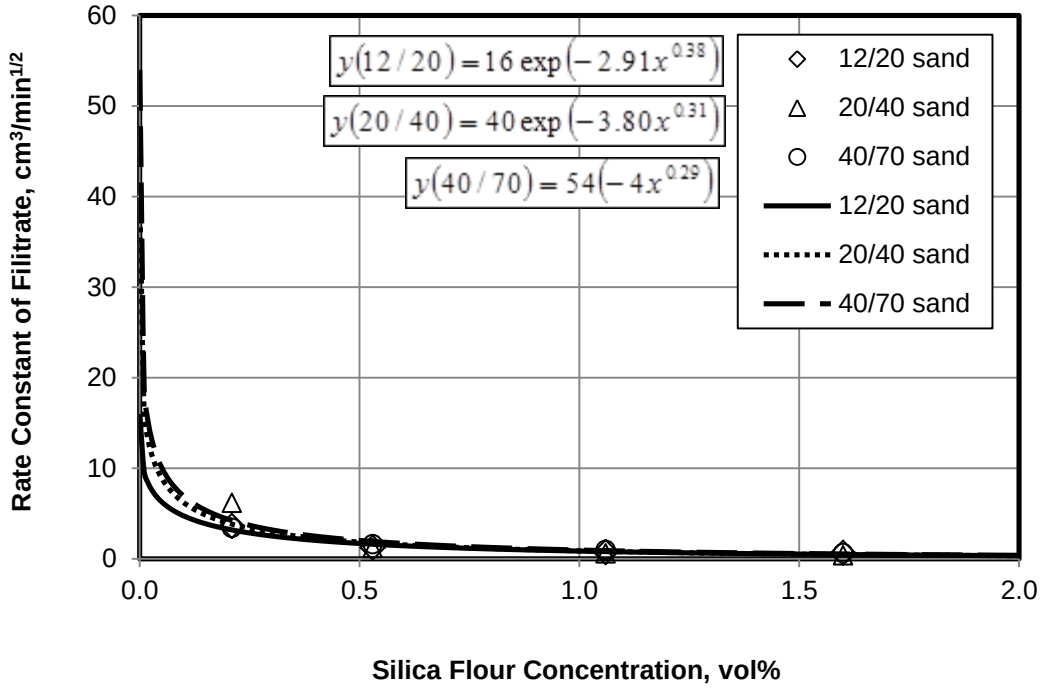

Fig. 9.16: Rate constant of filtrate of 35 micron pore diameter filter disc at different silica flour concentrations and different sand sizes

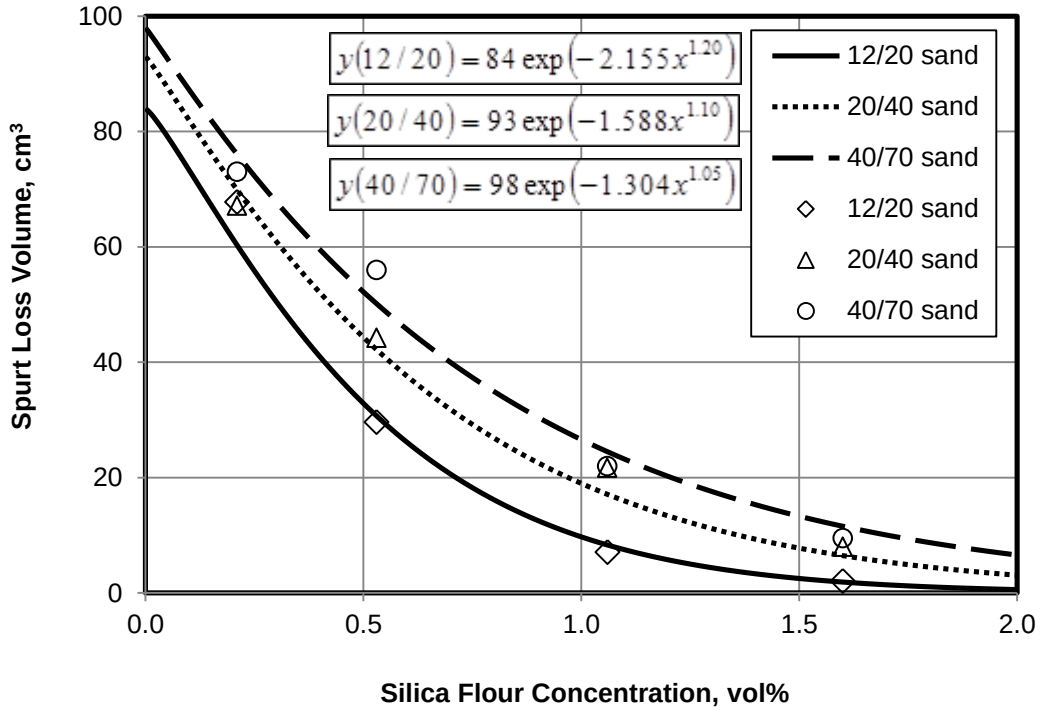

Fig. 9.17: Spurt loss volume of 35 micron pore diameter filter disc at different silica flour concentrations and different sand sizes

9.4 Conclusions

The main findings of the filtrate analysis of performance of the silica flour particle-gel system are the following:

- Filtrate analysis was used to evaluate the performance of the silica flour particle-gel applications in near-wellbore formation treatment and various important empirical correlations were developed which can assist in effective and successful designing for near-wellbore formation treatment with silica flour particle-gel system.
- The correlated filtrate volume obtained from the exponential relationship showed satisfactory match with the experimental filtrate volume.
- The effect of the silica flour concentration, sand size, and pore diameter of filter disc on the filtrate volume of the silica flour particle-gel system was investigated and a decrease in the filtrate volume by increasing the silica flour concentration and sand size and an increase in the filtrate volume by increasing the pore diameter of the filter disc were observed.
- The rate constants of filtrate and spurt loss volumes were determined and correlated successfully with the silica flour concentration, sand size, and pore diameter filter disc.

Chapter 10: Near-Wellbore Formation Treatment Design

10.1 Introduction

The objective of this chapter is to demonstrate the importance of the empirical correlations developed in this study for choosing suitable treatment fluids and evaluating the near-wellbore formation treatment under optimum application conditions. The developed empirical correlations are used to determine the treatment fluid properties and the modification of the near-wellbore formation after the treatment process. Two cases of treatment design are presented involving synthetic examples of gel-particle suspension and silica flour particle-gel systems.

10.2 Synthetic Field Application of Gel-Particle Suspension

The synthetic field application represents a well under drilling operations (**Fig. 10.1**) and the parameters of the synthetic well and fiels reservor shown in **Table 10-1**. Drilling fluid loss occurred through the sandstone bed because of the high permeability of the sandstone bed. Gel-particle suspension is used to treat and modify the sandstone bed permeability to prevent the drilling fluid loss. **Table 10-2** shows the properties of the gel-particle suspension and the modification of the sandstone bed after treatment that should be determined to design the treatment process. For the near-wellbore formation treatment by the gel-particle suspension, empirical correlations were used for the treatment design. **Table 10-3** shows a summary of the empirical correlations developed in this study.

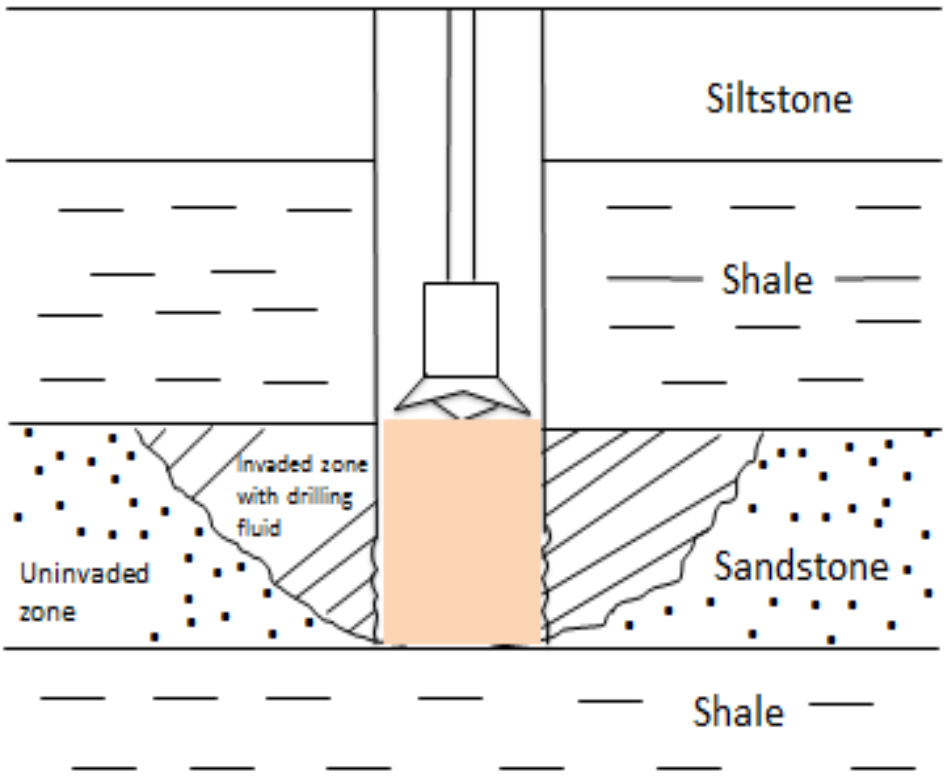

Fig. 10.1: Schematic of synthetic well under drilling process

TABLE 10-1: PARAMETERS OF SYNTHETIC WELL AND FIELD RESERVOIR
Hole size, casing ID = 8 in
Thickness of the sandstone bed = 200 ft
Penetrate of the invaded zone = 3ft
Porosity = 0.38
Permeability = 3800 md
BHT = 125 °F

TABLE 10-2: PARAMETERS OF THE GEL-PARTICLE SUSPENSION AND THE NEAR-WELLBORE FORMATION MODIFICATION

Suspension volume required (bbl)
Carrier fluid volume required (bbl)
Xanthan powder weight required (lb)
Polymer (gel particles) weight required (lb)
Injection flow rate of the suspension (bbl/day)
Time required to inject the suspension (hr)
Suspension viscosity (Pa.s)
Permeability reduction (dimensionless)
Resistance factor (dimensionless)

TABLE 10-3: SUMMARY OF THE EMPIRICAL CORRELATIONS OF THE GEL-PARTICLE SUSPENSION DEVELOPED IN THIS STUDY

Correlation Name	Empirical Correlation	Symbols
Viscosity correlation	$\mu = 0.00083C_p + 0.003$	μ: suspension viscosity, Pa.s C_p: suspension concentration, vol%
Differential pressure correlations	$\Delta P = 8.07\exp\left(0.55C_p\right)$ $\Delta P = 6.65 - 6.65\exp\left(0.0001q\right) + 115\left(\frac{q^{1.8}}{q^{1.8}+7136}\right)$ $\Delta P = 122\left[\frac{D_p}{D_p+265}\right] + 8.07$	ΔP: differential pressure, kPa q: injection flow rate, cm^3/hr D_p: gel-particle diameter, μm
Permeability reduction correlations	$\frac{K}{K_o} = 1 + 5.55\left(\frac{C_p^{0.64}}{C_p^{0.64} - 19.42}\right)$	$\frac{K}{K_o}$: permeability reduction, dimensionless

Correlation Name	Empirical Correlation	Symbols
	$\frac{K}{K_o} = 0.80\exp(-0.022q) + 0.20\exp(0.0028q)$ $\frac{K}{K_o} = 1 - 0.77\left[\frac{\left(D_p/D_T\right)^{1.8}}{\left(D_p/D_T\right)^{1.8} + 0.126}\right]$	
Resistance factor correlations	$F_r = 0.62 + 8\left[\frac{C_p}{C_p + 0.80}\right] + 0.33\exp\left(0.66C_p^{1.4}\right)$ $F_r = -16 + 22\left(\frac{q}{q+38}\right) + 16\exp\left(-75E-07q^2\right)$ $F_r = 1 + 35.09\left(\frac{D_p}{D_p + 141.62}\right)$	F_r: resistance factor, dimensionless
Power-law equation	$\beta = 54R_{ep}^{0.511} + 1$	β: pore-throat/particle-diameter ratio, dimensionless
Exponential-law equation	$\beta = 690\left[1 - \exp\left(-0.07R_{ep}^{0.5}\right)\right] + 1$	R_{ep}: particle Reynold number, dimensionless
Thermal effect correlations	$\ln\mu = -3.357 + \left(\frac{465.17}{T-550}\right)$ $\ln\Delta P = 7.902 + \left(\frac{1684.7}{T-700}\right)$ $\ln\frac{K}{K_o} = -0.3411 - \left(\frac{133.76}{T-100}\right)$ $\ln F_r = -8.407 + \frac{10000}{T+600}$	T: temperature, k

The steps of the treatment design calculations are as follows.

The wellbore volume = 3.141 × 0.333^2 × 200 = 69.80 ft³. Wellbore + 3 ft penetration volume = 3.141 × 3.333^2 × 200 = 6980 ft³. Volume for 3 ft matrix penetration = (6980-69.80) × 0.38 = 2626 ft³. Volume for casing fill + 20% = 69.80 + (0.2 × 69.80) = 83.76 ft³. Volume of suspension required = 83.76 + 2626 = 2709.76 ft³ (643.46 bbl). For 3 vol% gel particle suspension. Volume of gel particles required = 0.03 × 643.46 = 19.30 bbl. Volume of carrier fluid required = 643.46- 19.30 = 624.16 bbl. 0.25 gm of Xanthan powder was added to 500 cm³ (0.004193 bbl) water to prepare the carrier fluid. Weight of the Xanthan powder required = $\frac{624.16}{0.004193} \times 0.25 = 37214$gm = 37.214 kg (16.88lb). For the suspension experiments, 100 cm³/hr injection flow rate was used for sandpack of 1 in diameter. The suspension velocity (v) = $\frac{q}{A \times \phi}$. where A is the cross sectional area of the sandpack. $v = \frac{100}{5.066 \times 0.38} = 51.94$cm/hr. For same suspension velocity in the formation, the injection flow rate of the suspension in the Field (q): q = v × A × Φ. where A is the cross sectional treatment area of the sandstone bed. A = π × d × h. where d is the diameter of the well and h is the thickness of the sandstone bed. A = 3.141 × 0.667 × 200 = 419 ft². v = 51.94 cm/hr = 1.704 ft/hr. q = 1.704 × 419 × 0.38 = 271.32 ft³/hr = 64.43 bbl/hr = 1546 bbl/day. Time required to inject the suspension to the wellbore and the formation (t): t = Total volume of the suspension/ Injection flow rate of the suspension. t = 643.46/64.43 = 10 hrs. Viscosity of 3 vol% gel particle suspension at 125 °F (324.82 K) temperature: By using the correlation given in Table 10-1, suspension viscosity = 0.00442 Pa.s. Permeability reduction of 3800 md permeability of the sandstone at 125 °F temperature: By using the correlation given in Table 10-1, permeability reduction (K/K_o) = 0.39. Permeability decreased from 3800

md to 1482 md by the suspension treatment. Resistance factor (F_r) at 125 °F = 11.1 by using the correlation given in Table 10-1. **Table 10-4** shows the results of the design of the near-wellbore formation treatment by the gel-particle suspension to prevent the drilling fluid loss during the drilling operations. **Fig. 10.2** shows flow chart of the process of the near-wellbore formation treatment by gel-particle suspension.

TABLE 10-4: RESULTES OF THE NEAR-WELLBORE FORMATION TREATMENT DESIGNE BY THE GEL-PARTICLE SUSPENSION
Suspension volume required = 643.46 bbl
Carrier fluid volume required = 624.16 bbl
Xanthan powder weight required = 16.88 lb
Polymer (gel particles) volume required = 19.30 bbl
Injection flow rate of the suspension = 1546 bbl/day
Time required to inject the suspension = 10 hr
Suspension viscosity = 0.00442 Pa.s
Permeability reduction (K/K_o) = 0.39
Permeability after treatment = 1482 md
Resistance factor = 11.1

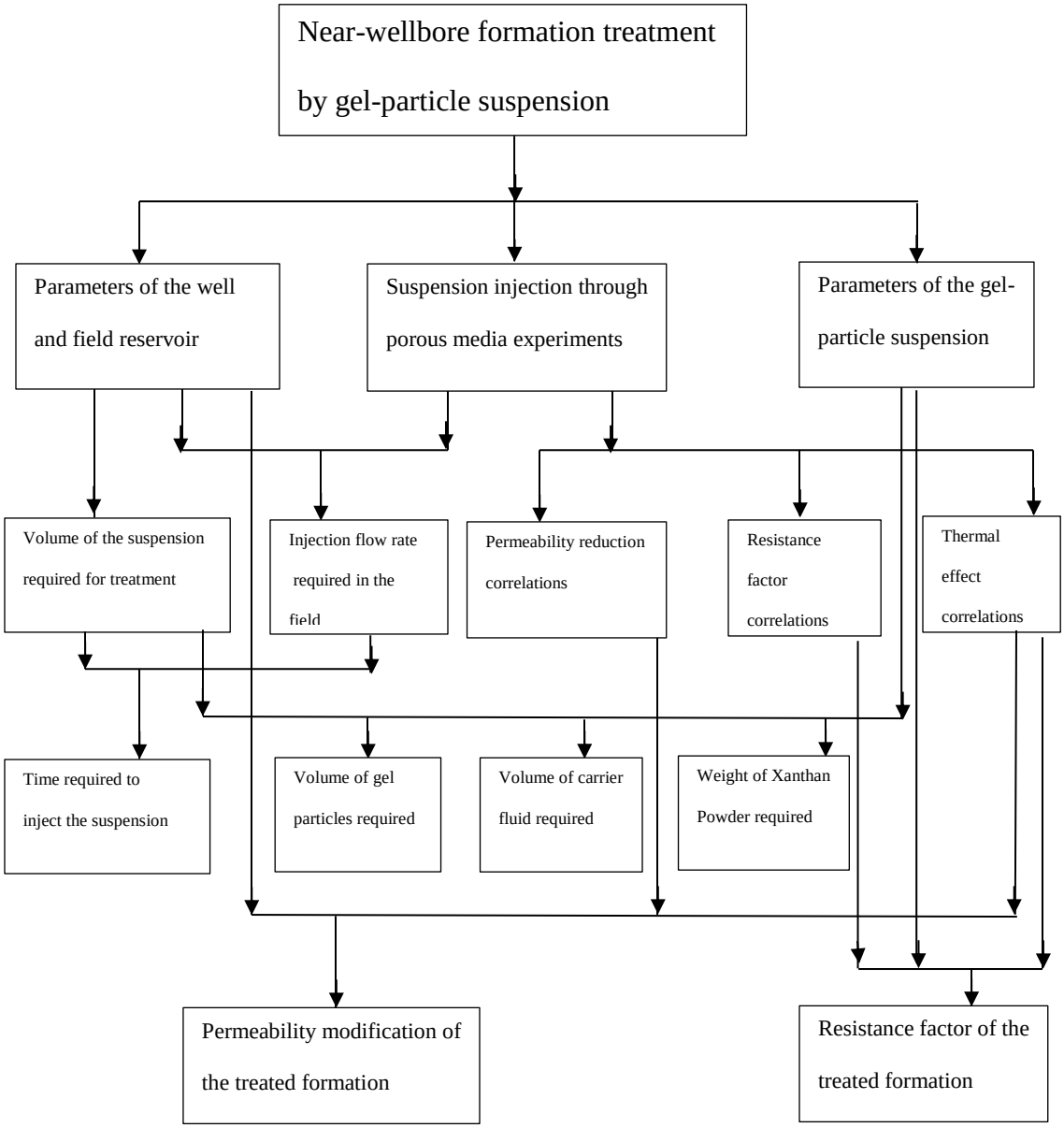

Fig. 10.2: Process of the near-wellbore formation treatment by gel-particle suspension

10.3 Synthetic Field Application of Silica Flour Particle-Gel System

The synthetic field application represents oil producing well (**Fig. 10.3**) of parameters show in **Table 10-5** and with three perforated zones (**Table 10-6**) (van Eijden et al. 2004). The middle sands were flushed and producing predominantly water. The well was producing 3000 bbl/day with a water cut of 63 %. Gel-cement system treatment was applied of the perforated zones at maximum pressure of 1500 psi for 30 minutes, thus the water shutoff was achieved by the cement plugged in the perforations and the gel penetrated three inch through the matrix (formation). The wellbore was washed to remove excess gel-cement and the well was shut in for 48 hrs. The upper and lower zones were re-perforated and the initial production was 4500 bbl/day at 40% water cut. The production logging tool (PLT) showed no flow coming from the middle zone. It was found that the main problem for the gel-cement system is the interaction between the cement retarders and the gel. The cement worked as a fluid loss agent in the gel-cement system. van Eijden 2005 replaced the cement by a silica flour which is an inert material, and developed particle-gel system. 50 wt% of silica flour was used in the particle-gel system which causes logistics problem and results in wellsite handling issues (Dalrymple et al. 2008). Fluid loss experiments were conducted on different silica flour particle-gel systems to minimize and optimize the silica flour concentration, as shown in chapter 8. Silica flour particle-gel system of 4.20 wt% (1.60 vol%) silica flour concentration was developed from the fluid loss experiments, which can be used for the near-wellbore formation treatment. **Table 10-7** shows the components of the silica flour-particle gel system developed from the fluid loss experiments.

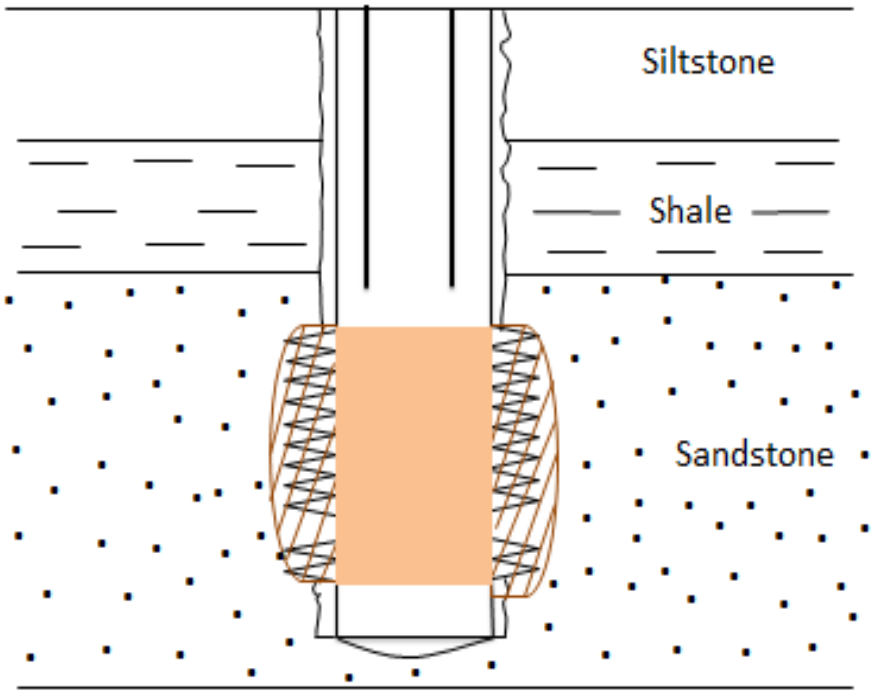

Fig. 10.3: Schematic of synthetic oil producing well

TABLE 10-5: PARAMETERS OF SYNTHETIC OIL PRODUCING WELL
Hole size, casing ID = 7.0 in
Tubing ID = 3.5 in
Oil production rate = 3000 bbl/day
Water cut = 63 %
Porosity = 0.22
BHP = 1500 psi
BHT = 90 °C

TABLE 10-6: PERFORATION ZONES OF SYNTHETIC PRODUCING OIL WELL		
Zone	Perforation Interval, m	Net Thickness, m
Upper zone	2864.0- 2867.0	3.0
	2872.0- 2873.0	1.0
	2873.5- 2878.0	4.5
	2883.0- 2892.0	9.0
Middle zone	2892.5- 2896.0	3.5
	2901.0- 2904.0	3.0
	2905.0- 2914.0	9.0
	2917.0- 2925.0	8.0
Lower zone	2933.0- 2944.0	11.0
	2943.0- 2948.0	5.0

The steps of the treatment design calculations as follows. The wellbore volume = 3.141 × 0.292^2 × 275.52 = 73.79 ft^3. Wellbore + 3 in penetration volume = 3.141 ×0.542^2 × 275.52 = 254.23 ft^3. Volume for 3 in formation penetration = (254.23- 73.79) × 0.20 = 36.09 ft^3. Volume for casing fill + 20% = 73.79 + (0.20 × 73.79) = 88.55 ft^3. Volume of gel-particle system required = 36.09 + 88.55 = 124.64 ft^3 = 932.29 gal = 29.60 bbl. Empirical correlations of the silica flour particle-gel system were developed from the experimental data, as shown in **Table 10-8**.

The developed empirical correlations were used for treatment design as

follows. For pore diameter of filter disc (D_s) = 35 micron and sand diameter (D_s) = 1260 micron (12/20 sand mesh). The critical silica flour concentration = 0.62 wt% by using the correlation given in Table 10-8. By using the correlation given in Table 10-8, the fluid loss for 4.20 wt% silica flour particle-gel system = 6 vol% and for 50 wt% silica flour particle-gel system = 0 vol%. This fluid loss for 100 cm^3 silica flour particle-gel system and the fluid loss for 29.60 bbl silica flour particle-gel system = 1.77 bbl. By using the correlation given in Table 10-8, the pressure initiate flow = 3478 kPa and for 50 wt% silica flour particle-gel system = 4510 kPa. By using the correlation given in Table 10-9, the filtrate rate constant for 4.20 wt% silica flour particle-gel system = 0.49 $cm^3/ min^{1/2}$ and for 50 wt% silica flour particle-gel system = 0 $cm^3/ min^{1/2}$. For 30 minute treatment time and 29.60 bbl particle-gel system, the filtrate volume = $0.49 \times (30)^{1/2}$ = 2.68 cm^3 for 100 cm^3 = 0.79 bbl for 29.60 bbl. By using the correlation given in Table 10-8, the spurt loss volume for 4.20 wt% silica flour particle-gel system = 1.80 cm^3 and for 50 wt% silica flour particle-gel system = 0 cm^3. This spurt loss volume for 100 cm^3 particle-gel system and for 29.60 bbl = 0.53bbl. Total filtrate volume = filtrate volume at 30 minutes + spurt loss volume = 0.79 + 0.53 = 1.32 bbl.

A comparison was conducted between the particle-gel system that was used for the field application and the particle-gel system that was developed from the experiments, as shown in **Table 10-9**. Table 10-9 shows that the difference between the results of the treatment design of both particle-gel systems is low, thus the 50 wt% silica flour concentration is very high and should be minimized. **Fig. 10.4** shows flow chart of the process of the near-wellbore water shutoff treatment by silica flour particle-gel system.

TABLE 10-7: COMPONENTS OF THE SILICA FLOUR PARTICLE-GEL SYSTEM DEVELOPED FROM FLUID LOSS EXPERIMENTS

Water = 16.02 bbl

Silica flour = 0.47 bbl

KCl = 1.89 bbl

Polymer 1 = 0.08 bbl

Polymer 2 = 9.51 bbl

Crosslinker = 1.63 bbl

Particle-gel system volume = 29.06 bbl

TABLE 10-8: SUMMARY OF THE EMPERICAL CORRELATIONS OF THE SILICA FLOUR PARTICLE-GEL SYSTEM

Correlation Name	Empirical Correlation	Symbols
Critical silica flour concentration correlation	$x_{cr} = -(4E-06D_F + 7E-05)Ds + (0.0214D_F + 0.1415)$	x_{cr}: critical silica flour conce-ntration, wt% D_F: pore diameter filter disc, micron D_s: sand diameter, micron F.L.: fluid loss, % C_s: silica flour concentration, wt% P: pressure initiate flow, kPa μ: silica flour particle-gel viscosity, Pa.s T: temperature, k
Fluid loss correlation	$F.L. = 100\exp[-(\ (66E-07D_F + 33E-05)D_s + (-0.045D_F + 2.06)\ )(C_s - (5E-06D_F + 6E-05)D_s + (0.021D_F + 0.157)\ )^{(-6E-06D_F + 2E-05)D_s + (0.0124D_F + 0.474)}\ ]$	
Pressure initiate flow correlation	$P = \dfrac{[(-0.043D_F + 3.278)D_s + (-161D_F + 8070)]}{(C_s - x_{cr})^{(-15E-06D_F + 3E-04)D_s + (0.013D_F + 0.686)}} \dfrac{(C_s - x_{cr})^{(-15E-06D_F + 3E-04)D_s + (0.013D_F + 686)}}{+(-0.00016D_s + 0.021D_F + 0.494)}$	
Thermal effect correlations	$\ln \mu = -5.914 + \left(\dfrac{545}{T - 120}\right)$ $\ln F.L. = 2.15 - \left(\dfrac{42.80}{T - 470}\right)$ $\ln P = 8.48 + \left(\dfrac{54.18}{T - 420}\right)$	

Correlation Name	Empirical Correlation	Symbols
Filtrate volume correlations for 35 micron disc and 12/20 mesh sand	$y(0.21\%) = 8.3\exp(2.063x^{0.02})$ $y(0.53\%) = 6\exp(1.623x^{0.03})$ $y(1.06\%) = 4\exp(0.670x^{0.12})$ $y(1.60\%) = 1\exp(0.927x^{0.02})$	y: filtrate volume, cm^3 x: filtrate time, min
Filtrate rate constant correlations for 35 micron disc	$y(12/20) = 16\exp(-2.91x^{0.38})$ $y(20/40) = 40\exp(-3.80x^{0.31})$ $y(40/70) = 54\exp(-4x^{0.29})$	y: filtrate rate constant, $cm^3/min^{1/2}$ x: silica flour concentration, vol%
Spurt loss volume correlations for 35 micron disc	$y(12/20) = 84\exp(-2.155x^{1.20})$ $y(20/40) = 93\exp(-1.588x^{1.10})$ $y(40/70) = 98\exp(-1.304x^{1.05})$	y: spurt loss volume, cm^3 x: silica flour concentration, vol%

TABLE 10-9: COMPARISON BETWEEN FIELD PARTICLE-GEL SYSTEM AND EXPERIMENT PARTICLE-GEL SYSTEM

Properties	Field Gel-Particle System	Experiment Gel-Particle System
Silica flour concentration (wt%)	50	4.20
Fluid loss (vol%)	0	6
Pressure initiate flow (kPa)	4510	3478
Filtrate rate constant ($cm^3/min^{1/2}$)	0	0.49
Filtrate volume at 30 minutes (bbl)	0	0.79
Spurt loss volume (bbl)	0	0.53
Total filtrate volume (bbl)	0	1.32

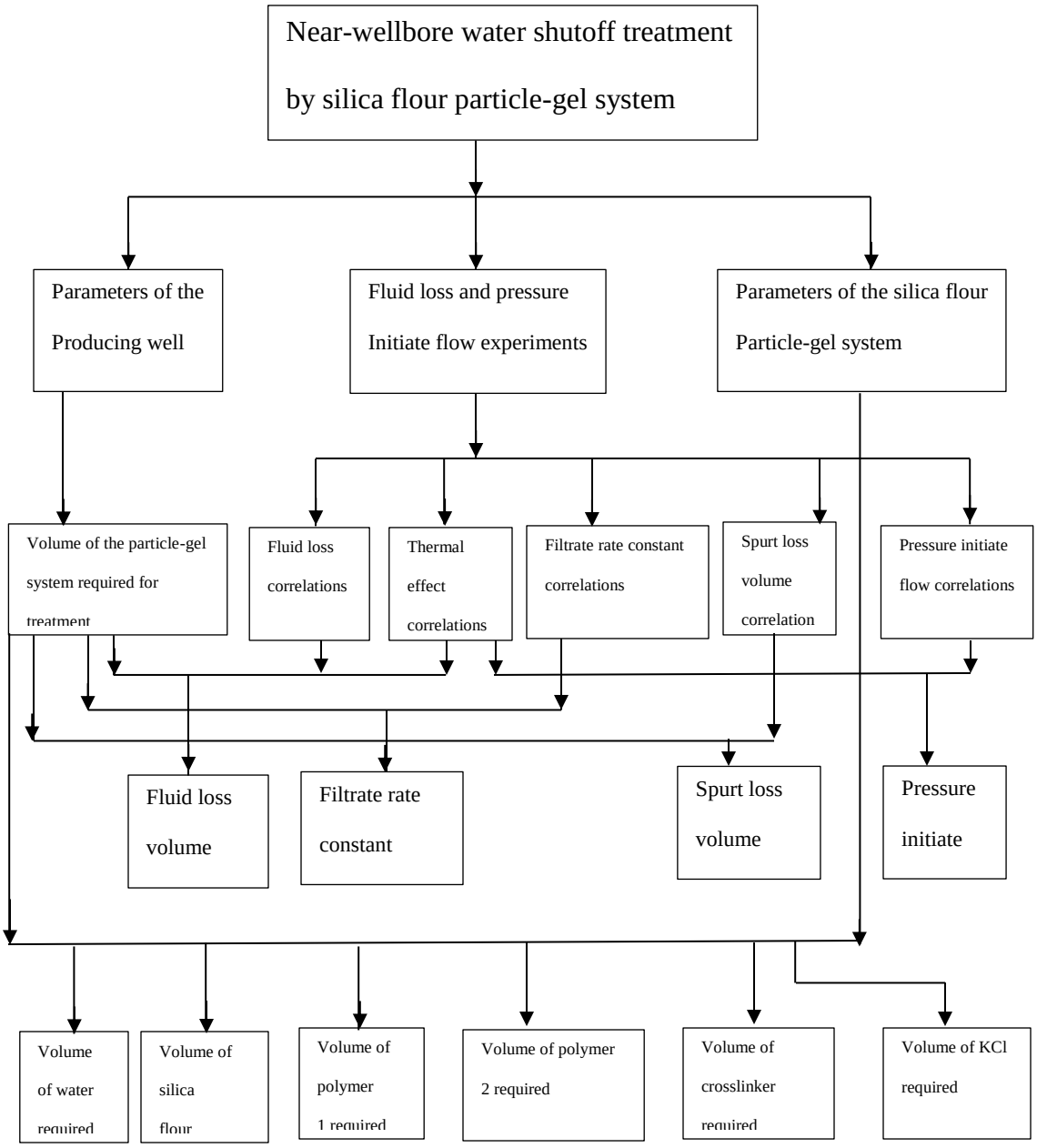

Fig. 10.4: Process of the near-wellbore water shutoff treatment by particle-gel system

Chapter 11: Summary, Discussion, and Conclusions

Heterogeneous formations around wellbore are been treated using gel particles suspensions and silica flour particle-gel slurry systems without much in depth investigations of the relevant and operating principles involved in the treatment of near-wellbore zones. Therefore, this work has focused on understanding of the operating principles and conditions by means of investigations of various issues involved in the effective treatment of heterogeneous formations by gel-particles suspensions injection and application of silica flour particle-gel systems. The discussion and conclusions of the various issues investigated in this dissertation can be summarized in the following sections. These will be presented in two groups experimental and theoretical studies.

11.1 Experimental Investigations

A- Fluid loss control treatment

In this study fluid loss control using gel particles suspension was investigated for the effect of gel particles concentration, gel particle diameter, flow rate, temperature, and particle diameter to pore-throat size on controlling lost circulation of drilling fluids during drilling operations. The experimental work demonstrated that the permeability modification of the high permeability formation increases by the gel particles concentration, gel particle diameter, and particle diameter to pore- throat size increases because the plugging of the pores by the gel particles increases. Also, the permeability modification become les s pronounced with flow rate increases because the particles

deposition over the pore surfaces decreases and mobilization of particles from pore surfaces increases by flow rate increases. The degree of pore-throat plugging and pore-surface deposition decreased when temperature increased and thus the permeability modification decreased when temperature increased.

B- Water shutoff treatment

In this study water shutoff treatment using silica flour particle-gel slurry system was investigated for the effect of silica flour concentration, temperature, sand size, pore diameter of formation material on controlling water production in hydrocarbon producing wells. The experimental work demonstrated that the fluid loss decreases and the pressure required to initiate water flow increases by silica flour concentration and sand size increase because the silica flour trapped in the pores of formation and forming a filter cake. The fluid loss increases and the pressure required to initiate flow decreases by pore diameter of formation and temperature increase because the particle-gel slurry system pass through the pores of formation easily without forming filter cake.

11.2 Theoretical Studies

A- Fluid loss treatment

a- Development of empirical correlations in actual variables of gel particles concentration, gel particle diameter, flow rate, temperature, and particle diameter to pore-throat size which effect on the permeability modification of the near-wellbore formation. Further, the dimensionless forms of these correlations were also developed.

b- Theoretical descriptions of various plugging and unplugging mechanisms causing

permeability modification. Further, the correlations of rate constant of plugging and unplugging processes at various temperatures were also developed.

B- Water shutoff treatment

a- Development of empirical correlations in actual variables of silica flour concentration, temperature, sand size, and pore diameter of formation which effect the fluid loss of silica flour particle-gel slurry systems and the pressure required to initiate water flow after water shutoff formation treatment.

b- Theoretical description of filtration analysis of silica flour particle-gel system and empirical correlations of the rate constant of filtrate and spurt loss volume were developed.

C- Field scale treatment design

a- Fluid loss treatment design

The developed correlations were used in designing of near-wellbore formation treatment by the gel particle suspension to control the drilling fluid loss of a well under drilling operations and the required volume of the gel particles suspension and the components of the suspension were determined. The permeability modification of the near-wellbore formation after the treatment was also determined.

b- Water shutoff treatment design

The developed correlations were used in the design of the near-wellbore water shutoff treatment by the silica flour particle-gel slurry system to control the water production of an oil producing well and the required volume of the silica flour particle-gel slurry system and the components of the slurry were determined. The fluid loss of

the silica flour particle-gel slurry system and the pressure required to initiate water flow after the treatment were also determined.

11.3 Overall accomplishment and benefits

The correlations developed in this dissertation and the application demonstrated examples can be beneficial in scientifically-guided applications and understanding of fluid-loss control by gel particles suspension and water shutoff treatment by silica flour particle-gel slurry system for field applications. Specifically, the investigations and studies presenting in this work provide:

a- Dimensionless empirical correlations can help in applications in the field for conditions that may be different than conditions of the experimental studies conducted in this work because dimensionless numbers are applicable under similar conditions.

b- The equations describing the various plugging and unplugging mechanisms can help in developing calculational procedures for simulation and theoretical investigation of the consequences of field treatment.

c- The methodology demonstrating the applications of field fluid-loss control and water shutoff treatments provide a useful example of how the correlations developed in this study can be applied in optimal design of other practical field treatment cases.

References

Al-Ibadi, A. and Civan, F. 2012. Experimental Study of Gel Particles Transport through Porous Media. Paper SPE 153557 presented at the SPE Latin American and Caribbean Petroleum Engineering Conference, Mexico City, Mexico, 16- 18 April.

Al- Ibadi, A. and Civan, F. 2013a: Experimental Investigation and Correlation of Treatment in Weak and High- Permeability Formations by Gel Particles. Paper SPE 153557, Journal of SPE Production and Operations, Vol. 28, No. 4, pp. 387-401.

Al- Ibadi, A. and Civan, F. 2013b: Experimental Investigation and Correlation of Thermal Effects on Near-Wellbore Formation Treatment by Gel Particles. Paper SPE-164119 presented at the SPE International Symposium on Oilfield Chemistry, The Woodlands, TX, USA, 8-10 April.

Al- Ibadi, A. and Civan, F. 2013c: Evaluation of Near-Wellbore Formation Treatment by Gel Particles Using Dimensional Analysis. Paper SPE 164507 presented at the SPE Production and Operations Symposium, Oklahoma City, OK, USA, 23-26 March .

Al- Ibadi, A., Civan, F., and Eoff, L. 2015: Experimental Investigation and Correlation of Particle-Gel Systems of Near-Wellbore Water Shutoff Treatments. Paper SPE 173627 will be presented at the SPE Production and Operations Symposium, Oklahoma City, OK, USA, 1-5 March .

Ali, E., Bergen, F., Demestre, P., Biezen, E., and van Eijden, J. 2008. Effective Gas Shuttoff Treatments in a Fractured Carbonate Field in Oman. Paper SPE 102244

presented at the Annual Technical Conference and Exhibition, San Antonio, Texas, 24-27 September. DOI:10.2118/102244-MS.

Almohsin, A., Bai, B., Imqam, A., Wei, M., Kang, W., Delshad, M., Sepehrnoori, K. 2014. Transport of Nanogel through Porous Media and Its Resistance to Water Flow. Paper SPE 169078 presented at SPE Improved Oil Recovery Symposium, Tulsa, Oklahoma, USA, April 12-16.

Baghdikian, S., Sharma, M., Handy, L. 1989. Flow of Clay Suspensions Through Porous Media. Paper SPE 16257- PA, SPE Reservoir Engineering Journal, May 1989.

Bai, B., Liu, Y., and Coste, J., P. 2007. Performed Particle Gel Conformance Control: Transport Mechanism through Porous Media. SPE Reservoir Evaluation and Engineering 10176-184. SPE 89468- PA. DOI: 10.2118/89468- PA.

Bonet, J. and Wood, R.D. 2008. Nonlinear Continuum Mechanics for Finite Element Analysis, Second Edition, Cambridge University Press, New York.

Burya, Y. G., Yudin, I. K., Dechabo, V. A., Kosov, V. L., and Anisimov M. A. 2001. Light-Scattering Study of Petroleum Asphaltene Aggregation. Journal of Applied Optics, Vol. 40, No. 24, pp. 4028-4035.

Chauveteau, G., Omari, A., Tabary, R., Renard, M., and Rose, J. 2000. Controlling Gelatiom Time and Microgel Size for Water Shutoff. Paper SPE 59317 presented at the SPE/DOE Improved Oil Recovery Symposium, Tulsa, 3-5 April. DOI: 10.2118/59317- MS

Chauveteau, G., Omari, A Tabary, R., Renard, M.,Veerapen, J., and Rose, J. 2001. New Size- Controlled Microgels for Oil Production. Paper SPE 64988 presented at

the SPE International Symposium on Oilfield Chemistry, Houston, 13-16 February. DOI: 10.2118/64988- MS.

Chauveteau, G., Tabary, R., Le Bon, C., Renard, M., Feng, Y., and Omari, A. 2003.In-Depth Permeability Control by Adsorption of weak size-Controlled Microgels. Paper SPE 82228 presented at the SPE European Formation Damage Conference, The Hague, 13-14 May. DOI: 10.2118/82228- MS.

Churchill, S.W. 1997. A new approach to teaching dimensionless analysis. Chemical Engineering Education, 30, pp. 158-165.

Civan, F. 1990. A Generalized Model for Formation Damage by Rock-Fluid Interactions and Particulate Processes. Paper SPE 21183 presented at the SPE Latin American Petroleum Engineering Conference, Rio de Janeiro, Brazil, October 14-19.

Civan, F. 1996. A Multipurpose Formation Damage Model. Paper SPE 31101 presented at the SPE Formation Damage Symposium, Lafayette, Louisiana, USA, February 14-15.

Civan, F. 2000.Reservoir Formation Damage- Fundamentals, Modeling, Assessment, and Migration, Gulf Pub. Co., Houston, TX, 742p.

Civan, F. 2004. Temperature Dependence of Wettability Related Rock Properties C orrelated by the Arrhenius Equation. Petrophysics 45 (4): 350- 362.

Civan, F. 2005. Applicability of the VTF Type Asymptotic Exponential Functions for Ice, Hydrates, and Polystrene Latex. J. of Colloid and Interface Science 285: 429-432.

Civan, F. and Nguyen, V. , 2005, **"**Modeling Particle Migration and Deposition in Porous Media by Parallel Pathways with Exchange**,"** Chapter 11, Handbook of Porous

Media, Second Edition, Vafai, K. (Ed.), CRC Press,Taylor& Francis Group, LC, Boca Raton, FL, pp. 457-484.

Civan, F. 2006a. Viscosity Temperature Correlation for Crude Oils Using an Arrhenius Asymptotic Exponential Function. Petroleum Science and Technology 24 (6): 699-706.

Civan, F. 2006b. Discusion of a Practical Method for Anticipating Asphaltene Problems. SPEPO 21 (3): 411. SPE- 104235- PA. DOI: 10.2118/104235- PA.

Civan, F. 2007a. Reservoir Formation Damage Fundamentals, Modeling, Assessment and Mitigation, Second Edition, Elsevi-er, Gulf Professional. Pub., Burlington, MA, 1114p.

Civan, F. 2007b. Temperature Effect on Power for Particle Detachment from Pore Wall Described by an Arrhenius- Type Equation. Transport in Porous Media 67 (2): 329-334.

Civan, F. 2007c. Critical Modification to the Vogel- Tammann- Fulcher Equation for Temperature Effect on the Density of Water. Industral Engineering & Chemistry Research Journal 46 (17): 5810- 5814.

Civan, F. 2008. Use Exponential Functions to Correlate Temperature Dependence. Chemical Engineering Progress 104 (7): 46- 52.

Civan, F. 2010, Non-isothermal Permeability Impairment by Fines Migration and Deposition in Porous Media including Dispersive Transport, Transport in Porous Media: Vol. 85, Issue 1, pp. 233-258.

Civan, F. 2011a, Correlate Data Effectively, Chemical Engineering Progress, Vol. 107, No. 2, pp. 35-44.

Civan, F. 2011b. Porous Media Transport Phenomena. John Wiley and Sons, Hoboken, 463p.

Civan, F. and Rasmussen, M.L. 2005. Analytical Models for Porous Media Impairment by Particles in Rectilinear and Radial Flows. In Handbook of Porous Media, second edition, ed. K. Vafai, Chap. 12, 485–542. Boca Raton, Florida: CRC Press.

Coste, J.P., Liu, Y., Bai, B. et al.2000. In Depth Fluid Diversion by Pre Gelled Particles . Laboratory study and Pilot Testing. Paper SPE 59362 presented at the SPE/DOE Im proved Oil Recovery Symposium, Tulsa, 3-5 April. DOI: 10.2118/59362- MS.

Dalrymple, D., Eoff, L., Vasques, J., and van Eijden, J. 2008. Shallow Penetration Particle-Gel System for Water and Gas Shuttoff Applications. Paper SPE 114886 presented at the Russian Oil & Gas Technical Conference and Exhibition, Moscow, Russian, 28-30 October. DOI:10.2118/114886-MS.

Engel, A. 2000. The role of transparent exopolymer particle (TEP) in the increase in apparent particle stickiness (α) during the decline of a diatom bloom. Journal of Plankton Research 22: 485-497.

Feng, Q., Chen, X., and Zhang, G. 2013. Experimental and Numerical Study of Gel Particles Movement and Deposition in Porous Media After Polymer Flooding, Transport in Porous Media: Vol. 96. Issue 1.

Feng, Y., Tabary, R., Renard, M., Le Bon, Omari, A., and Chaveteau, G. 2003. Characteristics of Microgels Designed for Water Shutoff and Profile Control. Paper SPE 80203 presented at the SPE international.

Fileding, R. C. Jr., Gibbons, D. H, and Legrand, F. P. 1994 . In Depth Drive Fluid Diversion Using An Evaluation of Colloidal Dispersion Gels and New

Bulk Gels: An Operational Case History of North Rainbow Ranch Unit. Paper SPE 27773 presented at the SPE/DOE Improved Oil Recovery Symposium. Tulsa , 17-20 April . DOI: 10.2118/ 27773- MS.

Fulcher, G.S. 1925. Analysis of Recent Measurements of the Viscosity of Glasses. *J. Am. Ceram. Soc.* 8: 339–355.

Gao, T., Hu, H.H. and Castaneda, P.P. 2011. Rheology of a Suspension of Elastic Particles in a Viscous Shear Flow. J. Fluid Mech., Vol. 687, pp. 209-237.

Goldsztein, G.H. 2005. Volume of Suspension that Flows through a Small Orifice before It Clogs. SIAM Journal of Appl. Math., Vol. 66, No. 1, pp. 228-236.

Gruesbeck, C. and Collins, E. 1982. Entrapment and Deposition of Fine Particles in Porous Media. Journal of the Society of Petroleum Engineers: 847-856.

Iscan, A.G. and Civan, F. 2006. Correlation of Criteria for Perforation and Pore Plugging by Particles, Journal of Porous Media, Vol. 9, No. 6, pp. 541-558.

Iscan, A.G., Kok, M.V., and Civan, F. 2009. Investigation of Porosity and Permeability Impairment in Sandstones by X-Ray Analysis and Simulation," Energy Sources, Part A, Vol.31, No. 5, pp. 387-395.

Kiørboe, T., Andersen, K.P. and Dam, H.G. 1990. Coagulation efficiency and aggregate formation in marine phytoplankton. Marine Biology Journal 107(2): 235–245.

Lane, R. H and Seright , R. S. 2000. Gel Water Shutoff in Fractured or Faulted Horizontal Wells. Paper SPE 65527 presented at the SPE/ CIM International Conference on Horizontal Well Technology, Calgary, 6-8 November. DOI: 10.2118/ 65527- MS.

Littmann, w. 1988. Polymer Flooding, Elsevier Science Publishing Company Inc.

Messeenger J. U.1981. Lost Circulation, Pennwell Publishing Co., Tulsa,112P.

Monkos, K., 2003.A Method of Calculations of the Parameters in the VTFs Equation: An Application to the Porcine Serum Albumin Aqueous Solutions. *Current Topics in Biophysics* 27 (1–2): 17–21.

Muhammed, F., Bai, B., and Al Brahim, A. 2014. A Simple Technique to Determine the Strength of Millimeter-Sized Particle Gel. Paper SPE 169106 presented at SPE Improved Oil Recovery Symposium, Tulsa, Oklahoma, USA, April 12-16.

Peifeng, H., Jianjun, L., and Xiang, H. 2010. Pore Structure Effect on the Permeability of porous Media. Proceedings of 2010 International Symposium on Multi-field Coupling Theory of Rock and Soil Media and Its Applications, Chengdu City, CH-INA. ISBN: 978- 0- 9807687- 2- 5.

Potanin, A. A. and Uriev, N.B. 1991. Micro-rheological Models of Aggregated Suspensions in Shear Flow. Journal of Colloid and Interface Science 142(2): 385-395.

Prada, A., Civan, F., and Dalrymple, D. 2000. Evaluation of Gelation Systems for Conformance Control. Paper SPE 59322 presented at the Improved Oil Recovery Symposium, Tulsa, Oklahoma, 3-5 April.

Pu, C.S. 2008. Surface Deposition and Micro-Dispersed Migration Dynamics of in Liquid-Solid System. Petroleum Industry Press, Beijing.

Sato, T., Mitsuhori, K., Hirabayashi, S., Brumby, P.E., Nagao, J., Temma, N., and Narito, H. 2013. Microscale Numerical Simulation of the Permeability Reduction due to Trapping of Suspended Fine Particles Within Sand Sediments. Transport in Porou Media, Vol. 96, pp. 153-167.

Seright, R.S.1997. Use of Preformed gels for Conformance Control in Fractured System

. SPEPE, 12(1): 59-65. SPE- 35351- PA. DOI: 10. 2118/35351-PA.

Seright, R. S.2000. Gel Propagation Through Fractures. Paper SPE 59316 Presented at The SPE/ DOE Improved Oil Recovery Symposium, Tulsa, 3-5 April. DOI: 10.2118159316-MS.

Sydansk, R. D. and Southwell, G.P. 2000. More Than 12 Years Experience With a Succ essful Conformance- Control Polym-er- Gel Technology. SPEPF 15 (4): 270- 278. SPE – 66558- PA. DOI: 10.2118/66558- PA.

Tammann, G. and Hesse, W.1926. Die abhängigkeit der viskosität von der temperature bei unterkühlten flüssigkeitn. Z. *Anorg. Allg. Chem.* 156: 245–257.

Taylor, G.I. 1932. The Viscosity of a Fluid Containing Small Drops of Another Fluid. Proc. Roy. Soc., 138 A, pp. 41-48.

Taylor, G.I. 1934. The Deformation of Emulsions in Definable Fields of Flow. Proc. Roy. Soc., 146 A, pp. 501-523.

Tran, T.V., Civan, F., and Robb, I. 2009. Correlating Flowing Time and Condition for Perforation Plugging by Suspended Particles. Paper SPE 120473, presented at the 2009 SPE Production and Operations Symposium, Oklahoma City, OK, USA, 5-7 April.

Tran, T.V., Civan, F., and Robb, I. 2010a. Effect of Permeability Impairment by Suspended Particles on Invasion of Drilling Fluids. Paper SPE IADC/SPE 133724, presented at the IADC/SPE Asia Pacific Drilling Technology Conference and Exhibition, Ho Chi Minh City, Vietnam, 1-3 November 2010.

Tran, T.V., Civan, F., and Robb, I. 2010b. Correlating Flowing Time and Condition for Plugging of Rectangular Openings, Natural Fractures, and Slotted Liners by

Suspended Particles. Paper SPE 126310, presented at the 2010 SPE International Symposium and Exhibition on Formation Damage Control, Lafayette, Louisiana, USA, 10-12 February.

Van Driest, E.R. 1946. On dimensional analysis and the presentation of data in fluid flow problems. Journals of Applied Mechanics, 13, P. A34.

van Duuren, F. A. 1968. Defined velocity gradient model flocculator. Journal of the Sanitary Engineering Divison: Proceeding of the American Society of Civil Engineers 94: 671–682.

van Eijden, J., Arkesteijn, F., Akil, E., Vliet, J., Batenburg, D., and McGinn, P. 2004. Gel- cement, a water shut-off system: qualification in a Syria field. Paper SPE 88765 presented at the 11th Abu Dhabi International Petroleum Exhibition and Conference, Abu Dhabi, U.A.E., 10-13 October.

van Eijden, J., Arkesteijn, F., van Batenburg, D., and van Vliet, J. 2005. Development and Field Application of a Shallow Perforation Shuttoff System for HP-HT Oil Wells. Paper SPE 94518 presented at the 6th European Formation Damage Conference, Scheveningen, The Netherlands, 25-27 May. DOI: 10.2118/94518-MS.

Vogel, H. 1921. Das temperature-abhängigketsgesetz der viskosität von flüssigkeiten. *Phys. Zeit*. 22: 645– 646.

Wang, H. G., Guo, W. K., and Jiang, H. F. 2001. Study and Application of Weak Gel System Prepared by Complex Polymer Used for Depth Profile Modification. Paper SPE 65379 presented at the SPE International Symposium on Oilfield Chem-istry, Houston, 13- 16 February. DOI: 10.2118/65379- MS.

Wang, H., Sweatman, R., Engelman, B. et al. 2008. Best Practice in Understanding and

Managing Lost Circulation Challenges. SPE Drill & Compl 23 (2): 168–175. SPE95895-PA. http://dx.doi.org/10.2118/ 95895-PA.

Wang, J., Liu, H., and Wang, Z. 2012. Experimental Investigation on the Filtering Flow Law of Pre-gelled Particle in Porous Media. Transport in Porous Media, Vol. 94, pp. 69-86.

Wojtanowicz, A. K., Krilow, Z., and Langlinas, J. P. 1987. Study on the Effect of Pore Blocking Mechanisms on Formation Damage. Paper SPE 16233, Presented at SPE Production Operations Symposiums, Oklahoma City, Oklahoma, USA, March 8-10.

Zamani, A. and Maini, B. 2009. Flow of Dispersed Particles through Porous Media-Deep Bed Filtration. J. Pet. Sci. Eng., Vol. 69, pp. 71-88.

Zeinijahromi, A., Vaz, A. and Bedrikovetsky, P. 2012. Effects of Fines Migration on Well Productivity during Steady State Production. Journal of Porous Media, Vol. 15, pp. 665-679.

Zhang, H., and Bai, B. 2010. Preformed Particle Gel Transport Through Open Fractures and its Effect on Water Flow. Paper SPE-129908 presented at the SPE Improved Oil Recovery Symposium, Tulsa, OK, USA, 24-28 April.

Zheng, L.H., Kong, L., Cao, Y., Wang, H., and Han, Z. 2012. Anew Fuzzy Ball Working Fluid for Plugging Lost Circulation Paths in Depleted Reservoirs. Petroleum Science and Technology, Vol. 30, pp. 2517-1530.

Appendix A: Nomenclature

International system of units (SI units) were used in this dissertation and the units inside the parentheses represent the SI derived units that were used also in this dissertation.

a = empirical parameter, dimensionless

a_i = initial guesses of parameters (unit determined by the type of property)

a_1 = initial guesses (unit determined by the type of property)

a_2 = initial guesses (unit determined by the type of property)

a_3 = initial guesses (unit determined by the type of property)

A = empirical parameter (unit determined by the type of property)

A = cross sectional area of the sand pack, m^2 (cm^2)

A_1 = empirical parameter, dimensionless

A_2 = empirical parameter, dimensionless

A_k and C = fitting constant (E/Rg), K

b = empirical parameter, dimensionless

b_i = initial guesses of parameters (unit determined by the type of property)

b_1 = initial guesses (unit determined by the type of property)

b_2 = initial guesses (unit determined by the type of property)

b_3 = initial guesses (unit determined by the type of property)

b_4 = initial guesses (unit determined by the type of property)

b_5 = initial guesses (unit determined by the type of property)

b_6 = initial guesses (unit determined by the type of property)

b_7 = initial guesses (unit determined by the type of property)

b_8 = initial guesses (unit determined by the type of property)

b_9 = initial guesses (unit determined by the type of property)

B = empirical parameter (unit determined by the type of property)

B_s = left Cauchy-Green or Finger tensor, dimensionless

B_1 = empirical parameter, dimensionless

B_2 = empirical parameter, dimensionless

c = specific heat capacity, m^2/s^2K (cm^2/s^2K)

c_{gp} = gel particles mass concentration, kg/m^3 (mg/L)

c_w = produced fines concentration, %

C = empirical parameter, dimensionless

C_o = particle concentration at the time o, $no.dm^{-1}$

C_p = particle concentration, vol% or wt%

C_s = silica flour concentration, wt% or vol%

C_t = total amount of produced fines per unit well length, m^2

C_1 = empirical parameter, dimensionless

C_2 = empirical parameter, dimensionless

C_3 = empirical parameter, s^{-1} (min^{-1})

C_4 = empirical parameter, s^{-1} (min^{-1})

C_5 = empirical parameter, s^{-1} (min^{-1})

d_f = diameter of a frame sand grain, m (μm)

d_q = diameter of a fine particle, m (μm)

D_b = cell body diameter, m (μm)

D_F = pore diameter of filter disc, m (μm)

D_g = grain diameter, m (μm)

D_P = gel-particle diameter, m (μm or cm)

D_{pmax} = maximum gel-particle diameter, m (μm)

D_{pmin} = minimum gel-particle diameter, m (μm)

D_s = sand diameter, m (μm)

D_T = pore throat diameter, m (μm)

e_n = restitution coefficient, dimensionless

e_τ = friction coefficient, dimensionless

E = activation energy (J/kmol)

f = temperature dependent parameter (unit determined by the type of property)

f_c = pre- exponential coefficient (unit determined by the type of property)

F = deformation gradient tensor, dimensionless

F.L. = fluid loss, vol%

$(F.L.)_c$ = pre-exponential coefficient of fluid loss, vol%

F_r = resistance factor, dimensionless

$(F_r)_c$ = pre- exponential coefficient of resistance factor, dimensionless

F(x) = cumulative particle distribution, %

G = viscous forces in the fluid to the elastic forces in the elastic solid particle, dimensionless

G_m = mean shear rate of the Coutte Chamber system, s^{-1}

H = Hamaker coefficient of particle and surface interacting through the pore fluid present in between them, J

j = impedance, dimensionless

k = absolute permeability, 1 D= $9.869233*10^{-13}$ m^2 (md)

k_{max} = threshold number of particles for the first time, dimensionless

k_r = constant, dimensionless

k_{rowi} = oil relative permeability at initial water saturation, 1 D= $9.869233*10^{-13}$ m^2 (md)

k(V) = number of particles arriving simultaneously at the opening, dimensionless

K = suspension permeability, 1 D= $9.869233*10^{-13}$ m^2 (md)

K_o = initial permeability, 1 D= $9.869233*10^{-13}$ m^2 (md)

K_w = water permeability, 1 D= $9.869233*10^{-13}$ m^2 (md)

l = separation distance between the particle surfaces in filter cake, m (cm)

M = skin growth coefficient, dimensionless

N = average number of particles forming fractal aggregation, dimensionless

pi = productivity index, dimensionless

P = differential pressure, kPa

P_c = pre- exponential coefficient of pressure, kPa

P_f = position vector for a frame sand grain, m (μm)

P_o = initial pressure, kPa

P_q = position vector for a fine particle, m (μm)

q = injection flow rate, m^3/s (cm^3/min)

q_w = water flow rate, m^3/s (cm^3/h)

r = radius, m (μm)

r_1 = radii of the inner cylinder of the system, m (cm)

r_2 = radii of the outer cylinder of the system, m (cm)

r_e = drainage radius, m

r_w = well radius, m

R = instantaneous mean aggregate radius, m (μm)

R_{ep} = particle Reynolds number, dimensionless

Rg = universal gas constant , J/kmol- K

R_o = initial particle radius, m (μm)

R^2 = regression coefficient, dimensionless

S = gel particle area, m^2 (μm^2)

S_w = water saturation, %

SHR_{gp} = gel particle shear breaking ratio, dimensionless

SWR_{gp} = gel particle swelling ratio in polymer solution, dimensionless

t = time, s (min)

t_d = dimensionless plugging time, dimensionless

T = temperature, K ($^{\circ}C$)

T_c = critical temperature, K

T_{ck} = characteristic-limit absolute temperature, K

T_{ik} = reference absolute temperature, K

u_q = particle velocity before the collision, m/s

U = flow velocity, m/s

ν = velocity , m/s (cm/s)

ν_w = water flow velocity, m/s

V_f = volume of fluid loss, m^3 (cm^3)

V_{Gel} = volume of gel in 1 ml of suspension, m^3 (μm^3)

x = independent variable, dimensions determined by application

x = ratio of distance, dimensionless

x* = normalized value of the dimensionless group, dimensionless

x_{cr} = critical silica flour concentration, wt%

x_{min} = minimum value of the dimensionless group, dimensionless

x_{max} = maximum value of the dimensionless group, dimensionless

X = normalized particle diameter, dimensionless

y = dependent variable, dimensions determined by application

z = length of the sand pack, m (cm)

z_o = initial length of the sand pack, m (cm)

Greek

γ = empirical material parameter, dimensionless

$\dot{\gamma}$ = shear rate or velocity gradient, s^{-1}

β_a = formation damage coefficient for attachment, dimensionless

β_s = formation damage coefficient for straining, dimensionless

β = pore throat to- particle diameter ratio, dimensionless

α, β and λ = empirical parameter, dimensionless

λ_s = filtration coefficient for size exclusion fines capture, m^{-1}

λ = ratio of volume of dashed cylinder and volume of a particle, dimensionless

σ and σ_p = fraction of particle, %

σ_a = volumetric concentration of attached fines, %

σ_s = volumetric concentration of strained fines, %

$Ø$ = porosity, dimensionless

$Ø_o$ = initial porosity, dimensionless

μ_c = pre- exponential coefficient of viscosity, Pa.s

μ_f = fluid viscosity, Pa.s

μ_o = initial viscosity, Pa.s

μ = suspension viscosity, Pa.s

μ_w = water viscosity, Pa.s

θ = temperature, K ($^{\circ}$C)

ρ = suspension density, kg/m^3 (g/cm^3)

τ_{cr} = critical shear stress, Pa

τ_D = characteristics times τ_{char} for the DLA, dimensionless

τ_R = characteristics times τ_{char} for the RLA, dimensionless

τ_s = extra stress tensor, Pa

Φ = volume concentration of particle, p.p.m

η_s = shear modulus of the elastic solid particle, Pa

ω = angular velocity, s^{-1}

δ_{gp} = retention coefficient of gel particles, dimensionless

Abbreviations

BHP = bottom-hole pressure

BHT = bottom-hole temperature

CT = computed tomography

DLA = diffusion-limited aggregation

3D = three-dimensional

F.L. = fluid loss

HPHT = high pressure high temperature

LBM = Lattice Boltzmann method

LCM = lost circulation material

LDPSDA = laser diffraction particle size distribution analysis

NMR = Nuclear Magnetic Resonance

NPT = non- productive time

PG = preformed gel

PLT = production logging tool

PPG = preformed particle gel

PVI = pore volumes injected

RLA = reaction-limited aggregation

TEP = transparent exopolymer particle

VTF = Vogel- Tammann- Fulcher

Appendix B: Special Correlation Equations

The general expressions of the special equations used for correlations of experimental data are presented in the following, where x and y denote the independent and dependent variables considered in their applications. All these equations were correlated using Microsoft excel 2010.

Type 1:

$$\ln y = bx + \ln a \tag{B-1}$$

where y is the steady-state differential pressure (kPa); x is the injection flow rate (≤100) (cm3/h) and a and b are empirical parameters.

Type 2:

$$\frac{1}{y} = \frac{b}{a}\left(\frac{1}{x^{\alpha}}\right) + \frac{1}{a} \tag{B-2}$$

where y is the steady-state differential pressure (kPa) or intercept of the unplugging region (dimensionless) or dimensionless group ($K\Delta P\mu_o v_o Z_o / K_o \Delta P_o \mu v Z$); x is the injection flow rate (≥100) (cm^3/h) or pore volume injected (dimensionless) or normalized dimensionless group ($\mu t/\rho Z^2$)* or normalized dimensionless group ($\mu t/\rho D_p^2$)* or normalized dimensionless group ($t^2 c\theta/Z^2$)*; and a, b, and α are empirical parameters.

Type 3:

$$\frac{1}{y - y_o} = \frac{b}{a}\left(\frac{1}{x}\right) + \frac{1}{a} \tag{B-3}$$

where y_o is the initial differential pressure, in kPa; y is the steady-state differential pressure, in kPa; x is the gel-particle diameter, in μm; and a and b are empirical parameters.

Type 4:

$$\frac{1}{y-1}=\frac{b}{a}\left(\frac{1}{x^{\alpha}}\right)+\frac{1}{a} \qquad \text{(B-4)}$$

where y is the permeability reduction (dimensionless) or intercept of the plugging region (dimensionless); x is the gel-particle volume fraction (%) or gel-particle diameter (μm) or particle diameter/pore-throat size (dimensionless) or pore volume injected (dimensionless); and a, b, and α are empirical parameters.

Type 5:

$$\frac{1}{y-1}=\frac{b}{a}\left(\frac{1}{x}\right)+\frac{1}{a} \qquad \text{(B-5)}$$

where y is the resistance factor (dimensionless); x is the gel-particle volume fraction (≤1) (%) or gel particle diameter (μm); and a and b are empirical parameters.

Type 6:

$$\ln y = bx^{\alpha}+\ln a \qquad \text{(B-6)}$$

where y is the resistance factor (dimensionless) or rate constant of the plugging and unplugging region (dimensionless) or fluid loss (%) or filtrate volume (cm^3) or rate constant of filtrate ($cm^3/min^{1/2}$) or spurt loss volume (cm^3); x is the gel-particle volume fraction (≥1) (%) or injection flow rate (≥100) (cm3/h) or pore volume injected (dimensionless) or silica flour concentration (wt% or vol%) or filtrate time (min); and a, b, and α are empirical parameters.

Type 7:

$$\frac{1}{y} = \frac{b}{a}\left(\frac{1}{x}\right) + \frac{1}{a} \qquad \text{(B-7)}$$

where y is the resistance factor (dimensionless) or dimensionless group ($K\Delta P\mu_o v_o Z_o / K_o \Delta P_o \mu v Z$) or dimensionless group (V_f/D_F^3) or dimensionless group (V_f/D_s^3); x is the injection flow rate (≤100) (cm3/h) or normalized dimensionless group ($\mu t/\rho Z^2$)* or normalized dimensionless group (vt/Z)* or dimensionless group (vt/D_F) or dimensionless group (vt/D_s); and a and b are empirical parameters.

Type 8:

$$\log\left[\frac{y - C_1}{A_1}\right] = B_1 \log x \qquad \text{(B-8)}$$

where y is the pore-throat/particle size ratio (dimensionless); x is the particle Reynolds number (dimensionless); and A_1, B_1, and C_1 are empirical parameters (dimensionless).

Type 9:

$$\ln\left[1 - \frac{y - C_2}{A_2}\right] = -B_2 x^{\lambda} \qquad \text{(B-9)}$$

where y is the pore-throat/particle size ratio (dimensionless); x is the particle Reynolds number (dimensionless); A_2, B_2, and C_2 are empirical parameters; and λ is the empirical exponent.

Type 10:

$$\ln y = b(x - x_{cr})^{\alpha} + \ln a \qquad \text{(B-10)}$$

where y is the fluid loss (%); x is the silica flour concentration (wt%); x_{cr} is the critical silica flour concentration (wt%); and a, b, and α are empirical parameters.

Type 11:

$$\frac{1}{y} = \frac{b}{a}\left(\frac{1}{(x - x_{cr})^{\alpha}}\right) + \frac{1}{a} \qquad \text{(B-11)}$$

where y is the pressure initiate flow (psig); x is the silica flour concentration (wt%); x_{cr} is the critical silica flour concentration (wt%); and a, b, and α are empirical parameters.

Appendix C: Empirical correlations of the differential pressure, permeability reduction, and resistance factor

A- The experimental data of the differential pressure across the proppant pack during the gel-particle-suspension injection were correlated with the injection flow rate and the gel particle diameter and empirical correlations were developed by applying Eqs. B-1, B-2, and B-3 given in Appendix B, as shown in Fgs. C.1 to C.3.

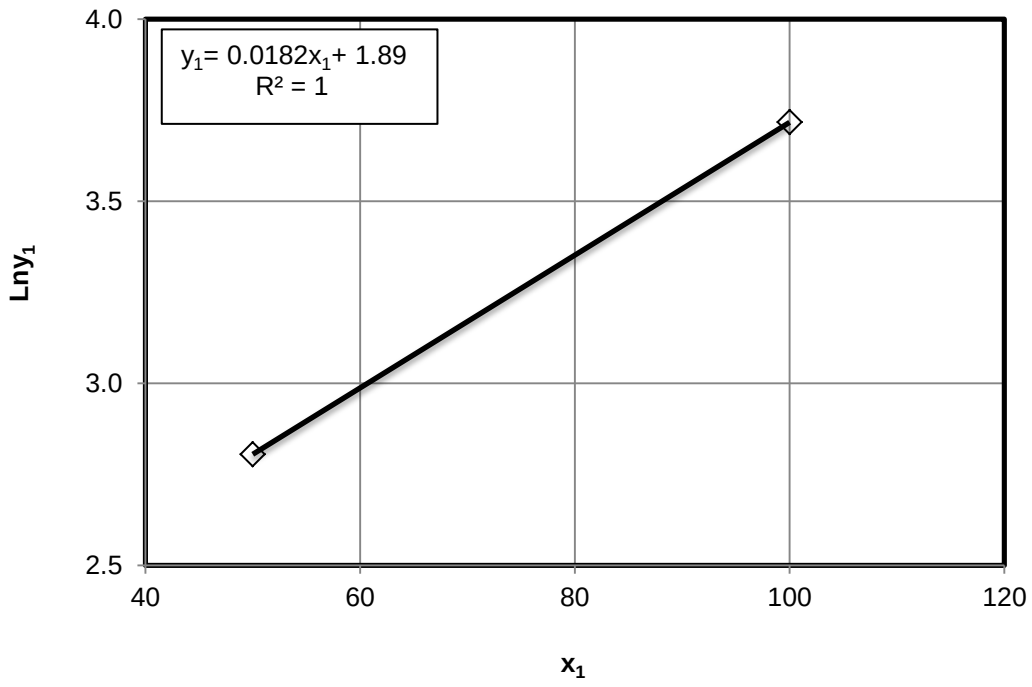

Fig. C.1: Straight line plot of Eq. B-1 at 50 cm³/hr and100 cm³/hr flow rates to develop the empirical correlation of the differential pressure at 3 vol% and 23.5 °C, as shown in Fig. 5.14

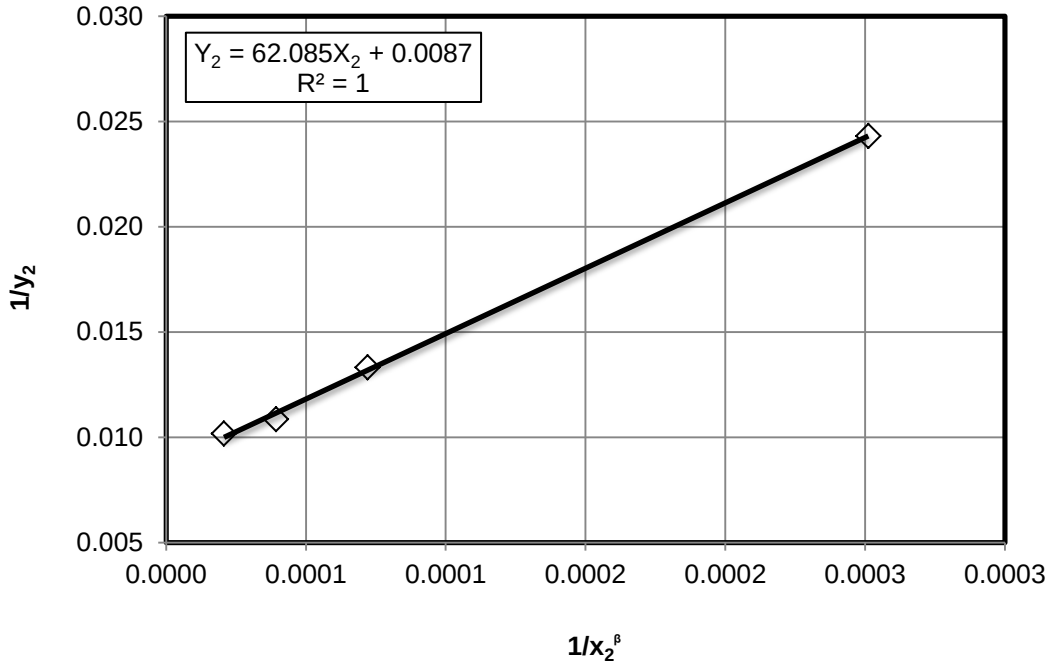

Fig. C.2: Straight line plot of Eq. B-2 at 100 cm³/hr, 200 cm³/hr, 280 cm³/hr and 400 cm³/hr flow rates to develop the empirical correlation of the differential pressure at 3 vol% and 23.5 °C, as shown in Fig. 5.14

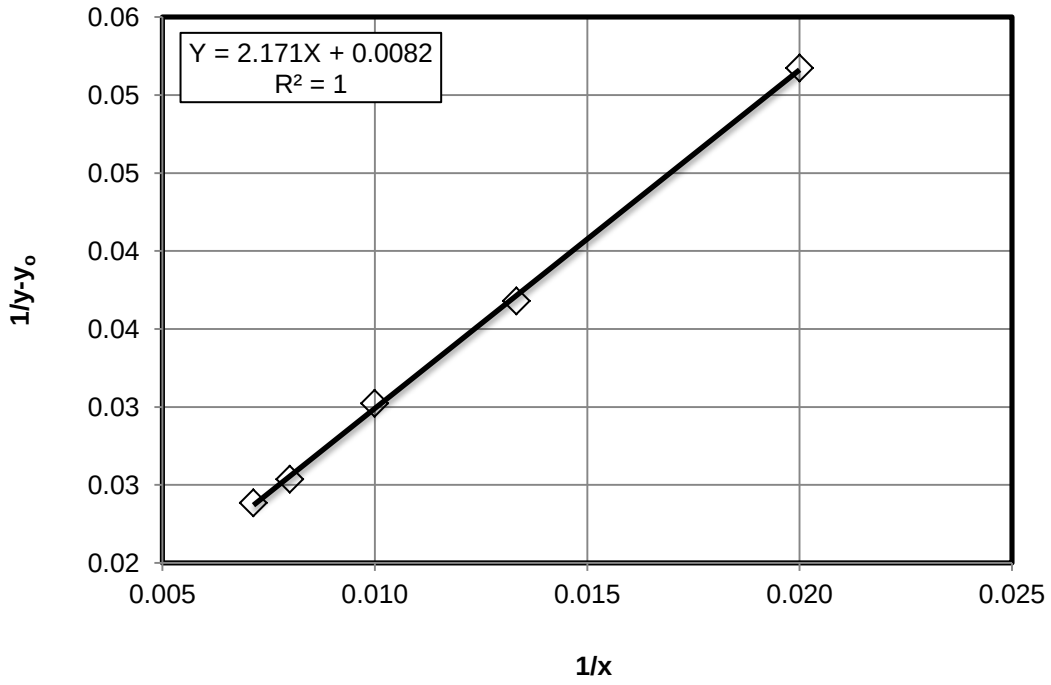

Fig. C.3: Straight line plot of Eq. B-3 at different gel- particle diameters to develop the empirical correlation of the differential pressure at 3 vol% and 23.5 °C, as shown in Fig. 5.15

B- The experimental data of the permeability reduction during the gel-particle-suspension injection were correlated with the gel-particle concentration, the gel particle diameter and the particle diameter to pore throat size ratio and empirical correlations were developed by applying Eq. B-4 given in Appendix B, as shown in Fgs. C.4 to C.6.

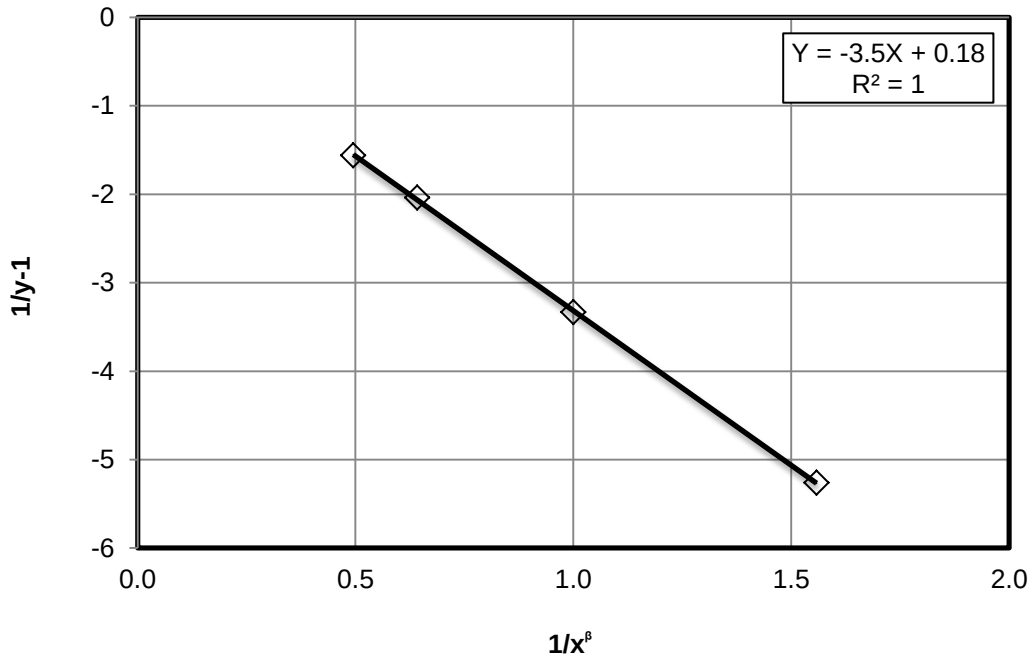

Fig. C.4: Straight line plot of Eq. B-4 at different gel-particle concentrations to develop the empirical correlation of the permeability reduction at 100 cm^3/h and 23.5 °C, as shown in Fig. 5.16

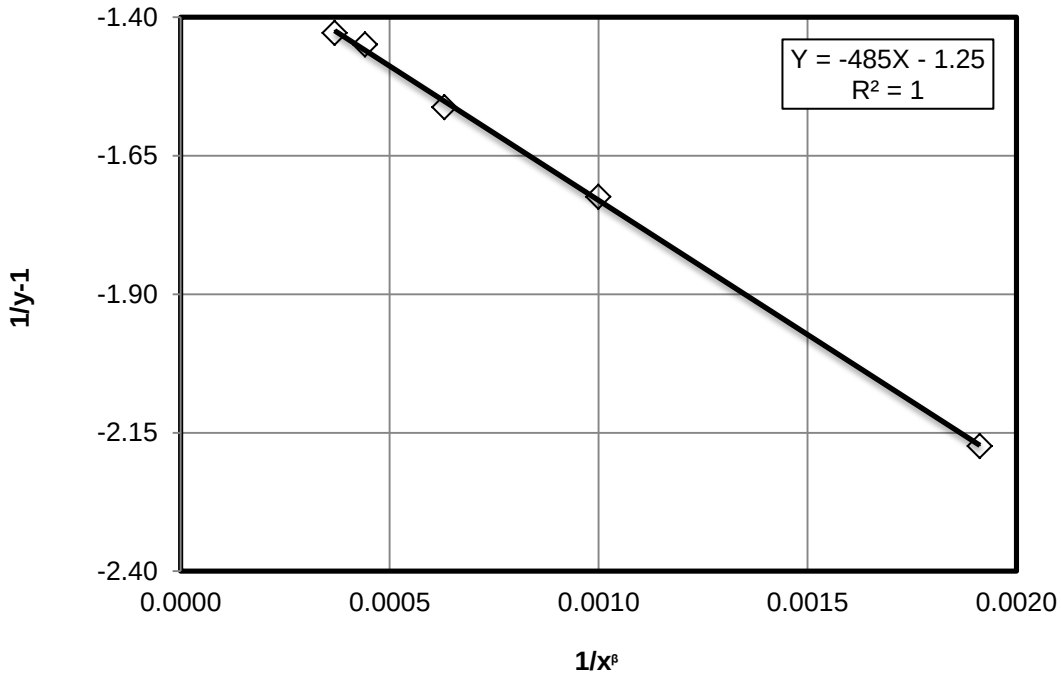

Fig. C.5: Straight line plot of Eq. B-4 at different gel-particle diameters to develop the empirical correlation of the permeability reduction at 100 cm^3/h and 23.5 °C, as shown in Fig. 5.18

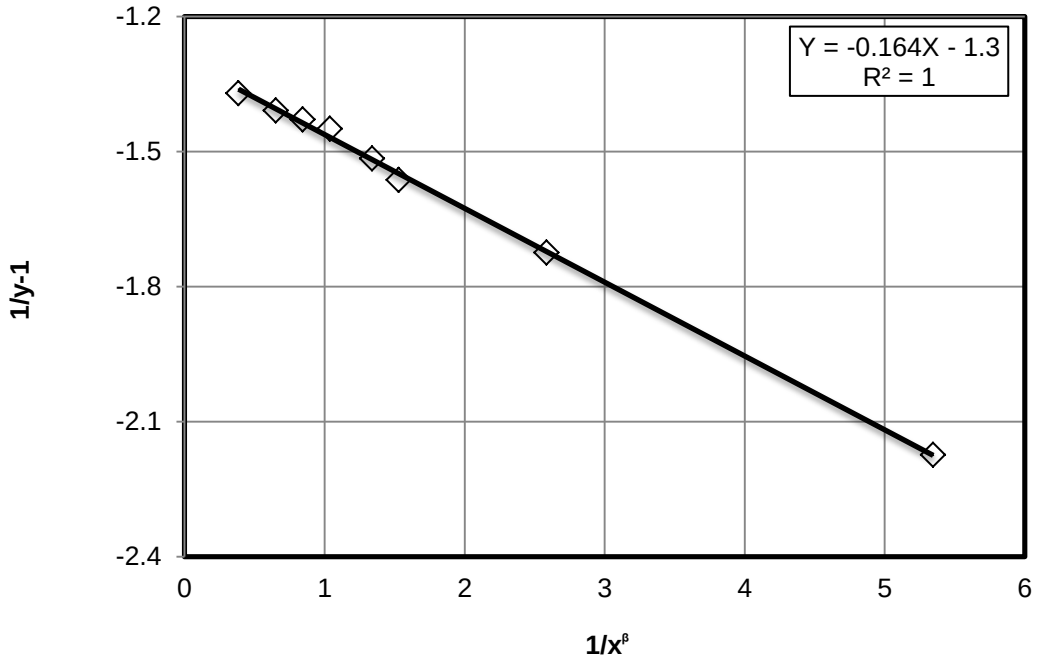

Fig. C.6: Straight line plot of Eq. B-4 at different particle diameter to pore throat size ratios to develop the empirical correlation of the permeability reduction at 100 cm^3/h and 23.5 °C, as shown in Fig. 5.19

C- The experimental data of the resistance factor during the gel-particle-suspension injection were correlated with the gel-particle concentration, the gel particle diameter and the injection flow rate and empirical correlations were developed by applying Eqs. B-5, B-6, and B-7 given in Appendix B, as shown in Fgs. C.7 to C.11.

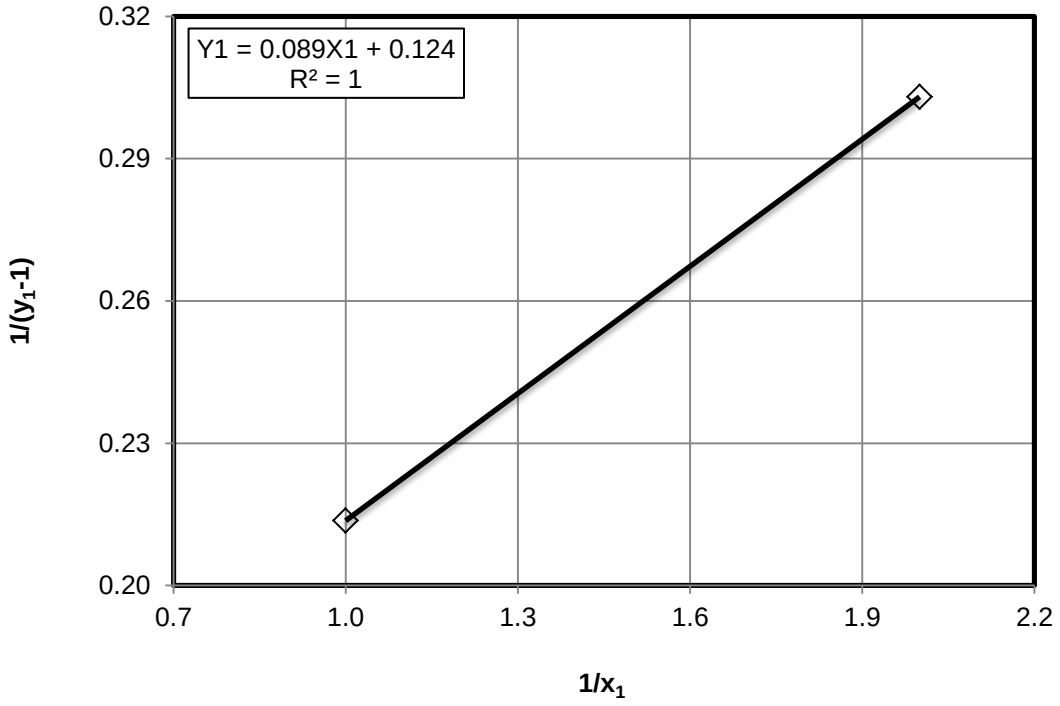

Fig. C.7: Straight line plot of Eq. B-5 at 0.5 vol% and 1 vol% gel-particle concentrations to develop the empirical correlation of the resistance factor at 100 cm^3/h and 23.5 °C, as shown in Fig. 5.20

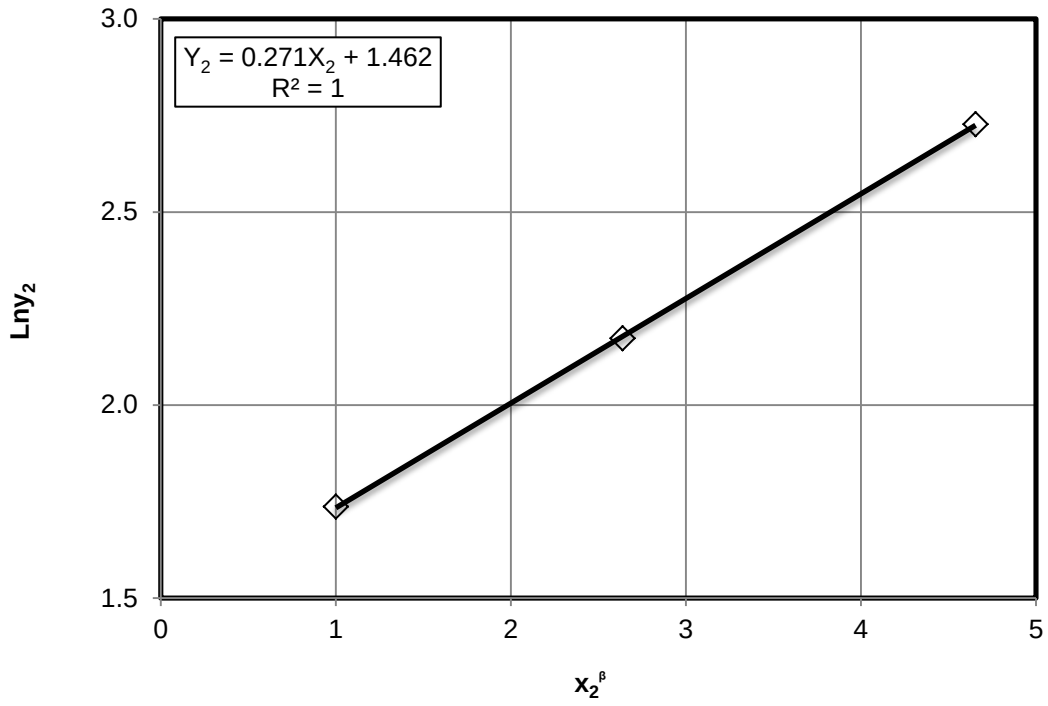

Fig. C.8: Straight line plot of Eq. B-6 at 1 vol%, 2 vol% and 3 vol% gel-particle concentrations to develop the empirical correlation of the resistance factor at 100 cm^3/h and 23.5 °C, as shown in Fig. 5.20

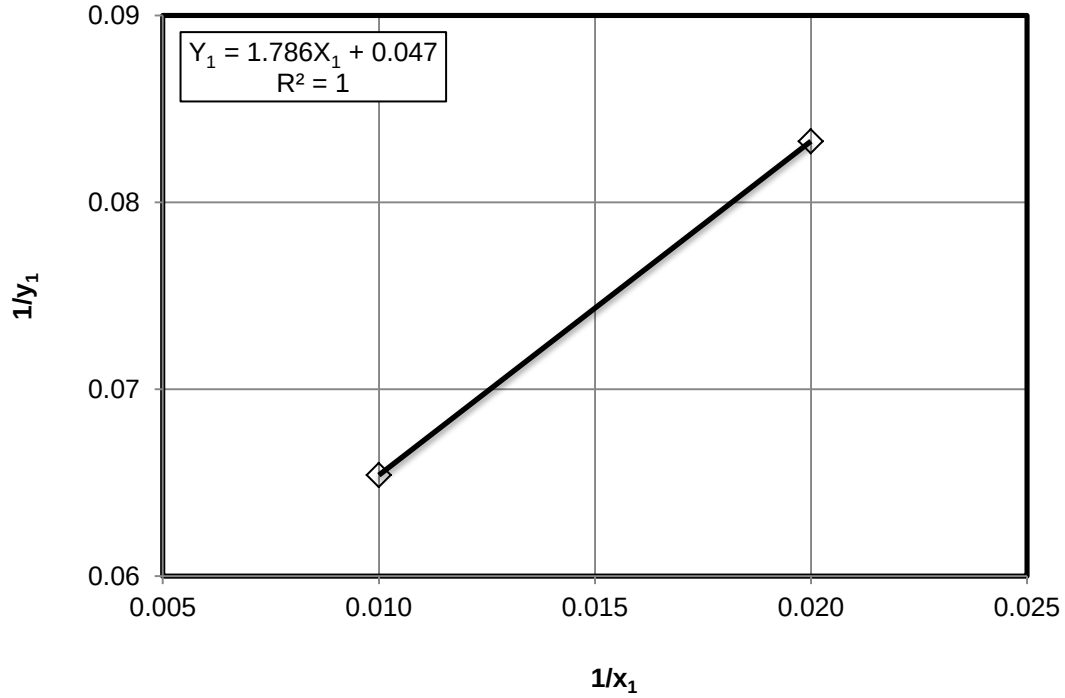

Fig. C.9: Straight line plot of Eq. B-7 at 50 cm^3/hr and 100 cm^3/hr flow rates to develop the empirical correlation of the resistance factor at 3 vol% and 23.5 °C, as shown in Fig. 5.21

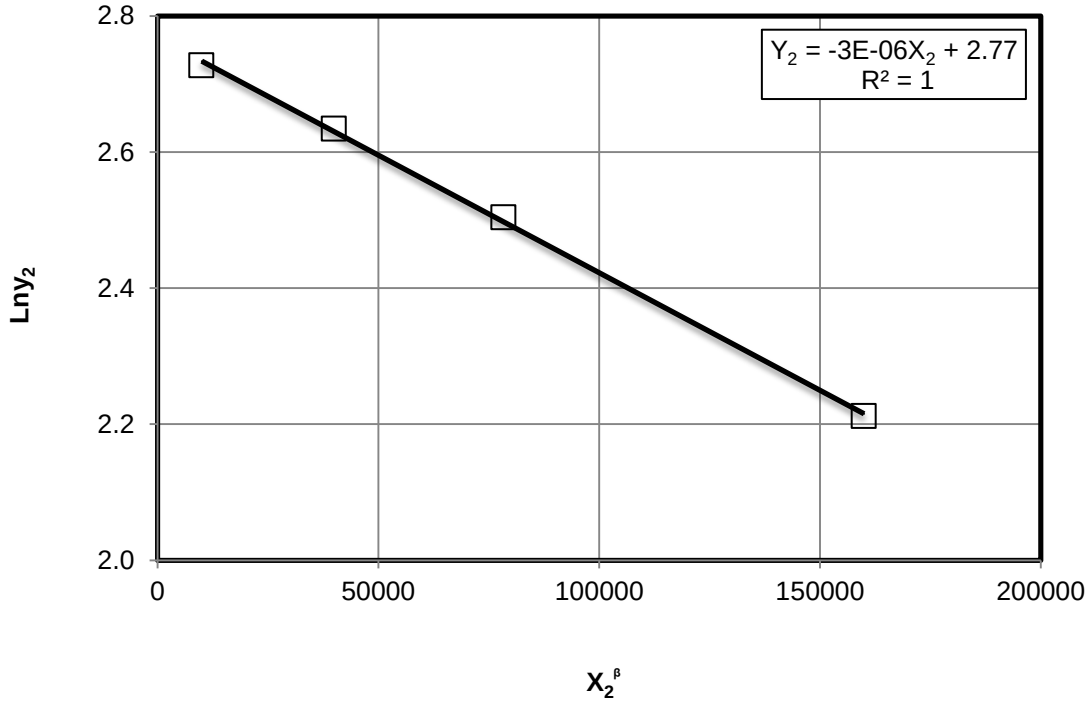

Fig. C.10: Straight line plot of Eq. B-6 at 100 cm³/hr, 200 cm³/hr, 280 cm³/hr and 400 cm³/hr flow rates to develop the empirical correlation of the resistance factor at 3 vol% and 23.5 °C, as shown in Fig. 5.21

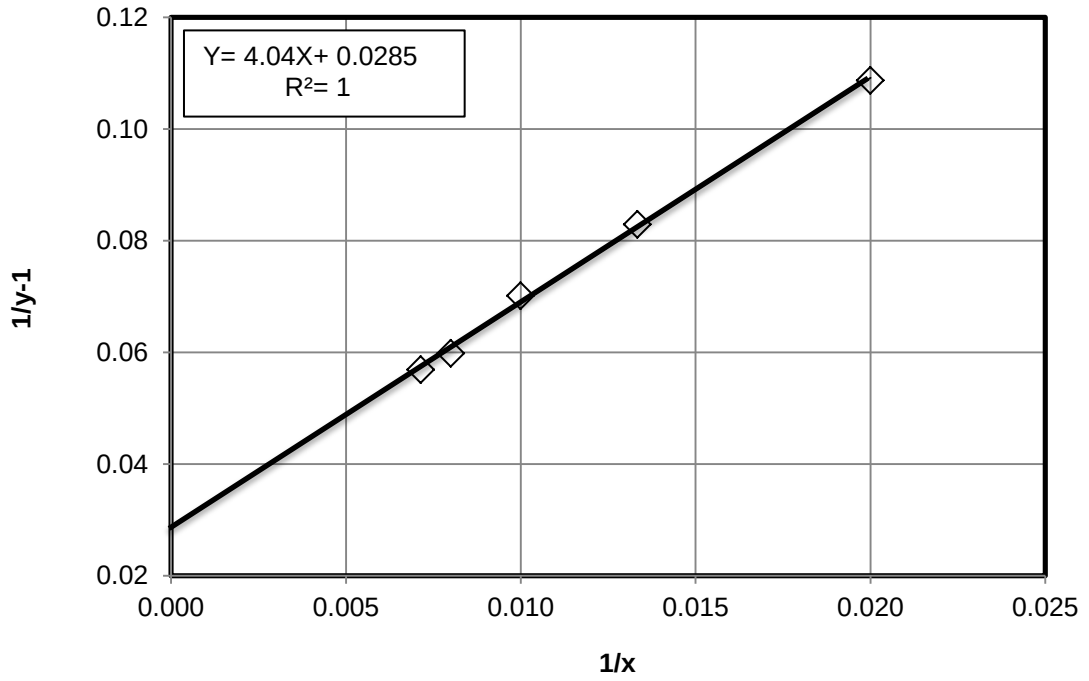

Fig. C. 11: Straight line plot of Eq. B-5 at different gel-particle diameter to develop the empirical correlation of the resistance factor at 100 cm³/h and 23.5 °C, as shown in Fig. 5.22

Appendix D: The power-law and exponential-law equations

The experimental data of the pore-throat/particle size ratio were correlated with the particle Reynolds number and power-law and exponential-law equations were developed by applying Eqs. B-8 and B-9 given in Appendix B.

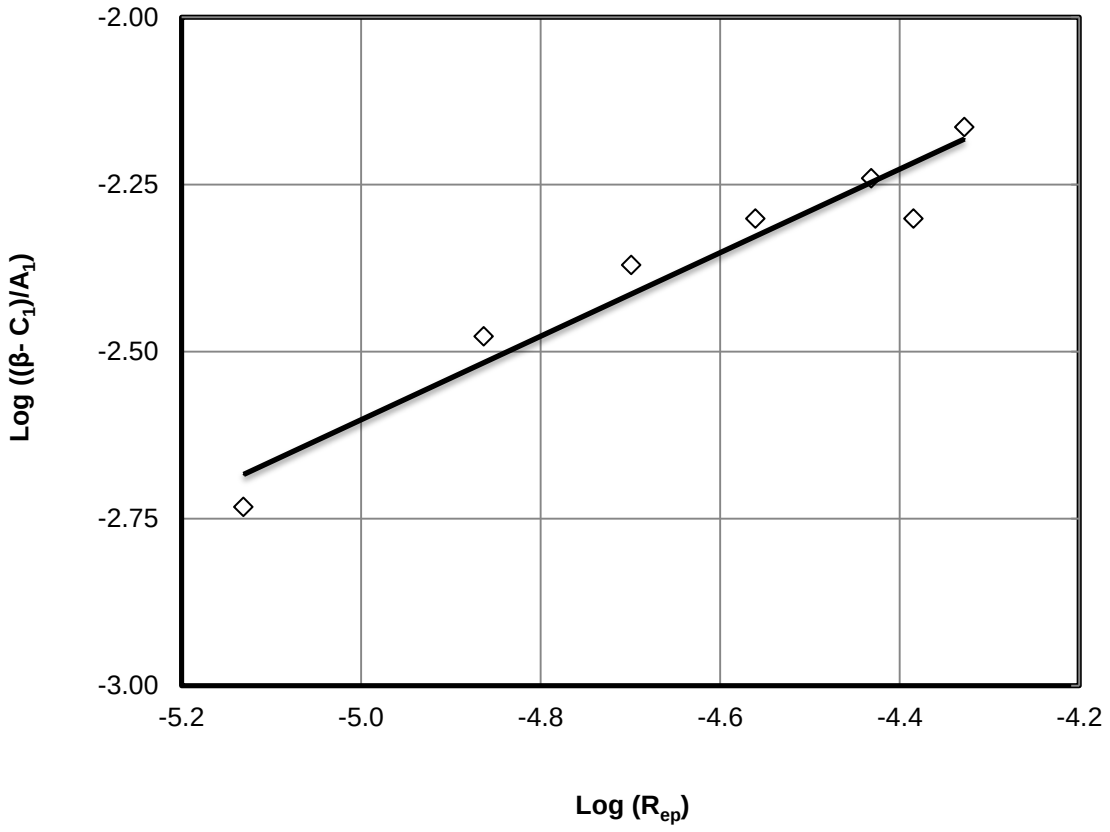

Fig. D.1: Straight line plot of Eq. B-8 at different gel particle concentrations and different gel particle diameters to develop the power-law equation, shown in Fig. 5.23.

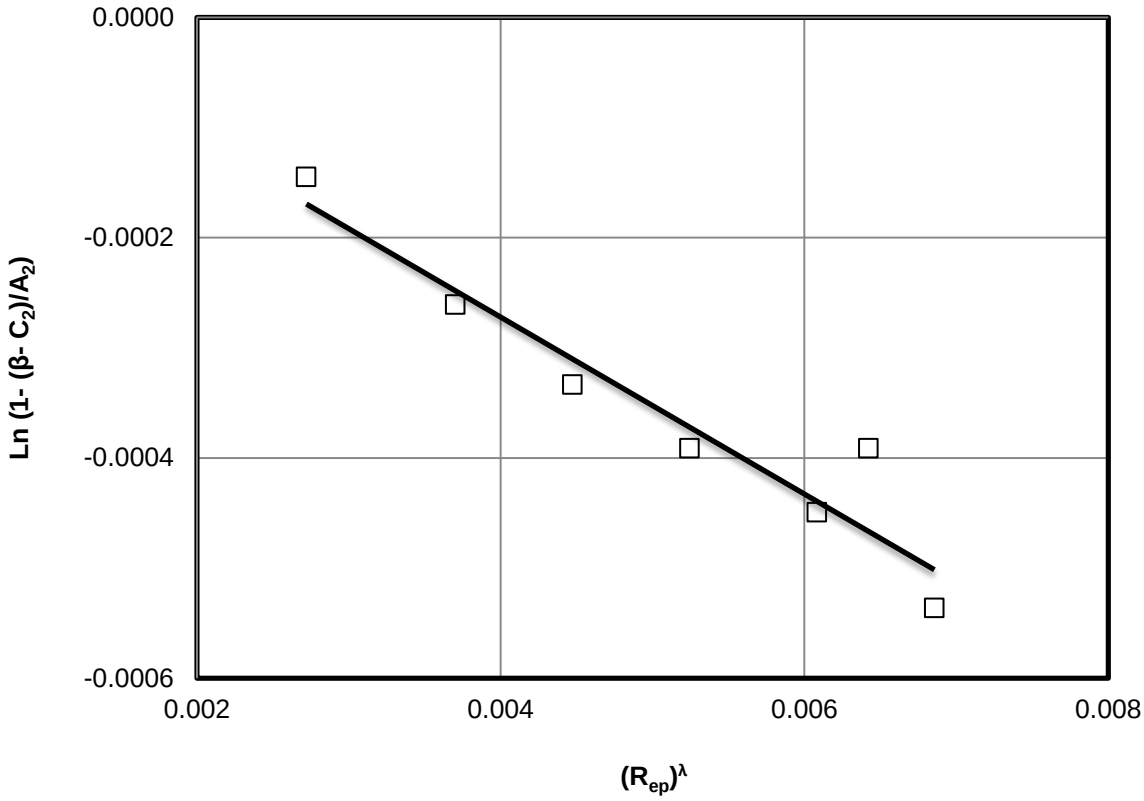

Fig. D.2: Straight line plot of Eq. B-9 at different gel particle concentrations and different gel particle diameters to develop the power-law equation, shown in Fig. 5.23.

Appendix E: Correlations of Thermal Effect on plugging/Unplugging Processes

The correlations of the thermal effect on the rate and intercept constants of plugging and unplugging regions were developed by the following steps:

1- The rate constant of the plugging and unplugging regions were correlated with the pore volumes injected at various temperatures and empirical correlations were developed, as shown in Figs. E.1 and E.2, by applying Eq. B-6 given in Appendix B.

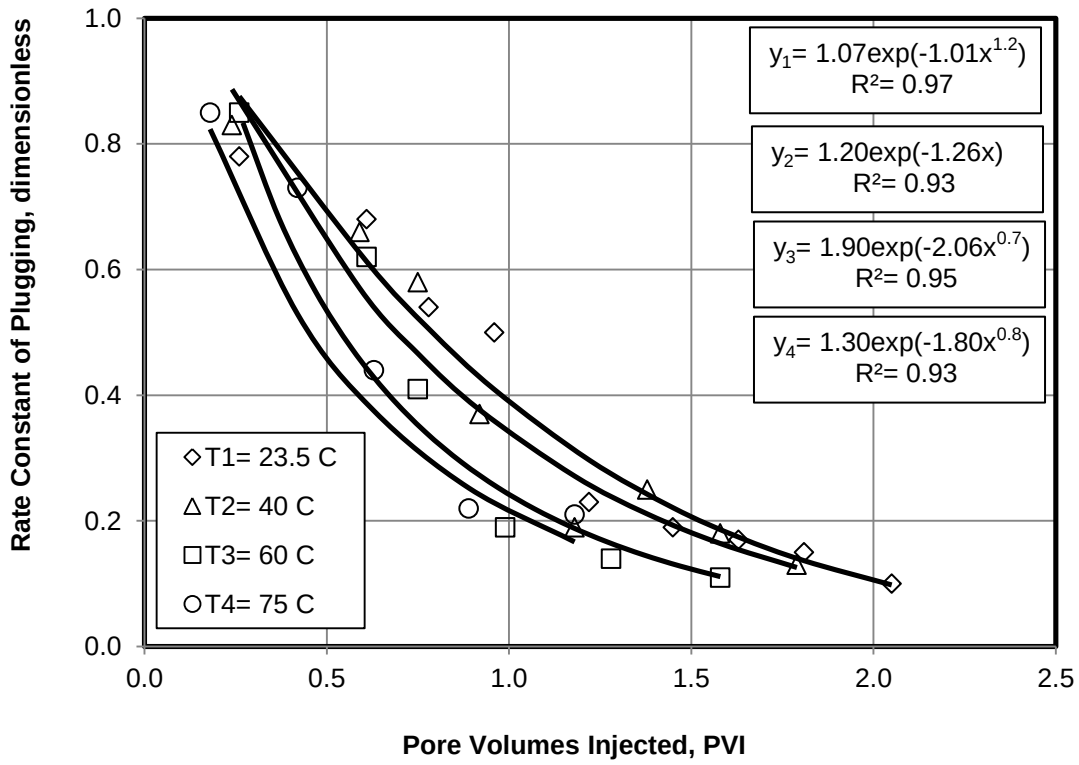

Fig. E.1: The relationship between rate constant of plugging and pore volumes injected at various temperatures

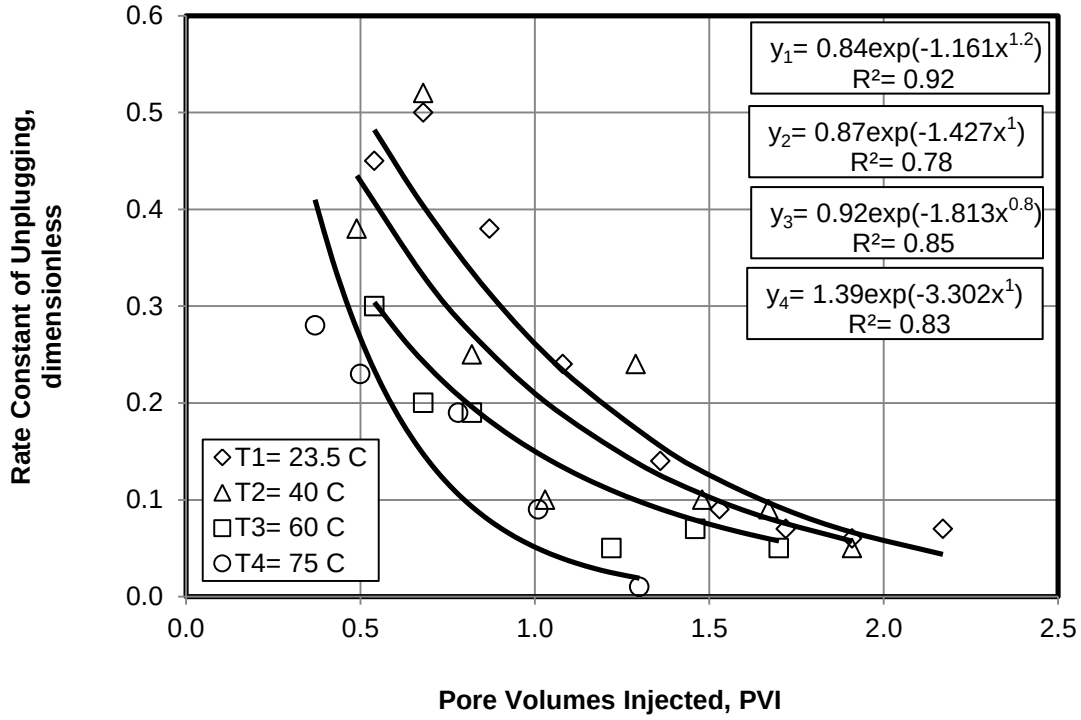

Fig. E.2: The relationship between rate constant of unplugging and pore volumes injected at various temperatures

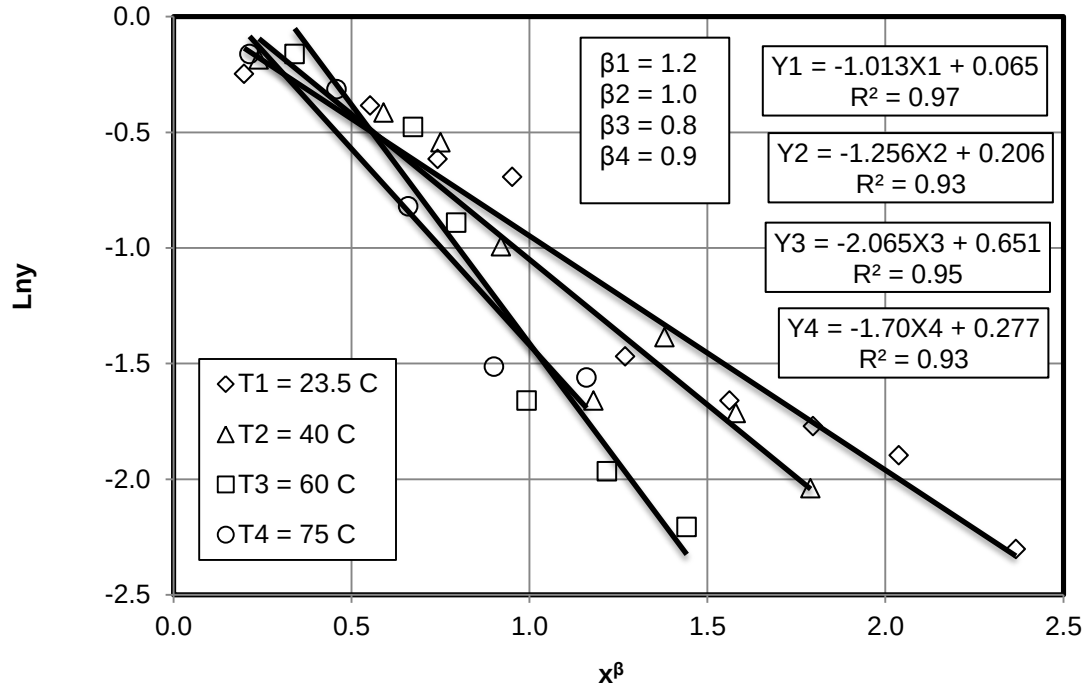

Fig. E.3: Straight line plot of Eq. B-6 at different temperatures to develop the empirical correlation of the rate constants of the plugging regions, as shown in Fig. E.1

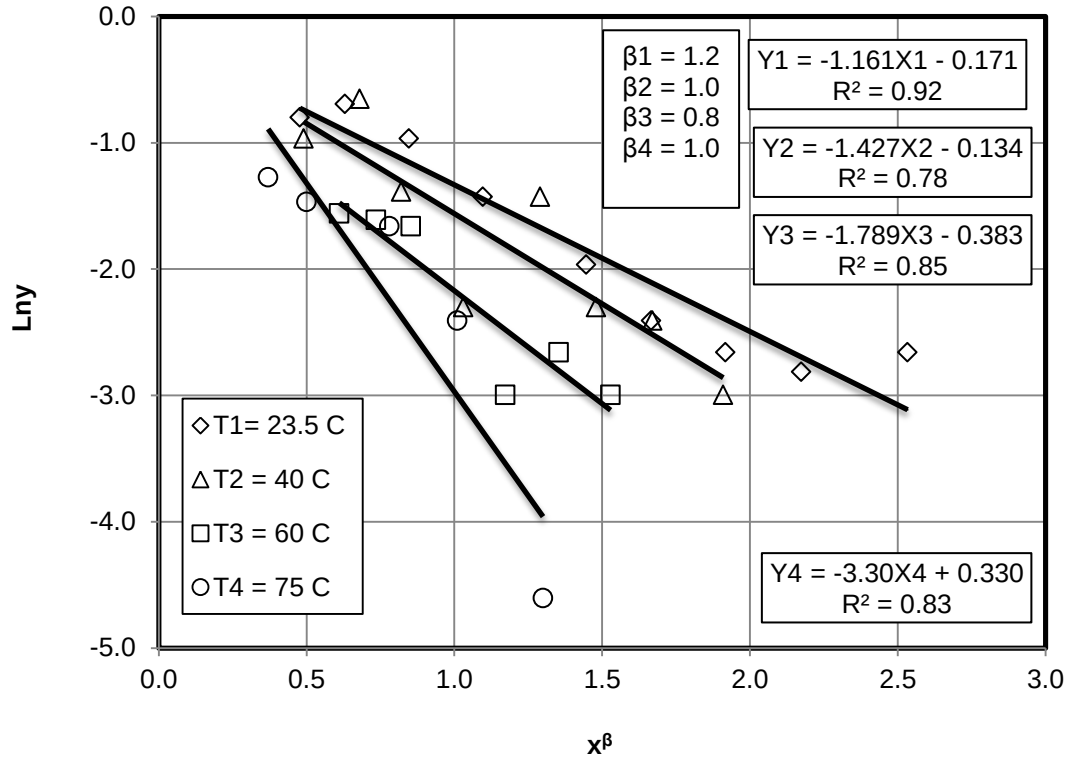

Fig. E.4: Straight line plot of Eq. B-6 at different temperatures to develop the empirical correlation of the rate constants of the unplugging regions, as shown in Fig. E.2

2- The intercept of the plugging and unplugging regions were correlated with the pore volumes injected at various temperatures and empirical correlations were developed, as shown in Figs. E.5 and E.6, by applying Eq. B-6 given in Appendix B.

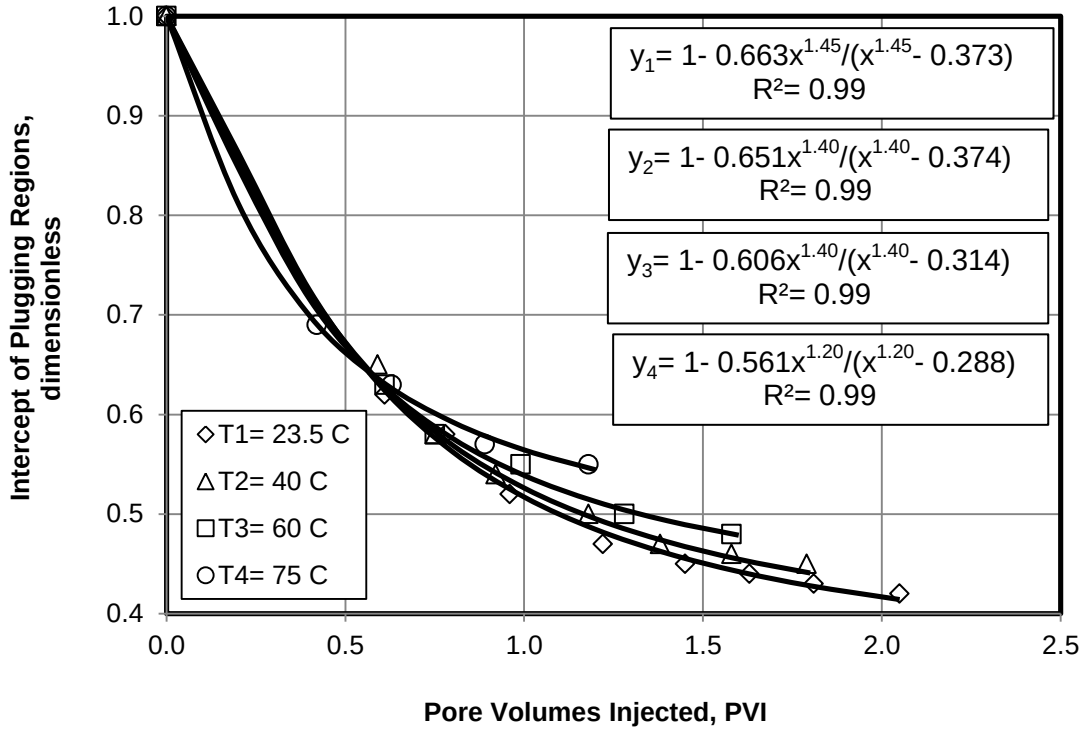

Fig. E.5: The relationship between intercept of plugging regions and pore volumes injected at various temperatures

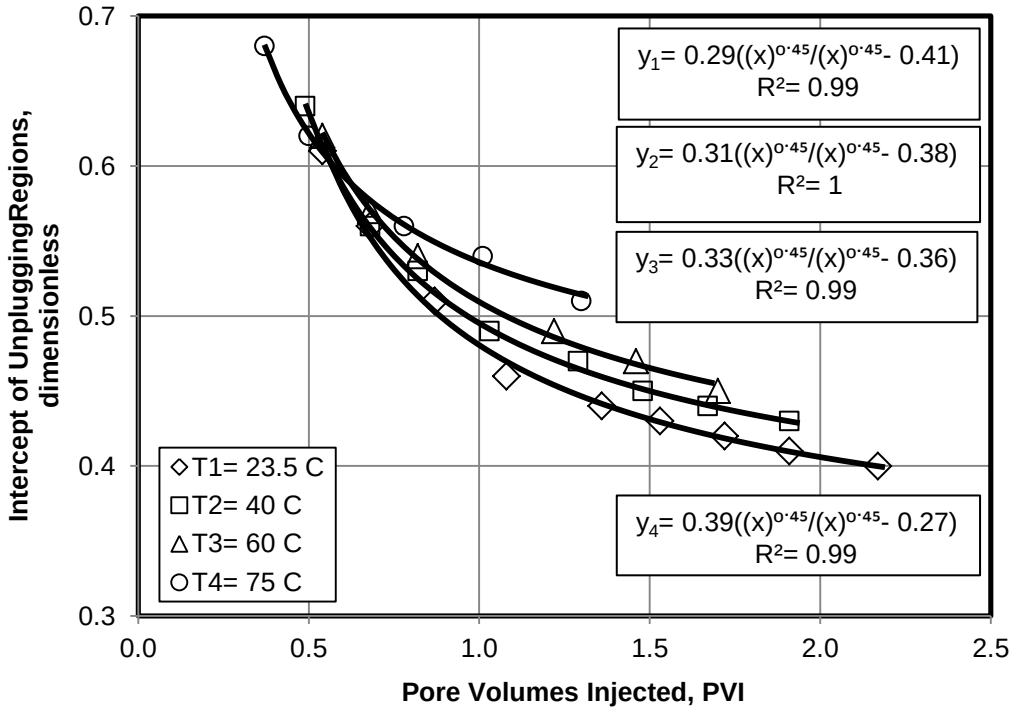

Fig. E.6: The relationship between intercept of unplugging regions and pore volumes injected at various temperatures

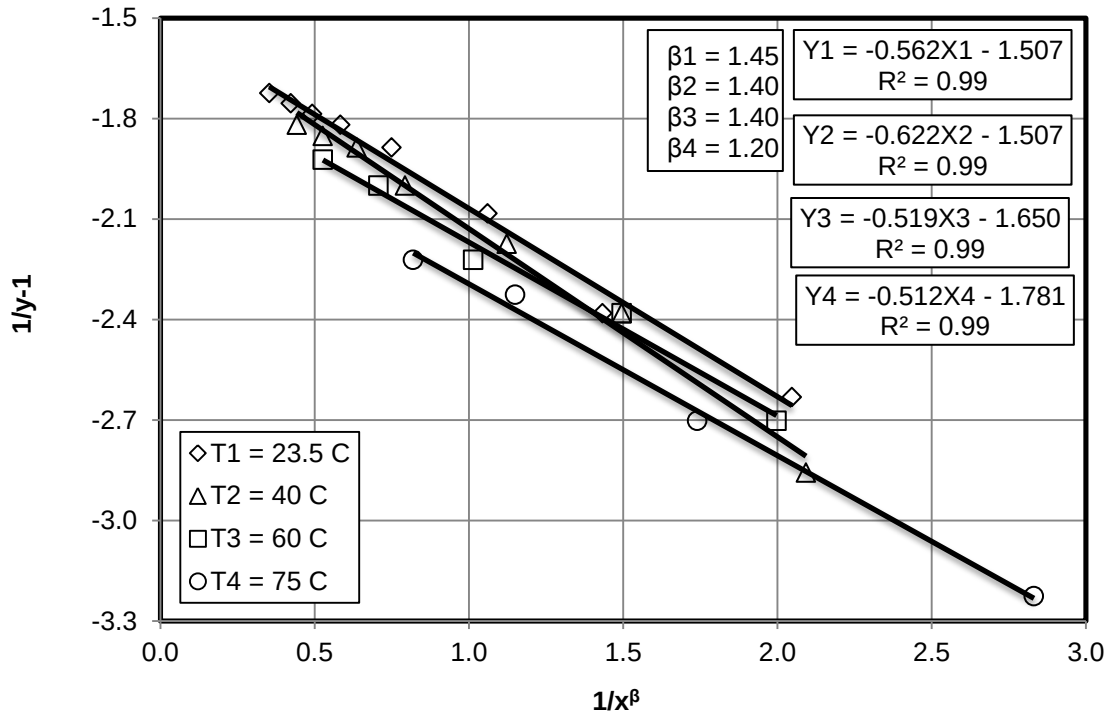

Fig. E.7: Straight line plot of Eq. B-4 at different temperature to develop the empirical correlation of the intercepts of the plugging regions, as shown in Fig. E.5

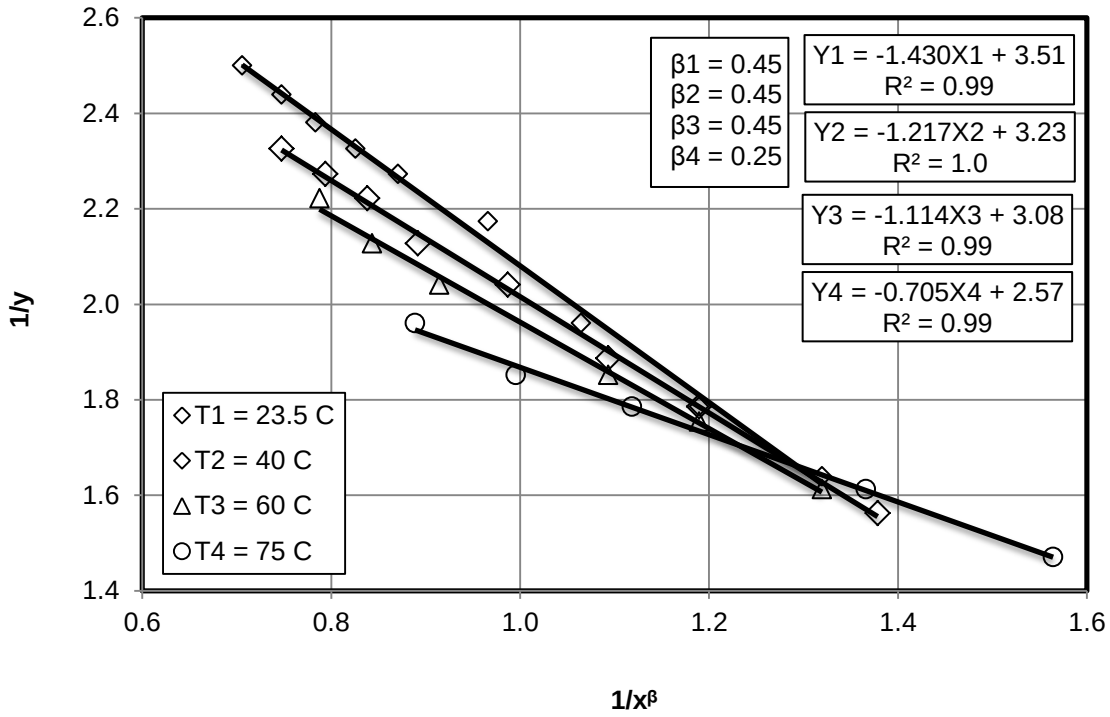

Fig. E.8: Straight line plot of Eq. B-2 at different temperature to develop the empirical correlation of the intercepts of the unplugging regions, as shown in Fig. E.6

3- The values of A,B, and β of the correlations in Figs. E.1, E.2, E.5 and E.6 were plotted and correlated as linear functions and substituted in Eqs. 6.7 and 6.8 to develop correlations of the thermal effect on the rate and intercept constants of plugging and unplugging regions, as shown in Figs. 6.20 to 6.23.

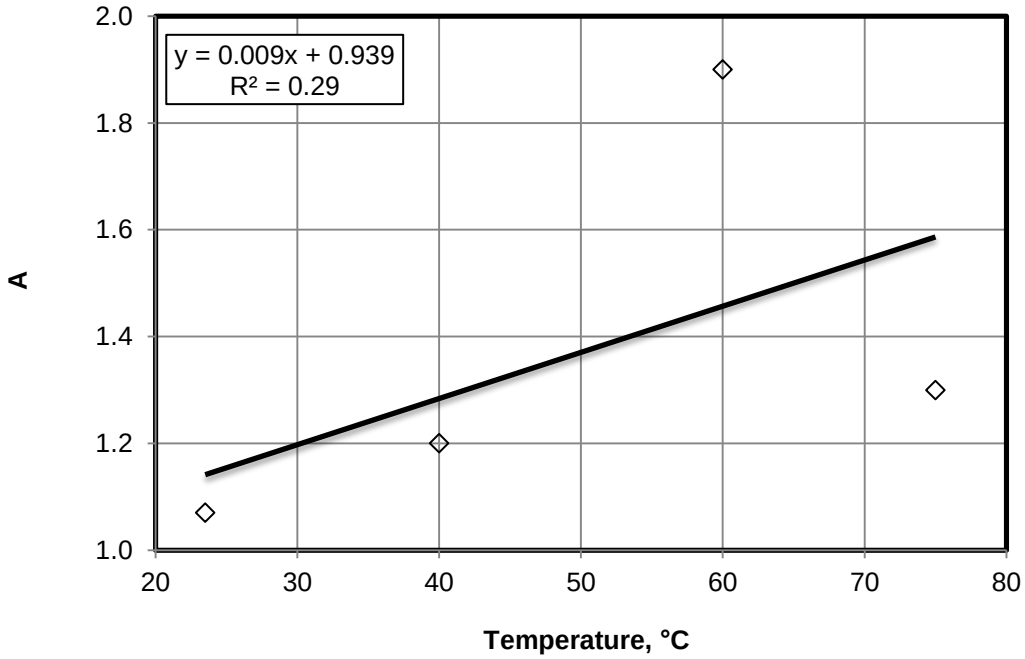

Fig. E.9: Linear function plot of A values at different temperatures for rate constants of plugging

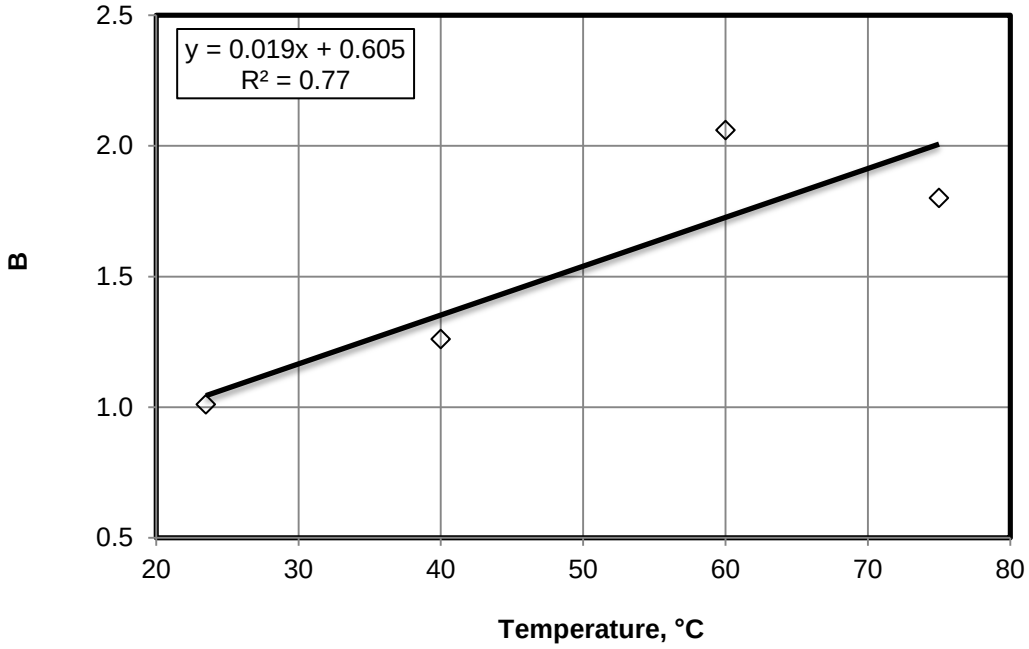

Fig. E.10: Linear function plot of B values at different temperatures for rate constants of plugging

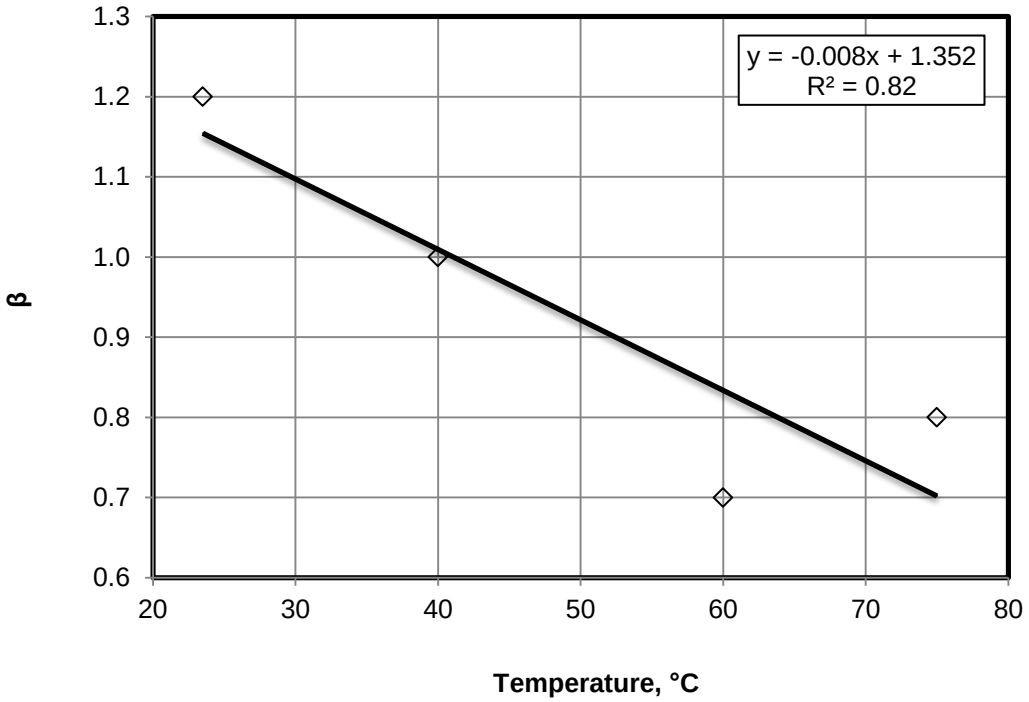

Fig. E.11: Linear function plot of β values at different temperatures for rate constants of plugging

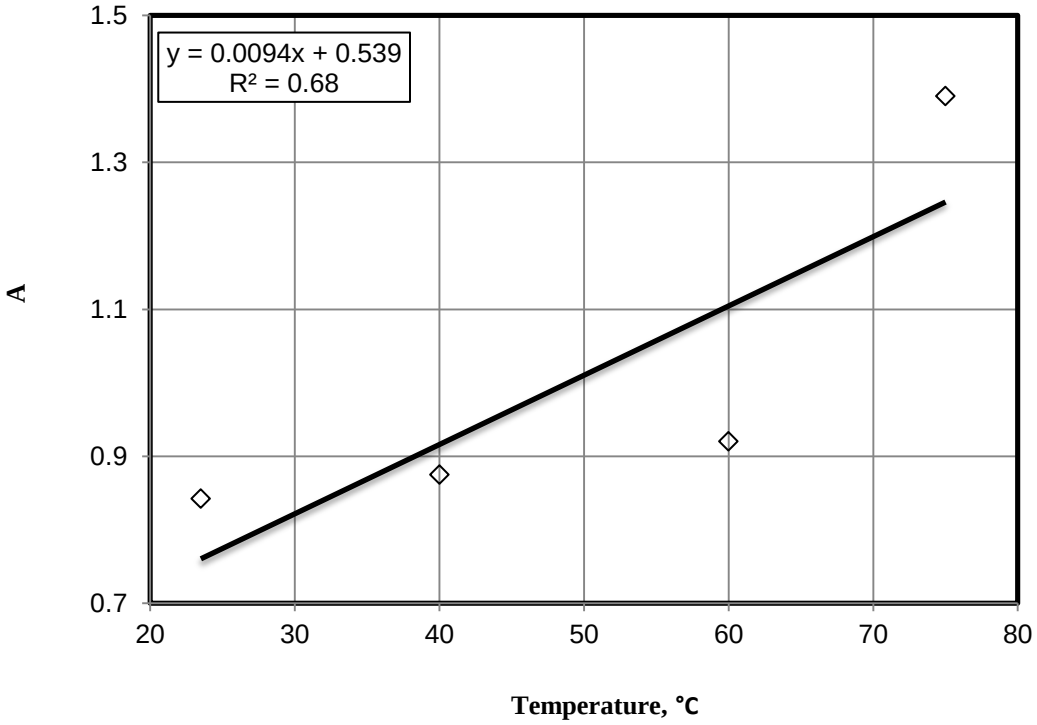

Fig. E.12: Linear function plot of A values at different temperatures for rate constants of unplugging

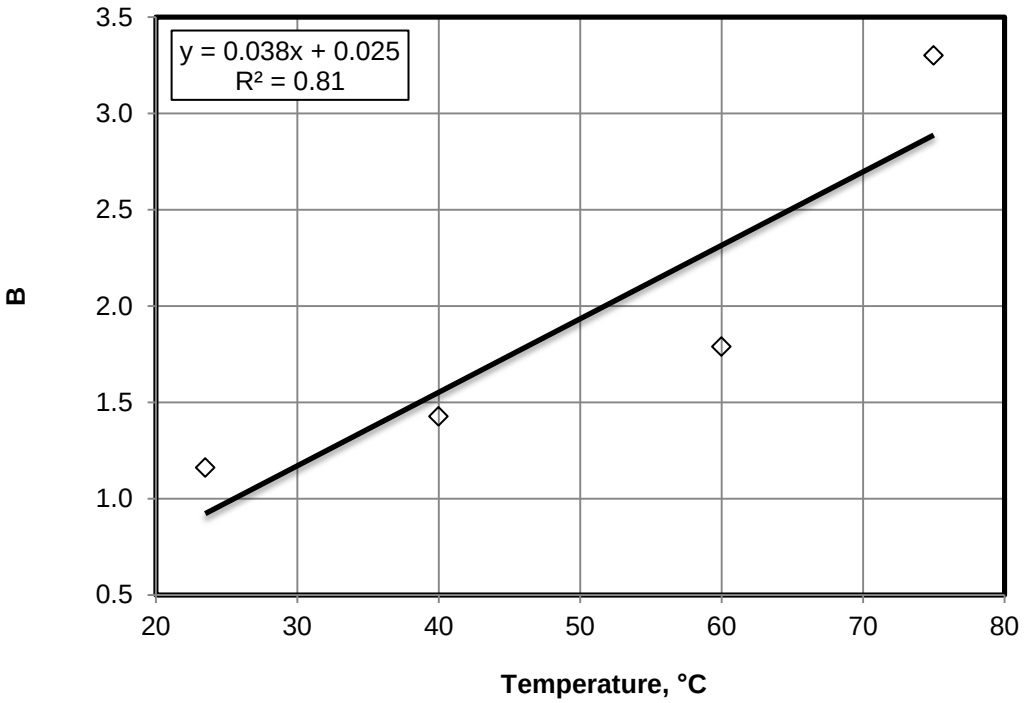

Fig. E.13: Linear function plot of B values at different temperatures for rate constants of unplugging

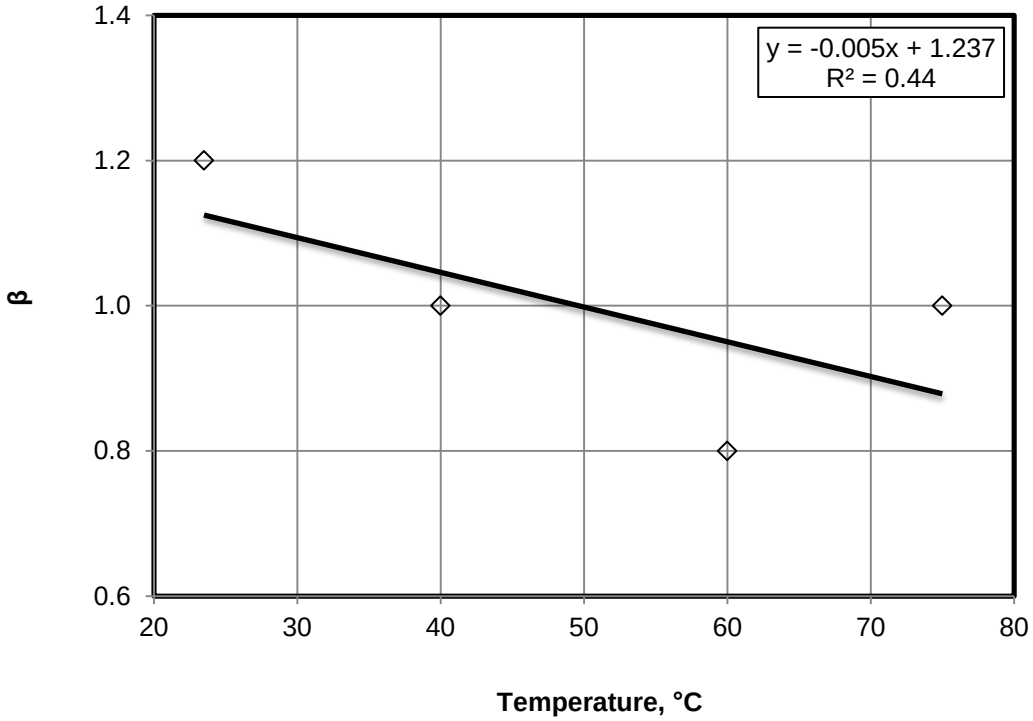

Fig. E.14: Linear function plot of β values at different temperatures for rate constants of unplugging

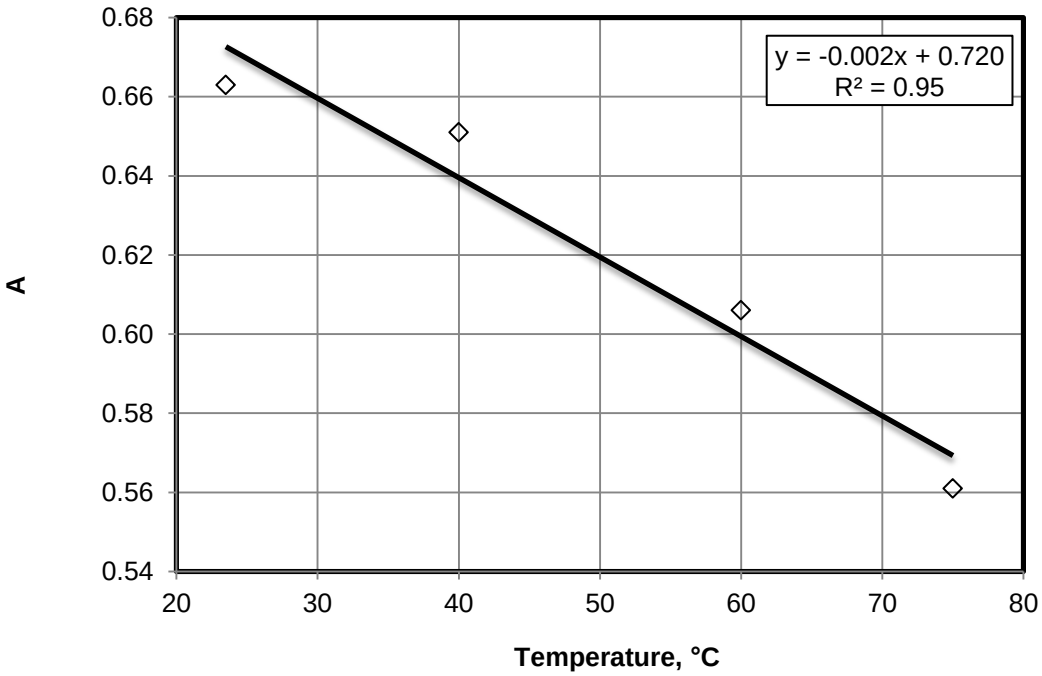

Fig. E.15: Linear function plot of A values at different temperatures for intercept of plugging regions

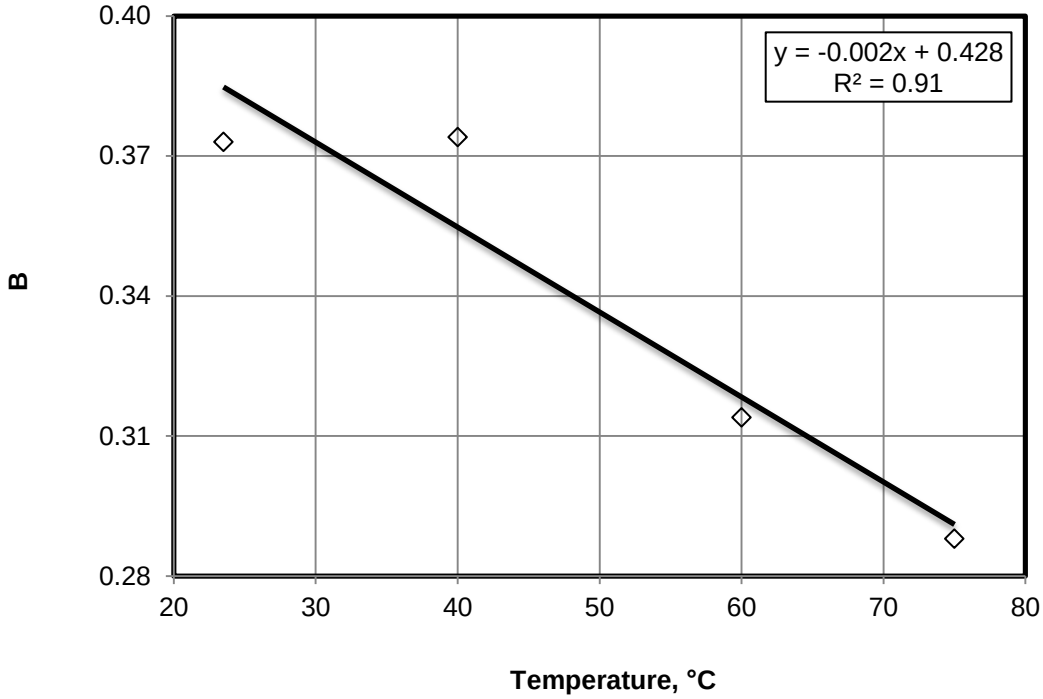

Fig. E.16: Linear function plot of B values at different temperatures for intercept of plugging regions

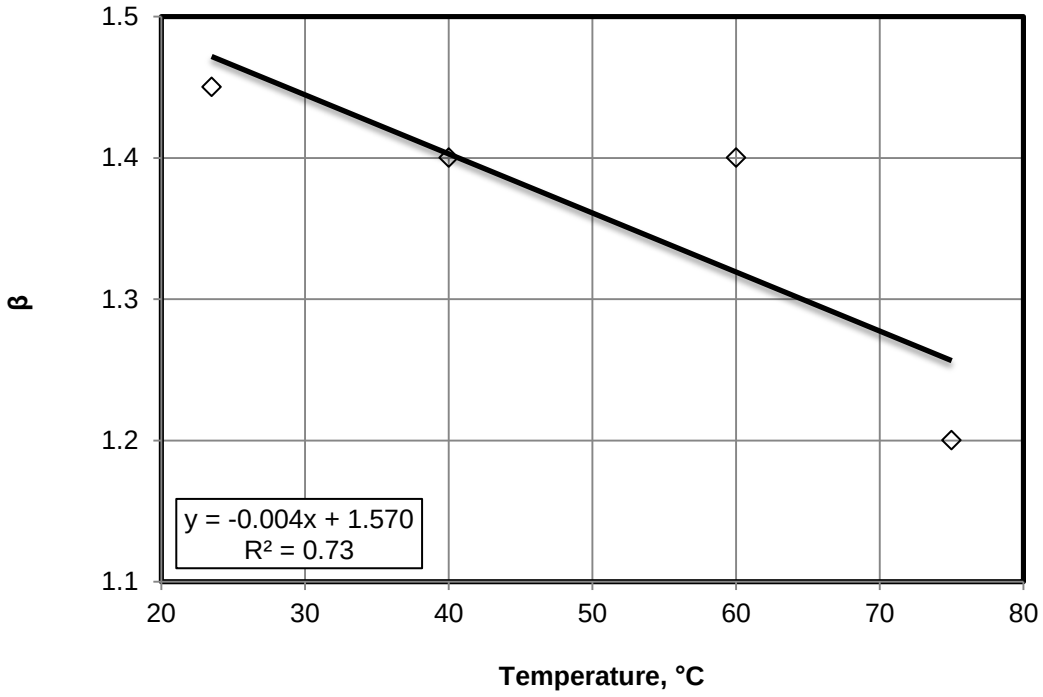

Fig. E.17: Linear function plot of β values at different temperatures for intercept of plugging regions

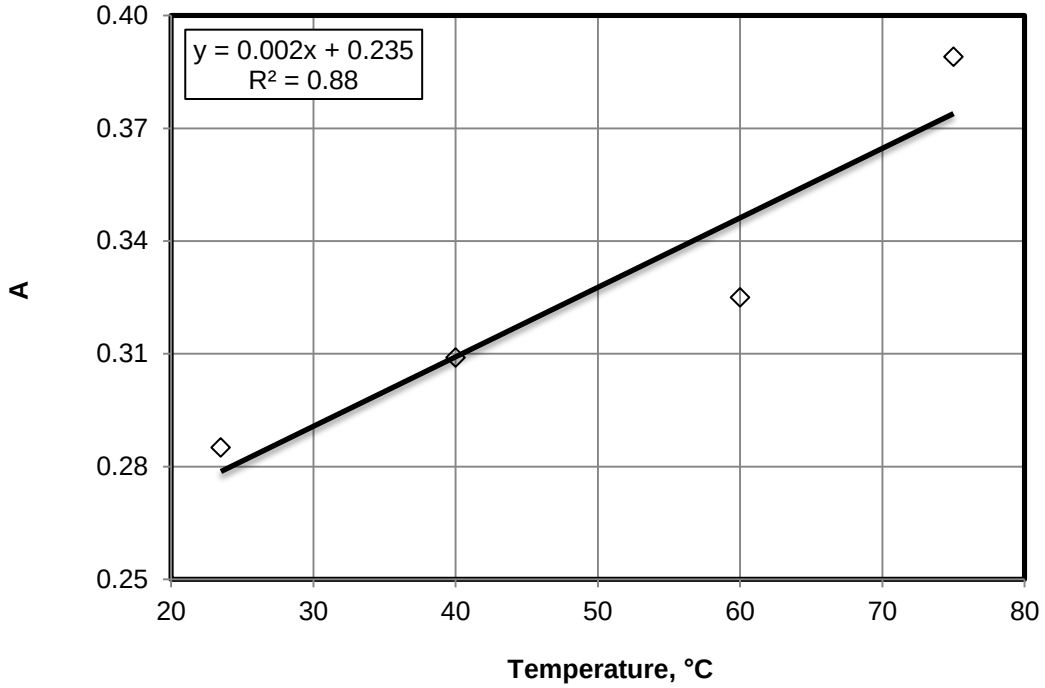

Fig. E.18: Linear function plot of A values at different temperatures for intercept of unplugging regions

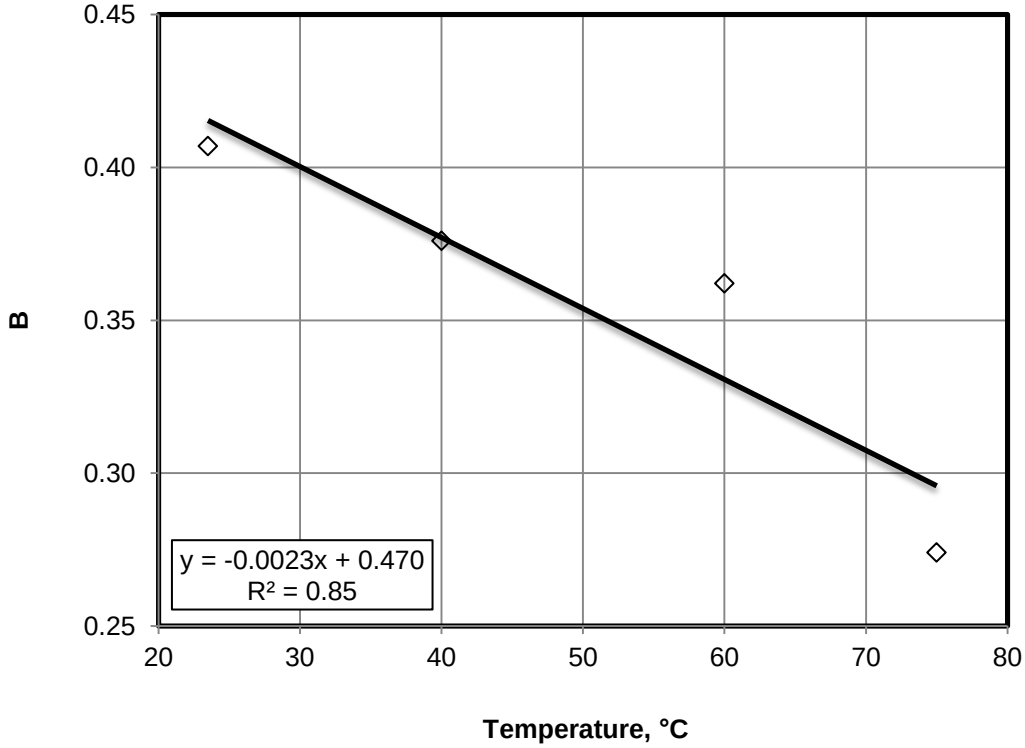

Fig. E.19: Linear function plot of B values at different temperatures for intercept of unplugging region

Appendix F: Correlations of the normalized dimensionless groups

The dimensionless groups values were normalized by used of Eq. 7.4 and were correlated at different concentrations, flow rates, gel particle sizes, and temperatures by applying Eqs. B-2 and B-7 given in Appendix B, as shown in the following figures:

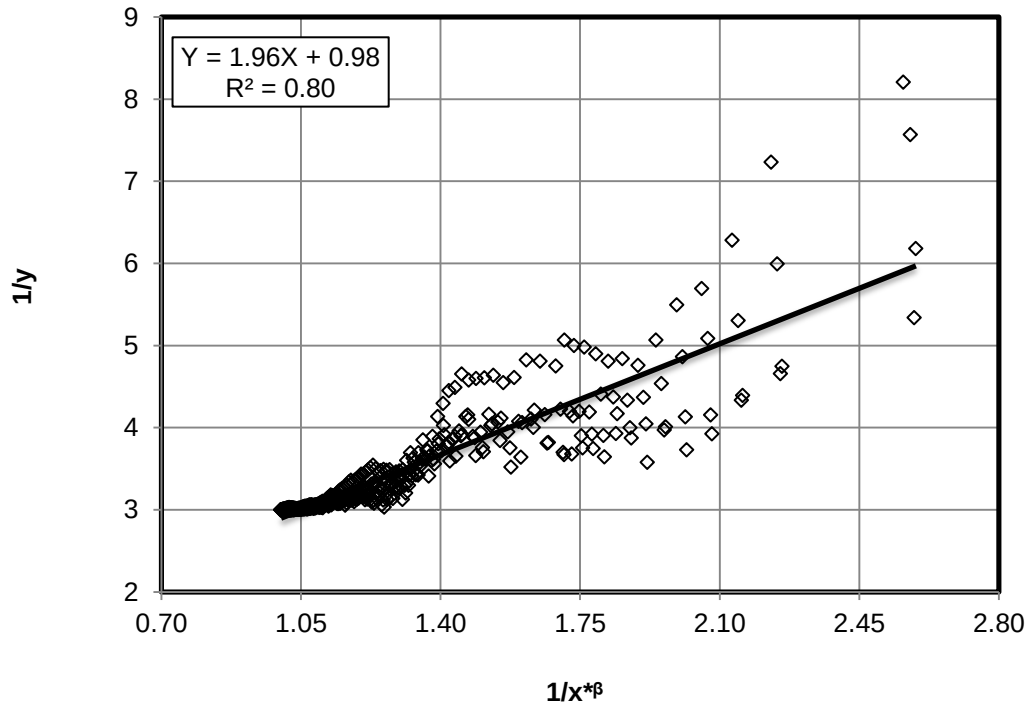

Fig. F.1: Straight line plot of Eq. B-2 for the normalized dimensionless group π_4 for the permeability reduction at different temperatures, as shown in Fig. 7.11

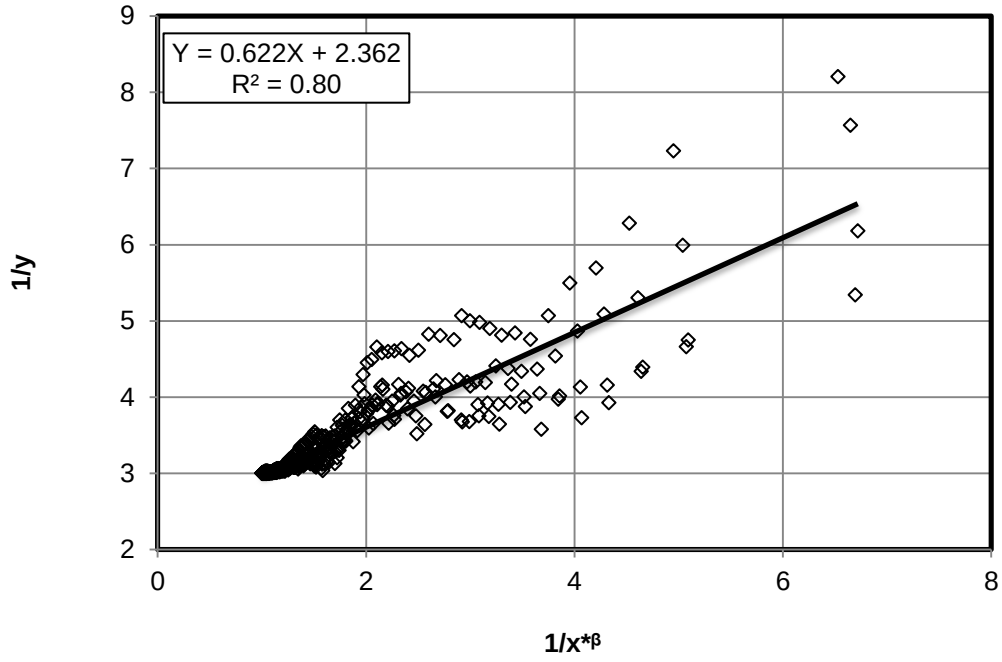

Fig. F.2: Straight line plot of Eq. B-2 for the normalized dimensionless group π_9 for the permeability reduction at different temperatures, as shown in Fig. 7.12

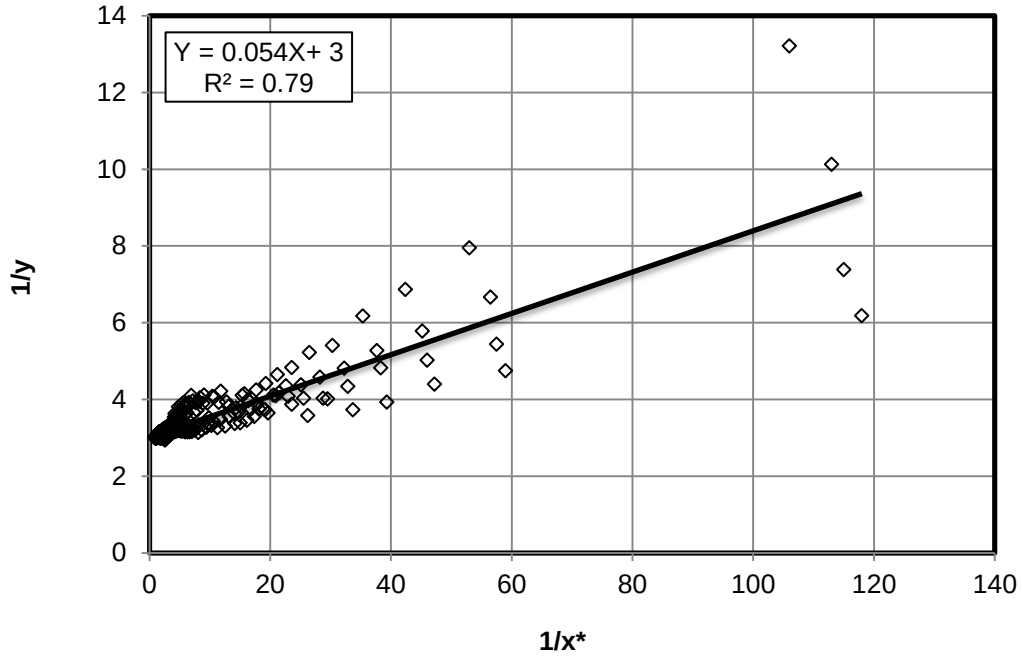

Fig. F.3: Straight line plot of Eq. B-7 for the normalized dimensionless group π_4 for the permeability reduction at different gel particles concentrations, as shown in Fig. 7.13

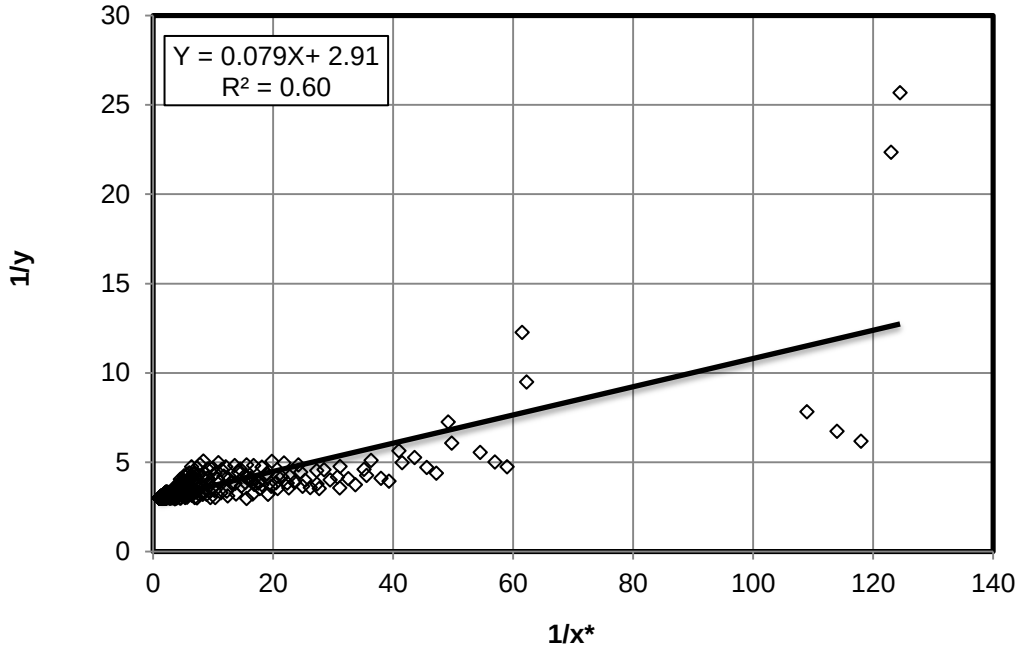

Fig. F.4: Straight line plot of Eq. B-7 for the normalized dimensionless group π_6 for the permeability reduction at different flow rates, as shown in Fig. 7.14

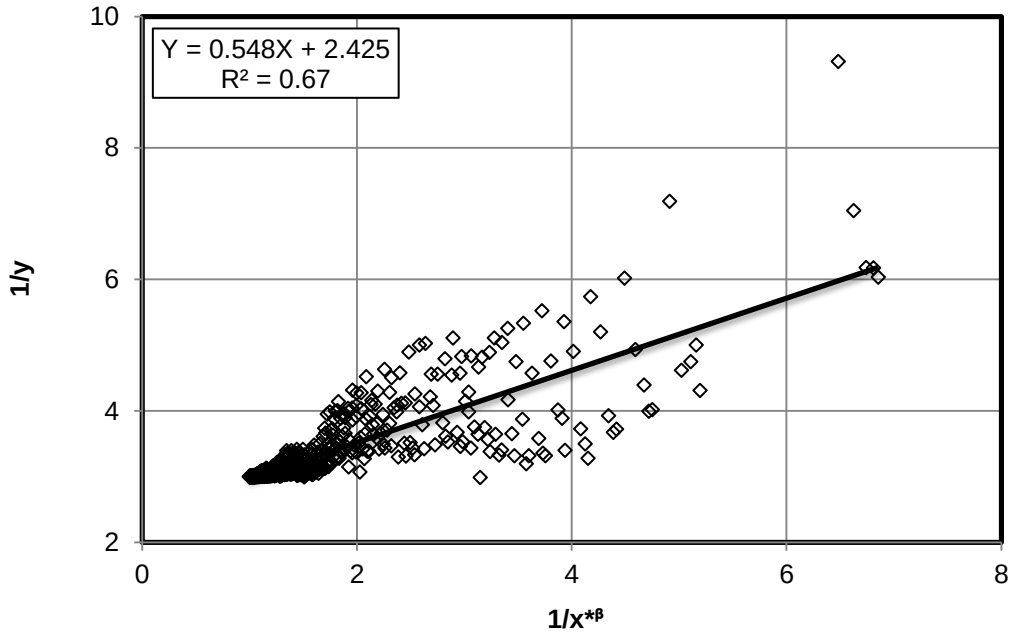

Fig. F.5: Straight line plot of Eq. B-2 for the normalized dimensionless group π_5 for the permeability reduction of the sand pack of 1061 µm grain diameter at different gel particles sizes, as shown in Fig. 7.15

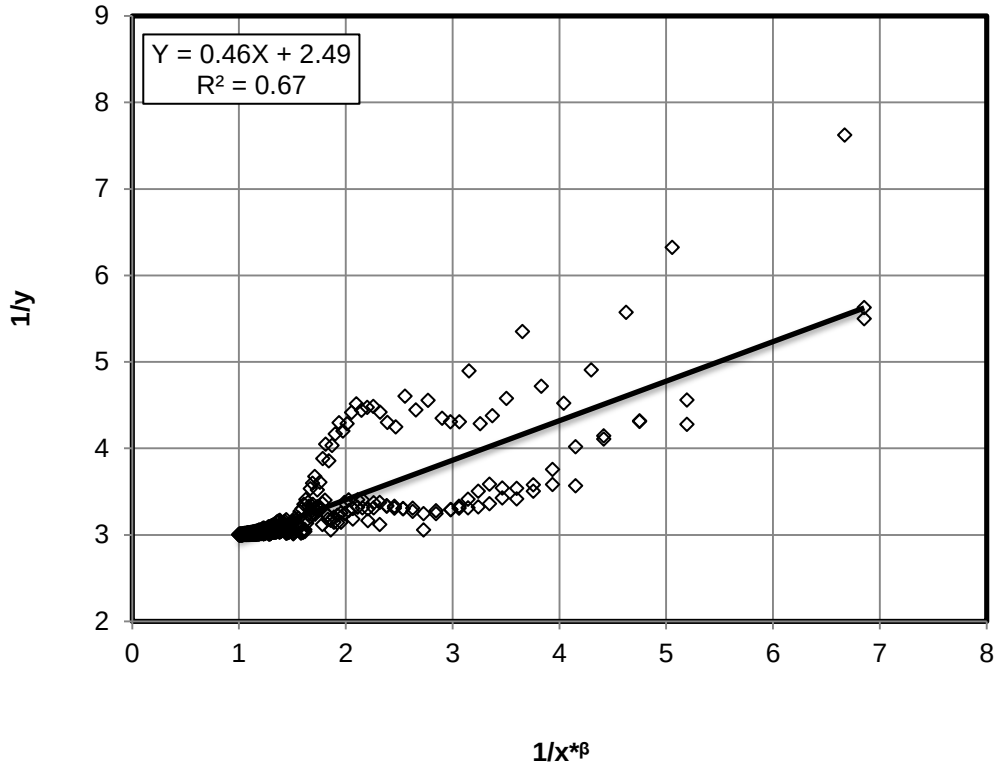

Fig. F.6: Straight line plot of Eq. B-2 for the normalized dimensionless group π_5 for the permeability reduction of the sand pack of 650 µm grain diameter at different gel particles sizes, as shown in Fig. 7.16

Appendix G: Correlation of the fluid loss

General empirical correlation of fluid loss at any pore diameter of filter disc, sand size and silica flour concentration was developed as described in the following.

1- The experimental data of the fluid loss was correlated with the silica flour concentration and exponential relationships were developed for 35, 10, and 5 micron pore diameter of filter disc at different sand sizes, as shown in Figs. G.1 to G.3, by applying Eq. B-6 given in Appendix B, as shown in Figs. G.4 to G.6.

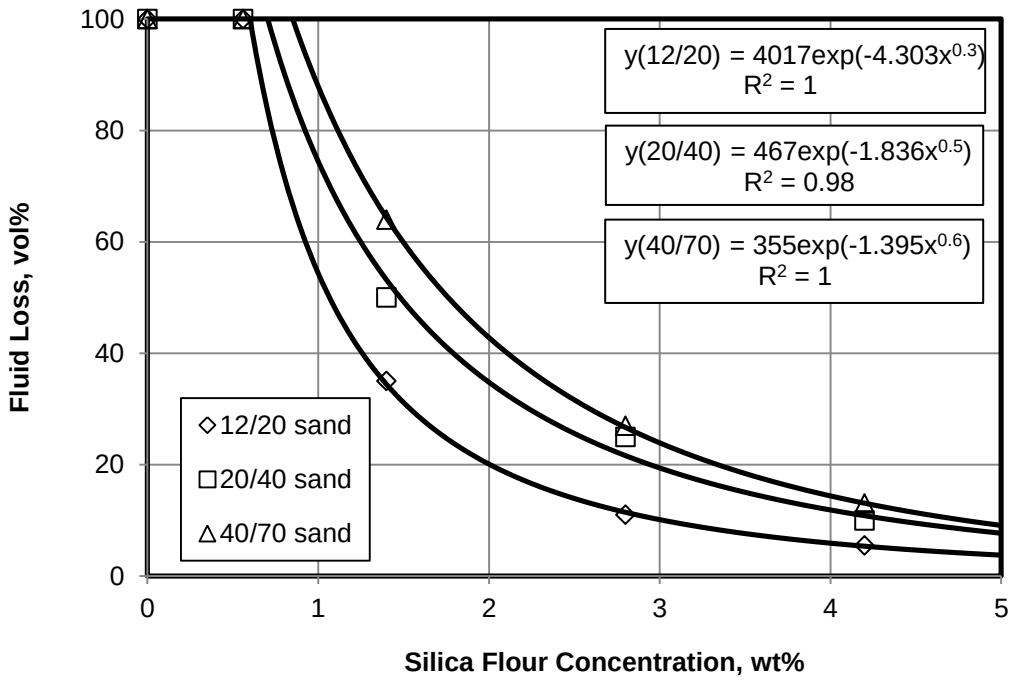

Fig. G.1: Correlate the experimental results of fluid loss at different silica flour concentrations for 35 micron average pore diameter of filter disc and different sand sizes

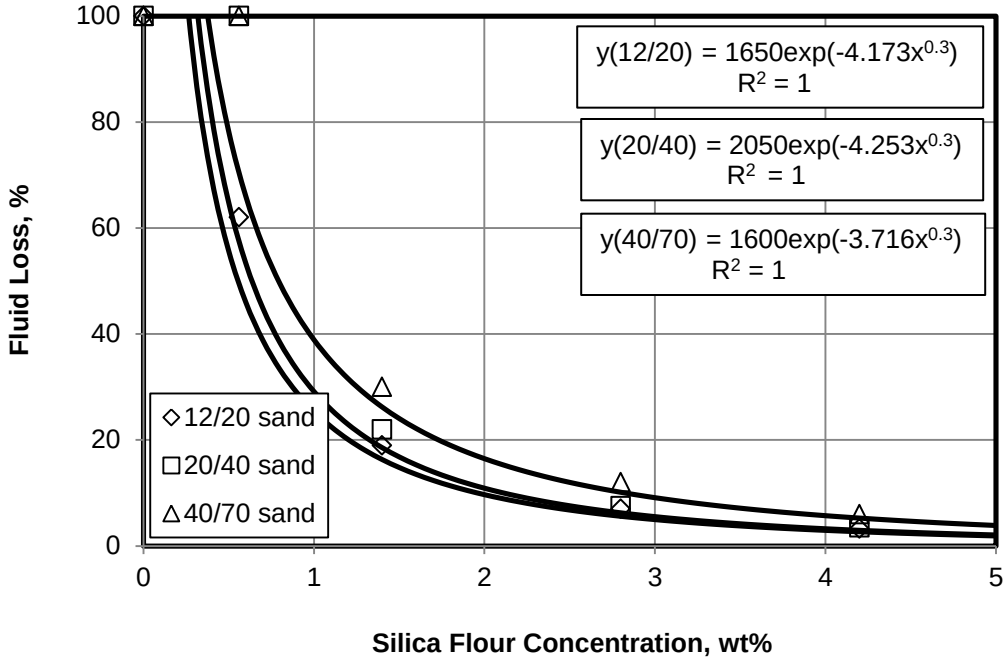

Fig. G.2: Correlate the experimental results of fluid loss at different silica flour concentrations for 10 micron average pore diameter of filter disc and different sand sizes

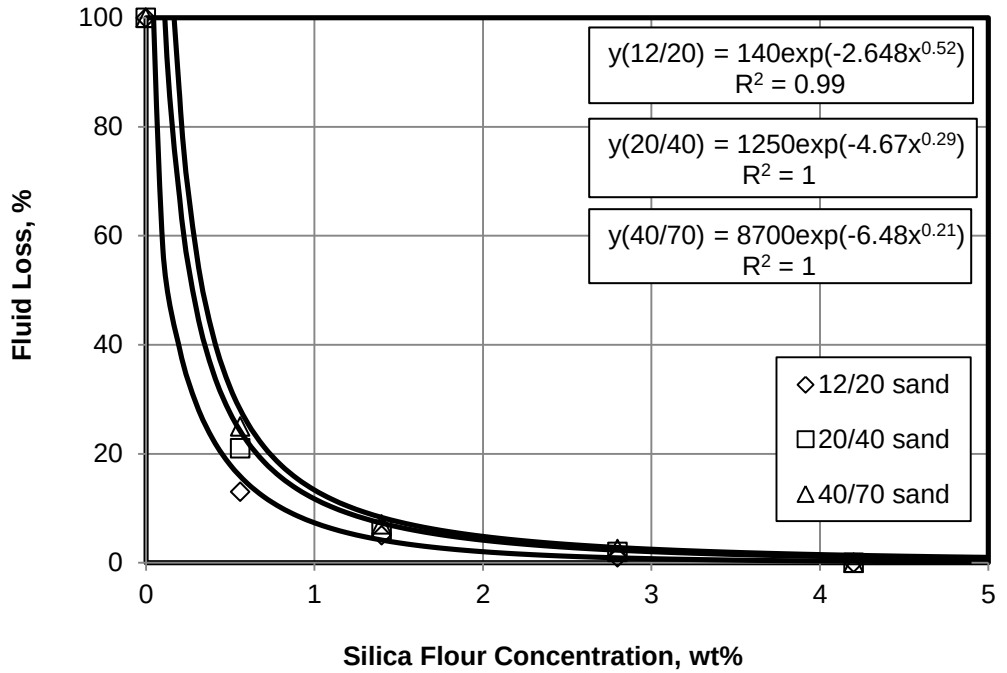

Fig. G.3: Correlate the experimental results of fluid loss at different silica flour concentrations for 5 micron average pore diameter of filter disc and different sand sizes

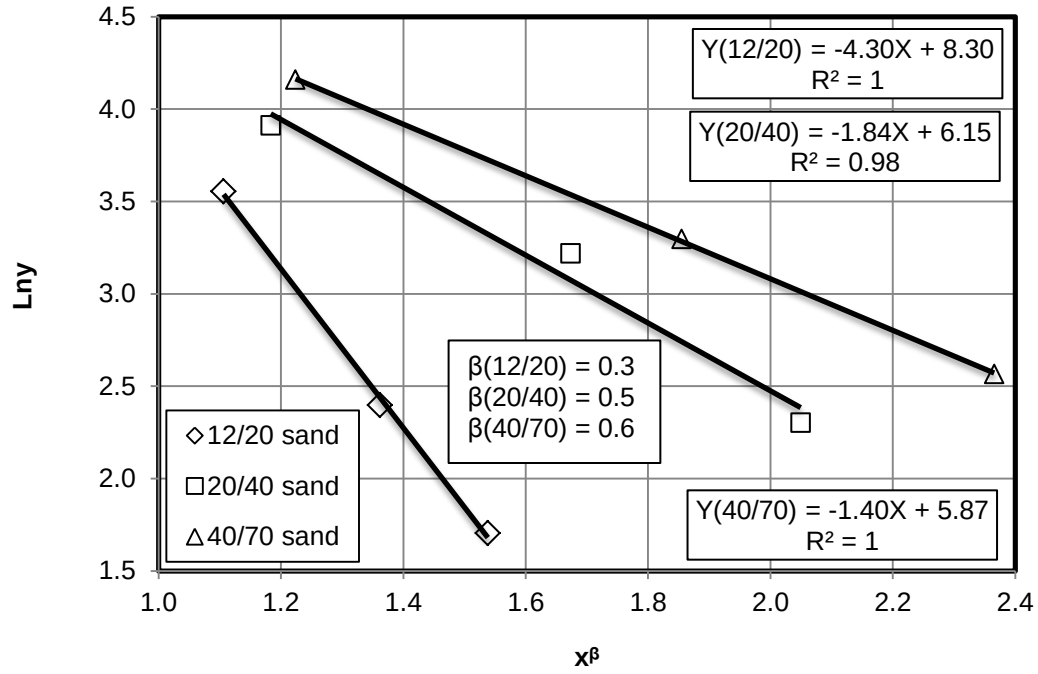

Fig. G.4: Straight line plot of Eq. B-6 to develop the exponential relationship of the fluid loss for 35 micron pore diameter of filter disc at different silica flour concentrations and different sand sizes, as shown in Fig. G.1

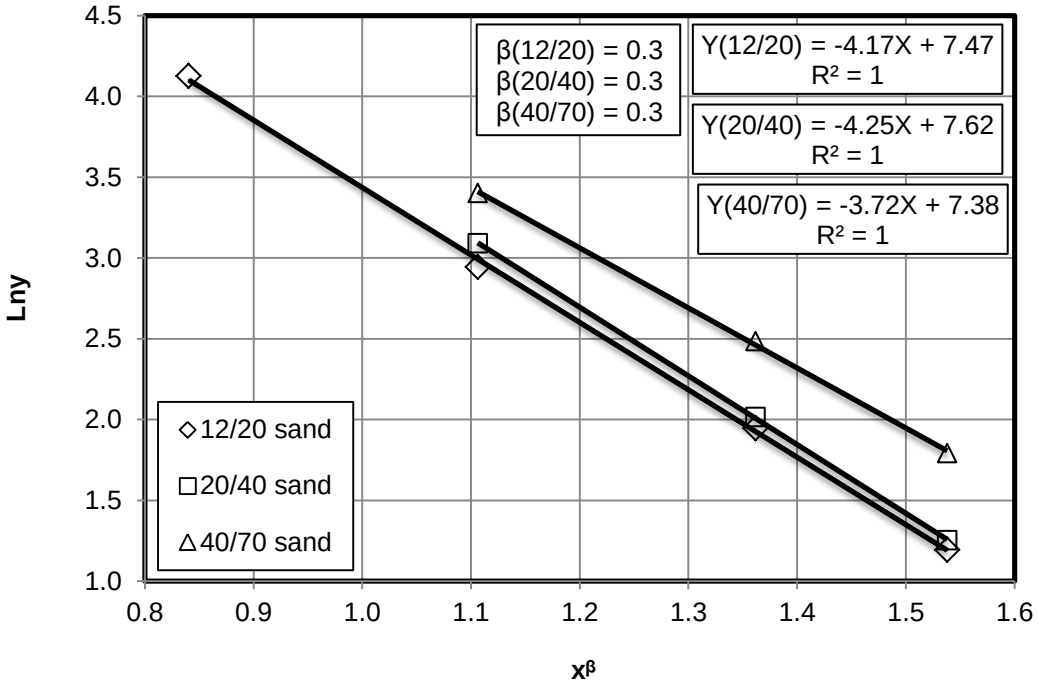

Fig. G.5: Straight line plot of Eq. B-6 to develop the exponential relationship of the fluid loss for 10 micron pore diameter of filter disc at different silica flour concentrations and different sand sizes, as shown in Fig. G.2

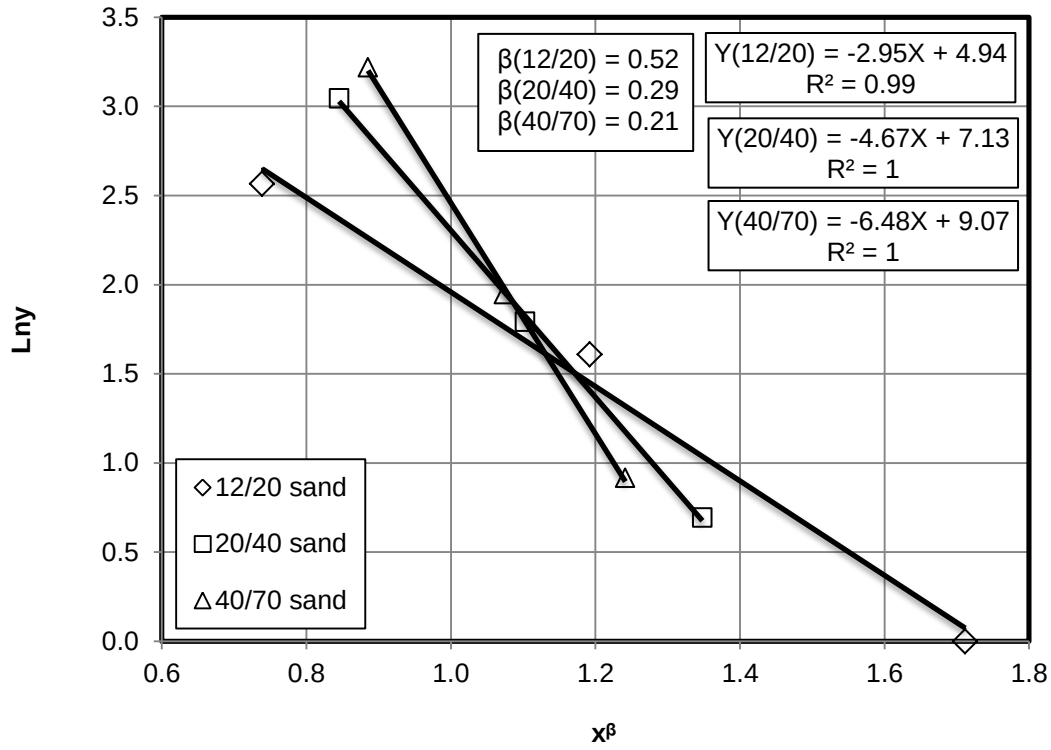

Fig. G.6: Straight line plot of Eq. B-6 to develop the exponential relationship of the fluid loss for 5 micron pore diameter of filter disc at different silica flour concentrations and different sand sizes, as shown in Fig. G.3

2- The fluid loss was correlated with the critical silica flour concentration for 35, 10, and 5 micron pore diameter of filter disc at different sand sizes, as shown in Figs. G.7 to G.9, by applying Eq. B-10 given in Appendix B, as shown in Figs. G.10 to G.12.

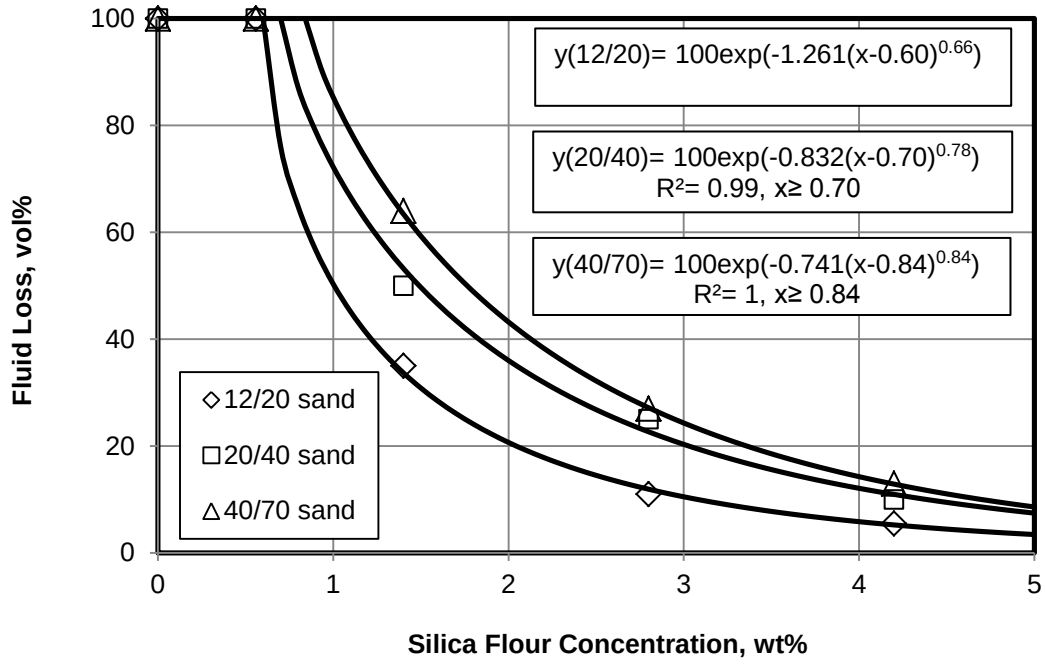

Fig. G.7: Correlate the experimental results of fluid loss with the critical silica flour concentrations for 35 micron average pore diameter of filter disc and different sand sizes

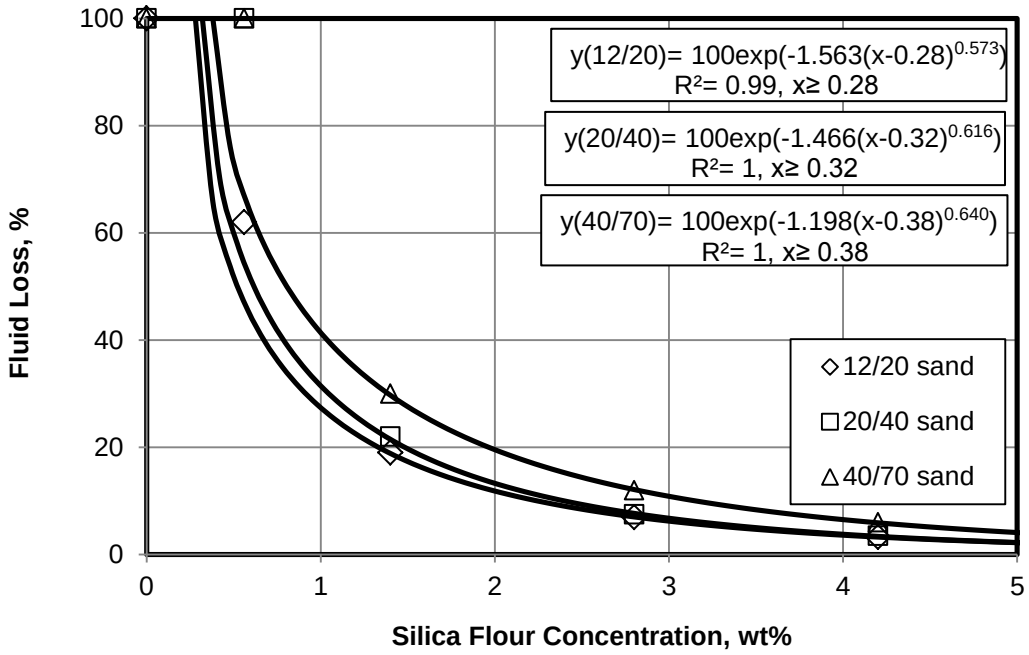

Fig. G.8: Correlate the experimental results of fluid loss with the critical silica flour concentrations for 10 micron average pore diameter of filter disc and different sand sizes

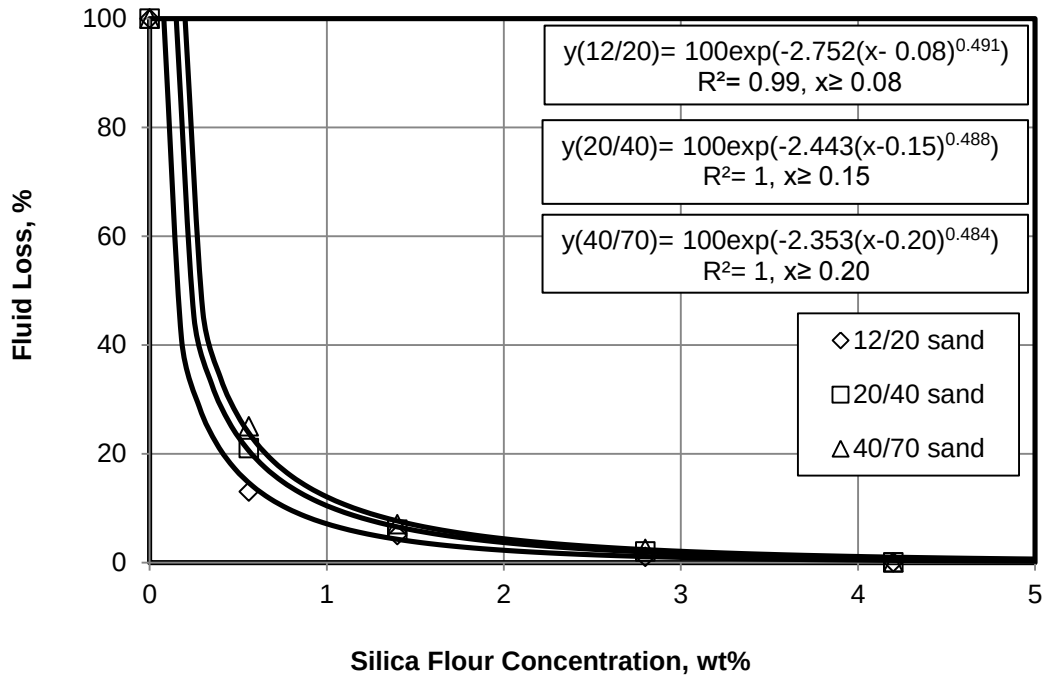

Fig. G.9: Correlate the experimental results of fluid loss with the critical silica flour concentrations for 5 micron average pore diameter of filter disc and different sand size

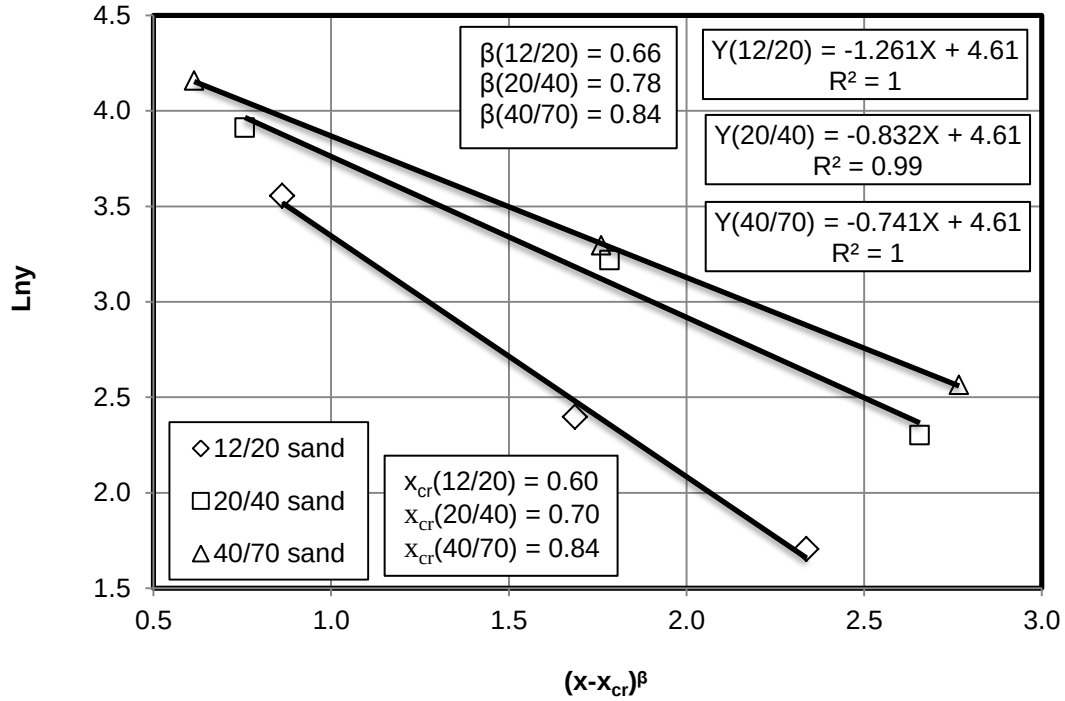

Fig. G.10: Straight line plot of Eq. B-10 to correlate the fluid loss with the critical silica flour concentration for 35 micron pore diameter of filter disc at different sand sizes, as shown in Fig. G.7

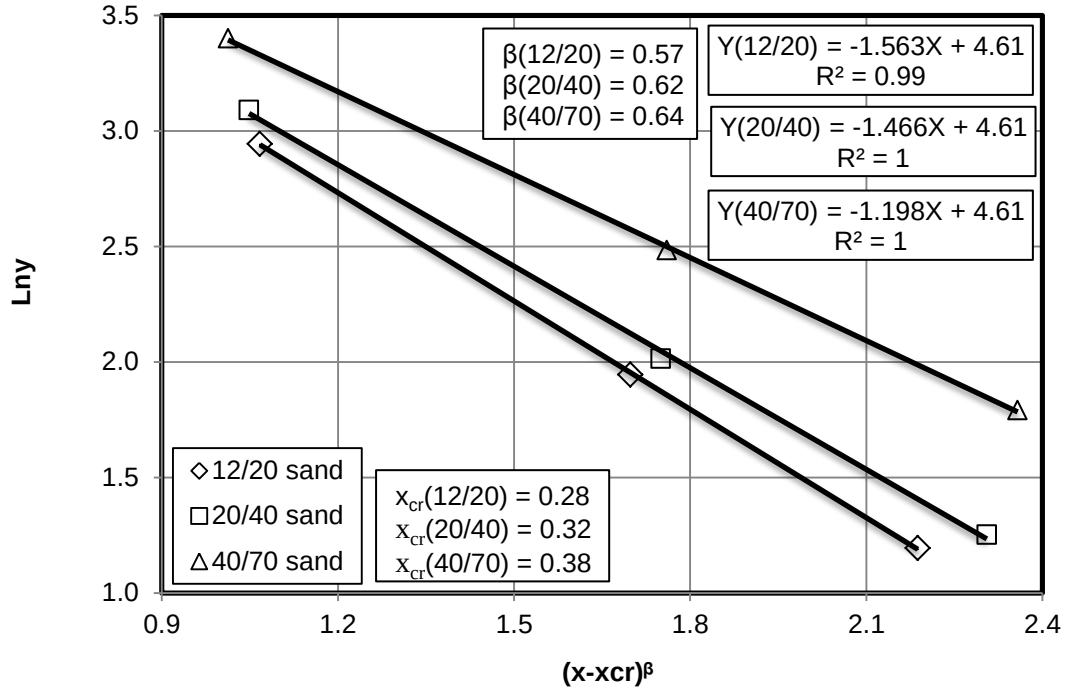

Fig. G.11: Straight line plot of Eq. B-10 to correlate the fluid loss with the critical silica flour concentration for 10 micron pore diameter of filter disc at different sand sizes, as shown in Fig. G.8

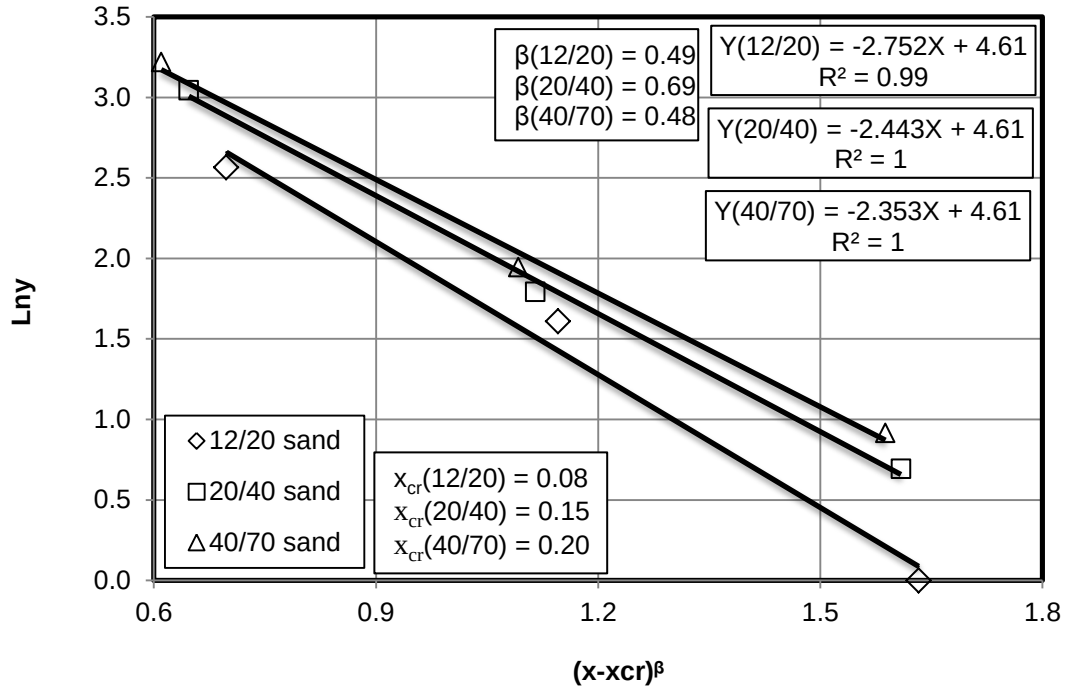

Fig. G.12: Straight line plot of Eq. B-10 to correlate the fluid loss with the critical silica flour concentration for 5 micron pore diameter of filter disc at different sand sizes, as shown in Fig. G.9

3- The values of B, α, and x_{cr} of the exponential relationships were plotted and correlated as linear functions and substituted in Eq. 8.2 to develop charts of fluid loss for same pore diameter of filter disc and different sand sizes, as shown in Figs. 8.3 to 8.5.

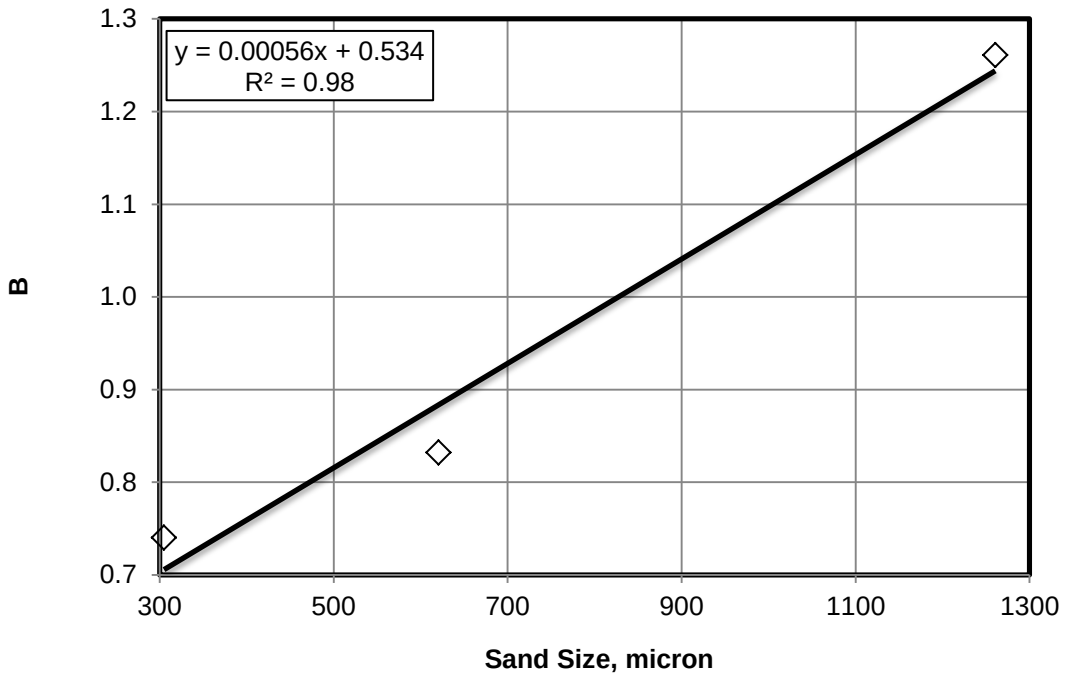

Fig. G.13: Linear function plot of B values at different sand sizes for 35 micron pore diameter of filter disc

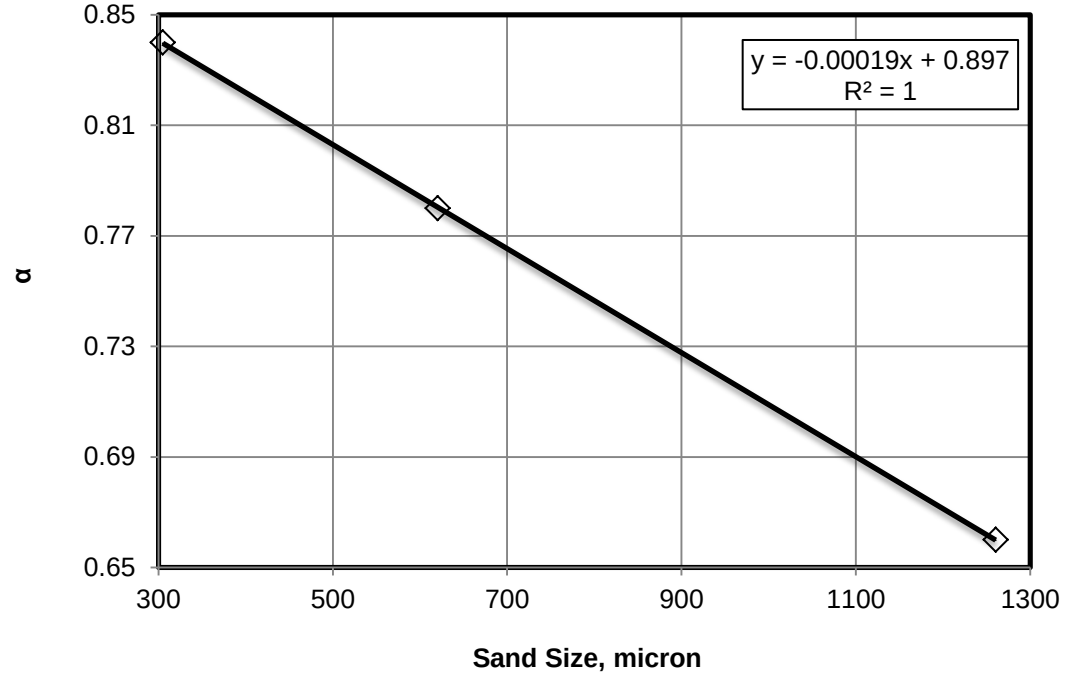

Fig. G.14: Linear function plot of α values at different sand sizes for 35 micron pore diameter of filter disc

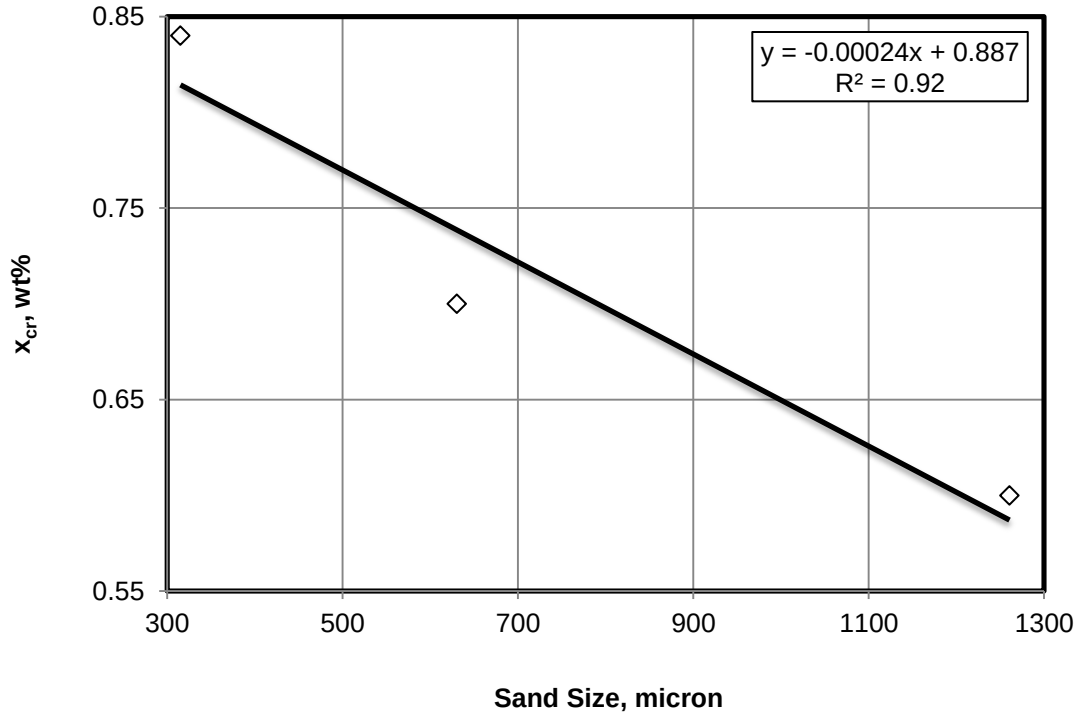

Fig. G.15: Linear function plot of x_{cr} values at different sand sizes for 35 micron pore diameter of filter disc

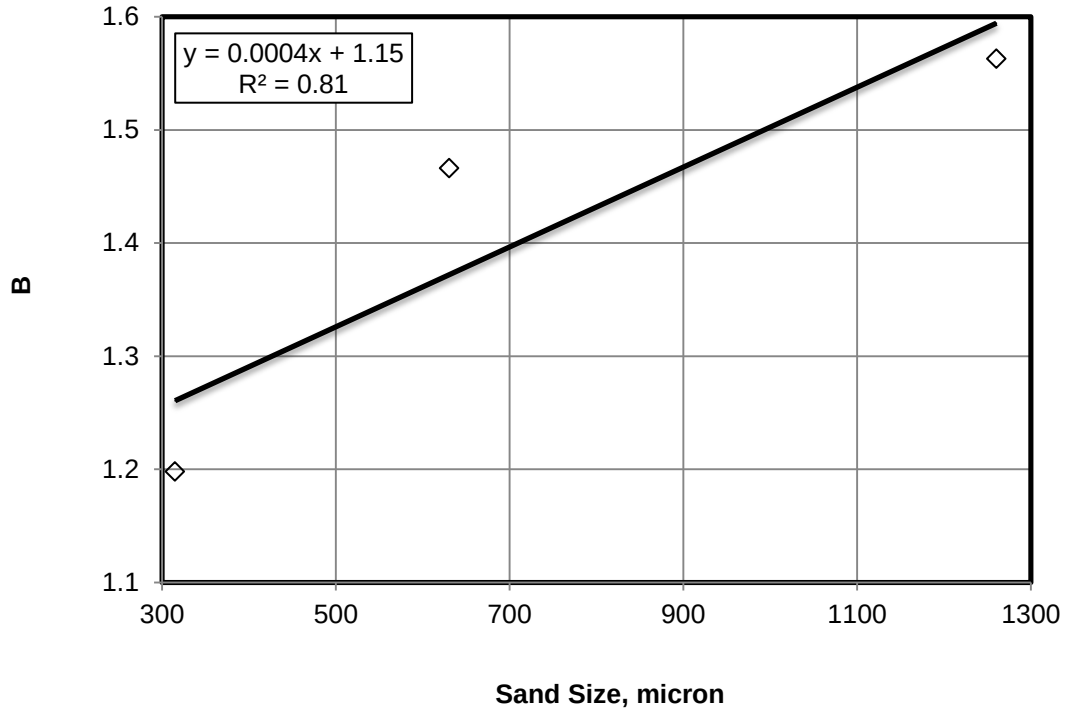

Fig. G.16: Linear function plot of B values at different sand sizes for 10 micron pore diameter of filter disc

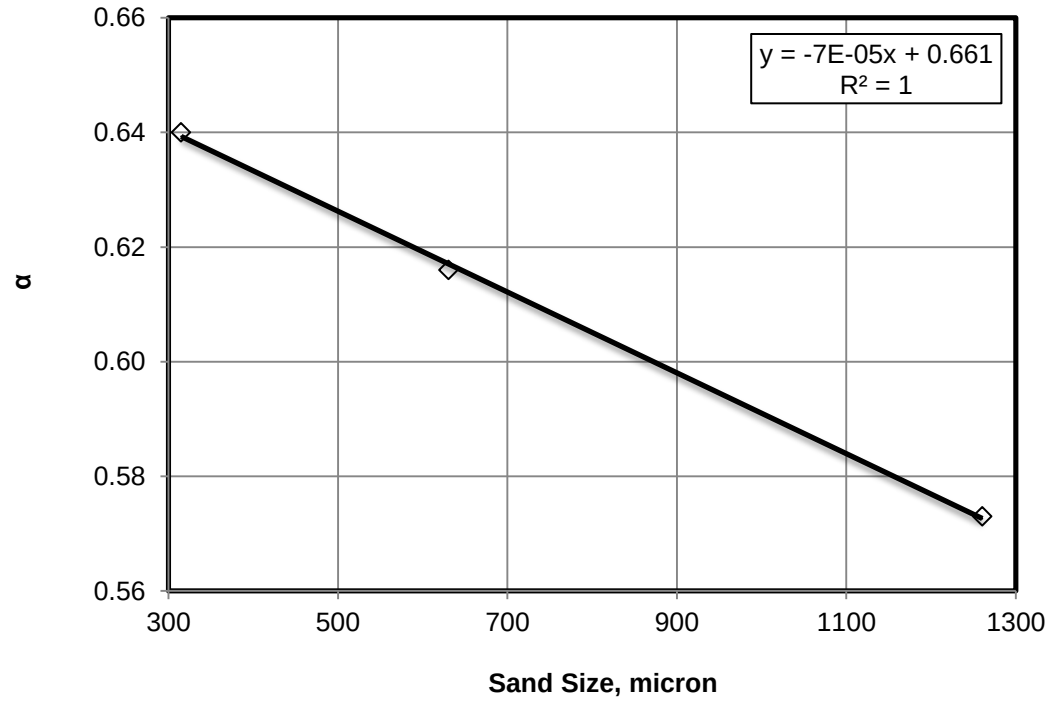

Fig. G.17: Linear function plot of α values at different sand sizes for 10 micron pore diameter of filter disc

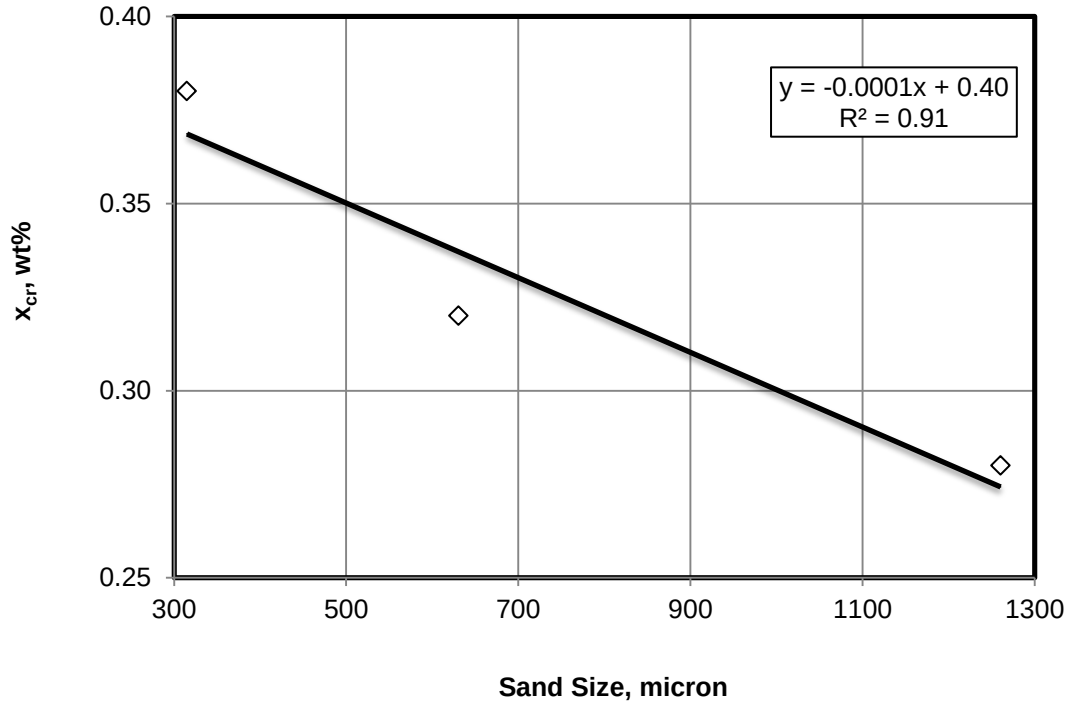

Fig. G.18: Linear function plot of x_{cr} values at different sand sizes for 10 micron pore diameter of filter disc

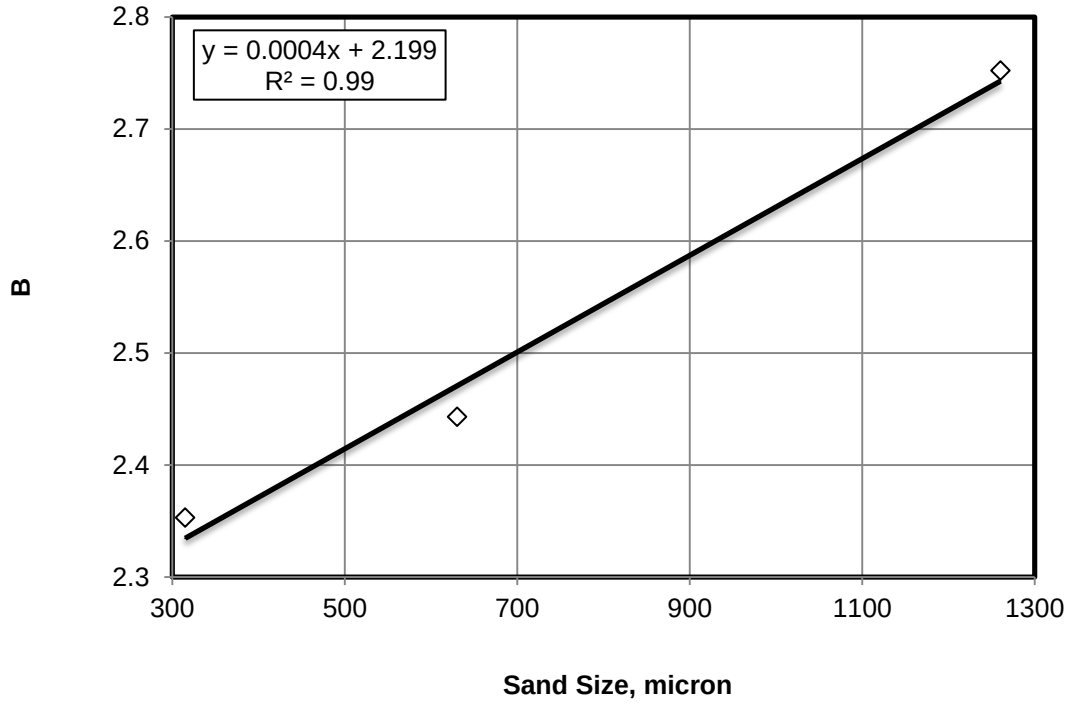

Fig. G.19: Linear function plot of B values at different sand sizes for 5 micron pore diameter of filter disc

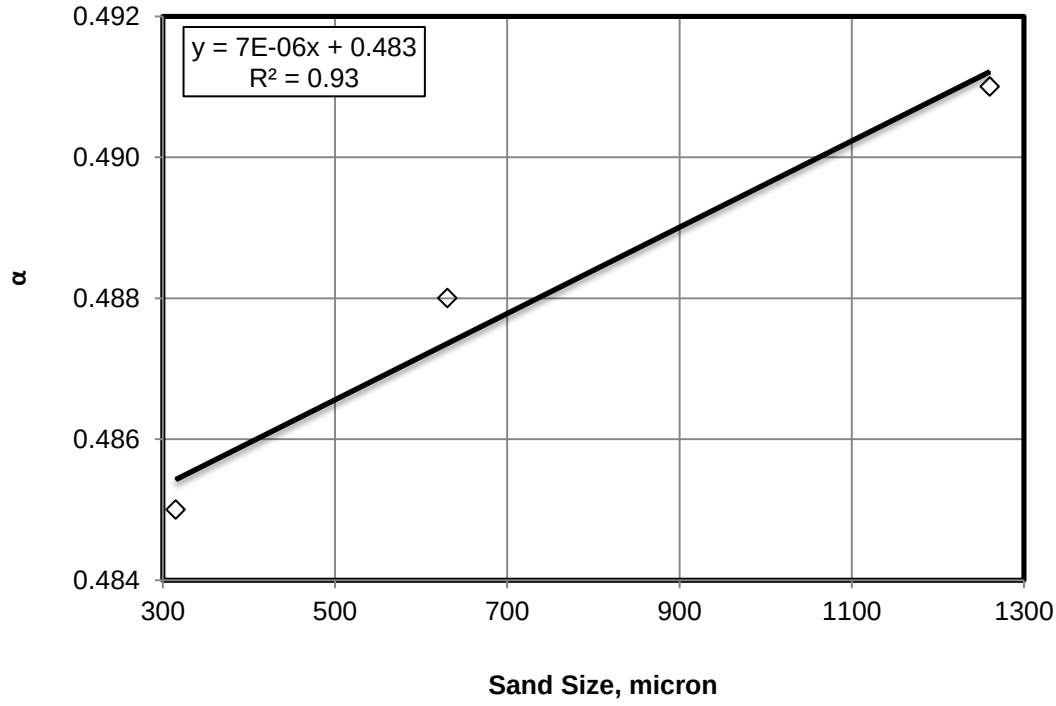

Fig. G.20: Linear function plot of α values at different sand sizes for 5 micron pore diameter of filter disc

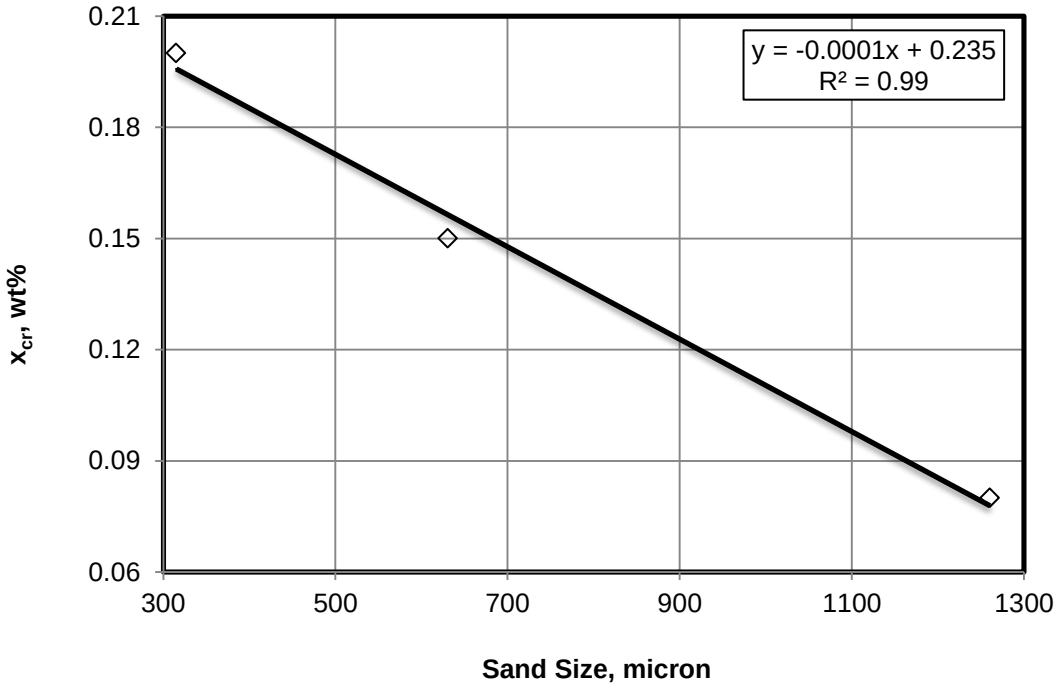

Fig. G.21: Linear function plot of x_{cr} values at different sand sizes for 5 micron pore diameter of filter disc

4- The values of a_1, b_1, a_2, b_2, a_3, and b_3 of Eq. 8.3 were plotted against pore diameter of filter disc and correlated as linear functions and substituted in Eq. 8.3 to develop general empirical correlation of fluid loss at any pore diameter of filter disc and sand size, as illustrated in Eq. 8.4.

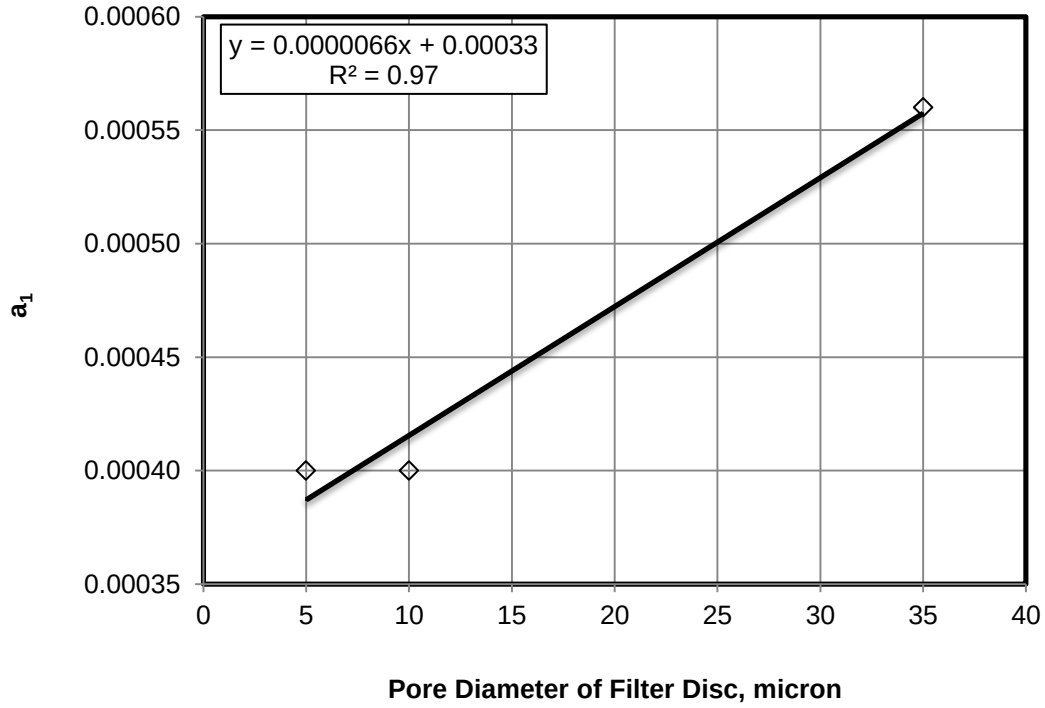

Fig. G.22: Linear function plot of a_1 at different pore diameters of filter discs

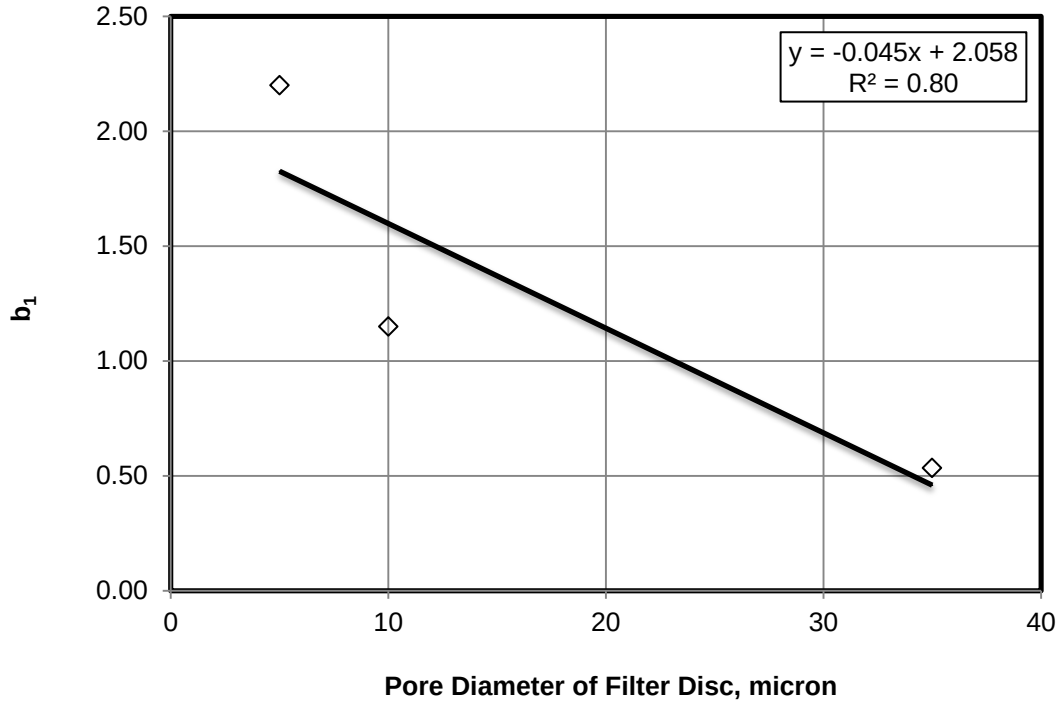

Fig. G.23: Linear function plot of b_1 at different pore diameters of filter discs

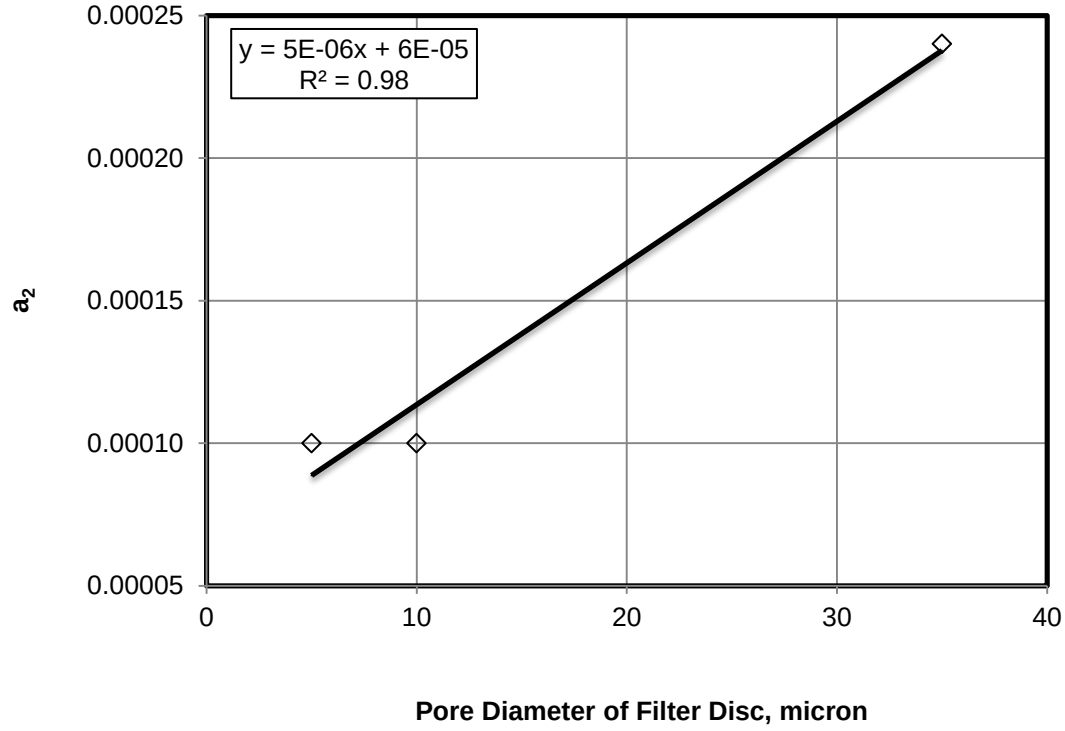

Fig. G.24: Linear function plot of a_2 at different pore diameters of filter discs

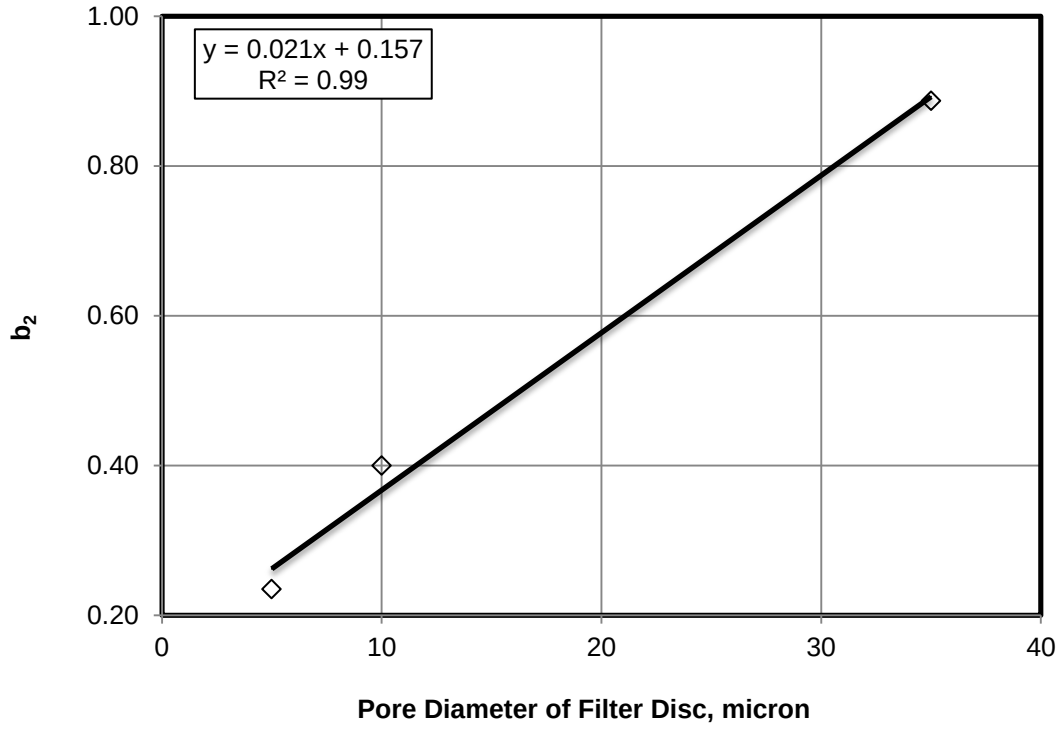

Fig. G.25: Linear function plot of b_2 at different pore diameters of filter discs

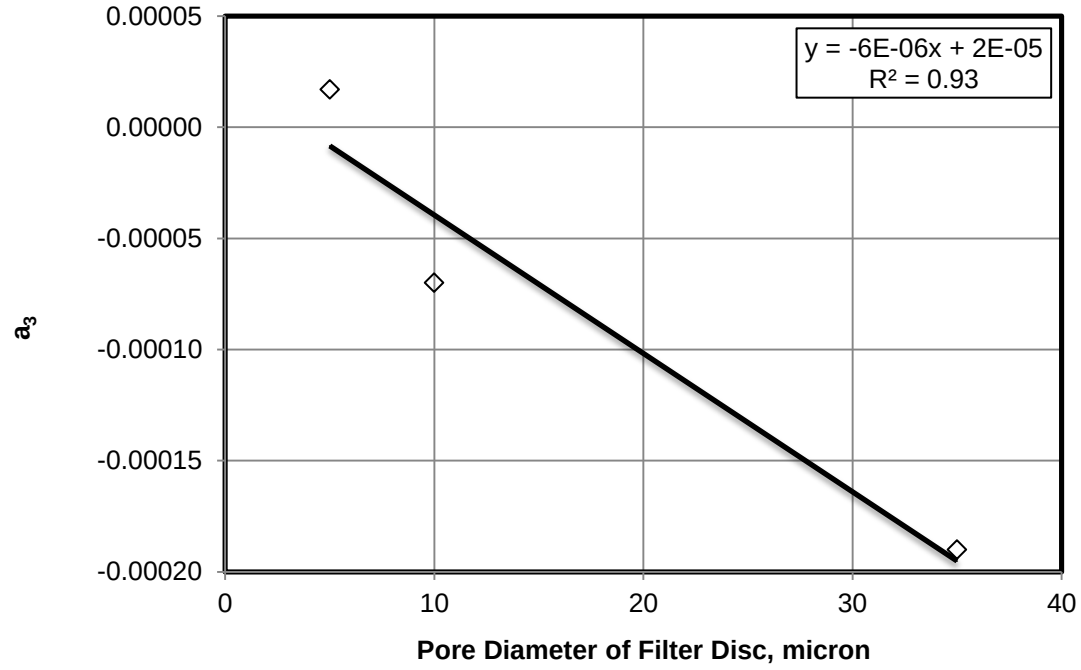

Fig. G.26: Linear function plot of a_3 at different pore diameters of filter discs

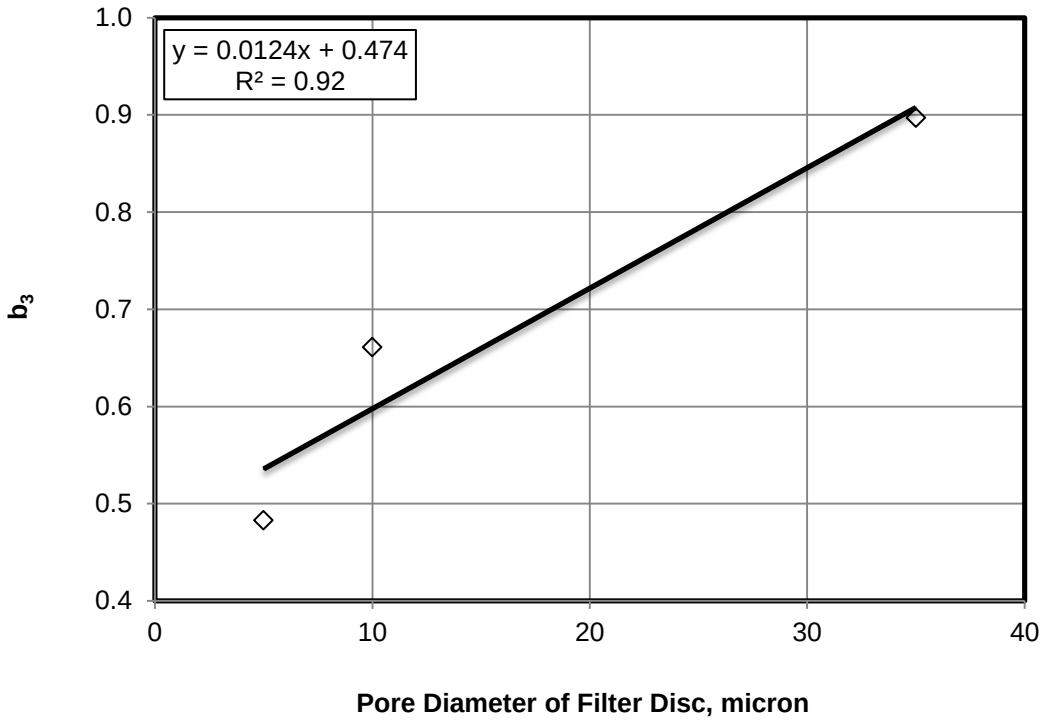

Fig. G.27: Linear function plot of b_3 at different pore diameters of filter discs

Appendix H: Correlation of critical silica flour concentration

The empirical correlation of critical silica flour concentration at any pore diameter of filter disc and sand size was developed as described in the following.

1- The values of critical silica flour concentration of same pore diameter of filter disc were plotted against sand size and correlated as linear function, as shown in Fig. H.1.

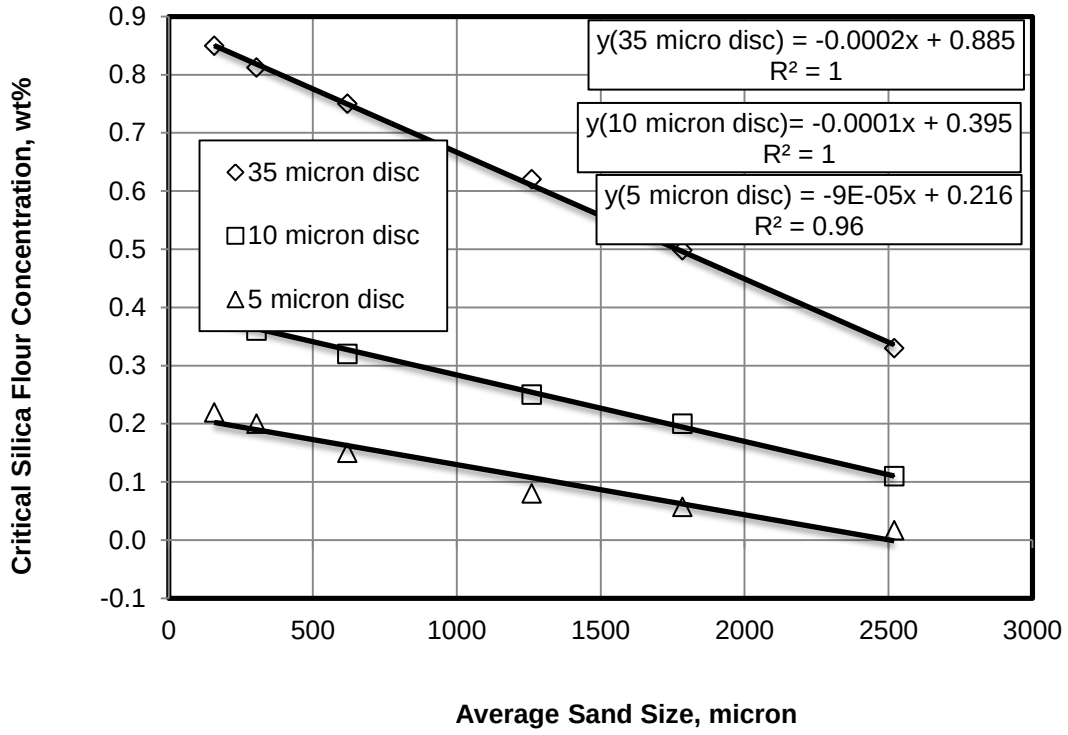

Fig. H.1: Correlate the critical silica flour concentrations for 35, 10, and 5 micron pore diameter of filter discs and different sand sizes

2- The values of A_s and B_s of the linear function of the critical silica flour concentration were plotted against the sand size and correlated as linear functions and substituted in the linear function of the critical silica flour concentration to develop general empirical correlation can be used at any pore diameter of filter disc and sand size, as shown in Eq. 8.5.

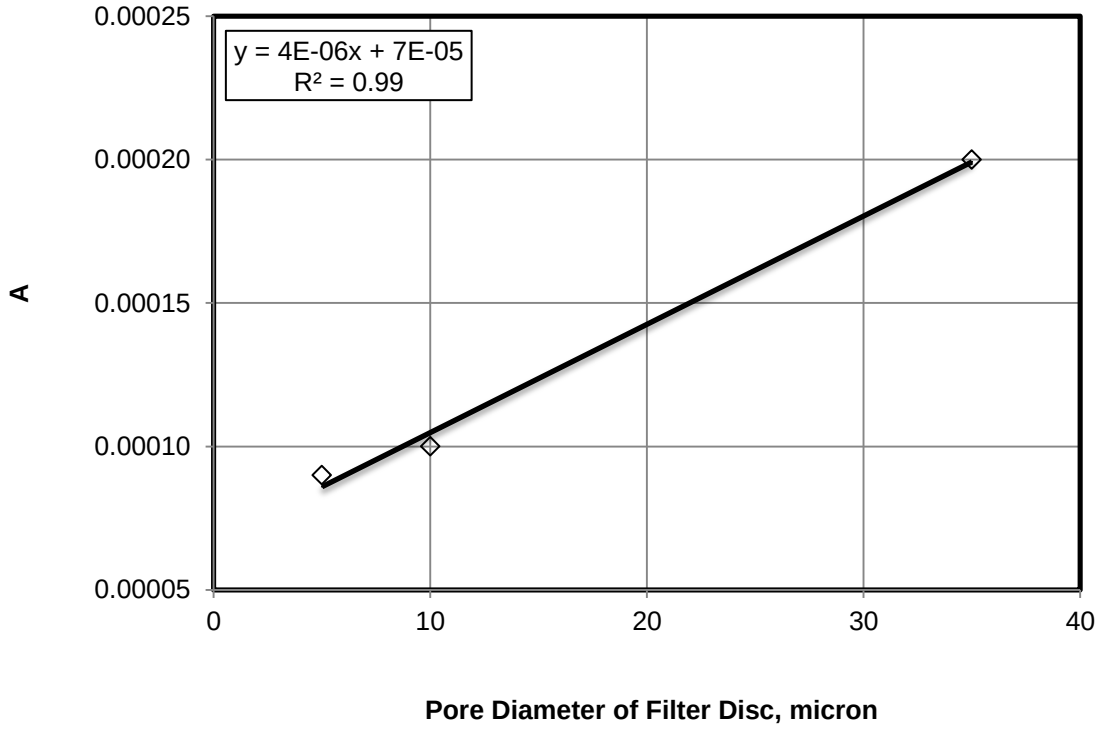

Fig. H.2: Linear function plot of A values at different pore diameter of filter discs

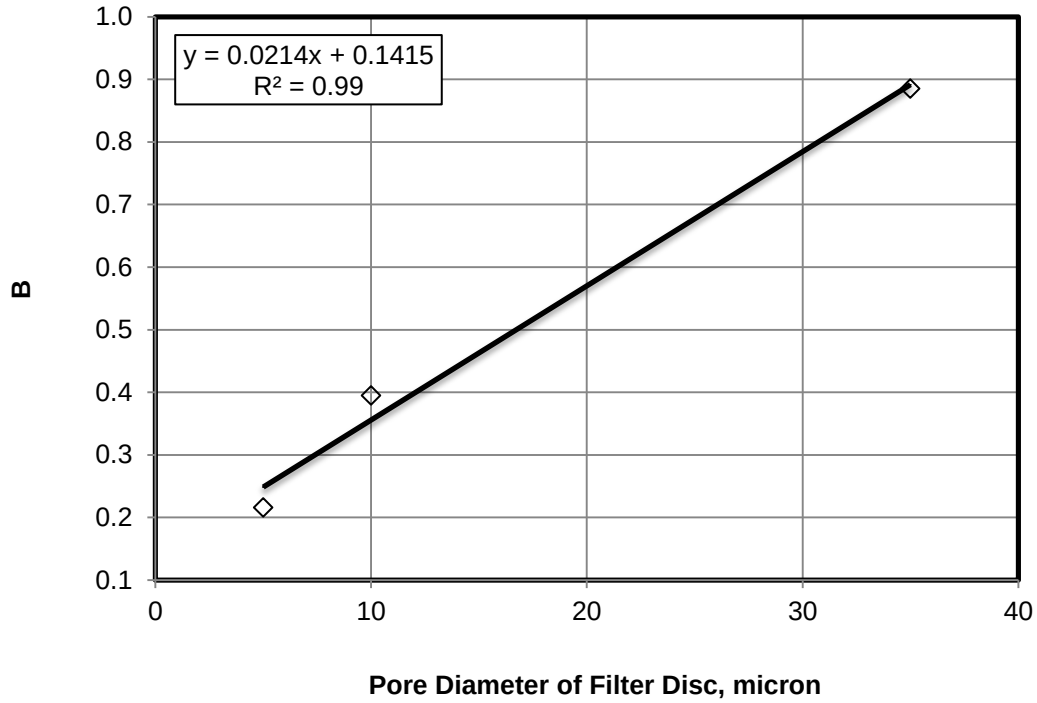

Fig. H.3: Linear function plot of B values at different pore diameter of filter discs

Appendix I: Correlation of the pressure initiate flow

The empirical correlation of pressure to initiate flow at any pore diameter of filter disc, sand size and silica flour concentration was developed as described in the following.

1- The experimental data of the pressure initiate flow was correlated with the critical silica flour concentration and relationships were developed for 35, 10, and 5 micron pore diameter of filter disc at different sand sizes, as shown in Figs. I.1 to I.3, by applying Eq. B-11 given in Appendix B.

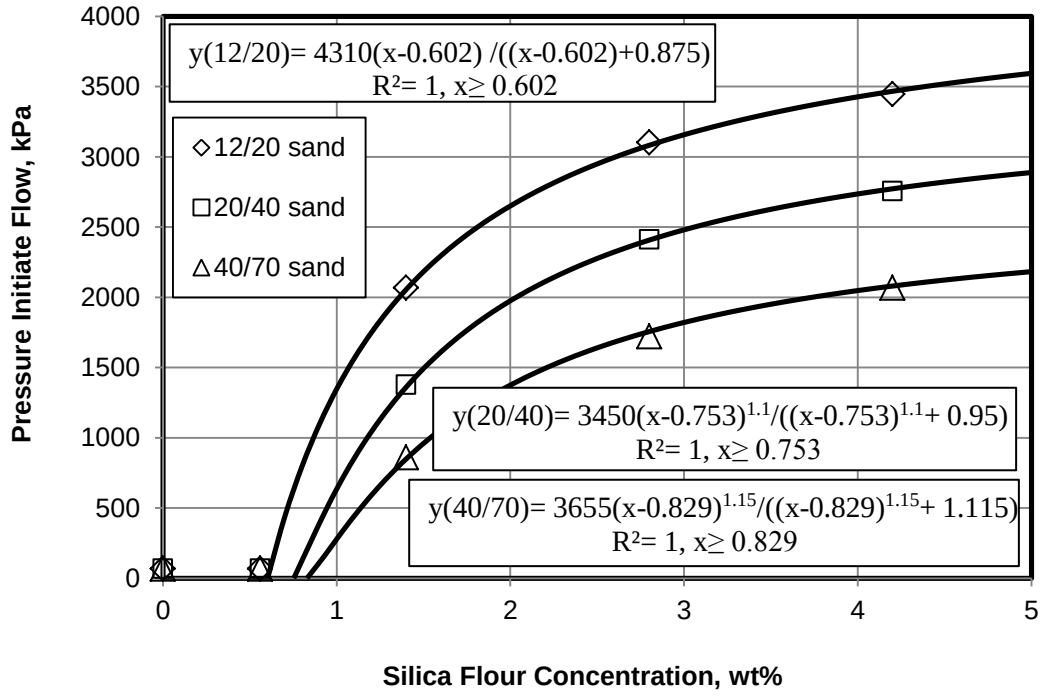

Fig. I.1: Correlate the experimental results of pressure initiate flow with the critical silica flour concentrations for 35 micron average pore diameter of filter disc and different sand sizes

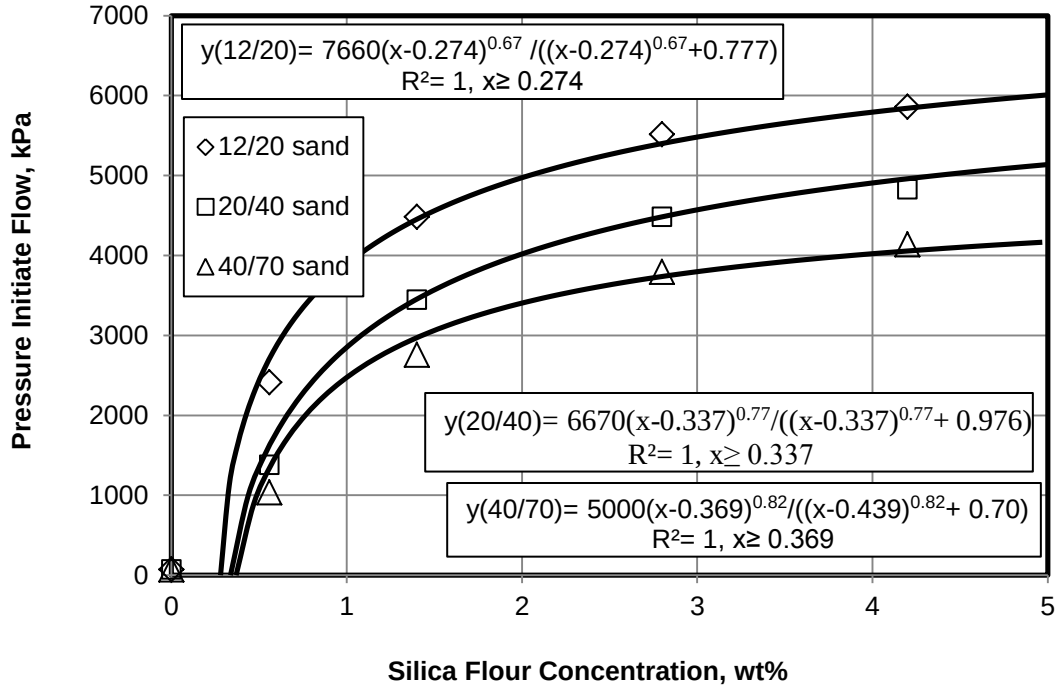

Fig. I.2: Correlate the experimental results of pressure initiate flow with the critical silica flour concentrations for 10 micron average pore diameter of filter disc and different sand sizes

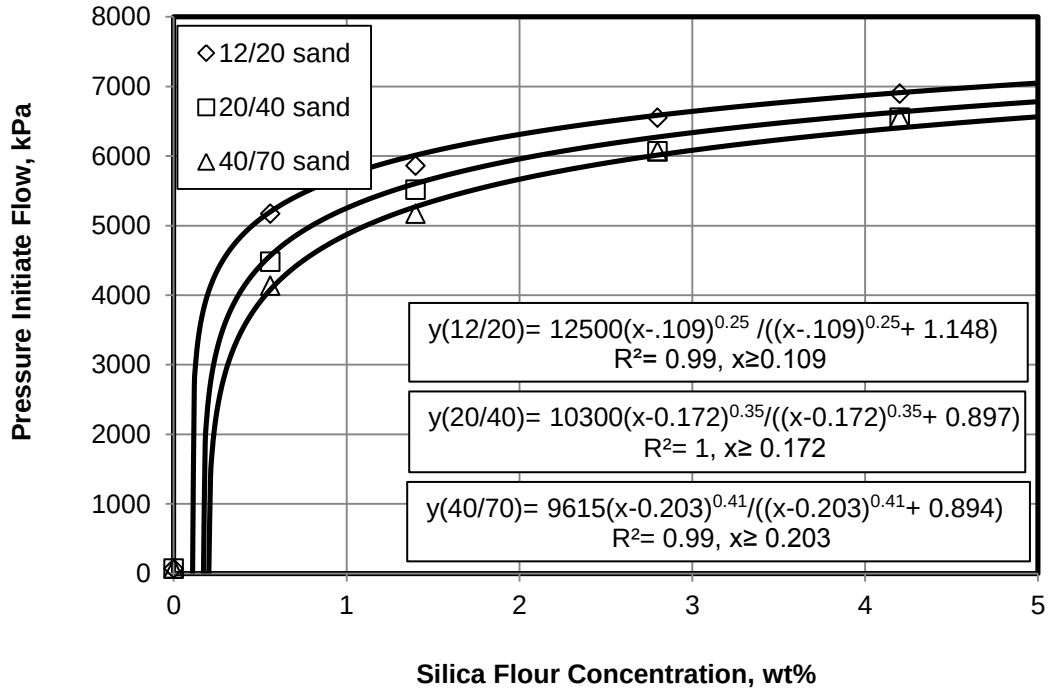

Fig. I.3: Correlate the experimental results of pressure initiate flow with the critical silica flour concentrations for 5 micron average pore diameter of filter disc and different sand size

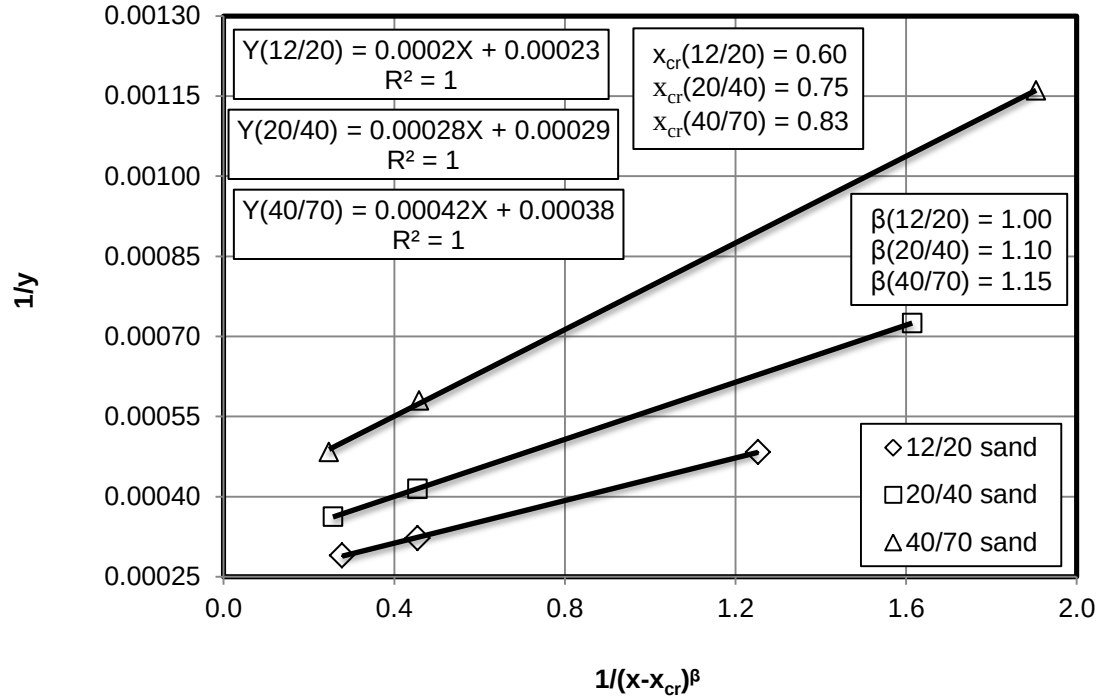

Fig. I.4: Straight line plot of Eq. B-11 to develop the relationship of the pressure initiate flow at different silica flour concentration for 35 micron pore diameter of filter disc at different sand sizes, as shown in Fig. I.1

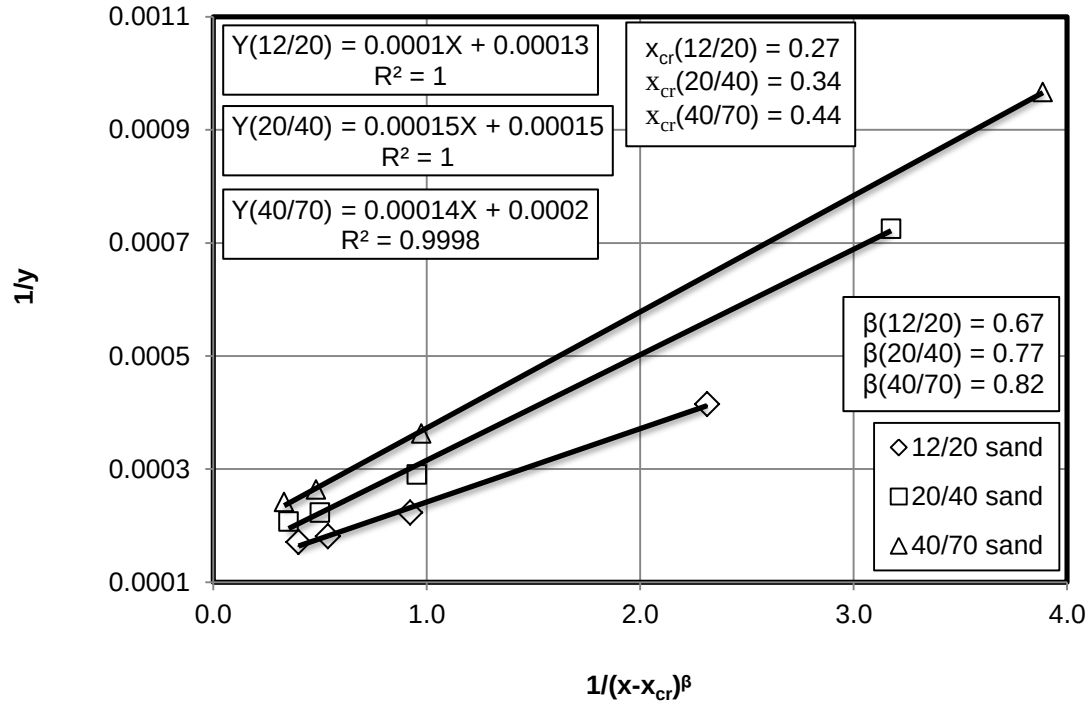

Fig. I.5: Straight line plot of Eq. B-11 to develop the relationship of the pressure initiate flow at different silica flour concentration for 10 micron pore diameter of filter disc at different sand sizes, as shown in Fig. I.2

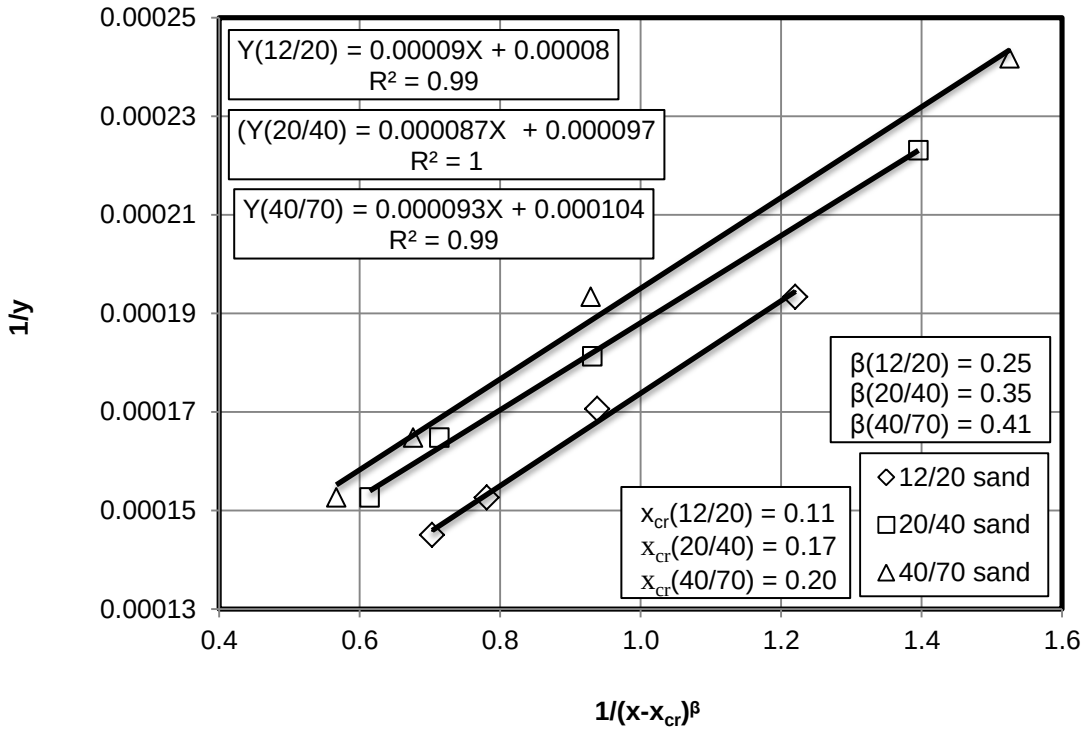

Fig. I.6: Straight line plot of Eq. B-11 to develop the relationship of the pressure initiate flow at different silica flour concentration for 5 micron pore diameter of filter disc at different sand sizes, as shown in Fig. I.3

2- The values of A, B, and α of the relationships were plotted and correlated as linear functions and substituted in Eq. 8.6 to develop charts of pressure to initiate flow for same pore diameter of filter disc and different sand sizes, as shown in Figs. 8.9 to 8.11.

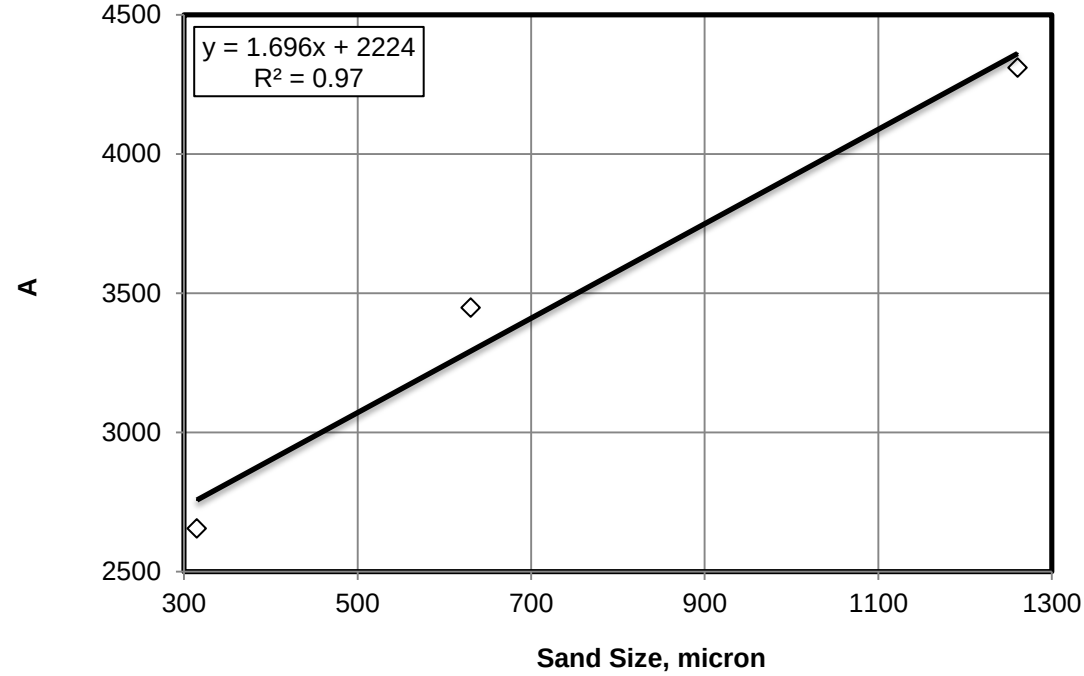

Fig. I.7: Linear function plot of A values at different sand sizes for 35 micron pore diameter of filter disc

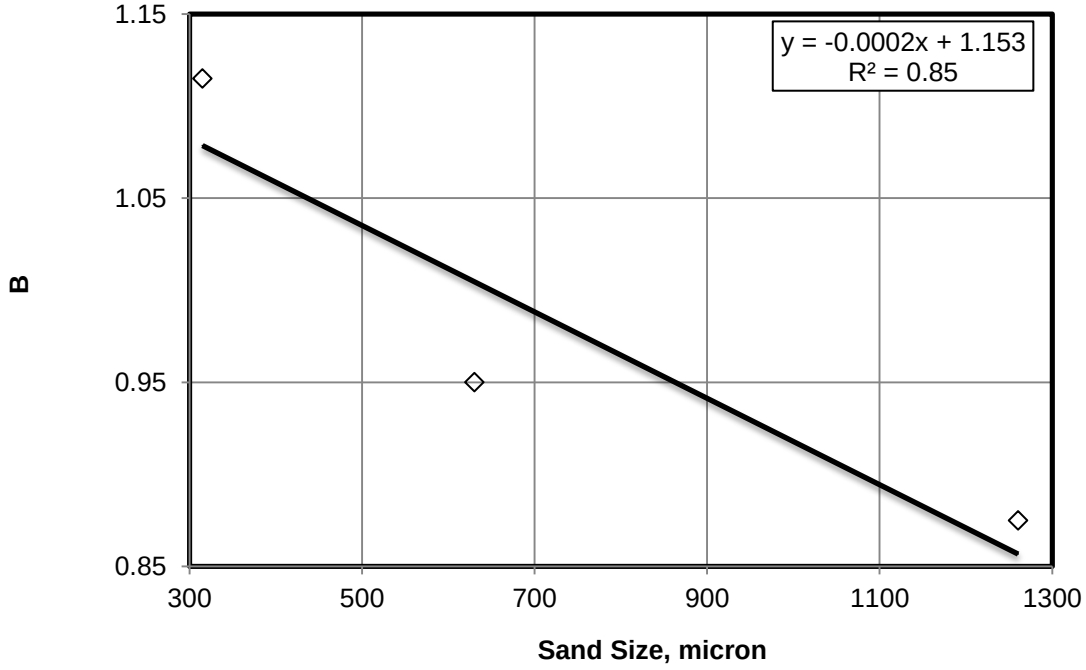

Fig. I.8: Linear function plot of B values at different sand sizes for 35 micron pore diameter of filter disc

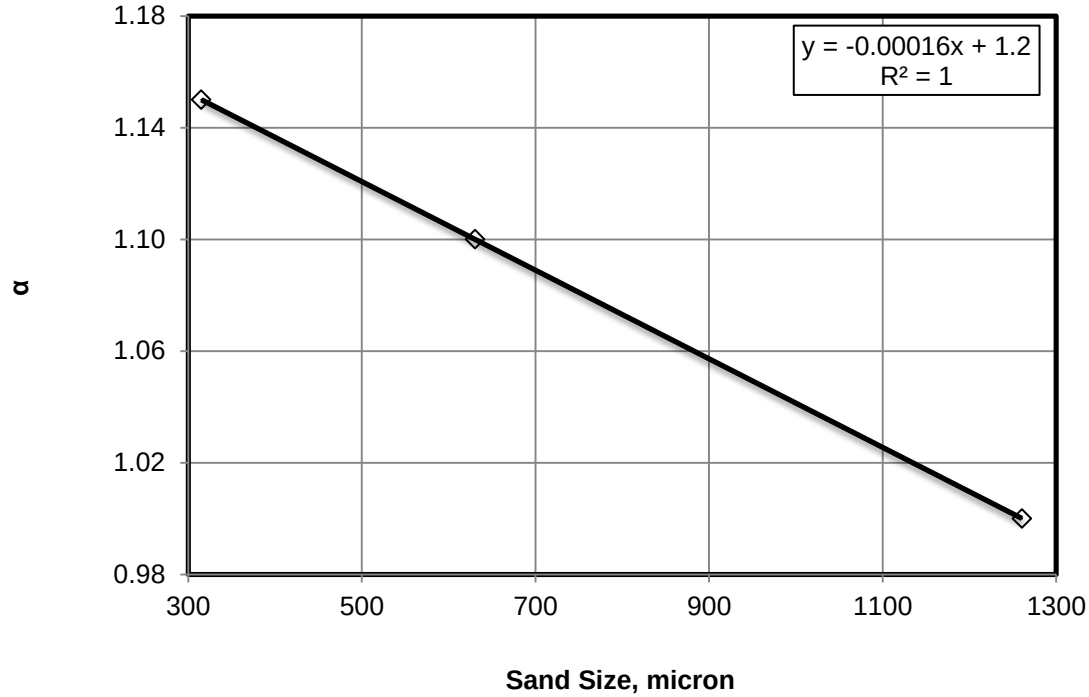

Fig. I.9: Linear function plot of α values at different sand sizes for 35 micron pore diameter of filter disc

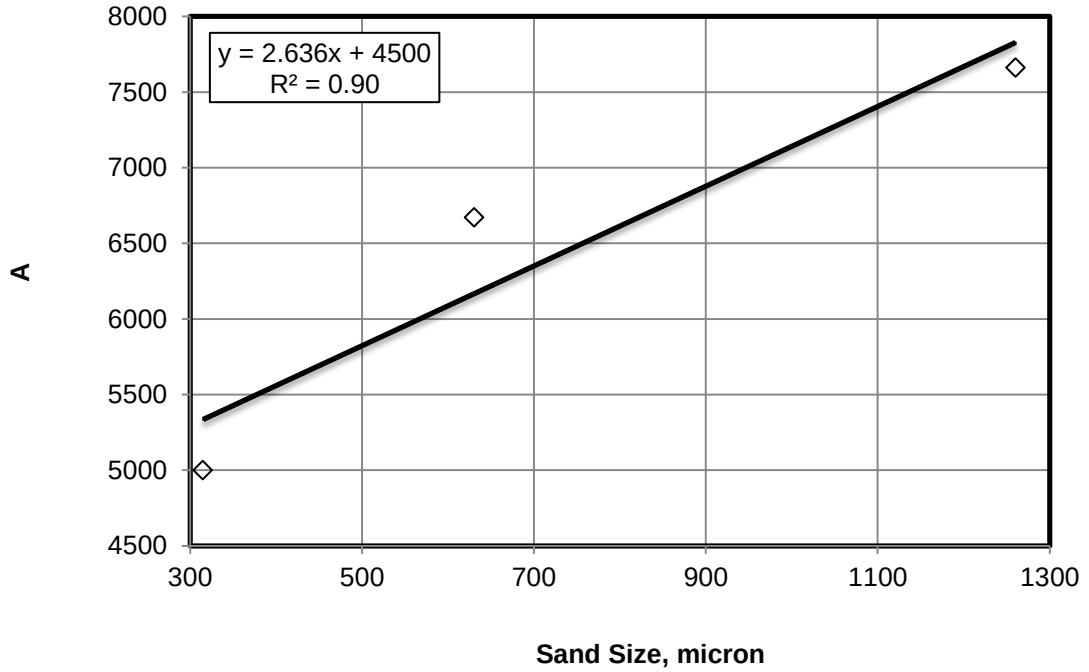

Fig. I.10: Linear function plot of A values at different sand sizes for 10 micron pore diameter of filter disc

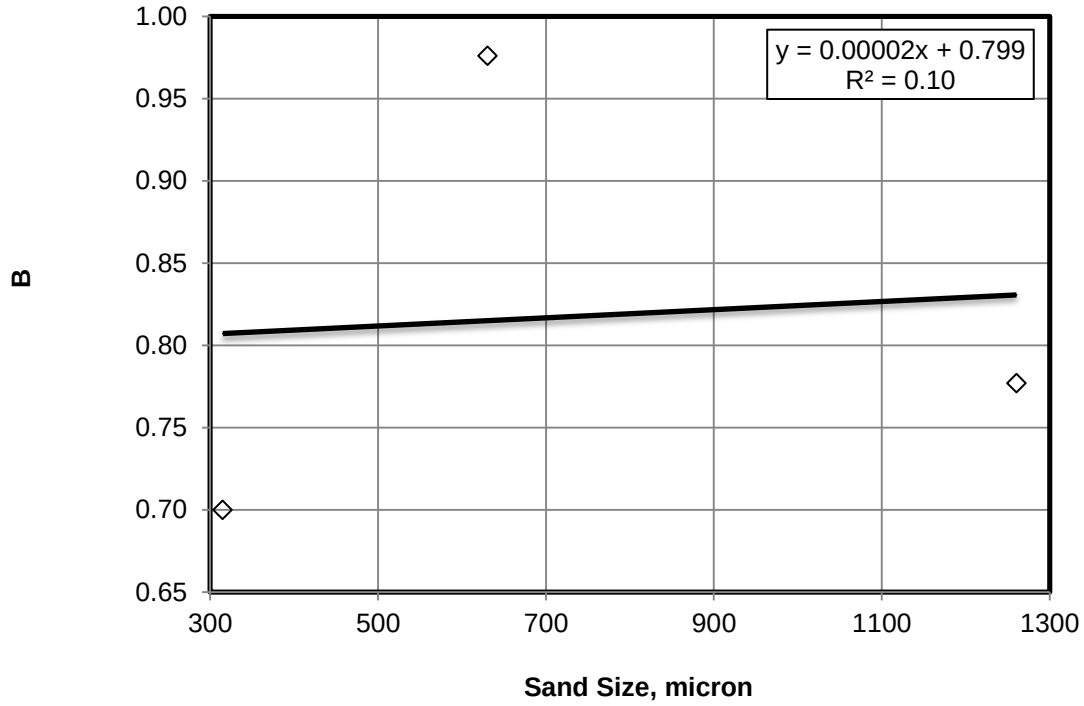

Fig. I.11: Linear function plot of B values at different sand sizes for 10 micron pore diameter of filter disc

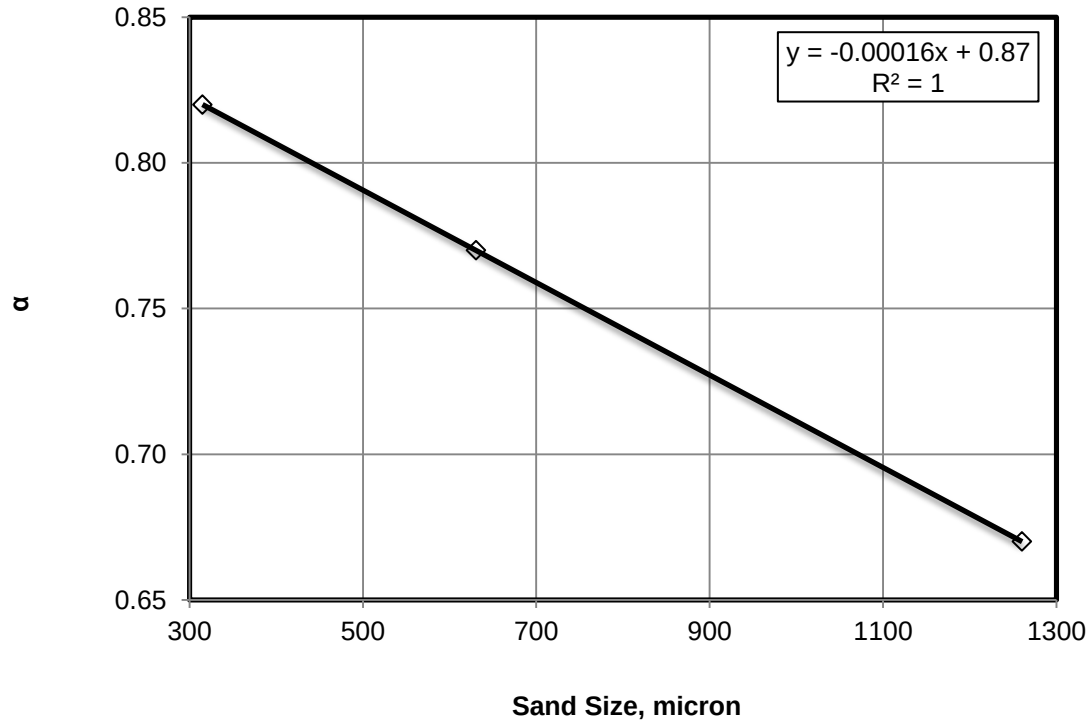

Fig. I.12: Linear function plot of α values at different sand sizes for 10 micron pore diameter of filter disc

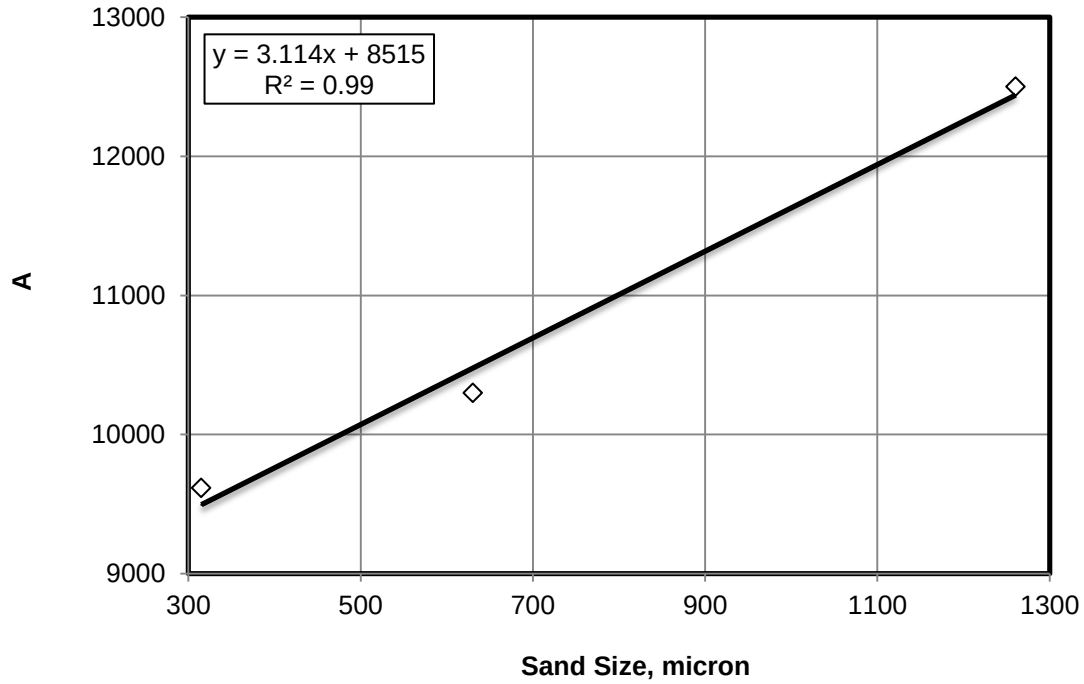

Fig. I.13: Linear function plot of A values at different sand sizes for 5 micron pore diameter of filter disc

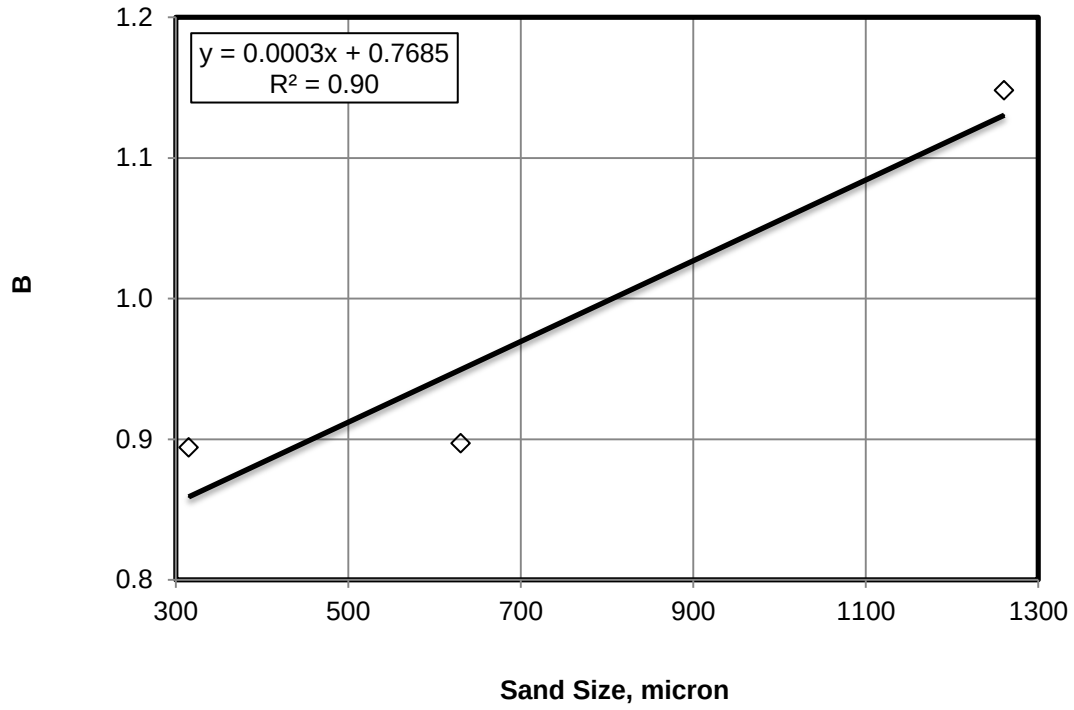

Fig. I.14: Linear function plot of B values at different sand sizes for 5 micron pore diameter of filter disc

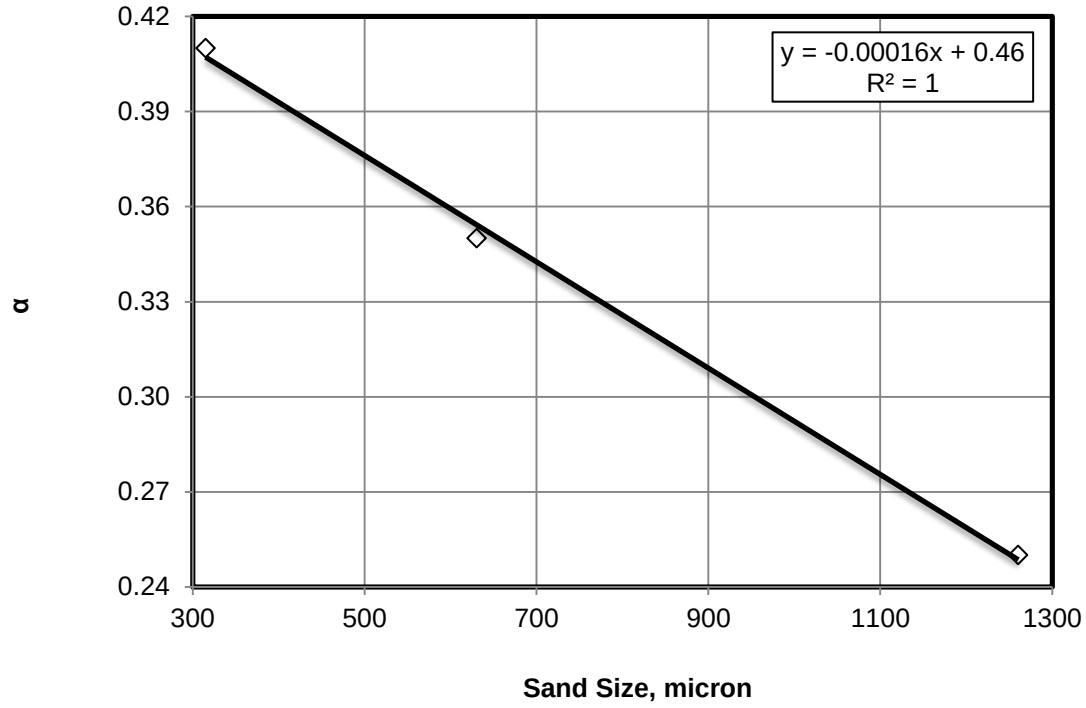

Fig. I.15: Linear function plot of α values at different sand sizes for 5 micron pore diameter of filter disc

3- The values of a_1, b_1, a_2, b_2, a_3, and b_3 of Eq. 8.7 were plotted against pore diameter of filter disc and correlated as linear functions and substituted in Eq. 8.7 to develop general empirical correlation of fluid loss at any pore diameter of filter disc and sand size, according to Eq. 8.8.

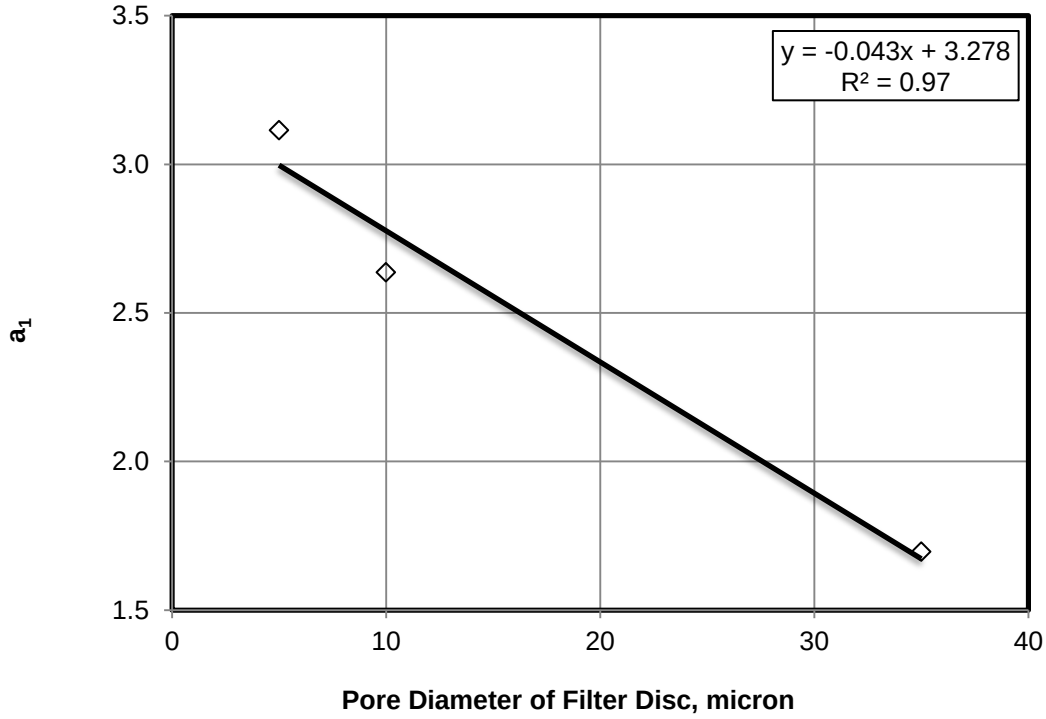

Fig. I.16: Linear function plot of a_1 at different pore diameters of filter discs

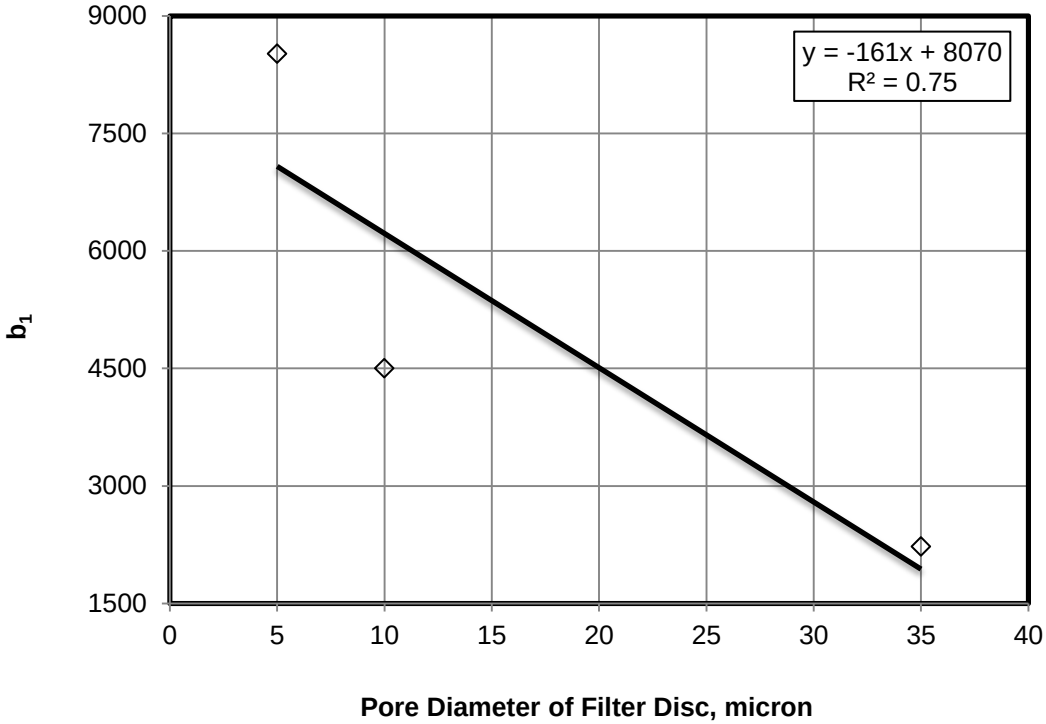

Fig. I.17: Linear function plot of b_1 at different pore diameters of filter discs

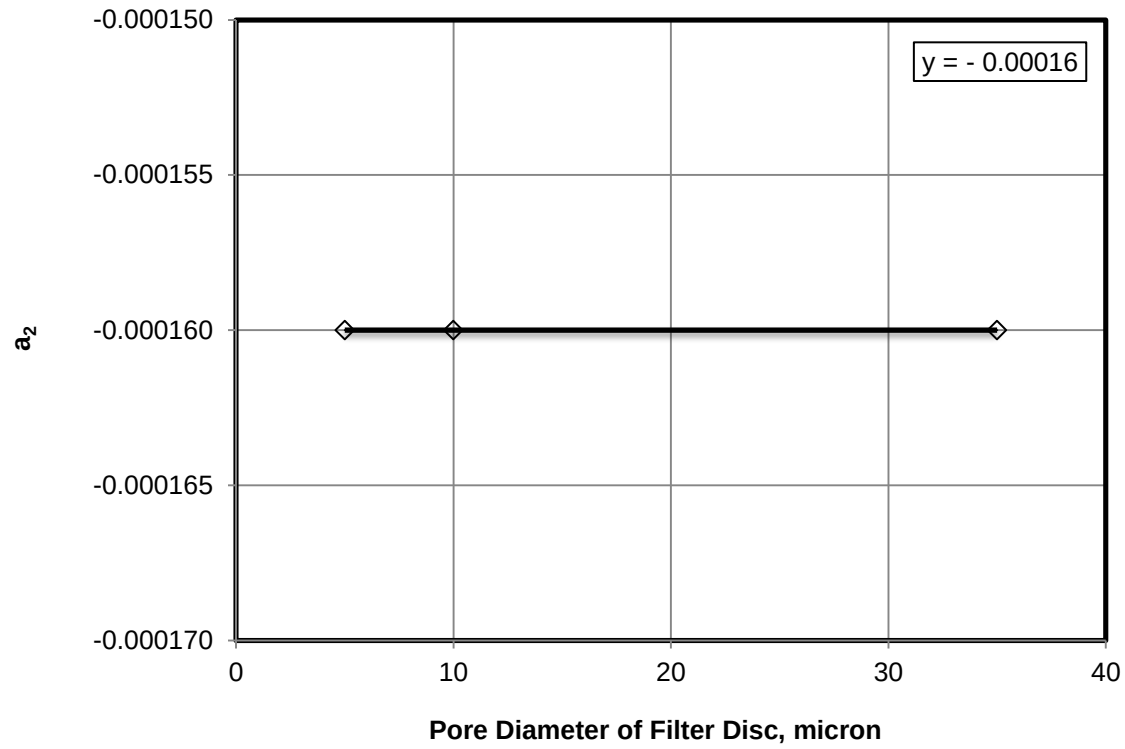

Fig. I.18: Linear function plot of a_2 at different pore diameters of filter discs

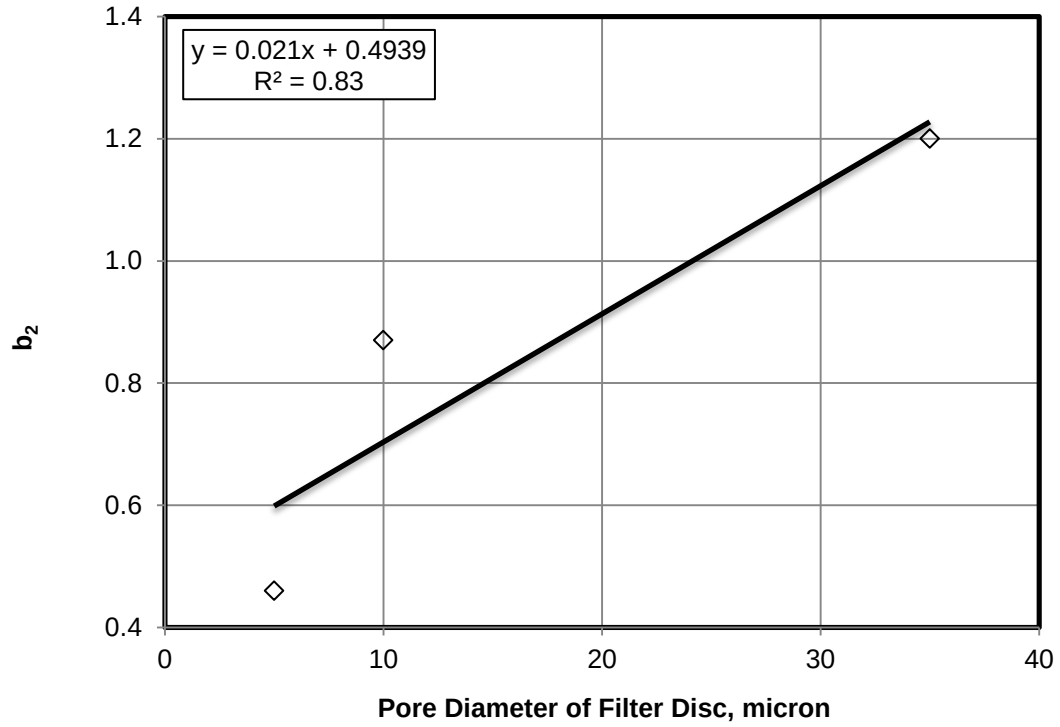

Fig. I.19: Linear function plot of b_2 at different pore diameters of filter discs

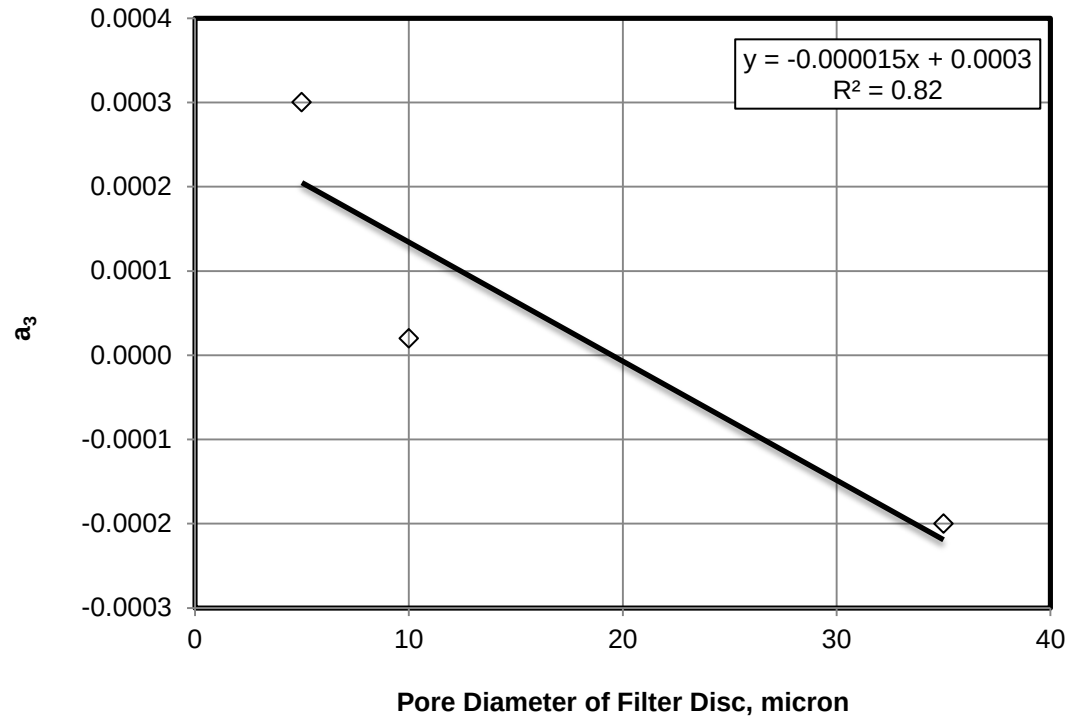

Fig. I.20: Linear function plot of a_3 at different pore diameters of filter discs

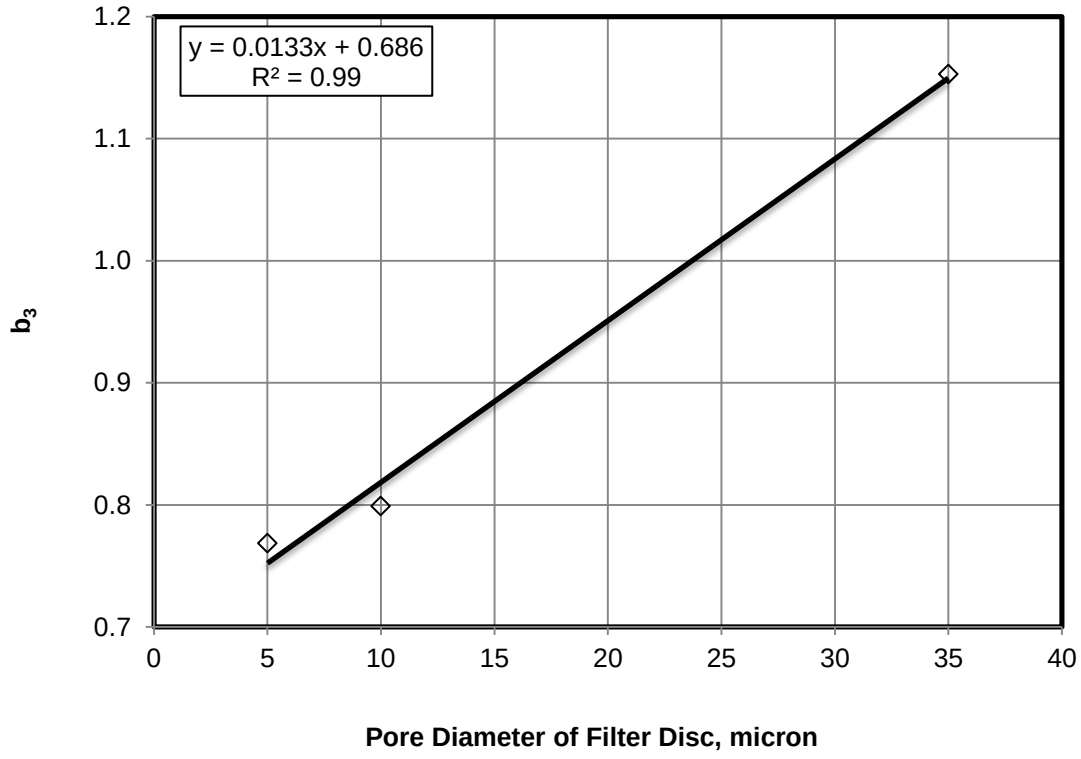

Fig. I.21: Linear function plot of b_3 at different pore diameters of filter discs

Appendix J: Correlation of the filtrate volume

The experimental data of the filtrate volume of the silica flour particle-gel system were correlated with the filtrate time and empirical correlations were developed for 35, 10, and 5 micron pore diameter of filter disc, 12/20, 20/40, and 40/70 sand mesh, and different silica flour concentrations, as shown in Figs. 9.1 to 9.3 and 9.6 to 9.11, by applying Eq. B-6 given in Appendix B.

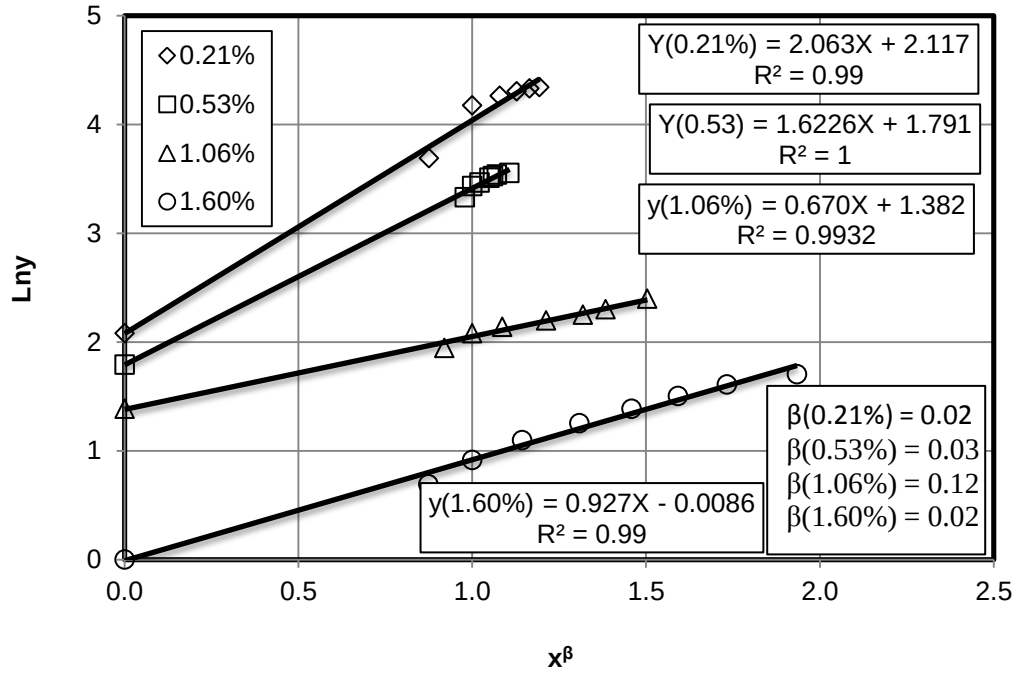

Fig. J.1: Straight line plot of Eq. B-6 to develop the exponential relationship of the filtrate volume at different silica flour concentration for 35 micron pore diameter of filter disc and 12/20 sand mesh, as shown in Fig. 9.1

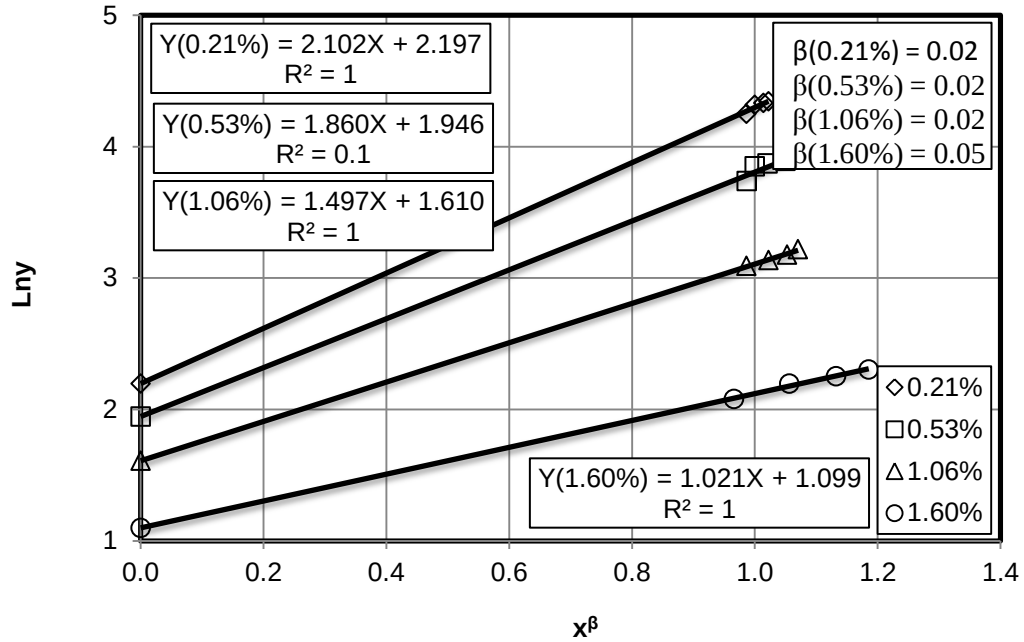

Fig. J.2: Straight line plot of Eq. B-6 to develop the exponential relationship of the filtrate volume at different silica flour concentration for 35 micron pore diameter of filter disc and 20/40 sand mesh, as shown in Fig. 9.2

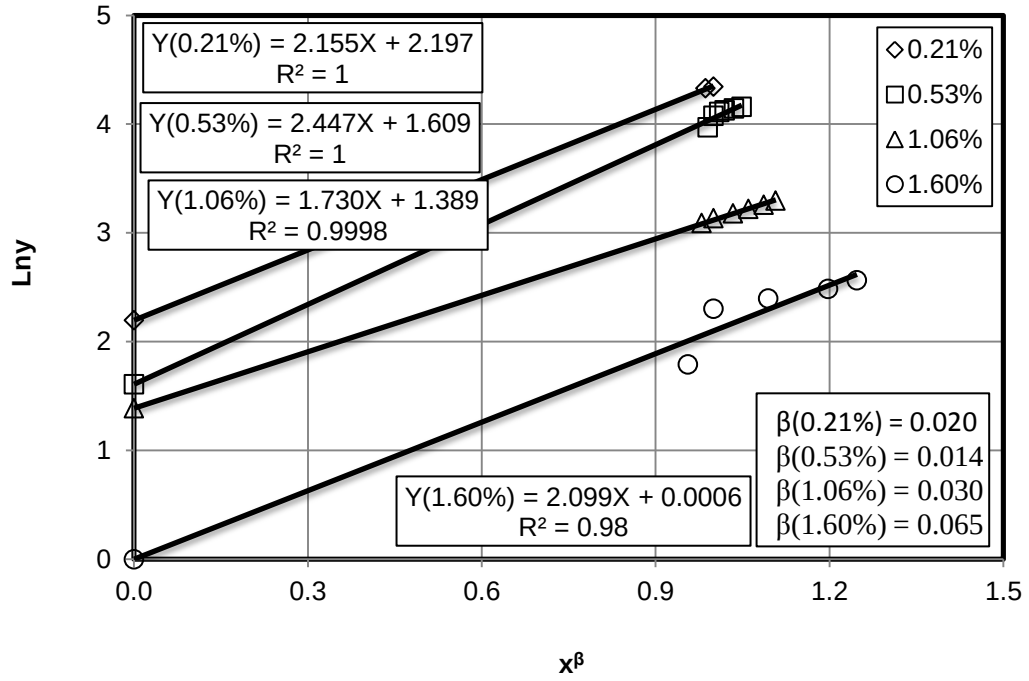

Fig. J.3: Straight line plot of Eq. B-6 to develop the exponential relationship of the filtrate volume at different silica flour concentration for 35 micron pore diameter of filter disc and 40/70 sand mesh, as shown in Fig. 9.3

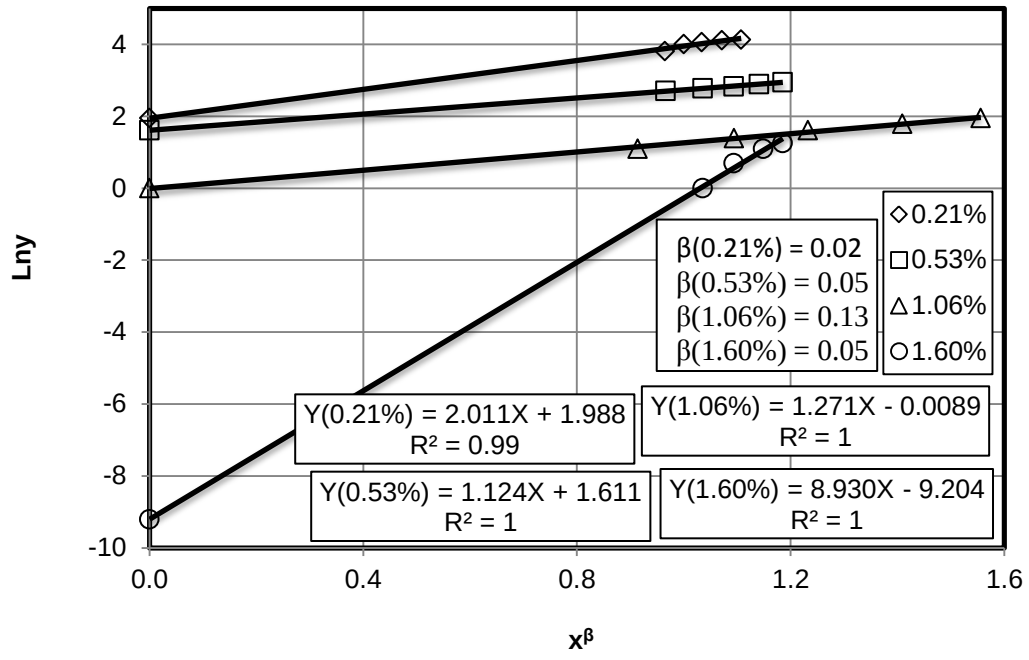

Fig. J.4: Straight line plot of Eq. B-6 to develop the exponential relationship of the filtrate volume at different silica flour concentration for 10 micron pore diameter of filter disc and 12/20 sand mesh, as shown in Fig. 9.6

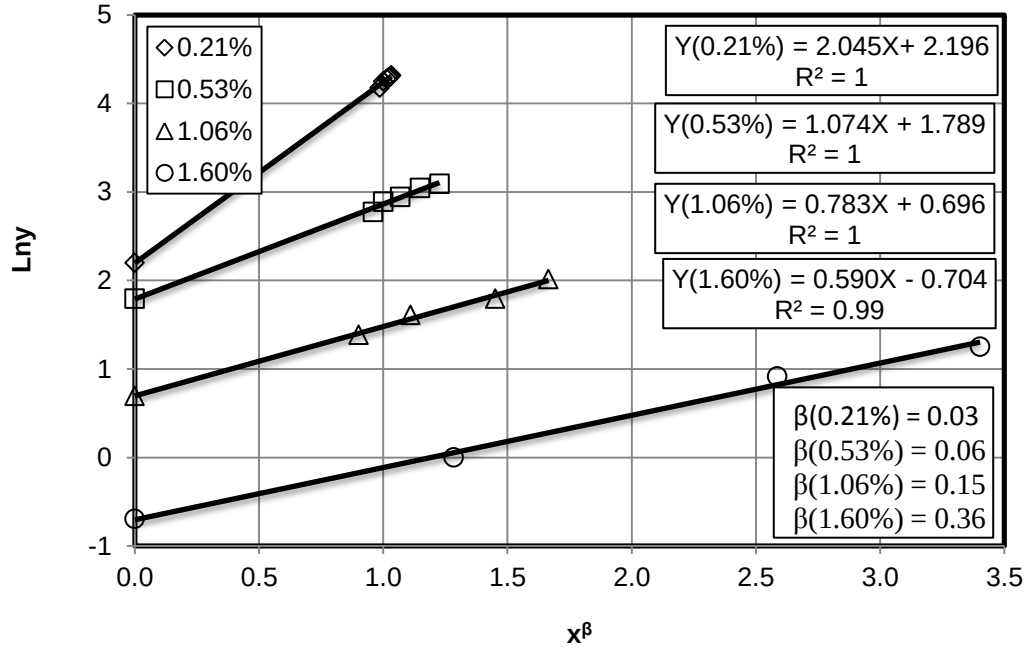

Fig. J.5: Straight line plot of Eq. B-6 to develop the exponential relationship of the filtrate volume at different silica flour concentration for 10 micron pore diameter of filter disc and 20/40 sand mesh, as shown in Fig. 9.7

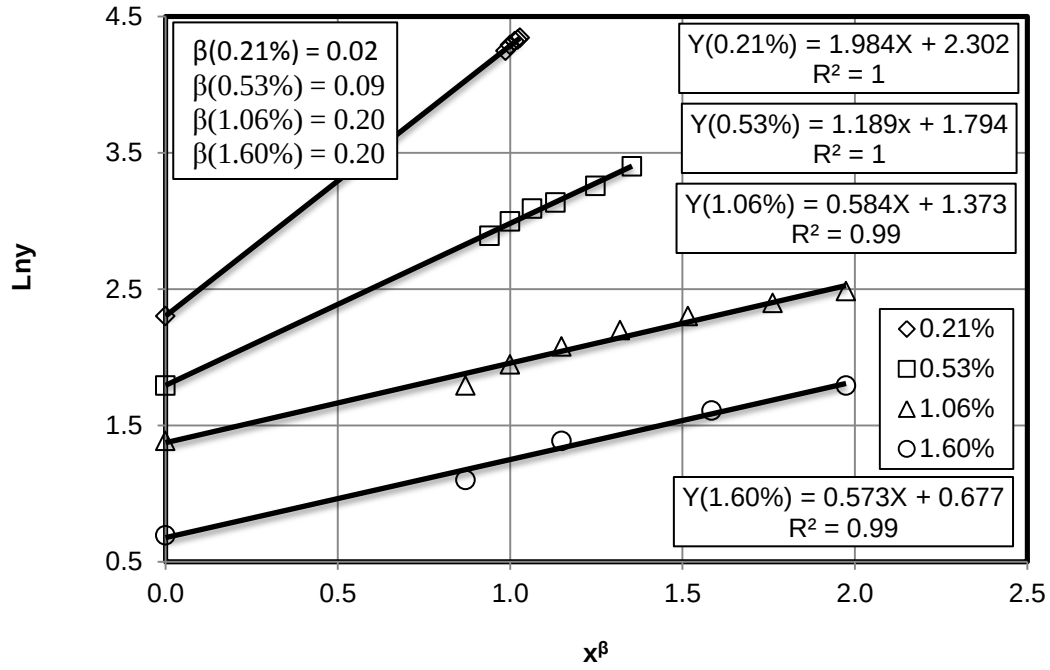

Fig. J.6: Straight line plot of Eq. B-6 to develop the exponential relationship of the filtrate volume at different silica flour concentration for 10 micron pore diameter of filter disc and 40/70 sand mesh, as shown in Fig. 9.8

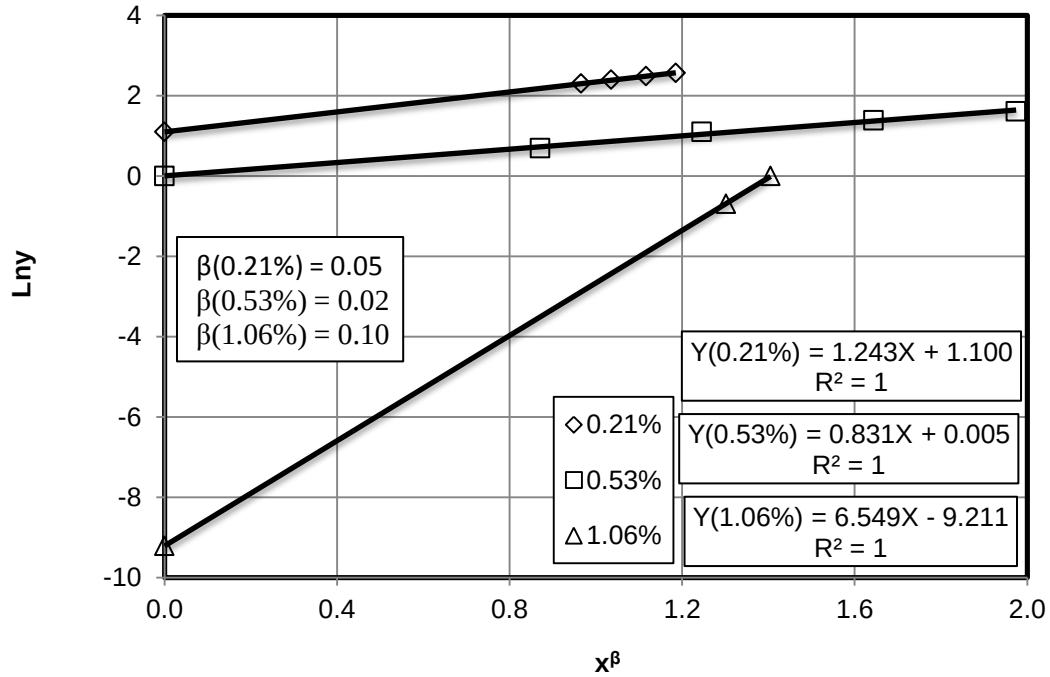

Fig. J.7: Straight line plot of Eq. B-6 to develop the exponential relationship of the filtrate volume at different silica flour concentration for 5 micron pore diameter of filter disc and 12/20 sand mesh, as shown in Fig. 9.9

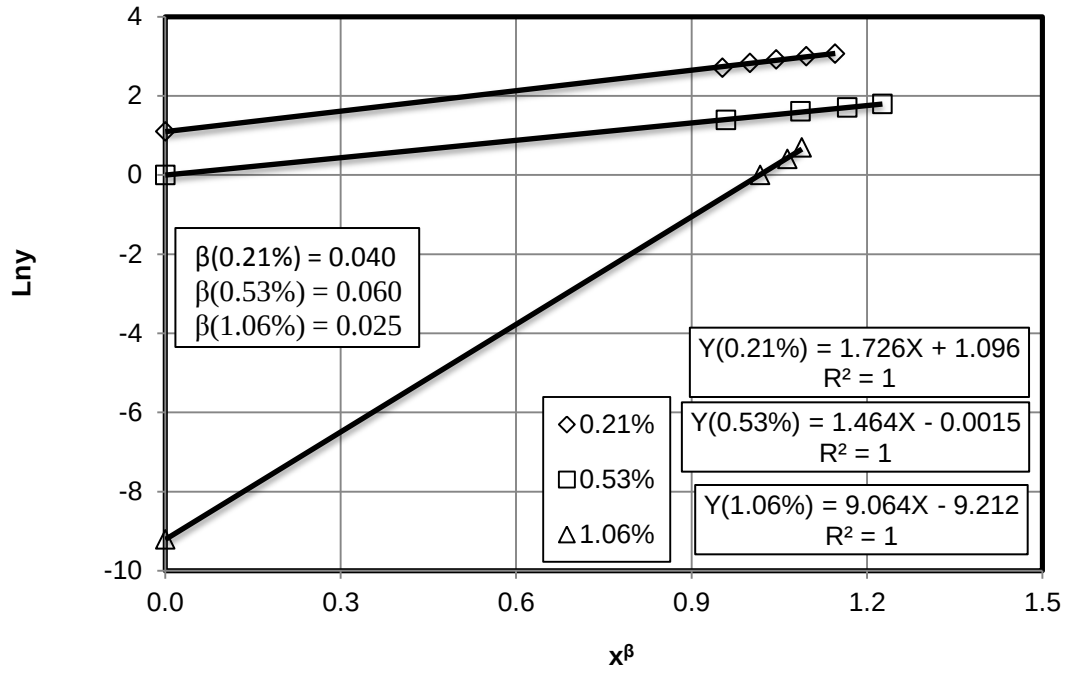

Fig. J.8: Straight line plot of Eq. B-6 to develop the exponential relationship of the filtrate volume at different silica flour concentration for 5 micron pore diameter of filter disc and 20/40 sand mesh, as shown in Fig. 9.10

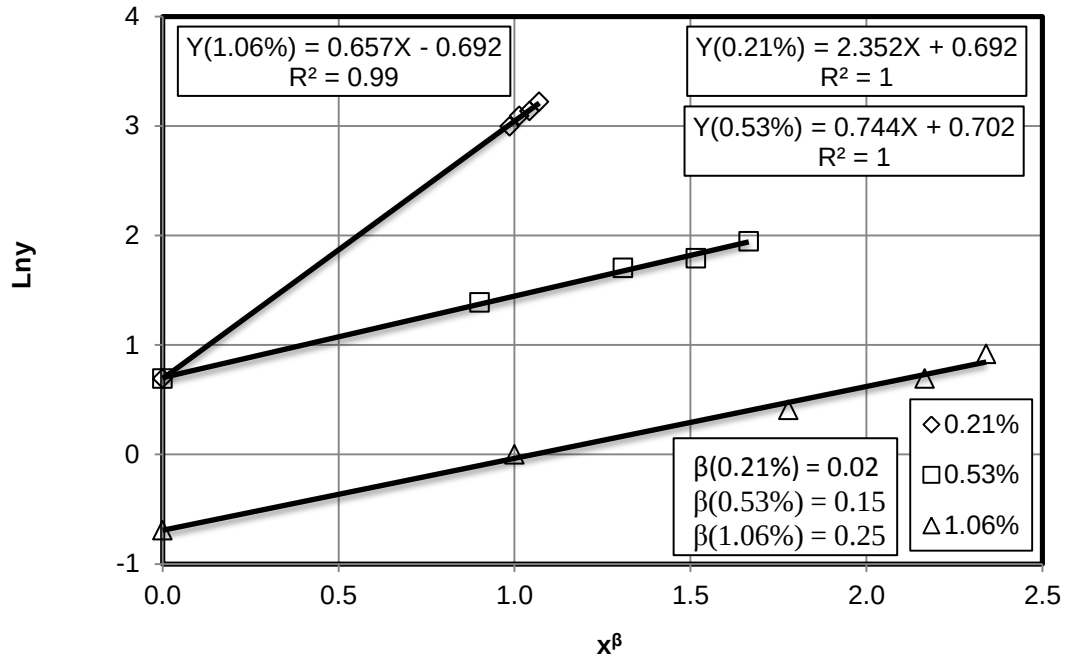

Fig. J.9: Straight line plot of Eq. B-6 to develop the exponential relationship of the filtrate volume at different silica flour concentration for 5 micron pore diameter of filter disc and 40/70 sand mesh, as shown in Fig. 9.11

Appendix K: Correlation of the rate constant of filtrate and spurt loss volume

The exponential correlations of the rate constant of filtrate and spurt loss volume of the silica flour particle-gel system were developed by the following steps:

1- The rate constant of filtrate were correlated with the silica flour concentration at different sand sizes and 35 micron pore diameter of filter disc and exponential correlations were developed, as shown in Figs. K.1 and K.2, by applying Eq. B-6 given in Appendix B.

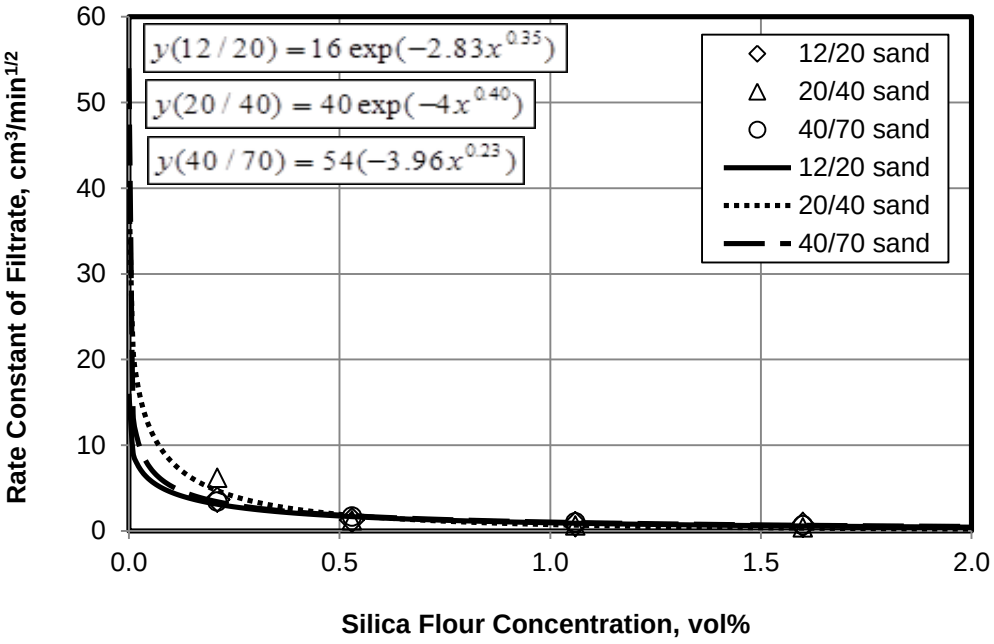

Fig. K.1: The relationship between rate constant of filtrate and silica flour concentration at 35 micron pore diameter filter disc and different sand sizes

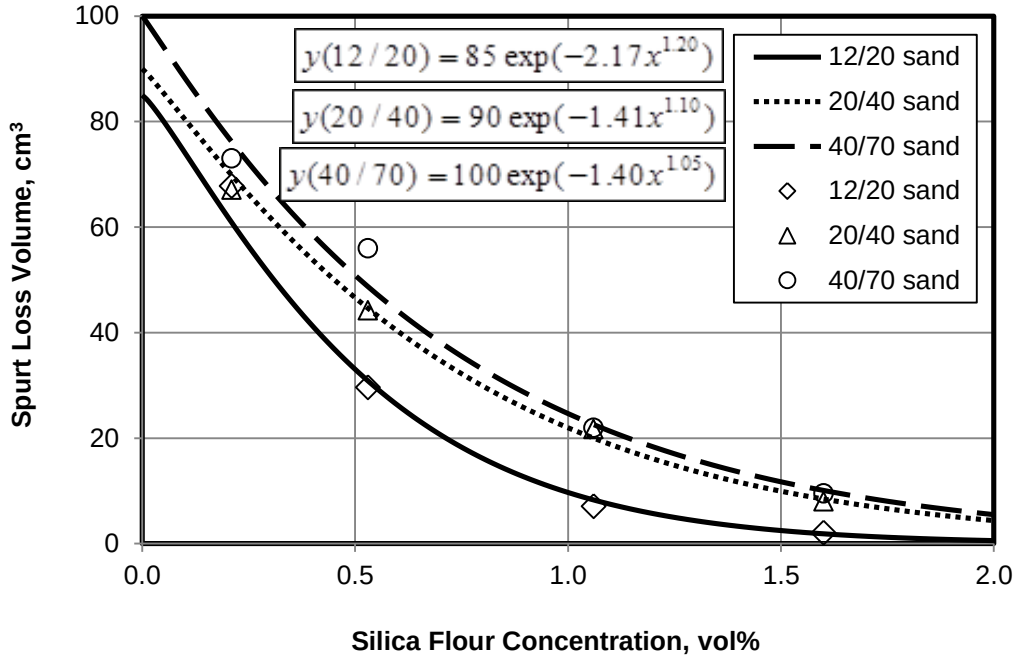

Fig. K.2: The relationship between spurt loss volume and silica flour concentration at 35 micron pore diameter filter disc and different sand size

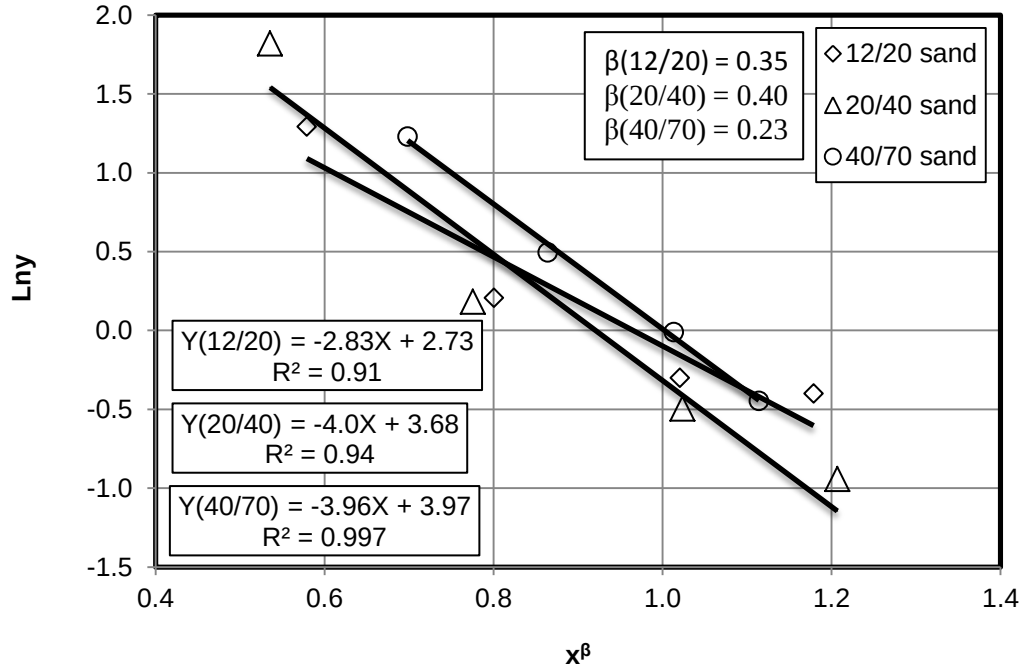

Fig. K.3: Straight line plot of Eq. B-6 at 35 micron pore diameter of filter disc to develop the exponential correlation of the rate constant of filtrate of different sand sizes, as shown in Fig. K.1

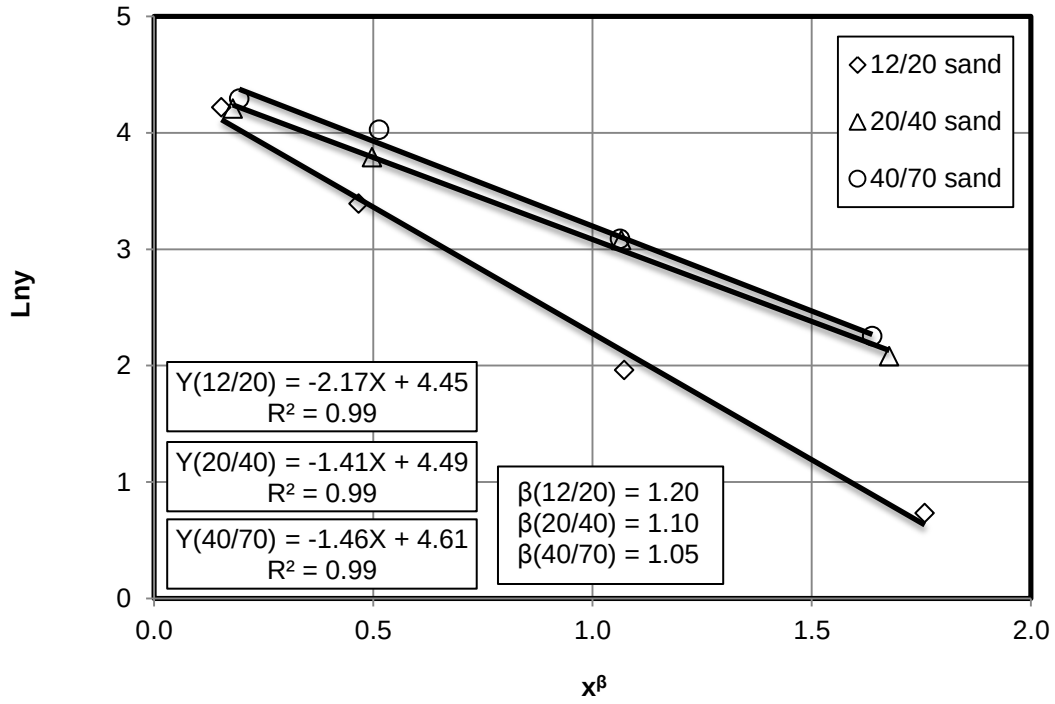

Fig. K.4: Straight line plot of Eq. B-6 at 35 micron pore diameter of filter disc to develop the exponential correlation of the spurt loss volume of sand sizes, as shown in Fig. K.2

2- The values of A,B, and β of the correlations in Figs. K.1 and K.2 were plotted and correlated as linear functions and substituted in Eq. 6.7 to develop correlations of rate constant of filtrate and spurt loss volume of the silica flour particle-gel system at 35 micron pore diameter of filter disc, as shown in Figs. 9.22 and 9.23.

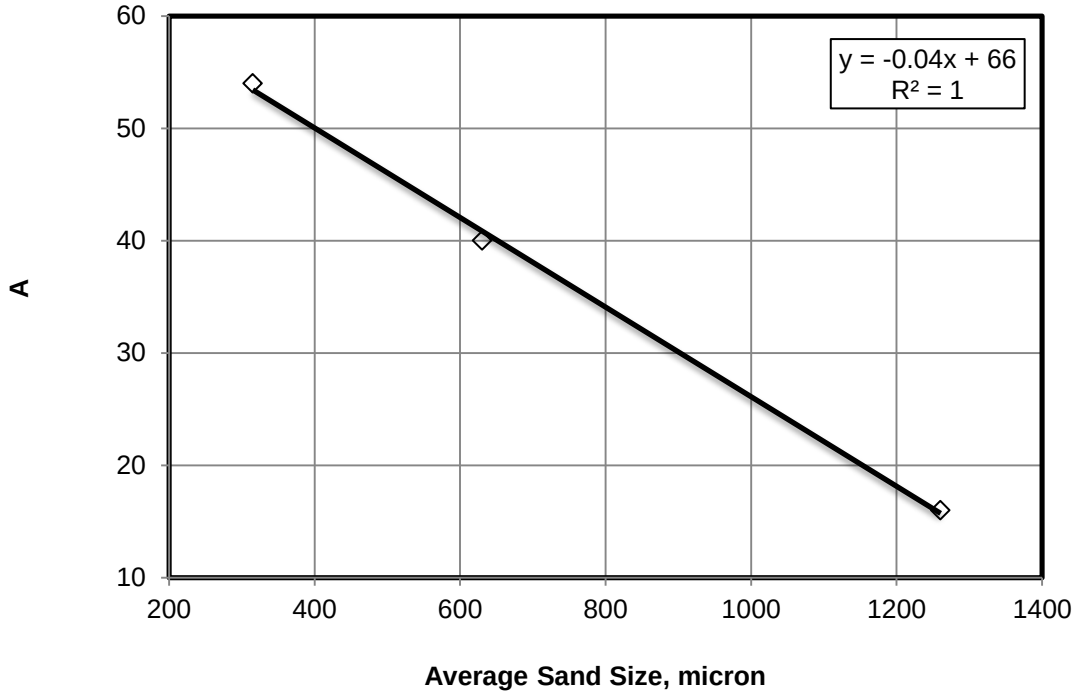

Fig. K.5: Linear function plot of A values at different sand sizes for the rate constants of filtrate of 35 micron pore diameter filter disc

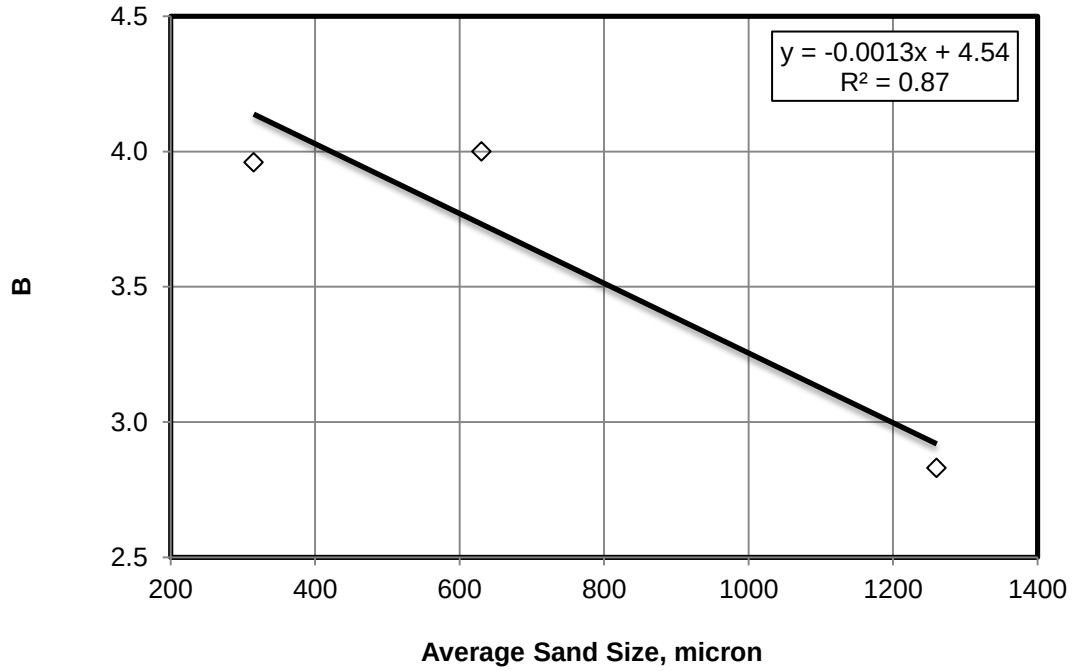

Fig. K.6: Linear function plot of B values at different sand sizes for the rate constants of filtrate of 35 micron pore diameter filter disc

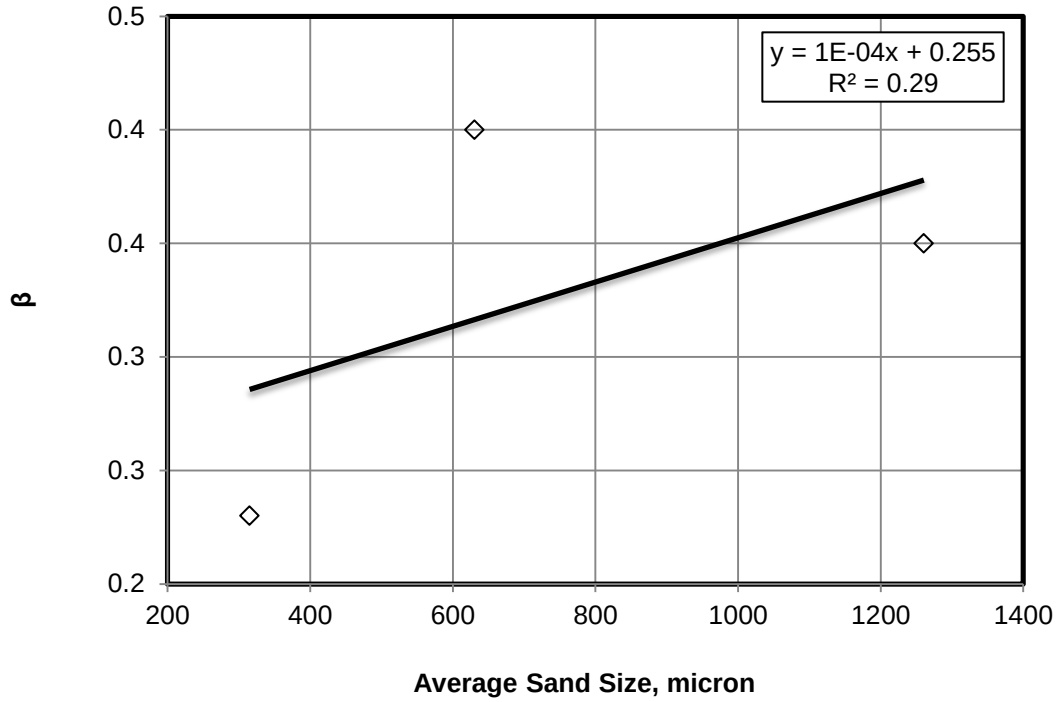

Fig. K.7: Linear function plot of β values at different sand sizes for the rate constants of filtrate of 35 micron pore diameter filter disc

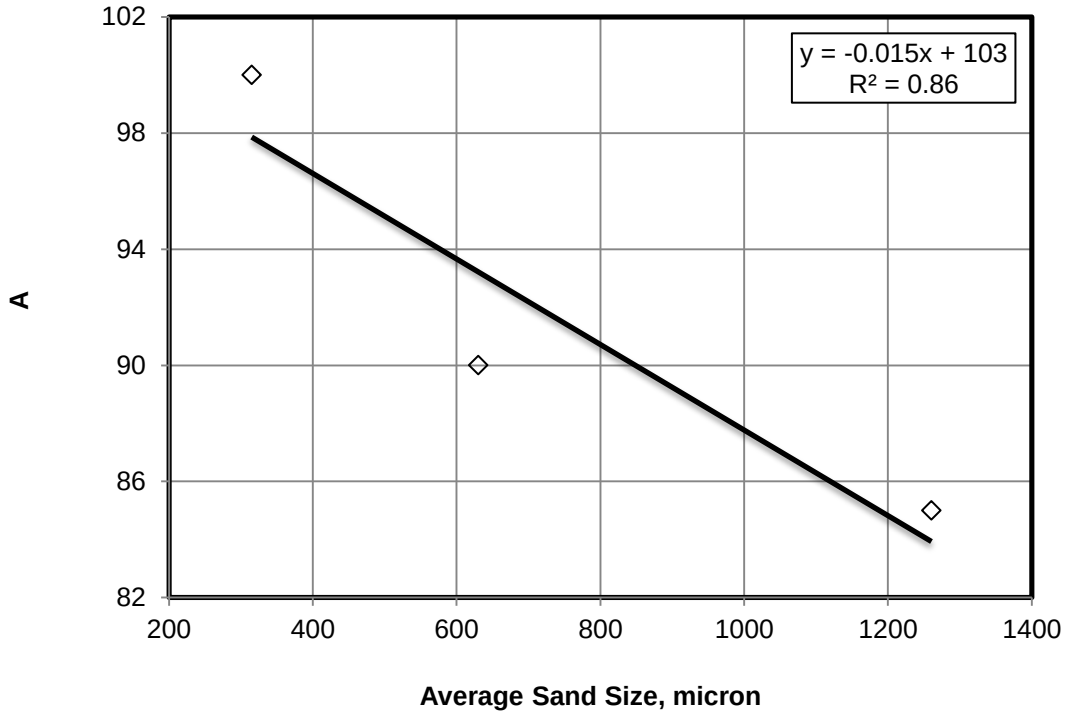

Fig. K.8: Linear function plot of A values at different sand sizes for the spurt loss volume of filtrate of 35 micron pore diameter filter disc

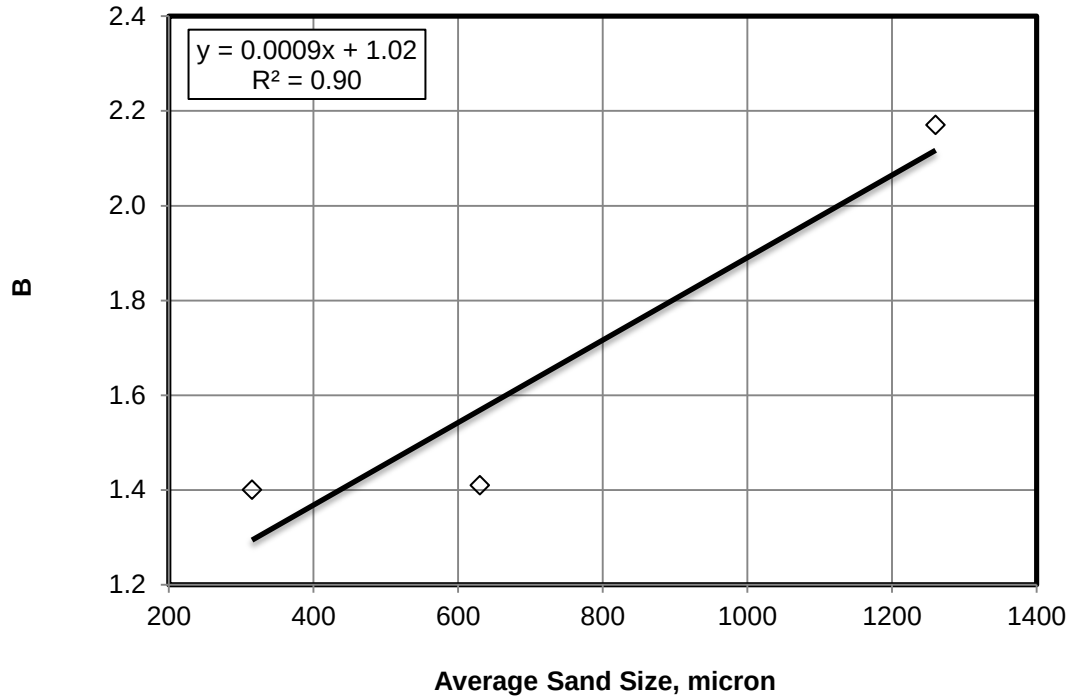

Fig. K.9: Linear function plot of B values at different sand sizes for the spurt loss volume of filtrate of 35 micron pore diameter filter disc

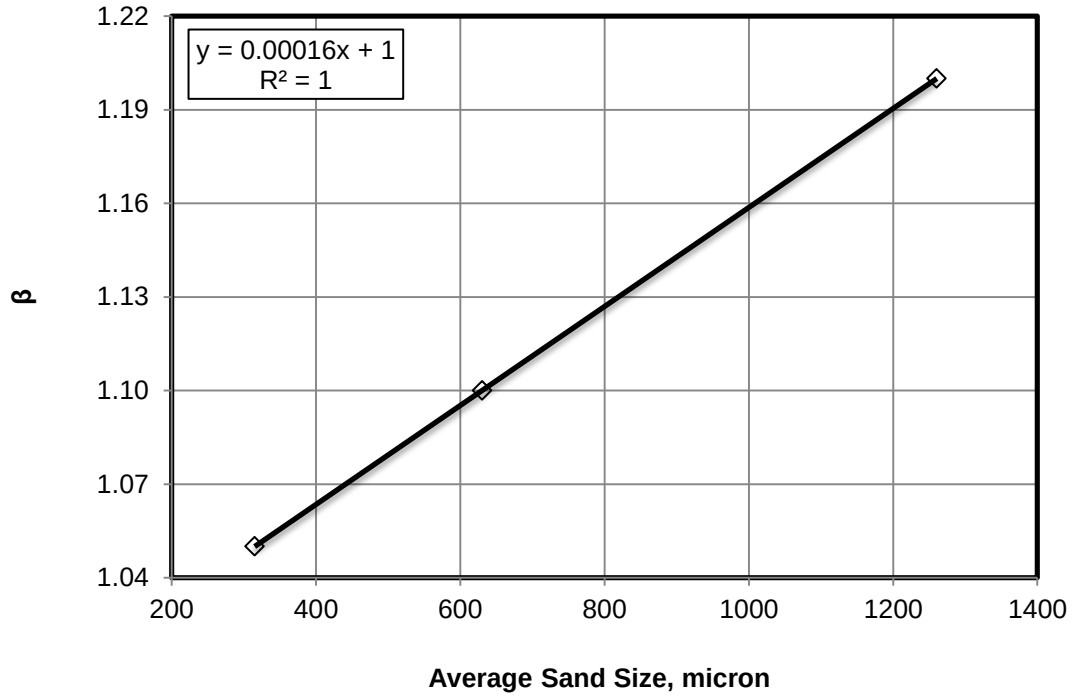

Fig. K.10: Linear function plot of β values at different sand sizes for the spurt loss volume of filtrate of 35 micron pore diameter filter disc